College de France lecture 2021: Interactions between atoms in quantum gases, from van der Waals universality to Fano–Feshbach resonances

Jean Dalibard

▶ **To cite this version:**

Jean Dalibard. College de France lecture 2021: Interactions between atoms in quantum gases, from van der Waals universality to Fano–Feshbach resonances. Doctoral. France. 2021. hal-03762409

HAL Id: hal-03762409
https://hal.science/hal-03762409

Submitted on 19 Oct 2022

HAL is a multi-disciplinary open access archive for the deposit and dissemination of scientific research documents, whether they are published or not. The documents may come from teaching and research institutions in France or abroad, or from public or private research centers.

L'archive ouverte pluridisciplinaire **HAL**, est destinée au dépôt et à la diffusion de documents scientifiques de niveau recherche, publiés ou non, émanant des établissements d'enseignement et de recherche français ou étrangers, des laboratoires publics ou privés.

Interactions between Atoms in Quantum Gases

From van der Waals universality to Fano–Feshbach resonances

Jean Dalibard
Collège de France, chair *Atoms and Radiation*

Lecture series 2021

Contents

Introduction

This lecture series is devoted to the study of interactions between neutral atoms. Taken literally, this is an extremely ambitious program since it covers the fields of molecular physics and quantum chemistry. It is therefore out of the question to realize this program in all its generality. We will focus on the case of cold atoms, for which the de Broglie wavelength is much larger than the range of the interatomic potentials. This assumption will bring considerable simplifications by reducing a complicated interaction potential to the knowledge of a few numbers, like the scattering length or the effective range.

In this year's course, we will focus more specifically on the two-body problem: what is the nature of the interaction between a pair of atoms, what is the connection between the bound states of this pair and the result of an elastic collision between the two particles, can this interaction be controlled and manipulated by external fields? These are questions that have been asked ever since the foundations of quantum mechanics were clarified (Heitler & London 1927; Feynman 1939), but which have come back to the forefront in the last twenty years, with the spectacular developments in quantum gas physics.

The intense research activity on quantum gases is directly linked to these interactions: if they were absent, we would be dealing with the ideal gas model, an interesting problem leading for example to Bose–Einstein condensation, but solved and understood a long time ago. Interactions between atoms change the picture completely; they are at the origin of new phase transitions, such as the Kosterlitz–Thouless transition or the Mott superfluid–insulator transition, treated within the framework of this chair in previous courses. They allow the realization of original composite objects, such as solitons or quantum vortices. The strength of these interactions can be brought to the maximum value allowed by quantum physics, which establishes a link between these cold atomic gases and some strongly interacting systems known in nuclear or particle physics.

The study of the two-body problem is only a first step towards a detailed understanding of interacting quantum gases. Its richness will be enough to keep us busy in this year's course, but this study will have to be completed in a later course: we will then have to explain how the "two-body" concepts we are going to derive here translate into the macroscopic properties of a fluid. We will also postpone to a future course the important but difficult problem of few-body physics: the concepts and tools we will set up here will naturally serve as a basis for these further developments.

I warmly thank Bertrand Evrard and Raphael Lopes for their proofreading of a first version of these notes.

These notes were translated from French using as a first step an automatic translator. This procedure may have introduced some typos or mistakes in the equations. In case of doubt please consult the French version. Thanks in advance for signaling these typos.

Chapter I

The interaction potential between two atoms

In this first chapter, we will specify the physical processes that govern the interaction between two atoms: how do these atoms behave when they approach each other? Is there attraction, repulsion, possibility of forming a bound state? These questions belong to both chemistry and physics, but we will see that the most important elements for us are not necessarily those that are emphasized in "traditional" courses of chemistry and molecular physics. In particular, the fact that we approach the problem from the point of view of cold atoms and quantum gases will give a central role to the long-range behavior of the interaction potential.

To understand this point, let us recall that for a gas of atoms at a temperature of the order of a microkelvin, or even below, the wavelength associated with each atom is large compared to the usual size of a diatomic molecule. This wavelength is typically several hundred nanometers, compared to a sub-nanometer size for a usual dimer. The delocalization of cold atoms, an immediate consequence of the Heisenberg inequality, thus leads to a "smoothing" of the interatomic potential, in a sense that we will specify in the following lectures.

We will consider in this chapter a pair of atoms each prepared in its electronic ground state. The description of the collision requires the determination of the interaction potential $V(\boldsymbol{r})$ between these two partners, $\boldsymbol{r}$ designating here the vector joining their centers of mass. In the most general case, this potential depends on the spin state of each of the two atoms; it can be anisotropic, i.e. it depends on the orientation of the $\boldsymbol{r}$ vector in space. This will be the case if we consider, for example, magnetic dipole interactions between polarized atoms: if the magnetic moment of the two atoms is oriented along z, we know that the magnetic interaction will be attractive if $\boldsymbol{r}$ is parallel to the z axis, and repulsive if it is perpendicular to it. In this lecture series, we will essentially restrict ourselves to the case of an isotropic potential, where V depends only on the modulus of $\boldsymbol{r}$. This restriction is not very strong: it allows us to treat the effects which are dominant in most situations.

As we have written above, considering collisions between cold atoms makes the behavior of the long-range potential play an important role. We will therefore start with the case of atoms relatively far from each other to show that the corresponding interaction, called *van der Waals interaction*, behaves like

$$V(r) = -\frac{C_6}{r^6}, \tag{1}$$

where the coefficient C_6 is positive. It is thus in all cases an attractive interaction: for most atomic species, it can alone form bound dimers, even if the binding energies are very low compared to the usual molecules encountered in chemistry.

We will then discuss the description of the "true" chemical bond that appears when the atoms are close to each other. It results from the possibility for the external electrons to jump from one atom to the other by tunneling. We will examine the length and energy scales associated with this tunneling interaction and we will finish by taking into account the statistical nature, fermions or bosons, of the electrons and nuclei involved.

This last point obviously plays a central role for quantum gases.

To keep this chapter to a reasonable size, we will limit ourselves to the homo-nuclear case, i.e. two identical collision partners. The heteronuclear case is of course also very interesting and we refer interested readers to the comprehensive review articles of Weiner, Bagnato, et al. (1999), Köhler, Góral, et al. (2006), and Chin, Grimm, et al. (2010). Moreover, we will consider here only interactions between neutral atoms. The problem of the interaction between neutral atoms and ions in the context of cold gas physics is reviewed in the recent article by Tomza, Jachymski, et al. (2019).

1 The van der Waals interaction

Consider two neutral atoms, A and B, separated by a distance r. The first effect, and the most important one from the point of view of cold atom physics, is the long-range interaction that appears between these two atoms when they are far enough apart. The "distance" criterion is obtained by comparing the distance r to the size of the electron cloud of each atom, this size being a few angströms. The atoms are considered to be far apart if their two electron clouds do not overlap, i.e. , if there is no point in space where the electron wave functions of A and B are both significantly non-zero. When this criterion is satisfied, the exchange terms responsible for the chemical bonding that we will study in § 4 are absent and only the van der Waals interaction matters.

1-1 The electric dipole-dipole interaction

We are interested here in the electromagnetic interaction of two separate systems, each composed of a nucleus and electrons, and each with zero total charge. The most convenient way to treat this problem is to proceed with a multipole expansion. The first term is the electric dipole-dipole interaction:

$$U_{\mathrm{dip}} = \frac{1}{4\pi\epsilon_0 r^3}\left[\boldsymbol{D}_A \cdot \boldsymbol{D}_B - 3\left(\boldsymbol{u}\cdot\boldsymbol{D}_A\right)\left(\boldsymbol{u}\cdot\boldsymbol{D}_B\right)\right], \tag{2}$$

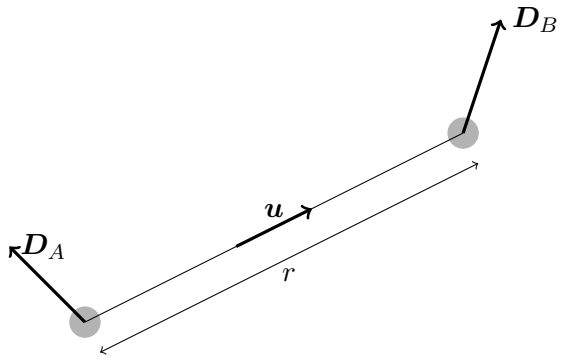

Figure 1. *Dipoles $\boldsymbol{D}_A$ and $\boldsymbol{D}_B$ separated by a distance r.*

where $\boldsymbol{u}$ is the unit vector joining the centers of mass of atoms A and B (figure 1). The dipole operator $\boldsymbol{D}_A$ is given by

$$\boldsymbol{D}_A = \sum_j q(\boldsymbol{r}_j - \boldsymbol{r}_A), \tag{3}$$

where the sum relates to all electrons of atom A, and an equivalent definition for $\boldsymbol{D}_B$. The following terms of the development involve the quadrupolar, octupolar,... electrostatic interactions, as well as magnetic terms generated by the electron currents and spins within each atom. For the following discussion, we will focus on the contribution of the term (2), which is dominant.

1-2 Principle of the perturbative approach

We proceed here to a perturbative treatment of the dipole-dipole interaction given in (2), to determine the modification to the energy E_0 of the ground state. We will denote this modification $\Delta E_0^{(k)}$, where k is the order of the perturbation.

Interactions at first order. The first point to note is that the average electric dipole is always zero for an isolated atom placed in its ground state.

This results from the time-reversal invariance of the electromagnetic interactions responsible for atomic stability. For a hydrogen atom for example, the electronic ground state is the 1s state whose wave function is given by

$$\psi(\boldsymbol{r}) = \frac{\mathrm{e}^{-r/a_0}}{\sqrt{\pi a_0^3}}, \tag{4}$$

where we have assumed the center of the atom placed at the origin of the coordinates and where $a_0 = \hbar^2/(m_e e^2)$ is the Bohr radius, with m_e the mass of the electron and $e^2 = q^2/(4\pi\epsilon_0)$. This wave function is spherically symmetric and we have

$$\langle 1\mathrm{s}|\ q\hat{\boldsymbol{r}}|1\mathrm{s}\rangle = 0. \tag{5}$$

Note that the possible existence of an electronic or nuclear spin degeneracy does not modify this result, which concerns the orbital part of the atomic wave functions. It follows that if we take the two atoms A and B in their electronic ground state ψ_0, the average interaction U_{dip} is always zero

$$\Delta E_0^{(1)} = \langle A:\psi_0; B:\psi_0|\ \hat{U}_{\mathrm{dip}}\ |A:\psi_0; B:\psi_0\rangle = 0. \tag{6}$$

At the first order of perturbation theory, the two atoms "do not see each other": there is no interaction energy between them.

Interactions at second order. The situation is radically changed when we go to the second order of perturbation theory. Before describing the physics underlying the interaction that appears at this order, let us recall a general mathematical result concerning perturbation theory. Let us start from a Hamiltonian $\hat{H}_0$, characterized by its eigenstates and eigenenergies $|\psi_n\rangle$ and E_n with n integer and $E_0 \leq E_1 \leq \ldots$. We suppose that a perturbation $\hat{U}$ is added to $\hat{H}_0$ and we look for the energy shift of the ground level E_0. If the first order term $\langle\psi_0|\hat{U}|\psi_0\rangle$ is null, as it is the case for the problem we are interested in [*cf.* (6)], then the dominant term that appears at second order in U,

$$\Delta E_0^{(2)} = -\sum_{n\neq 0} \frac{|U_{0n}|^2}{E_n - E_0}, \quad U_{0n} = \langle\psi_0|\hat{U}|\psi_n\rangle, \tag{7}$$

is always negative (figure 2): all the terms of the sum written above are in effect positive or zero if E_0 is the minimal energy of the system. We can immediately deduce that our two atoms will attract each other, at least in

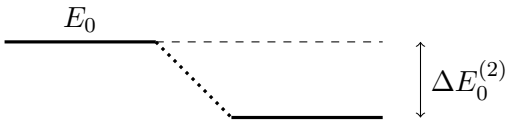

Figure 2. *Second order energy shift for the ground state given in (7). This term is always negative.*

a certain range of distances: the introduction of the coupling U will indeed lower their energy, compared to its value for $r = \infty$.

1-3 Induced dipoles and correlations between atoms

Let us now examine the underlying physics responsible for this attraction. For an atomic electron, the mean square of the dipole operator is not zero. Returning to the hydrogen atom, a simple calculation gives

$$\langle 1\mathrm{s}|\ r^2\ |1\mathrm{s}\rangle = 3a_0^2. \tag{8}$$

In a semi-classical picture, we can therefore represent each dipole as a random variable $\boldsymbol{D}(t)$, with zero mean, but non-zero variance. The instantaneous dipole $\boldsymbol{D}_A(t)$ creates an electric field at the location of atom B, which responds by polarizing itself: an induced dipole appears in the atom B, with an amplitude related to $\boldsymbol{D}_A(t)$. This induced dipole in B in turn creates an electric field at the location of atom A, and this field interacts with the initial dipole $\boldsymbol{D}_A(t)$ (we neglect here the delay effects in this round trip between A and B). In this scheme, the atom B plays the role of a mirror, which sends back to A an image of the dipole $D_A(t)$ to which it gave birth.

The interaction between $\boldsymbol{D}_A$ and this electric field leads to an energy term varying as $\boldsymbol{D}_A^2$, which is non-zero. We have reasoned here by looking at the influence of the fluctuating dipole A on itself, via the polarization of the atom B. Of course, the reciprocal mechanism also exists, with the fluctuating dipole $\boldsymbol{D}_B(t)$ polarizing atom A, which sends back a "reflection" of the initial fluctuation and gives rise to a $\boldsymbol{D}_B^2$ interaction.

It is instructive to look at the same problem from a "more quantum" angle by considering the first-order state vector of perturbation theory. Recall

first that if a Hamiltonian $\hat{H}_0$ has as its eigenstate basis the $|\psi_n\rangle$'s of energy E_n and if we add a static perturbation $\hat{U}$, the $|\psi_n^{(1)}\rangle$ state at first order in V is written in the case of a non-degenerate level:

$$|\psi_n^{(1)}\rangle = |\psi_n\rangle + \sum_{k\neq n} \frac{\langle\psi_k|\hat{U}|\psi_n\rangle}{E_n - E_k}\,|\psi_k\rangle, \tag{9}$$

where we have by convention chosen null the projection of $|\delta\psi_n^{(1)}\rangle = |\psi_n^{(1)}\rangle - |\psi_n\rangle$ on $|\psi_n\rangle$ itself.

To simplify the notations, let us take the case of two hydrogen atoms in their electronic ground state 1s, each of energy $E_1 = -E_{\rm I}$ where $E_{\rm I} = e^2/2a_0 = 13.6\,\text{eV}$ designates the ionization energy of a hydrogen atom. The unperturbed state is

$$|\Psi\rangle = |A:1\text{s};\ B:1\text{s}\rangle \equiv |1\text{s};1\text{s}\rangle. \tag{10}$$

Let us assume that the axis AB is parallel to the axis z so that $\hat{U}_{\rm dip}$ is written

$$\hat{U}_{\rm dip} = \frac{e^2}{r^3}\left[\hat{x}_A\hat{x}_B \,+\, \hat{y}_A\hat{y}_B \,-\, 2\,\hat{z}_A\hat{z}_B\right], \tag{11}$$

where $\hat{x}_A$, $\hat{y}_A$, $\hat{z}_A$ denote the three components of the position operator of the electron of atom A (and idem for B).

Starting from the ground state 1s (angular momentum 0), the position operators $\hat{x},\hat{y},\hat{z}$ have a nonzero matrix element only with the p states (angular momentum 1). The dominant element in the sum (9) is obtained when we consider the first excited state 2p, corresponding to the principal quantum number $n=2$, of energy $E_2 = -E_{\rm I}/4$. We limit ourselves to the contribution of this state for simplicity. We also introduce the p level basis composed of the p_α with $\alpha = x,y,z$. These states form the basis commonly used in chemistry for a space of angular momentum $J=1$. We will also use that $\langle 2\text{p}_x|\,\hat{x}\,|1\text{s}\rangle = \langle 2\text{p}_y|\,\hat{y}\,|1\text{s}\rangle = \langle 2\text{p}_z|\,\hat{z}\,|1\text{s}\rangle \propto a_0$ and $\langle 2\text{p}_\alpha|\,\hat{r}_\beta\,|1\text{s}\rangle = 0$ if $\alpha\neq\beta$.

Under these conditions, there are only 3 terms that contribute to the generic expression (9) at first order in $U_{\rm dip}$:

$$|1\text{s};1\text{s}\rangle + \sum_{\alpha=x,y,z} \frac{\langle 2\text{p}_\alpha;2\text{p}_\alpha|\hat{U}_{\rm dip}|1\text{s};1\text{s}\rangle}{2E_1 - 2E_2}|2\text{p}_\alpha;2\text{p}_\alpha\rangle \tag{12}$$

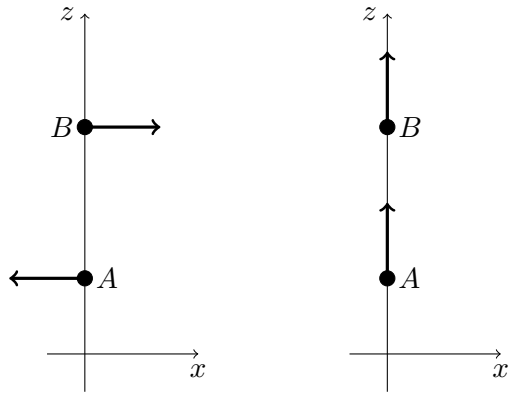

Figure 3. *Left: dipoles induced by the contribution in $|2p_x;2p_x\rangle$ to the state (13). Right: same for the contribution in $|2p_z;2p_z\rangle$.*

that we write

$$|1\text{s};1\text{s}\rangle - \epsilon\left(|2\text{p}_x;2\text{p}_x\rangle + |2\text{p}_y;2\text{p}_y\rangle - 2\,|2\text{p}_z;2\text{p}_z\rangle\right) \tag{13}$$

with

$$\epsilon = \frac{e^2}{2r^3}\,\frac{(\langle 2\text{p}_z|\,\hat{z}\,|1\text{s}\rangle)^2}{E_2 - E_1}, \qquad \epsilon > 0. \tag{14}$$

The expression (13) is interesting because it shows the quantum correlations that appear between the two atoms. Taken individually, the dipole moment of each atom remains zero at this order of the calculation: $\langle\Psi^{(1)}|\hat{x}_A\,|\Psi^{(1)}\rangle = 0$. On the other hand, if atom A is found in the 2p_x state, then we see that atom B is also in the 2p_x state. Moreover, the probability amplitude $-\epsilon$ to find $|2\text{p}_x;2\text{p}_x\rangle$ has the opposite sign to that of the starting state $|1\text{s};1\text{s}\rangle$. This means that the two dipoles along x are anti-correlated, i.e. they have opposite directions (figure 3):

$$\langle\Psi^{(1)}|\,\hat{x}_A\hat{x}_B\,|\Psi^{(1)}\rangle \;= -2\epsilon\left(\langle 1\text{s}|\,\hat{x}\,|2\text{p}_x\rangle\right)^2 \;<\; 0. \tag{15}$$

Since the centers of these dipoles are located on a line parallel to z (figure 3, left), this configuration is attractive. The same is true for the y direction. On the contrary, the dipoles along z are positively correlated: $\langle\hat{z}_A\hat{z}_B\rangle > 0$

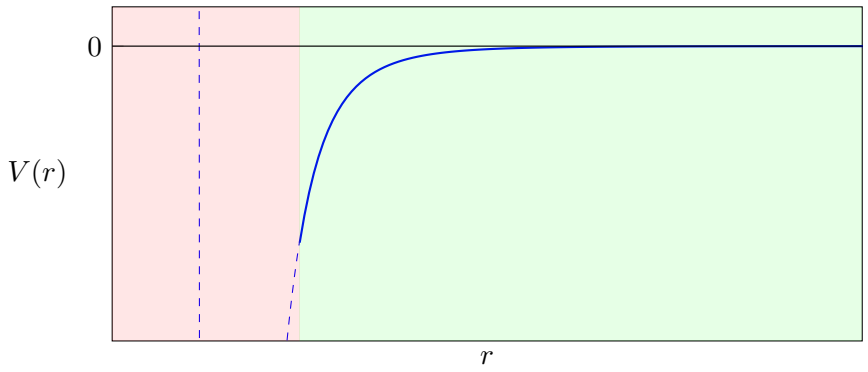

Figure 4. *$V(r) = -C_6/r^6$ van der Waals interaction. This interaction is dominant at long distance (area colored in green). At short distance (zone colored in red), the exchange interaction and the repulsion between nuclei become preponderant.*

(figure 3, right). This also corresponds to an attractive configuration, since the z axis is parallel to the AB axis.

1-4 The van der Waals coefficient C_6

Let us now turn to the discussion of the interaction energy itself. Since this energy is obtained to second order in $U_{\rm dip}$ [cf. eq. (7)] and $U_{\rm dip}$ is itself proportional to $1/r^3$, it follows that the energy varies as $1/r^6$ and therefore takes the form first proposed by London (1930) (figure 4):

$$V(r) = -\frac{C_6}{r^6}. \tag{16}$$

The precise determination of the C_6 coefficient requires a numerical calculation of the wave functions of the excited atomic states, then the estimation of the matrix elements of the electric dipole operator between the ground state and these excited states. One can consult for example:

- For hydrogen : Kolos & Roothaan 1960.
- For helium and other noble gases: Tang, Toennies, et al. 1995; Tang & Toennies 2003; Zhao & Truhlar 2006.
- For alkali metal atoms: Derevianko, Babb, et al. (2001) and Mitroy & Bromley (2003),Coxon & Hajigeorgiou (2010).
- For alkaline earth atoms: Mitroy & Bromley (2003), Porsev & Derevianko (2006), Li, Xie, et al. (2010), Yin, Li, et al. (2010), and Heaven, Merritt, et al. (2011).
- For erbium and dysprosium : Lepers, Wyart, et al. (2014) and Li, Wyart, et al. (2017) (a non-negligible anisotropy appears in this case due to the complex structure of the electronic ground state).

The purpose of this section is to give a simple estimate of the C_6 coefficient for atoms commonly used in cold atom experiments, such as alkali metal atoms (one peripheral electron) or alkaline earth atoms (two peripheral electrons).

To obtain this estimate, we will use the same approximation as in the previous paragraph (§ 1-3), when discussing the correlations present in the perturbed state. We will assume that in the sum over all excited states that appears in the energy shift at order 2, the essential contribution comes from the resonance line of the atom, which connects the ground state g to a particular excited level e. Let us model this line as a transition from the ground state of angular momentum $J_g = 0$ to the excited level of angular momentum $J_e = 1$; the level $|e\rangle$ corresponds to a space of dimension 3, of which a possible basis is formed by the three orbitals $|e_\alpha\rangle$, $\alpha = x, y, z$, already used above.

We note $\omega = (E_e - E_g)/\hbar$ the frequency of the selected transition and we restrict the sum to one level (i.e. three states)

$$\Delta E^{(2)} = -\sum_{\alpha=x,y,z} \frac{|\langle e_\alpha; e_\alpha|\hat{U}_{\rm dip}\,|g; g\rangle|^2}{2\hbar\omega}. \tag{17}$$

The numerator involves the matrix elements $\langle e_\alpha|\hat{D}_\alpha|g\rangle$ which also enter in the expression of the natural width (inverse of the lifetime) of the e level,

calculated within the electric dipole approximation:

$$\Gamma = \frac{\omega^3 d^2}{3\pi\epsilon_0 \hbar c^3}, \tag{18}$$

where $d = \langle e||D||g\rangle$ is the *reduced dipole* between g and e.

Let us insert the expression (11) of the potential $\hat{V}$ into the energy shift (17). The contributions of $\hat{D}_x$, $\hat{D}_y$, $\hat{D}_z$ sum with weights $1:1:4$ to give

$$\Delta E^{(2)} = -\frac{27}{16}\,\frac{\Gamma}{\omega}\,\frac{\hbar\Gamma}{(kr)^6} \tag{19}$$

where $k = \omega/c = 2\pi/\lambda$ is the wave number of the transition of frequency ω and wavelength λ. This very simple expression brings out the scaling law $C_6 \propto \Gamma^2\lambda^7$.

Table 1 gives the approximate values of C_6 obtained by the law (19), compared to the most accurate numerical results (see also figure 5). Recall that the natural width $\Gamma/2\pi$ of a resonance line is typically of the order of 5 to 50 MHz (lifetime of e from 3 to 30 ns), and the corresponding wavelengths are of the order of a fraction of a micron. The ratio Γ/ω, which is the small dimensionless parameter involved in the perturbative development and which appears in (19), is thus $\sim 3\times10^{-9}$–3×10^{-8}.

For all atomic species in this table, the agreement is excellent (error lower than 20 %) except for those of the lanthanide family such as erbium, dysprosium and ytterbium for which the approximation consisting in limiting to only one resonance line is problematic (Safronova, Porsev, et al. 2012; Porsev, Safronova, et al. 2014)

Beyond the dipole-dipole interaction. The dipole-dipole interaction term is only the first element of the multipole expansion, which comprises an infinite number of terms, in $-C_{2n}/r^{2n}$ with $n = 3, 4, 5, \ldots$. Each value of n corresponds to a given multipole order: $n = 3$ for the dipole, $n = 4$ for the quadrupole, etc. The coefficients C_{2n} are called *dispersion coefficients*. For the discussions in this course, we will just keep the first term $-C_6/r^6$ which is dominant at long distance, but an accurate comparison of the calculated potential with the experimental measurements requires to take into account several terms of this sum (for example up to $n = 12$ for the He-He potential by Tang, Toennies, et al. (1995)). Let us also note an approximate recurrence relation linking the different dispersion coefficients:

$$C_{2n} \approx \left(\frac{C_{2n-2}}{C_{2n-4}}\right)^3 C_{2n-6} \tag{20}$$

which allows one to calculate all these coefficients once the first three are known [see Tang, Toennies, et al. (1995) and refs. in].

system	C_6 [a.u.]	$\Gamma/2\pi$ [MHz]	λ [nm]	C_6 approximated [a.u.]
Li-Li	1389	5.87	671	1340
Na-Na	1556	9.80	589	1500
K-K	3897	6.04	767	3610
Rb-Rb	4691	6.07	780	4100
Cs-Cs	6870	5.22	852	5629
Mg-Mg	627	80.9	235	630
Ca-Ca	2121	34.6	423	1840
Sr-Sr	3103	32.0	461	2750
Er-Er	1760	29.7	401	930
Dy-Dy	2275	32.2	421	1550
Yb-Yb	1929	29	399	860

Table 1. *Values of the van der Waals coefficient C_6 for some atomic species frequently used in cold atom experiments. Column 2 gives the value found in the literature, resulting from a detailed analysis summing the contributions of the different atomic transitions (see the different references in the text). Column 5 gives the value found by restricting to the main resonance line [*cf. *eq. (19)], whose characteristics (width and wavelength) are presented in columns 3 and 4. In the literature, C_6 is traditionally expressed in atomic units (a.u.), i.e. $E_0 a_0^6$ with $E_0 = e^2/a_0 = 1$ Hartree. We have $a_0 = 0.5292\,\text{Å}$ and $e^2/a_0 = 27.21\,eV$, so that the atomic unit for C_6 is $9.55\times10^{-80}\,Jm^6$. Recall that we have assumed throughout this course $e^2 = q^2/4\pi\epsilon_0$ with $q = 1.602\times10^{-19}$C.*

Delay effects. We have explained the origin of the van der Waals interaction by starting with the instantaneous dipole of atom A that creates a field polarizing atom B, and this induced dipole in turn creates a field on the A atom. In doing so, we have neglected any delay effect in the establishment

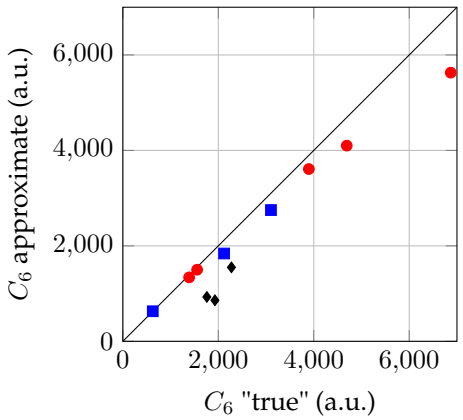

Figure 5. *Relation between the experimentally measured value for the coefficient C_6 and its approximated value (19). The values of the table 1 are used here. The red discs correspond to the alkali-metal species, the blue squares to the alkaline earth species and the black lozenges to the lanthanides.*

of these fields. This is an approximation which is only valid if the atoms are not too far apart. More precisely, we have seen that the dynamics of each atom is dominated by its resonance transition of frequency ω. If the propagation time r/c of the electromagnetic field between the two atoms is small compared to $1/\omega$, it will be legitimate to neglect the phase shift induced by this propagation. The criterion of validity of the $1/r^6$ law is therefore given by:

$$\text{Negligible delay effects if} \quad \frac{r}{c} \ll \frac{1}{\omega} \quad \Leftrightarrow \quad kr \ll 1. \tag{21}$$

For more distant atoms, delay effects must be taken into account and lead to the replacement of the $1/r^6$ law by the faster $1/r^7$ decay (Casimir & Polder 1948). Note, however, that these retardation effects are in practice extremely small and do not play a significant role in the determination of the scattering lengths which we will study later. As a check, one can estimate the interaction energy (19) for $kr = 1$ and one finds energies of the order of one picokelvin only.

2 Van der Waals interaction for excited atoms

In this lecture series, we will mainly focus on the case where the interacting atoms are placed in their electronic ground state. Nevertheless, it is useful at this stage to say a few words about the case where at least one of the two atoms is placed in an excited electronic state.

2-1 Pair of atoms with an electronic excitation

We start our study with the case where only one of the two atoms is in an excited electronic state. To simplify the discussion, we keep the model of an atomic transition $J_g = 0 \leftrightarrow J_e = 1$. We will see that the major difference with the previous case is that the dipole-dipole coupling now acts at order 1, and thus gives rise to a $1/r^3$ interaction, with a larger range than for atoms in their ground state.

The subspace associated to the physical situation we are interested in is of dimension 6, with as possible basis

$$\{|g; e_\alpha\rangle, |e_\alpha; g\rangle\}, \quad \alpha = x, y, z. \tag{22}$$

In the absence of coupling, this subspace is degenerate. To take into account the coupling $\hat{U}_{\rm dip}$ at order 1 of the perturbation theory, we have to diagonalize the 6×6 matrix corresponding to the restriction of $\hat{U}_{\rm dip}$ to the subspace generated by (22).

Fortunately, this diagonalization is less complex than it seems. Let us take as before the axis z parallel to the vector joining A to B. For a given index α, the operator $\hat{U}_{\rm dip}$ has a non-zero component only between $|g; e_\alpha\rangle$ and $|e_\alpha; g\rangle$ with for example:

$$\langle g; e_x| \hat{U}_{\rm dip} |e_x; g\rangle = \frac{e^2}{r^3} |\langle g| \hat{x} |e_x\rangle|^2 = \frac{3}{4} \frac{\hbar\Gamma}{(kr)^3} \tag{23}$$

with an identical result when we make the substitution $x \to y$, and a result multiplied by -2 when we make the substitution $x \to z$.

Therefore, the diagonalization of the 6×6 matrix can be reduced to the

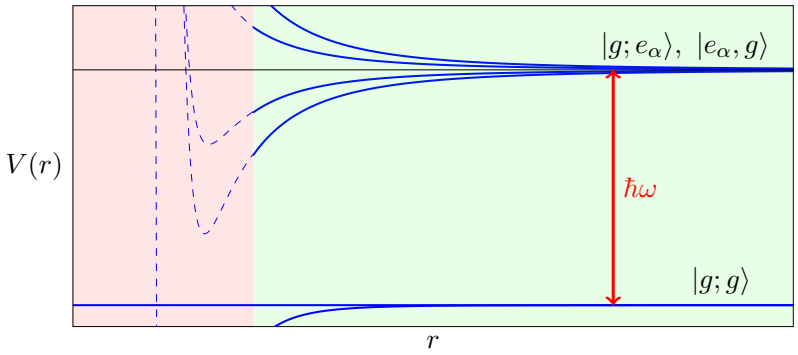

Figure 6. *Energy levels of a pair of atoms with electronic excitation for a model transition $J_g = 0 \leftrightarrow J_e = 1$.*

diagonalization of three 2×2 submatrices:

$$[V_{x,y}] = \frac{3}{4}\frac{\hbar\Gamma}{(kr)^3}\begin{pmatrix}0 & 1\\ 1 & 0\end{pmatrix} \qquad \text{and} \quad [V_z] = -2[V_{x,y}]. \tag{24}$$

The diagonalization is immediate and gives the following energies and eigenstates (with a global shift of $\hbar\omega$ with respect to the ground state $|g;g\rangle$):

$$E = \pm\frac{3}{4}\frac{\hbar\Gamma}{(kr)^3} \qquad \frac{1}{\sqrt{2}}\left(|e_\alpha;g\rangle \pm |g;e_\alpha\rangle\right), \quad \alpha = x,y \tag{25}$$

and

$$E = \pm\frac{3}{2}\frac{\hbar\Gamma}{(kr)^3} \qquad \frac{1}{\sqrt{2}}\left(|e_z;g\rangle \mp |g;e_z\rangle\right). \tag{26}$$

This result, which is plotted in Figure 6, calls for several remarks:

- The dependence $(1/r^3)$ on the distance r is much weaker than for the case of a pair of atoms in their electronic ground state $(1/r^6)$. This potential will therefore be felt at larger distances.
- This potential emerges at first order of perturbation theory, whereas the one found in (19) came at second order. This is why the factor $\Gamma/\omega \sim 10^{-7}$ which appeared in (19) is absent here.
- The eigenstates in (25) and (26) involve the excited electronic state e which is radiatively unstable and can de-excite by emitting a photon, with a lifetime Γ^{-1} when the atom is isolated. These eigenstates are therefore also unstable. When the atoms are close together, the precise calculation of the lifetime of these states requires an elaborate formalism and we will not do it here. Let us simply note that if we evaluate the matrix element of the dipole operator between each of these states and the ground state $|g;g\rangle$, we find that three of these states lead to a zero value: they are *subradiant states*, of long lifetime. For the three other states, the dipole is multiplied by $\sqrt{2}$ compared to the case of an isolated atom; their lifetime is thus reduced by a factor of 2, they are *superradiant states*.

2-2 Van der Waals interaction for Rydberg atoms

Let us now say a few words about the case where the atoms are each prepared in an excited state. We consider alkali metal atoms and suppose that the external electron of each atom has been brought into a highly excited state $|e\rangle \equiv |n,\ell,j,m\rangle$ with $n \gg 1$, i.e. , a Rydberg state. If the atoms are far enough apart, one can always treat perturbatively the electric dipole-dipole interaction $\hat{U}_{\rm dip}$ between them. As for the case of two ground-state atoms, the first non-zero term of the energy appears at order 2 :

$$\Delta E = -\sum_{e',e''}\frac{\left|\langle e',e''|\hat{U}_{\rm dip}|e,e\rangle\right|^2}{E_{e'}+E_{e''}-2E_e}, \tag{27}$$

where the sum covers all possible states for the outer electrons of the atoms. In practice, the matrix element of the electric dipole operator that appears in the numerator is governed by selection rules that strongly restrict the class of eligible states. For example, if $|e\rangle$ is an s state, of orbital angular momentum $\ell = 0$, the only $|e'\rangle, |e''\rangle$ states that can contribute are p states, of orbital angular momentum $\ell = 1$.

Since the operator $\hat{U}_{\rm dip}$ is proportional to $1/r^3$, where r is the distance between the two atoms, the energy shift $\Delta E(r)$ can always be put in the form $\Delta E = -C_6/r^6$. However, contrary to the case where the two atoms were in their ground state and the van der Waals interaction was always

attractive ($C_6 > 0$), we cannot say anything about the sign of C_6 this time. The energy denominators involved in (27) can indeed be negative as well as positive.

In fact, it often happens that the sum involved in (27) is dominated by a single term, such that $E_{e'} + E_{e''}$ is very close to $2E_e$. Saffman, Walker, et al. (2010) give the example of the rubidium state $|e\rangle = |60\mathrm{p}_{3/2}\rangle$, for which the dominant term in the sum comes from the $|60\mathrm{s}, 61\mathrm{s}\rangle$ pair, the energy denominator being only $h \times 0.3\,\mathrm{GHz}$.

We will not describe in detail this interaction between Rydberg atoms because it is a subject rich enough to deserve a course on its own. We will simply mention two points that radically distinguish it from the case of atoms in their ground state:

- The coefficient C_6 is considerably larger than that found for the ground state. This increase results from two factors: (i) the numerator of (27) involves the matrix element of the position operator between a state $|n, \ell\rangle$ and a neighboring state $|n', \ell \pm 1\rangle$ with $n' \approx n$. This matrix element varies as n^2, so that the numerator of (27) varies as $(n^2)^4 = n^8$. (ii) The denominator of (27) involves energy differences of neighboring hydrogen states. As the energy of each state varies as $1/n^2$, this difference varies as $1/n^3$. In the end, we find that the coefficient varies as $\frac{n^8}{1/n^3} = n^{11}$, an exponent rarely found in scaling laws in physics! We show in figure 7 the verification of this scaling law.

- The above reasoning is based on perturbation theory. But the very large value predicted for C_6 indicates that when the atoms move closer together, the energy shift ΔE will quickly become of the order of the energy differences $E_{e'} + E_{e''} - 2E_e$ which intervene in the denominator of (27). When this is the case, perturbation theory can no longer be applied and one switches to a regime where the interaction potential varies as $1/r^3$, as in the previous paragraph (§ 2-1) devoted to the resonant dipole-dipole interaction. This switch corresponds to the transition from the van der Waals regime to the Förster regime (Walker & Saffman 2008).

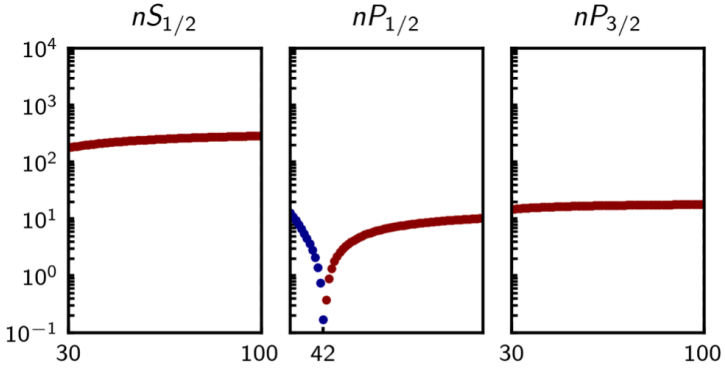

Figure 7. *Test of the scaling law $|C_6| \propto n^{11}$ for a pair of rubidium atoms prepared in a Rydberg state. The parameter $|C_6|/(n/60)^{11}$ is plotted as a function of the principal quantum number n. The scaling law is well verified for a pair of atoms in the $|ns, ns\rangle$ or $|np_{3/2}, np_{3/2}\rangle$ state. In the case of $|np_{1/2}, np_{1/2}\rangle$ pairs, accidental compensations in the different contributions to C_6 lead to a near cancellation of this coefficient for $n = 42$. Figure taken from Sylvain de Léséleuc's PhD thesis, Paris-Saclay University, 2018.*

3 The van der Waals dimers

3-1 When the covalent bond is absent

In chemistry, van der Waals interaction is usually only a small contribution to the binding energy of a molecule. The dominant contributions, either covalent or ionic, come from electron exchanges between atoms. These exchanges, which we will discuss in § 4, only occur when the electron clouds of the atoms overlap, typically for distances r less than a few angströms. They lead to potential wells, i.e. binding energies of the molecules, much larger than those produced by the van der Waals interaction. For example, for $C_6 = 100$ atomic units, we find that the potential well created by the van der Waals attraction at a distance $r = 5\,\text{Å}$ is $6 \times 10^{-22}\,\mathrm{J}$, or 4 meV. A typical covalent bond leads to energies that are rather on the order of one electron volt.

However, there is a whole class of atoms, rare gas or alkaline earth for example, for which the covalent bond cannot occur because their peripheral atomic layer is complete: the exchange process at the basis of the chemical bond is therefore blocked. In some textbooks, one can read that as a consequence, the diatomic molecule built with these atoms, He_2 or Be_2, cannot exist. This assertion is in all rigor erroneous: the He_2 or Be_2 edifice exists and it is stable, in the sense that it has an energy lower than that of two infinitely separated atoms. Its existence relies on van der Waals attraction, with the overlap of electron clouds at short distances creating essentially a repulsive potential.

3-2 The example of rare gases

A simple model of interaction energy between two noble gas atoms has been proposed by Tang & Toennies (1984), then deepened and justified from first principles by several authors. One can consult Tang & Toennies (2003) for a detailed description of this potential called TT (Tang-Toennies). The idea of this potential is (i) to start from the development

$$-\sum_{n=3}^{N} \frac{C_{2n}}{r^{2n}} \tag{28}$$

at long distance, (ii) to screen it when r approaches 0 to avoid its divergence, and (iii) to substitute a repulsive short-range (Born–Mayer) potential, preventing the nuclei from getting too close to each other. In addition to the coefficients C_{2n} involved in (28), two parameters, A and b, must be given to describe this short-range screening and repulsion.

The TT potential is written more precisely

$$V(r) = A\mathrm{e}^{-br} - \sum_{n=3}^{N} f_n(br)\frac{C_{2n}}{r^{2n}} \tag{29}$$

where each screening function $f_n(x)$

$$f_n(x) = 1 - \mathrm{e}^{-x}\sum_{k=0}^{2n}\frac{x^k}{k!} \tag{30}$$

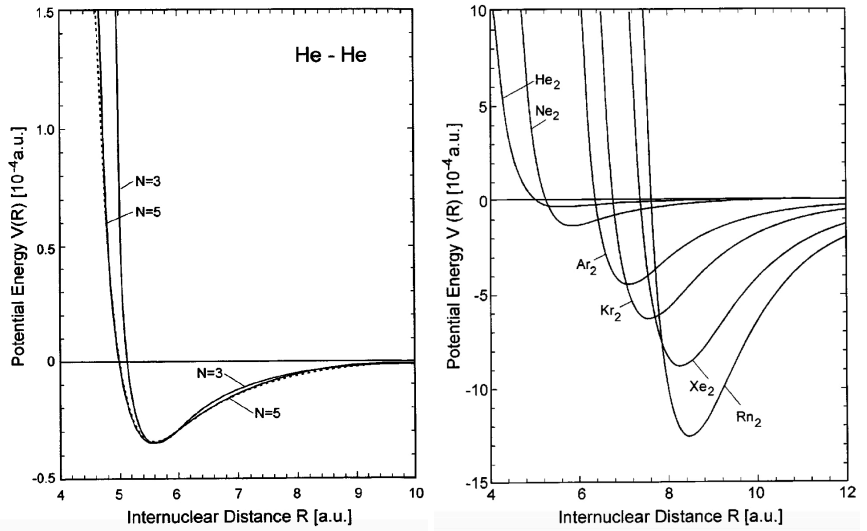

Figure 8. *Left: interaction potential between two helium atoms, obtained by keeping only the dipole-dipole term ($N = 3$) in (28), compared to the result obtained with dipole, quadrupole and octupole interactions ($N = 5$). The dashed potential is determined by a fit to the experimental data. Right: Interaction potential between rare gas atoms. The data are plotted in atomic units, $a_0 = 0.5292\,\mathring{A}$ for the distances and $e^2/a_0 = 27.21\,eV$ for the energies. Figures extracted from Tang & Toennies (2003).*

goes continuously from 0 to 1 when r increases from 0 to infinity. In practice, the restriction to $N = 5$, which amounts to keeping only the dipolar, quadrupolar and octupolar terms, gives a very good approximation of the real potential (figure 8, left). Once N is fixed, the coefficients A and b are adjusted to place the position $r_{\min}$ of the minimum of the potential and its depth $V_{\min}$ at the values determined from experimental or numerical results [see Barrow & Aziz (1988) for an example of this determination].

We have plotted in figure 8 (right) the potential obtained for the rare gases. We see that the depth of the potential well $V_{\min}$ and the position $r_{\min}$ of this minimum increase when we move down the periodic table. The values of the coefficients C_6 are reported in the table 2. These values

system	$r_{\min}$	$V_{\min} \times 10^4$	C_6
He-He	5.6	0.35	1.5
Ne-Ne	5.8	1.3	6.4
Ar-Ar	7.1	4.5	64
Kr-Kr	7.6	6.4	130
Xe-Xe	8.3	9.0	290
Rn-Rn	8.5	13	420
Be-Be	4.8	36.0	214
Mg-Mg	7.4	19.6	627
Ca-Ca	8.1	50.1	2121
Sr-Sr	8.8	49.3	3103

Table 2. *Parameters of van der Waals dimers formed from noble gases and alkaline earth atoms. These data are in atomic units, $a_0 = 0.5292\,\mathring{A}$ for distances and $e^2/a_0 = 27.21\,eV$ for energies.*

are extracted from Tang & Toennies (2003) and one can also consult Gerber (2006).

An important point is that for each noble gas species, including helium ^{4}He which corresponds to the shallowest well, this interaction potential gives rise to bound states [3 bound states for Ne_2, 6 bound states for Ar_2 for example (Ogilvie & Wang 1992)]. X_2 molecules (with X=rare gas atom) exist, even if their binding energy is low: the most bound is radon with a potential well of 13×10^{-4} atomic units, or 35 meV (400 Kelvins). The only missing dimer is $^3He_2$, which interacts with the same potential as $^4He_2$, but for which the quantum fluctuations related to the kinetic energy are larger (factor $3/4$ on the mass), which makes the bound state disappear.

Due to the lack of adequate lasers, it is not yet possible to cool and trap rare gases optically, at least when they are in their electronic ground state. But if this becomes possible, it is interesting to note that the resulting gases will be in a relatively strong interaction regime, at least for the heaviest elements. Indeed, as we will see in the following, the scattering length, which is the parameter characterizing the interactions between atoms at low temperature, varies as $(C_6)^{1/4}$. The C_6 coefficient of radon for example (400 atomic units) is only 3 to 10 times lower than that of alkali metal atoms, in spite of the fact that for the latter, the covalent bond gives rise to potential wells 100 times deeper. Unless there is a special scattering resonance, the scattering length for radon will differ by a factor of 2 at most from that of alkali metal atoms. One should therefore be wary of the intuition derived from room temperature chemistry when approaching the physics of interactions between ultra-cold atoms.

One notes on the table 2 that the dimers of rare gases are "large molecules". The distance between atoms for the He_2 molecule is 4 times larger than for the di-hydrogen molecule H_2. This is of course due to the long-range nature of the potential.

3-3 Experimental study of the He_2 molecule

The possible existence of the helium dimer has long been a subject of controversy. The question has been definitively settled in a beautiful experiment of wave physics by Schöllkopf & Toennies (1994). In this experiment, a supersonic beam of helium is formed from a high pressure container (15 bar) with a 5 micron diameter hole. The jet passing through this hole propagates in the vacuum, it cools down because of the supersonic expansion and thus becomes quasi-monokinetic ($\Delta v/v \lesssim 5\,\%$). The wavelength associated to each type of particle (atom, dimer, trimer), $\lambda = h/mv$, is then well defined. For a temperature of 30 K, we find $\lambda = 0.18$ nm for He atoms.

This beam is collimated by two 10 micron wide slits, located 47 cm apart, and then passes through a periodic grating on which the particles can be diffracted (figure 9). The period of the grating is $d = 200\,\mu$m and we expect to observe diffraction peaks at angles $\theta_n \approx n\lambda/d$.

An example of signal is shown in Figure 2. We see a main peak on the left, corresponding to non-diffracted particles. On the right, for an angle θ_1, the large peak corresponds to the first diffraction order ($n = 1$) of the atoms. The interesting signal is located between these two large peaks: we see two smaller peaks at $\theta_2 = \theta_1/2$ and $\theta_3 = \theta_1/3$, which correspond to particles whose wavelength is respectively 2 and 3 times smaller than those of atoms. They are respectively due to the dimers and the trimers, which go at the same speed as the atoms because of the collisions at the exit of the source, and have a mass 2 (resp. 3) times larger.

The helium dimer is a nice example of the objects of interest in this

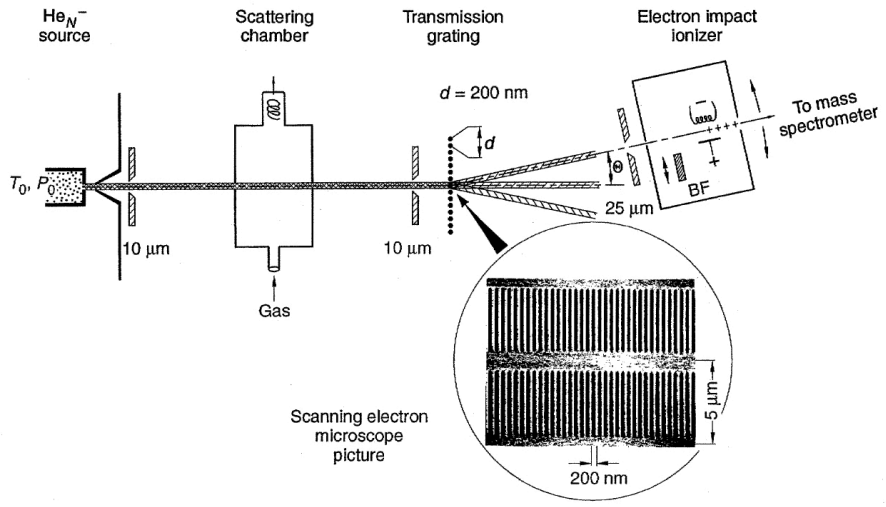

Figure 9. *Experimental scheme using diffraction of matter waves to detect the presence of helium dimers and trimers in a supersonic beam of atomic helium. Figure taken from Schöllkopf & Toennies (1994).*

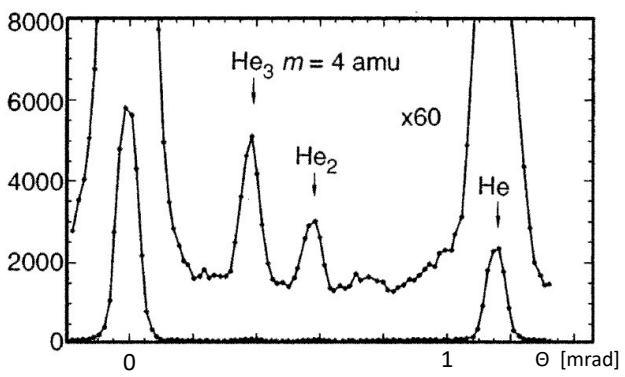

Figure 10. *Angular distribution of diffracted particles. Since the beam is monokinetic, the comparison of the diffraction angles allows one to directly trace the mass of the diffracted particles. The large peak on the left corresponds to the non-diffracted beam and the large peak on the right to the first diffraction order for helium atoms. The two smaller intermediate peaks reveal the existence of He_2 dimers and He_3 trimers. Figure extracted from Schöllkopf & Toennies (1994).*

course. In particular, its binding energy ($\sim 10^{-7}$ eV) is much smaller than the depth of the potential well visible in figure 8 ($\sim 10^{-3}$ eV). This indicates that the dimer is only very marginally bound (Grisenti, Schöllkopf, et al. 2000). Correlatively, the average distance between the two atoms, ~ 50 Å, is much larger than the distance $r_{\min} \sim 3$ Å at which the interaction energy is minimal. This is the signature of a scattering resonance, a notion that will be clarified in the following chapters.

Let us mention that the trimer is also a fascinating object. It is indeed a weakly bound three-body state, a precursor of the states predicted by Efimov (1971) [see also Lim, Duffy, et al. (1977) for the specific case of helium]. More precisely, the state highlighted by Schöllkopf & Toennies (1994) and shown in figure 10 is the ground state of the trimer and its size is of the order of 10 Å. More recently, Kunitski, Zeller, et al. (2015) have revealed the first excited state of this trimer (in fact, the only possible excited state), whose size exceeds 100 Å and which can be seen as a true Efimov state.

3-4 The alkaline earth atoms

The alkaline earth atoms belong to the second column of the periodic table: Be, Mg, Ca, Sr, the last three being used in cold atom experiments. They have two outer electrons in an s-type level, which means that this layer is complete, the two electrons forming a spin singlet state. Therefore, the exchange processes responsible for covalent bond cannot occur and the attractive part of the potential is essentially due to van der Waals interactions, as for rare gases. One can then use a TT type potential [cf. (29)] to describe their interaction in an approximate way [see e.g. Li, Xie, et al. (2010) for Mg and Yin, Li, et al. (2010) for Ca]. There are also numerical methods of high accuracy, see for example Zhao & Truhlar (2006), Gerber (2006), and Heaven, Merritt, et al. (2011).

The interaction potentials for Ca and Sr are shown in figure 11, together with those of the "neighboring" rare gases Ar and Kr. The figure also shows the interaction potential for mercury (Yin, Li, et al. 2010). For the physics

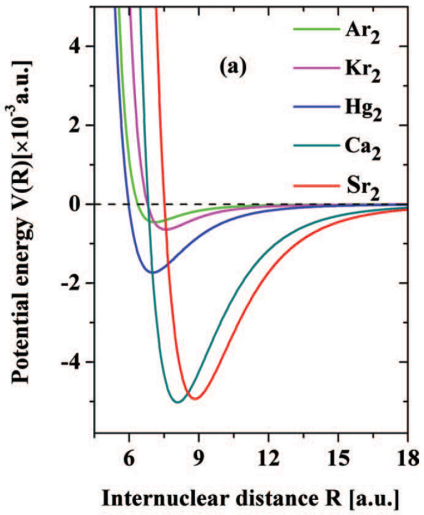

Figure 11. *Interaction potential for Ca, Sr and Hg. The potentials of the noble gases Ar and Kr are shown for comparison. Figure extracted from Yin, Li, et al. (2010).*

of cold atoms, the two important points are that:

- The coefficient C_6 takes for each species a significant value, comparable to those of the alkali metal atom on the same line of the periodic table: Na↔Mg, K↔Ca, Rb↔Sr (see table 1).
- The dimers all have a relatively large number of bound states; the interatomic potential for the lightest of them (Be) leads to 10 or 11 bound states, and this number increases as one moves down the periodic table, the atoms becoming heavier and the C_6 coefficient increasing.

As we will see in the remainder of the course, these two points are sufficient to ensure that the typical scattering length is proportional to $C_6^{1/4}$ and comparable to that of alkali metal atoms, for which the covalent bond exists. At very low temperatures, the gases formed with these atoms will therefore have interaction energies similar to those of sodium or rubidium gases, for example.

4 The "real" chemical bond

In the last section of this chapter, we are interested in the covalent bond, which allows the formation of strongly bound homonuclear dimers. This bonding results from the possibility for the electrons to tunnel from one nucleus to the other, which increases the extension of their wave function and thus decreases their kinetic energy. We will start our discussion with the simplest atomic species to describe theoretically, hydrogen. We will then generalize it to other atomic species relevant for cold atom experiments, the alkali metal species.

4-1 Born–Oppenheimer approximation

The description of the interaction between two hydrogen atoms is a 4-body problem, two nuclei (protons) noted A and B and two electrons noted 1 and 2. The 4-body problem is intrinsically very difficult to solve. Here, it is greatly simplified by the Born–Oppenheimer approximation that takes advantage of the very large difference between the mass M of a nucleus and the mass m_e of an electron. This approximation allows us to reduce to a two–body problem. Since this problem is itself globally translation invariant, it can be further reduced to a one-body problem, treatable with "standard" quantum physics methods.

To implement the Born-Oppenheimer approximation, one starts by fixing the positions of the nuclei in $\boldsymbol{r}_A$ and $\boldsymbol{r}_B$ and looks for the eigenstates of the total energy (kinetic+potential) of the electrons moving in the Coulomb field created by the nuclei. Once this energy is known, at least in an approximate way, we use it as an effective potential energy, noted $V(r_{AB})$, to describe the motion of the nuclei. The Born-Oppenheimer approximation is a variant of the adiabatic approximation that we have encountered several times in previous years' courses: since the mass m_e of the electron is small, the electronic variables evolve with short time constants. These time constants correspond to an energy typical of atomic physics, i.e. about ten electron-volts for hydrogen. Because of this fast evolution, the electronic variables can adapt almost instantaneously to the much slower motion of the nuclei.

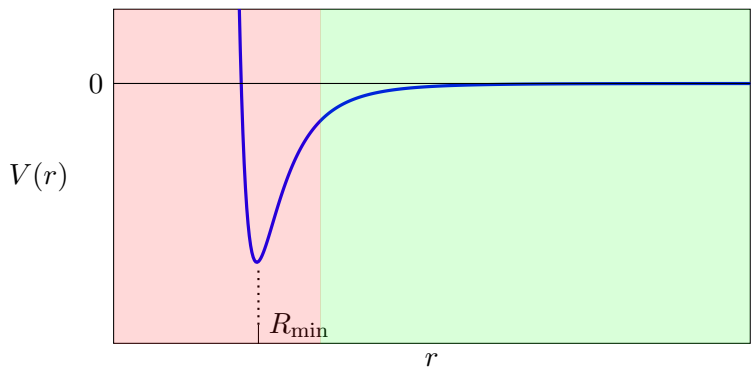

Figure 12. *Schematic representation of the effective potential $V(r)$ between the nuclei A and B, obtained after Born–Oppenheimer approximation. We have plotted here only the potential corresponding to the minimum energy of the electrons, calculated for each value of the distance $r = |\boldsymbol{r}_A - \boldsymbol{r}_B|$. In the green colored area, the van der Waals interaction is dominant.*

We will specify in the following paragraphs how to obtain an expression for $V(r)$. Let us assume for the moment that this expression is known, with the typical shape represented in figure 12. This potential tends to 0 when the two nuclei are far apart ($r \to \infty$), it has a minimum for a particular value $R_{\min}$ of the distance between nuclei, and it diverges when the nuclei become very close to each other ($r \to 0$). The problem of the interaction between the two hydrogen atoms is then reduced to the two-body problem described by the Hamiltonian

$$\hat{H} = \frac{\hat{p}_A^2}{2M} + \frac{\hat{p}_B^2}{2M} + \hat{V}\left(|\boldsymbol{r}_A - \boldsymbol{r}_B|\right). \tag{31}$$

This Hamiltonian allows both:

- The treatment of the chemical bond of the dihydrogen molecule H_2. We then look for bound states in this potential. In particular, the position $R_{\min}$ of the minimum gives the size of the ground-state molecule at equilibrium and $V(R_{\min})$ its binding energy.
- The treatment of the elastic collision between two hydrogen atoms. We consider atoms with initial momenta $\boldsymbol{p}_A, \boldsymbol{p}_B$ and we look for the distribution of possible final momenta $\boldsymbol{p}'_A, \boldsymbol{p}'_B$.

In both cases, the problem is simplified by the fact that the system described by the Hamiltonian (31) is translationally invariant, which allows to separate the dynamics into a center-of-mass component, unaffected by the potential V, and the part dealing with the relative variable. More precisely, we define

$$\boldsymbol{R} = \frac{1}{2}(\boldsymbol{r}_A + \boldsymbol{r}_B), \quad \boldsymbol{r} = \boldsymbol{r}_A - \boldsymbol{r}_B \tag{32}$$

with the conjugated moments

$$\boldsymbol{P} = \boldsymbol{p}_A + \boldsymbol{p}_B, \quad \boldsymbol{p} = \frac{1}{2}(\boldsymbol{p}_A - \boldsymbol{p}_B) \tag{33}$$

which allows to write $\hat{H}$ in the form:

$$\hat{H} = \hat{H}_{\text{com}} + \hat{H}_{\text{rel}} \tag{34}$$

with

$$\hat{H}_{\text{com}} = \frac{\hat{P}^2}{2(2M)}, \qquad \hat{H}_{\text{rel}} = \frac{\hat{p}^2}{2m_{\text{r}}} + \hat{V}(r) \tag{35}$$

where we have introduced the reduced mass $m_{\text{r}} = m/2$. If we define the origin of the energies such that $V(r) \to 0$ when $r \to \infty$ [cf. figure 12], the eigenstates of negative energy of $\hat{H}_{\text{rel}}$ correspond to the different bound states of the molecule H_2, with various degrees of excitation of the levels of vibration and rotation of the nuclei. The positive energy states are used to describe a collision between the two atoms.

The knowledge of the potential $V(r)$ gives the energy scale relevant to the molecular motion and allows one to validate the Born–Oppenheimer approximation. For example, in the development of $V(r)$ close to $R_{\min}$:

$$V(r) = V(R_{\min}) + \frac{1}{2} m_{\text{r}} \omega^2 \left(r - R_{\min}\right)^2 + \dots \tag{36}$$

the quantity $\omega/2\pi$ corresponds to the vibration frequency of the molecule around its equilibrium position. For H_2, this frequency is 1.3×10^{14} Hz, corresponding to an energy $\hbar\omega = 0.5$ eV, which is indeed small in front of the characteristic energies of the electron motion (10 eV).

Born-Oppenheimer approximation or adiabatic approximation? The starting point of the Born-Oppenheimer approximation is the large mass difference between the nuclei and the electrons, which allows one to determine the energy levels $V_n(r_{AB})$ of the electrons for a given distance r_{AB} between the nuclei. We then treat each of these energy levels as a potential governing the evolution of the nuclei. This approach is very similar to the one underlying the adiabatic approximation, where the electron state adjusts almost instantaneously to the much slower motion of the nuclei. There is however an additional ingredient that appears in the adiabatic approximation, once the energy levels $V_n(r_{AB})$ and the associated electronic states $|\psi_n(r_{AB})\rangle$ are known; these are the geometric potentials (scalar and vector) related to the variation with r_{AB} of the electronic states $|\psi_n(r_{AB})\rangle$. These geometric potentials, related in particular to the Berry phase, played a central role in the 2014 course, which was devoted to artificial magnetism for cold atomic gases. In molecular physics, their effects, mostly weak, are completely neglected in the Born–Oppenheimer approximation. For a thorough discussion of their order of magnitude, one may consult Comparat (1999).

4-2 The Heitler–London method

Once the Born–Oppenheimer approximation has been performed, the procedure to be followed to obtain an approximate but reliable value of the potential $V(r)$ is described in many textbooks [see for example Demtröder (2010)] and is inspired by the method introduced by Heitler & London (1927). The Hamiltonian describing the motion of the two electrons, each with mass m_e, is written:

$$\hat{H}_{\rm el}(\boldsymbol{r}_A, \boldsymbol{r}_B) = \frac{\hat{p}_1^2}{2m_e} + \frac{\hat{p}_2^2}{2m_e} + \hat{V}_{\rm Coulomb} + 2E_{\rm I} \tag{37}$$

with

$$\hat{V}_{\rm Coulomb} = -\frac{e^2}{r_{1A}} - \frac{e^2}{r_{1B}} - \frac{e^2}{r_{2A}} - \frac{e^2}{r_{2B}} + \frac{e^2}{r_{12}} + \frac{e^2}{r_{AB}}, \tag{38}$$

with as before $e^2 = q^2/(4\pi\epsilon_0)$ and $\boldsymbol{r}_{\alpha\beta} = \boldsymbol{r}_\alpha - \boldsymbol{r}_\beta$. This Hamiltonian contains:

- The two kinetic energy terms.
- All the Coulomb interaction terms. We are dealing here with 4 charged particles, each of which can interact with the 3 others, and so there are $\frac{1}{2}(4\times 3) = 6$ terms, 4 being attractive and 2 repulsive. Note that we have taken into account here the repulsion energy between the two nuclei e^2/r_{AB}, even if this term represents at this stage only a constant energy for the electron motion.
- We have also added[1] the constant $2E_{\rm I}$ where $E_{\rm I} = 13.6\,{\rm eV}$ is the ionization energy of a hydrogen atom; this allows to set the zero-energy reference for the situation where the two hydrogen atoms are each in their electronic ground state and infinitely far from each other.

Let us forget for the moment that electrons and protons have a spin $1/2$ and that they are indistinguishable particles that must obey the Pauli principle. The starting point of the Heitler–London theory is that for $r_{AB} \to \infty$, the ground level of $\hat{H}_{\rm el}$ is doubly degenerate. It can be obtained in two different ways, corresponding to the possible assignments of the electrons 1 and 2 to the nuclei A and B:

$$|\Psi_{\rm I}\rangle = |1:\psi_A; 2:\psi_B\rangle, \qquad |\Psi_{\rm II}\rangle = |1:\psi_B; 2:\psi_A\rangle \tag{39}$$

or in "wave function" point of view:

$$\Psi_{\rm I}(\boldsymbol{r}_1, \boldsymbol{r}_2) = \psi_A(\boldsymbol{r}_1)\psi_B(\boldsymbol{r}_2), \qquad \Psi_{\rm II}(\boldsymbol{r}_1, \boldsymbol{r}_2) = \psi_B(\boldsymbol{r}_1)\psi_A(\boldsymbol{r}_2). \tag{40}$$

Here $\psi_A(\boldsymbol{r}_1)$ is the state of the electron 1 placed in the ground state 1s around the nucleus A, itself located in $\boldsymbol{r}_A$:

$$\psi_A(\boldsymbol{r}_1) = \frac{{\rm e}^{-r_{1A}/a_0}}{\sqrt{\pi a_0^3}}, \tag{41}$$

where $a_0 = \hbar^2/(m_e e^2)$ is the Bohr radius, already used above. The idea is then to use the variational method in this two-dimensional space: for each value of the distance between nuclei r_{AB}, we look for the linear combinations of $\Psi = \alpha\Psi_{\rm I} + \beta\Psi_{\rm II}$ which lead to an extremum of the mean energy

$$E(\alpha, \beta, r_{AB}) = \frac{\langle\Psi|\hat{H}_{\rm el}(\boldsymbol{r}_A, \boldsymbol{r}_B)|\Psi\rangle}{\langle\Psi|\Psi\rangle}. \tag{42}$$

[1] Without this term, the zero energy would correspond to the physical situation where the 4 particles, protons and electrons, are each infinitely far from the three others.

For well chosen test functions (which is the case here), we expect that these extrema are close to some of the energy levels of $\hat{H}_{\rm el}(\boldsymbol{r}_A, \boldsymbol{r}_B)$. Since the wave functions $\Psi_{\rm I,II}$ are real, we can limit our study to the case where the variational parameters α, β are also real.

Note 1. The method used here is not a first-order perturbation theory, even if the result obtained below involves the matrix elements of $\hat{H}$ between the states $\Psi_{\rm I,II}$. Indeed, the $\Psi_{\rm I,II}$ states are not eigenstates of a single Hamiltonian that one would obtain from $\hat{H}_{\rm el}$. More precisely, $\Psi_{\rm I}$ is an eigenstate of

$$\hat{H}_0^{(1)} = \frac{p_1^2}{2m_e} + \frac{p_2^2}{2m_e} - \frac{e^2}{r_{1A}} - \frac{e^2}{r_{2B}} \tag{43}$$

whereas $\Psi_{\rm II}$ is eigenstate of

$$\hat{H}_0^{(2)} = \frac{p_1^2}{2m_e} + \frac{p_2^2}{2m_e} - \frac{e^2}{r_{1B}} - \frac{e^2}{r_{2A}}. \tag{44}$$

We are therefore not in the canonical case of first-order degenerate perturbation theory, where the degeneracy of two eigenstates of the same Hamiltonian $\hat{H}_0$ is lifted by a perturbation $\hat{V}$ coupling these two states.

Note 2. From now on, we will identify the distance between nuclei r_{AB} with the distance r between atoms, since the center of gravity of an atom practically coincides with its nucleus, thanks to the large mass difference between nuclei and electrons.

4-3 Bonding and antibonding orbitals

The search for the extrema of the energy functional (42) is done without major difficulty [see e.g. Schiff (1968)]. As one would expect given the symmetry of the problem, the extrema are obtained for symmetric and antisymmetric linear combinations of $\Psi_{\rm I}$ and $\Psi_{\rm II}$:

$$A(1)B(2) \pm B(1)A(2) \tag{45}$$

where we have noted for simplicity $\psi_A(\boldsymbol{r}_1) \equiv A(1)$, etc.

A relatively long calculation allows to put these extremal energies in the form of an effective potential for the motion of the nuclei

$$V_{\rm eff,\pm}(r_{AB}) = \frac{\varepsilon_{\rm dir} \pm \varepsilon_{\rm exc}}{1 \pm \Delta^2}. \tag{46}$$

Let us briefly discuss the origin of the two energies $\varepsilon_{\rm dir,exc}$ and the dimensionless coefficient Δ appearing in this expression, these three terms being functions of the interatomic distance r.

- The direct energy $\varepsilon_{\rm dir}$ is given by:

$$\varepsilon_{\rm dir}(r) = \langle 1:\psi_A;\ 2:\psi_B | \hat{H}_{\rm el} | 1:\psi_A;\ 2:\psi_B \rangle \tag{47}$$

  and corresponds to the matrix elements of $\hat{H}_{\rm el}$ where each electron remains attached to its original nucleus.

- The exchange energy $\varepsilon_{\rm exc}$ is given by:

$$\varepsilon_{\rm exc}(r) = \langle 1:\psi_B;\ 2:\psi_A | \hat{H}_{\rm el} | 1:\psi_A;\ 2:\psi_B \rangle \tag{48}$$

  and describes a process where the operator $\hat{H}_{\rm el}$ swaps the assignment of electrons to nuclei from $A(1)B(2)$ to $B(1)A(2)$.

- The dimensionless term Δ represents the overlap between the two 1s states located respectively on the A nucleus and the B nucleus:

$$\Delta(r) = \langle \psi_A | \psi_B \rangle. \tag{49}$$

By construction, the terms $\varepsilon_{\rm exc}(r)$ and $\Delta(r)$ are nonzero only if there exist points in space where the functions $\psi_A(\boldsymbol{r})$ and $\psi_B(\boldsymbol{r})$ both take nonzero values. For example we find for the coefficient Δ

$$\Delta(r) = \int \psi_A(\boldsymbol{r}_1)\, \psi_B(\boldsymbol{r}_1)\, \mathrm{d}^3 r_1 = \left(1 + \frac{r}{a_0} + \frac{r^2}{3a_0^2}\right) \mathrm{e}^{-r/a_0}. \tag{50}$$

which decreases exponentially fast with the internuclear distance r.

All the integrals involved in this problem are given by Slater (1968). When the set of test functions is limited to the 1s states, this exponential decay also appears for the direct term. But this is not always the case:

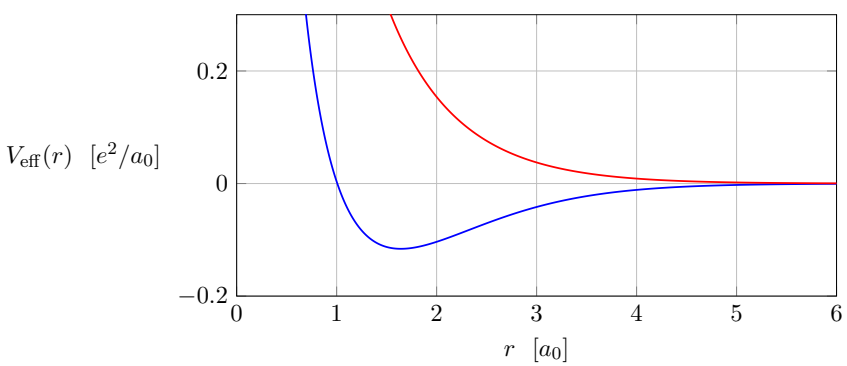

Figure 13. *Effective potentials $V_{\text{eff},+}$ (blue) and $V_{\text{eff},-}$ (red) between two hydrogen atoms calculated for the test functions (45) (Heitler–London method). All integrals necessary for the calculation are given in Slater (1968), table 21-1.*

we have seen in §1 that for an "enriched" choice of test functions, the van der Waals interaction emerges and is significant even if there is no overlap between wave functions.

Let us neglect for the moment the van der Waals interaction and stay with only the orbitals from the 1s states. A numerical calculation shows that $V_{\text{eff},+}(r) < V_{\text{eff},-}(r)$ for all r. The variations of these energies with the distance r are plotted in figure 13. They both tend to $+\infty$ in $r = 0$ and to 0 exponentially fast when $r \to \infty$. The potential $V_{\text{eff},-}(r)$, always positive, is a decreasing function of r whereas $V_{\text{eff},+}(r)$ has a minimum of $-0.116\, e^2/a_0 = -3.15\,\text{eV}$ for $r = 1.64\, a_0 = 0.87\,\text{Å}$. We can verify numerically that this potential is deep enough to contain bound states corresponding to a stable four-body edifice (two protons and two electrons), i.e. the H_2 molecule.

Let us now take into account the fact that (i) the two electrons are spin 1/2 particles and (ii) they are indistinguishable (Pauli's principle):

(i) The existence of the electron spin increases the degeneracy of the levels. Let us choose a quantization axis for the spins and note $|\pm\rangle$ the two possible spin states for an electron. There are thus 4 possible states for the electron pair and the degeneracy of the gound level when the atoms are infinitely far from each other is now $2 \times 4 = 8$ [*cf.* eq. (39) for the two states of the orbital part]. When r is not infinite, each of the two energy levels $V_{\text{eff},\pm}(r)$ is degenerated 4 times.

(ii) Let us now consider the Pauli principle. As always, the unique role of this principle is to restrict the size of the Hilbert space by imposing that the global "orbital+spin" state of the two electrons is antisymmetric in the $1 \leftrightarrow 2$ exchange. Since the spatial wave functions found above are symmetric or antisymmetric in this exchange, it is sufficient to choose the spin state with opposite exchange symmetry:

- The state associated with the $+$ sign in (45,46), which leads to a local minimum of the effective potential and a bound state of the H_2 dimer, must be antisymmetric with respect to spin, which corresponds to the singlet state:

$$\frac{1}{\sqrt{2}}\left(|1+,2-\rangle - |1-,2+\rangle\right). \tag{51}$$

  This state is often called a bonding orbital and corresponds to the covalent chemical bond.

- The state associated with the $-$ sign in (45,46) must be spin symmetric and thus an element of the triplet space (dimension 3) generated by :

$$|1+,2+\rangle,\ \frac{1}{\sqrt{2}}\left(|1+,2-\rangle + |1-,2+\rangle\right),\ |1-,2-\rangle. \tag{52}$$

  This set of states is called an antibonding orbital.

In the end, we arrive at two distinct interaction channels $V_{\text{eff},\pm}(r)$ depending on whether the total spin $\boldsymbol{S} = \boldsymbol{s}_1 + \boldsymbol{s}_2$ of the two electrons is in the singlet state $S = 0$ or the triplet state $S = 1$. We can therefore summarize these two channels by the general formula:

$$V(r) = V_0(r) + \frac{\hat{s}_1 \cdot \hat{s}_2}{\hbar^2} V_1(r) \tag{53}$$

where the operator

$$\hat{\boldsymbol{s}}_1 \cdot \hat{\boldsymbol{s}}_2 = \frac{1}{2}\left[(\hat{\boldsymbol{s}}_1 + \hat{\boldsymbol{s}}_2)^2 - \hat{s}_1^2 - \hat{s}_2^2\right] = \frac{1}{2}\left[\hat{S}^2 - \frac{3}{2}\right] \tag{54}$$

takes the values $-3\hbar^2/4$ and $\hbar^2/4$ in the singlet and triplet states and

$$V_0 = \frac{1}{4}\left(V_{\text{eff},+} + 3V_{\text{eff},-}\right) \qquad V_1 = V_{\text{eff},-} - V_{\text{eff},+}. \tag{55}$$

Let us insist on the fact that this convenient writing does not imply that the difference between the singlet and triplet potentials originates in a spin-spin interaction.

Origin of the chemical bond. Within this simple model, we can estimate the average energy terms for the bonding and antibonding orbitals. It is therefore possible to determine the process that leads to the existence of a minimum for the bonding orbital and thus to the chemical bond. One finds that the dominant process is the lowering of kinetic energy due to the symmetrization of the spatial wave function:

$$A(1)B(2) + B(1)A(2). \tag{56}$$

This symmetrization makes the $\Psi(1,2)$ wave function "flatter" over a large region of space, and thus decreases its kinetic energy which is proportional to the integral of $|\boldsymbol{\nabla}_1\Psi|^2 + |\boldsymbol{\nabla}_2\Psi|^2$ over space. On the contrary, the spatially antisymmetric state must cancel at any point $\boldsymbol{r}_1 = \boldsymbol{r}_2$. It is thus confined in a reduced region compared to the symmetric state and its kinetic energy is larger. Note that the Coulomb energy is larger for the symmetric state than for the antisymmetric state since the two electrons have a significant probability of being close to each other. However, this penalty due to the increase in electrostatic potential energy is more than compensated by the gain due to the decrease in kinetic energy.

4-4 Improving the description of the interaction

Experimentally, one finds that the potential well for the bonding orbital of the hydrogen molecule has a depth[2] of 4.75 eV. The very simple approach developed above gives a depth of 3.15 eV, thus less large (which is normal for a variational method), but relatively close. As always with the variational method, one can improve the result, i.e. decrease the lower bound, by enriching the class of test functions.

A first possibility is to introduce an element of "ionic bonding" into the problem, i.e. to allow states where both electrons are bound to the same atom. This can be done while still considering only the 1s states, provided that the spin state is the singlet state so as to ensure global antisymmetry. We are thus led to take a class of test functions with the orbital part

$$\Big[A(1)B(2) + B(1)A(2)\Big] + \beta\Big[A(1)A(2) + B(1)B(2)\Big]. \tag{57}$$

The variable β is a variational parameter that is adjusted for each value of the inter-nuclear distance r, the case $\beta = 0$ corresponding to the bonding orbital found above. This simple change of the variational space increases the depth of the potential well to 3.8 eV, which is significantly closer to the experimental value (Slater 1968).

To go further, it is necessary to incorporate in the basis of test functions other states than the 1s states of the two atoms. In practice, this is done by parameterizing the wave functions of each electron by several tens of coefficients that are varied to minimize the energy. For the hydrogen molecule, the results obtained are in agreement with the experimental data (Kolos & Roothaan 1960; Kolos, Szalewicz, et al. 1986). In particular, this approach incorporates states where both atoms are in the $|2\mathrm{p}_\alpha; 2\mathrm{p}_\alpha\rangle$ state, with $\alpha = x, y, z$, which allows to take into account the van der Waals interactions studied in § 1. The corresponding C_6 coefficient is of the order of 2 a.u.

Once the van der Waals interactions are included in the potential, we find as expected that the antibonding orbital is also attractive at large distances. It has a minimum in $R_{\min} = 4.2$ Å with depth 0.6 meV, that is $\sim 10^4$ times less than for the bonding orbital [see for example Walraven (1990) and refs. in]. This very small value and the small mass of the H-nuclei result in this potential well being too shallow to support a bound state, similar to what we mentioned for ^{3}He in § 3-2.

[2] The potential minimum is located at $R_{\min} = 0.74$ Å and the well gives rise to 15 (vibrational) bound states (Kołos & Wolniewicz 1975).

4-5 Generalization to alkali metal species

The method we have just followed generalizes almost immediately to atoms with one outer electron, i.e. the column of alkali metal atoms, which are widely used in quantum gas physics. As for hydrogen, the electronic ground state of these atoms is an s state for the external electron, the electrons of the inner layers playing only a minor role in the establishment of the chemical bond. We thus recover the notion of bonding and antibonding orbitals, associated respectively with a singlet and triplet spin state for the two external electrons (one per atom composing the dimer). We will not detail here the characteristics of the corresponding potentials and we refer the reader to the following references:

- Lithium: LeRoy, Dattani, et al. (2009)
- Sodium: Araujo, Weinstein, et al. (2003),Matsunaga & Zavitsas (2004)
- Potassium: Zavitsas (2006)
- Rubidium: Deiß, Drews, et al. (2015)
- Cesium: Coxon & Hajigeorgiou (2010)

Let us simply point out that the van der Waals forces play a more important role here than for hydrogen. Indeed, these atoms are much more polarizable and the C_6 coefficients are considerably increased. It follows that the potential wells of the antibonding orbitals always contain a significant number of bound states: about ten for lithium and this number increases when we go down the periodic table. This point will play an important role to validate the use of the semi-classical method in the study of the interaction between two alkali metal atoms.

Influence of nuclear spin. So far, we have not taken into account the fact that atomic nuclei generally have a non-zero spin. To finish this first chapter, we now briefly indicate how this modifies the results obtained so far. To this nuclear spin is associated a magnetic moment that interacts with the magnetic moment of the electron, which gives rise to the hyperfine structure of the atomic levels. The electronic ground state of each atom is split

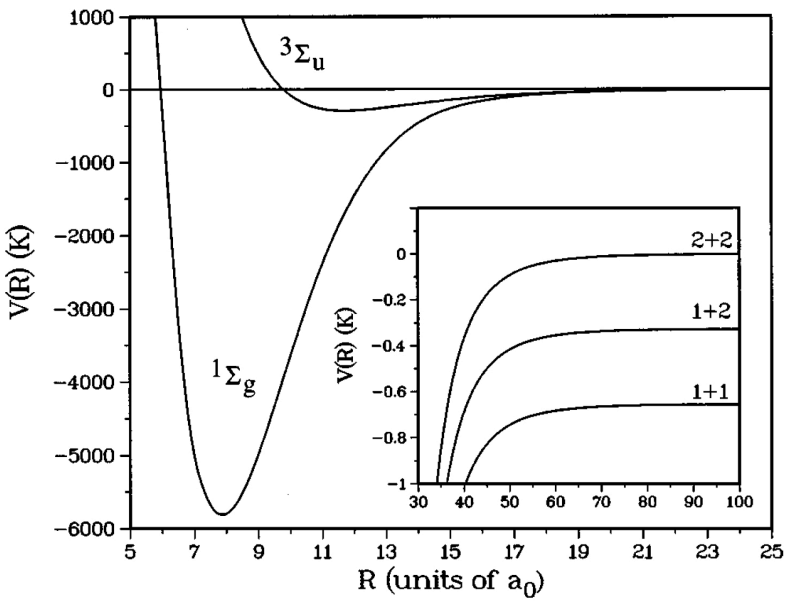

Figure 14. *Singlet (bonding orbital) and triplet (antibonding orbital) interaction potentials between two rubidium ^{87}Rb atoms, with the three channels associated with the possible hyperfine states of each atom. Figure extracted from Weiner, Bagnato, et al. (1999).*

into two sublevels of energy E_f and total angular momentum $f = i \pm 1/2$, resulting from the coupling $\propto \hat{\boldsymbol{s}} \cdot \hat{\boldsymbol{i}}$ of the electron spin angular momentum $s = 1/2$ and that of the nucleus, noted i. For hydrogen, the nucleus is a proton and we have $i = 1/2$. For several stable alkali metal atoms (^{7}Li, ^{23}Na, ^{39}K,^{87}Rb), we have $i = 3/2$ which leads to the two hyperfine levels $f = 1$ and $f = 2$.

Let us now consider our pair of atoms, each in its ground state. There are three possible values for the energy of the pair, as represented in figure 14 for rubidium 87, corresponding to the possibilities $\{f_1, f_2\}$ equal to $\{1, 1\}$, $\{1, 2\}$ or $\{2, 2\}$. It is important to note that these three possible channels of interaction are coupled together. Indeed, the dominant hyperfine Hamiltonian when the atoms are far apart, $\propto \hat{\boldsymbol{s}}_1 \cdot \hat{\boldsymbol{i}}_1 + \hat{\boldsymbol{s}}_2 \cdot \hat{\boldsymbol{i}}_2$ does not com-

mute with the one that gives rise to the bonding and antibonding orbitals, marked by the total electron spin $\hat{\boldsymbol{S}} = \hat{\boldsymbol{s}}_1 + \hat{\boldsymbol{s}}_2$. This coupling between collision channels will play an important role when we address the problem of Fano–Feshbach resonances.

Indiscernability of the nuclei. We have taken into account in the above the fact that electrons are indistinguishable particles (fermions), which led us to impose a total spin $S = 0$ on the bonding orbital (symmetric orbital state, hence antisymmetric spin state), and the opposite for the antibonding orbital of total spin $S = 1$. It is also necessary to take into account the fact that nuclei are indistinguishable particles, bosons or fermions depending on the integer or half-integer value of their spin. In fact, in the rest of this course, rather than symmetrizing or anti-symmetrizing the state of nuclei, we will work on the state of the atoms taken as a whole. For example, for a $3/2$ spin nucleus (fermion), the atom has an integer spin ($f = 1$ or $f = 2$); it will therefore be treated as a bosonic particle: we will impose that the wave function of the pair of atoms is symmetric in the global exchange of all the particles that compose them. This prescription, together with the fact that the electronic state has been chosen antisymmetric, ensures the required antisymmetry by exchange of the nuclei.

In practice, we will see in the next chapter that for a rotationally invariant potential, this symmetrization or antisymmetrization of the state of the atom pair is done by restricting the possible values of the total orbital angular momentum L to even or odd values.

Appendix: Interaction channels for alkali metal atoms

We specify in this appendix how one can identify the (many!) interaction and collision channels for alkali atoms. It is necessary to take into account both the spin of the external electron of each atom, $\boldsymbol{s}_1$ and $\boldsymbol{s}_2$, and the spin of each nucleus, $\boldsymbol{i}_1$ and $\boldsymbol{i}_2$. In the absence of an external magnetic field, there are two interactions related to these spins that must be taken into account:

- At large distances, the dominant interaction is the hyperfine interaction of each atom, described by the coupling

$$V_{\rm hf} = \alpha \left(\hat{\boldsymbol{s}}_1 \cdot \hat{\boldsymbol{i}}_1 + \hat{\boldsymbol{s}}_2 \cdot \hat{\boldsymbol{i}}_2 \right) \tag{58}$$

  which can be diagonalized by introducing the spin of each atom $\boldsymbol{f}_j = \boldsymbol{s}_j + \boldsymbol{i}_j$, $j = 1, 2$. This coupling gives rise to three energy levels (*cf.* insert in figure 14).

- At short distances, the dominant interaction is the effective interaction in $\hat{\boldsymbol{s}}_1 \cdot \hat{\boldsymbol{s}}_2$ which describes the difference between singlet and triplet potentials:

$$V(r) = V_0(r) + \frac{\hat{s}_1 \cdot \hat{s}_2}{\hbar^2} V_1(r). \tag{59}$$

There is no basis of the total spin space (of dimension $2 \times 4 \times 2 \times 4 = 64$ for $i_1 = i_2 = 3/2$) which allows to diagonalize simultaneously these two couplings. The problem of the interaction between these atoms thus necessarily involves a solution of the Schrödinger equation with different coupled channels.

We can however simplify the problem by considering the *total spin* operator

$$\hat{\boldsymbol{F}} = \hat{\boldsymbol{s}}_1 + \hat{\boldsymbol{i}}_1 + \hat{\boldsymbol{s}}_2 + \hat{\boldsymbol{i}}_2 \tag{60}$$

which commutes with these two couplings and is therefore a constant of motion. We can therefore classify the interaction channels according to the values of (F, M_F) where M_F is associated with the projection of $\boldsymbol{F}$ on a fixed axis. For a spin $i = 3/2$, F can take any integer value between 0 and 4. The next step is to take into account the orbital angular momentum $\boldsymbol{L}$ of the pair of atoms to make sure that the total state (orbital+spin) has the right symmetry with respect to the exchange of the two atoms. This may lead to eliminate some values of F, depending on the chosen orbital state. In the presence of an external magnetic field oriented along the z axis, the total spin F is no longer a constant of motion, but its projection F_z remains and the associated quantum number M_F can still be used to classify the different channels.

Chapter II

Elements of Scattering Theory

In the previous chapter, we explained the physical origin of the interaction potential between two neutral atoms and gave the orders of magnitude in energy and distance that characterize it. We now move on to the implementation of the theoretical tools that will allow us to quantitatively treat the collision between two atoms under the effect of this potential. In this chapter, we will present the general formalism called *scattering theory*, to concentrate in the next chapter on the case of low-energy collisions which govern the physics of quantum gases.

We have also underlined in the previous chapter that the interaction potential between two neutral atoms is in a very good approximation isotropic. This invariance by rotation allows to simplify considerably the description of the collision by taking advantage of the conservation of the relative orbital angular momentum of the two particles, a direct consequence of this invariance. In particular, we will explain how taking this symmetry into account allows us to describe the collision in terms of independent one-dimensional channels, each associated to a particular angular momentum ℓ. More precisely, we will see that we can associate to each channel a phase shift $\delta_\ell(k)$ between the incident wave and the scattered wave, $\boldsymbol{k}$ being here the relative wave vector between the two partners of the collision.

Throughout this year's course, we will be concerned with the two-body physics resulting from the interaction between a pair of atoms. However, the quantities that will appear in what follows, in particular the phase shifts $\delta_\ell(k)$, are directly usable to address the N-body problem, at least in certain limits. A simple illustration of this point lies in the formula of Beth & Uhlenbeck (1937), which relates the second virial coefficient b_2 of a gas of bosons or fermions to the phase shifts $\delta_\ell(k)$ [see for example Huang (1987)]:

$$b_2(T) = \pm\frac{1}{2^{5/2}} + \frac{2^{3/2}}{\pi}\int_0^{+\infty}\sum_\ell (2\ell+1)\frac{\mathrm{d}\delta_\ell}{\mathrm{d}k}\,\mathrm{e}^{-\hbar^2k^2/mk_\mathrm{B}T}\,\mathrm{d}k. \qquad (1)$$

Let us recall that the coefficient b_2 gives the first correction to the ideal gas model in the expansion of the equation of state of the fluid in powers of the fugacity $z = \mathrm{e}^{\mu/k_\mathrm{B}T}$:

$$\frac{P\lambda^3}{k_\mathrm{B}T} = z + b_2 z^2 + \mathcal{O}(z^3), \qquad (2)$$

where μ is the chemical potential, T the temperature, P the pressure and $\lambda = \hbar\sqrt{2\pi/mk_\mathrm{B}T}$ the thermal wavelength. The gas is assumed here to be polarized, i.e. to occupy only one spin state. In (1), the first term corresponds to the correction due to the quantum statistics for the ideal gas and the second term to the correction due to interactions. To simplify the writing, we assumed here that there was no contribution from bound dimer states. For a reason that will become clearer in the rest of this chapter, the sum on the angular momenta runs for even values of ℓ for bosons and odd values for fermions.

1 The scattering states

1-1 The two-body problem

We explained in the previous lecture how to approach the two-body problem by separating the motion of the center-of-mass from that of the relative particle. Starting from the Hamiltonian describing the motion of two atoms A and B of mass m interacting with the potential $V(r)$,

$$H_{\rm tot} = \frac{\boldsymbol{p}_A^2}{2m} + \frac{\boldsymbol{p}_B^2}{2m} + V(|\boldsymbol{r}_A - \boldsymbol{r}_B|) = H_{\rm com} + H_{\rm rel}, \tag{3}$$

we introduced the center-of-mass variables

$$\boldsymbol{R} = \frac{1}{2}(\boldsymbol{r}_A + \boldsymbol{r}_B), \quad \boldsymbol{P} = \boldsymbol{p}_A + \boldsymbol{p}_B, \tag{4}$$

and those of the relative variable

$$\boldsymbol{r} = \boldsymbol{r}_A - \boldsymbol{r}_B, \quad \boldsymbol{p} = \frac{1}{2}(\boldsymbol{p}_A - \boldsymbol{p}_B). \tag{5}$$

The center-of-mass Hamiltonian $H_{\rm com} = \boldsymbol{P}^2/4m$ is simply that of a free particle of mass $2m$ and is therefore of no particular interest: an eigenstate basis for this Hamiltonian is formed by the plane waves $\mathrm{e}^{\mathrm{i}\boldsymbol{K}\cdot\boldsymbol{R}}$ and we will assume in the following that we have placed ourselves in the center-of-mass reference frame, which amounts to taking $\boldsymbol{K} = 0$.

The interesting part of the physics of the collision between the two atoms is described by the relative Hamiltonian

$$H_{\rm rel} = \frac{\boldsymbol{p}^2}{2m_{\rm r}} + V(r), \tag{6}$$

where $m_{\rm r} = m/2$ is the reduced mass and we will thus be interested in the eigenstates of this operator:

$$\hat{H}_{\rm rel}\,\psi(\boldsymbol{r}) = E\,\psi(\boldsymbol{r}). \tag{7}$$

The problem of the collision between two particles can thus be reduced to the study of the scattering of a single particle by the external potential $V(r)$. This subject is treated in all textbooks on quantum physics [see for example Landau & Lifshitz (1975)] and we will simply summarize here the important results for the rest of the course.

Recall that these eigenstates are of two types:

- If the energy E is lower than $V(+\infty)$ – which we will take equal to 0 by convention –, then the state $\psi(\boldsymbol{r})$ is localized around 0, corresponding to a *bound state* of the di-atomic molecule AB. This is a *vibrational state* that corresponds to a certain degree of excitation of the AB elongation.
- If the energy E is larger than $V(+\infty)$, the state $\psi(\boldsymbol{r})$ is asymptotically free and thus describes a collision between A and B. This state is called a *stationary scattering state*.

In this section, we are interested in the collision process, thus in the case $E > 0$ and we will set $E = \hbar^2 k^2/2m_{\rm r}$.

1-2 The integral equation for scattering

To determine the scattering states, our starting point will be the eigenvalue equation (7) that we write:

$$\frac{\hbar^2}{2m_{\rm r}}\left(\nabla^2 + k^2\right)\psi(\boldsymbol{r}) = V(r)\,\psi(\boldsymbol{r}). \tag{8}$$

We will consider it as a differential equation where the right-hand side term $V(r)\,\psi(r)$ plays the role of a source and we will use the Green function method to solve it.

We start with a particular solution of the equation without a source term

$$\frac{\hbar^2}{2m_{\rm r}}\left(\nabla^2 + k^2\right)\psi(\boldsymbol{r}) = 0 \tag{9}$$

that we take as a plane wave $\mathrm{e}^{i\boldsymbol{k}\cdot\boldsymbol{r}}$. As we will see below, the orientation of the wave vector $\boldsymbol{k}$ corresponds to the direction of the relative momentum of the particles before the collision. To associate a solution of equation (8) with its source term to the solution $\mathrm{e}^{i\boldsymbol{k}\cdot\boldsymbol{r}}$ of the equation without source, we first determine the Green function of the free equation (9). This amounts to

solving

$$\frac{\hbar^2}{2m_{\rm r}}\left(\nabla^2 + k^2\right)\mathcal{G}_0(\boldsymbol{r}) = \delta(\boldsymbol{r}), \tag{10}$$

whose two solutions can be written :

$$\frac{\hbar^2}{2m_{\rm r}}\mathcal{G}_0^{(\pm)}(\boldsymbol{r}) = -\frac{\mathrm{e}^{\pm \mathrm{i}kr}}{4\pi r}. \tag{11}$$

For a reason that will become clear in the next paragraph, we will use here the Green function $\mathcal{G}_0^{(+)}$ which corresponds to an outgoing spherical wave.

Once this Green function is known, we can formally construct a solution $\psi_{\boldsymbol{k}}$ of (8) in the presence of the potential V as

$$\psi_{\boldsymbol{k}}(\boldsymbol{r}) = \mathrm{e}^{\mathrm{i}\boldsymbol{k}\cdot\boldsymbol{r}} + \int \mathcal{G}_0^{(+)}(\boldsymbol{r}-\boldsymbol{r}')\, V(\boldsymbol{r}')\, \psi_{\boldsymbol{k}}(\boldsymbol{r}')\, \mathrm{d}^3r'. \tag{12}$$

This equation is called *integral equation for scattering* or *Lippmann-Schwinger equation* (Lippmann & Schwinger 1950).

The equation (12) is an implicit equation, more precisely a Fredholm's equation of the second type: one must know $\psi_{\boldsymbol{k}}(\boldsymbol{r}')$ to evaluate the integral whose result then gives $\psi_{\boldsymbol{k}}(\boldsymbol{r})$. One could therefore doubt its relevance to our problem. In fact, its interest is real when the potential $V(\boldsymbol{r})$ has a limited range b, i.e. when we can consider it as negligible for $r > b$. In this case, (12) allows to link the values of $\psi_{\boldsymbol{k}}(\boldsymbol{r})$ at any point of space, in particular asymptotically far from $\boldsymbol{r} = 0$, to the values of $\psi_{\boldsymbol{k}}(\boldsymbol{r}')$ in the neighborhood of 0. Indeed, because of the presence of $V(\boldsymbol{r}')$ in the integral, only those points close to 0 contribute significantly to the integral.

On the mathematical side, let us point out that one can prove that (12) has a unique solution, provided that $V(\boldsymbol{r})$ is sufficiently regular. This property is no longer true when one tries to generalize this approach to the case of three or more particles [see for example Joachain (1975), § 5.6 and § 16.1].

Remarks

- The notion of range for $V(r)$ is clear when dealing with a square potential for example. We will have to define it further when we are interested in the van der Waals potential, which decreases as $1/r^6$ at infinity.

- The stationary scattering state $\psi_{\boldsymbol{k}}(\boldsymbol{r})$ has been defined via the outgoing Green function $\mathcal{G}_0^{(+)}$; strictly speaking, it should thus be denoted $\psi_{\boldsymbol{k}}^{(+)}(\boldsymbol{r})$ and called the outgoing scattering state. We will omit this $^{(+)}$ when there is no ambiguity. We can also define an incoming scattering steady state, denoted $\psi_{\boldsymbol{k}}^{(-)}(\boldsymbol{r})$, from $\mathcal{G}_0^{(-)}$. We will not need this type of state, except in § 2-3.

- We can verify that the stationary scattering states $\psi_{\boldsymbol{k}}^{(+)}(\boldsymbol{r})$ form an orthonormal set of functions of the Hilbert space when $\boldsymbol{k}$ describes the whole space of wave vectors. We can obtain a basis of the Hilbert space by adding to this set the possible bound states of $\hat{H}_0 + \hat{V}$. Similarly, we can form an orthonormal basis of the Hilbert space by using the set of $\psi_{\boldsymbol{k}}^{(-)}(\boldsymbol{r})$ completed by the same bound states. On the other hand, we cannot say anything at this stage about the scalar product of a $\psi_{\boldsymbol{k}}^{(+)}$ and a $\psi_{\boldsymbol{k}'}^{(-)}$. We will see in § 2-3 that this product in fact provides the matrix elements of the scattering operator $\hat{S}$.

1-3 The Born approximation

As we mentioned, the equation (12) is implicit since the integrand involves the unknown function $\psi_{\boldsymbol{k}}$. However, this expression lends itself well to an explicit perturbative expansion with respect to the potential V, since the integrand is itself proportional to V. More precisely, the calculation of the scattering state at order n in V requires for the right-hand side member the knowledge of $\psi_{\boldsymbol{k}}(\boldsymbol{r}')$ at order $n-1$ only. The perturbative expansion that can be generated in this way is called *Born expansion*.

Let's start with the result of this expansion at the lowest order. At order 0 in V, the scattering steady state is equal to the incident wave function $\mathrm{e}^{\mathrm{i}\boldsymbol{k}\cdot\boldsymbol{r}}$. The scattering steady state can thus be written at order 1 in V:

$$\psi_{\boldsymbol{k}}(\boldsymbol{r}) \approx \mathrm{e}^{\mathrm{i}\boldsymbol{k}\cdot\boldsymbol{r}} + \int \mathcal{G}_0^{(+)}(\boldsymbol{r}-\boldsymbol{r}')\, V(\boldsymbol{r}')\, \mathrm{e}^{\mathrm{i}\boldsymbol{k}\cdot\boldsymbol{r}'}\, \mathrm{d}^3r', \tag{13}$$

which is easily calculated (at least numerically) for any potential $V(\boldsymbol{r}')$.

This Born expansion can be conducted at any order and leads to the infinite series:

$$\begin{aligned}\psi_{\boldsymbol{k}}(\boldsymbol{r}) &= \mathrm{e}^{\mathrm{i}\boldsymbol{k}\cdot\boldsymbol{r}} \\ &+ \int \mathcal{G}_0^{(+)}(\boldsymbol{r}-\boldsymbol{r}')\, V(\boldsymbol{r}')\, \mathrm{e}^{\mathrm{i}\boldsymbol{k}\cdot\boldsymbol{r}'} \\ &+ \iint \mathcal{G}_0^{(+)}(\boldsymbol{r}-\boldsymbol{r}')\, V(\boldsymbol{r}')\, \mathcal{G}_0^{(+)}(\boldsymbol{r}'-\boldsymbol{r}'')\, V(\boldsymbol{r}'')\, \mathrm{e}^{\mathrm{i}\boldsymbol{k}\cdot\boldsymbol{r}''}\, \mathrm{d}^3r'\mathrm{d}^3r'' \\ &+ \ldots \end{aligned} \tag{14}$$

The discussion of the validity of the Born approximation, and more generally of the convergence of the Born expansion, is not a simple problem. One can consult for example Messiah (1962) and Landau & Lifshitz (1975). In the low-energy limit which will interest us in the following, the following condition is necessary: the attractive part of the potential $V(r)$ must be sufficiently shallow to not support any bound state. In practice, this is not the case for real interatomic potentials, as we have seen in chapter I. It is therefore not possible to use the Born approximation for these potentials. On the other hand, one may use model potentials for which this approximation is relevant.

2 The operatorial approach

The handling of integral expressions like (12) can be cumbersome, especially when one wants to proceed to expansion like Born's. To simplify the writing (without changing the problem in any way), one can adopt a more formal writing in terms of operators and Dirac kets. Beyond the simplification of the writing, this formal scattering theory has the advantage of being applicable to a larger class of problems, be it the scattering of material particles with an internal degree of freedom (spin), or the scattering of photons by atoms or phonons on impurities in a crystal.

2-1 The Green operators $\hat{G}_0$ and $\hat{G}$

The starting equation (8) of the previous paragraph can be put in the form

$$\left(E - \hat{H}_0\right)|\psi\rangle = \hat{V}|\psi\rangle, \tag{15}$$

where $\hat{H}_0$ is the Hamiltonian of a free particle of mass m_r: $\hat{H}_0 = \hat{\boldsymbol{p}}^2/2m_\mathrm{r}$. Its solution (12) is written

$$|\psi_{\boldsymbol{k}}\rangle = |\boldsymbol{k}\rangle + \hat{G}_0^{(+)}(E)\hat{V}|\psi_{\boldsymbol{k}}\rangle \tag{16}$$

where the operator $\hat{G}_0^{(+)}(E)$, called the *Green operator* or *resolvent* of the Hamiltonian $\hat{H}_0$, is formally written

$$\hat{G}_0^{(+)}(E) = \frac{1}{E - \hat{H}_0 + \mathrm{i}0_+} \tag{17}$$

to represent the inverse of $E - \hat{H}_0$. Note that we have to add an imaginary part to the denominator (here infinitely small and noted $\mathrm{i}0_+$) to avoid divergences when E is equal to an eigenvalue of $\hat{H}_0$. In practice, this imaginary part is treated via the equality in the sense of distributions:

$$\frac{1}{x - x_0 + \mathrm{i}0_+} = \mathcal{PP}\left(\frac{1}{x - x_0}\right) - \mathrm{i}\pi\delta(x - x_0), \tag{18}$$

where $\mathcal{PP}$ denotes the principal part integral. We can verify directly that

$$\langle\boldsymbol{r}|\hat{G}_0^{(+)}|\boldsymbol{r}'\rangle = \mathcal{G}_0^{(+)}(\boldsymbol{r}-\boldsymbol{r}'). \tag{19}$$

A similar relationship for the incoming Green function $\mathcal{G}_0^{(-)}$ is obtained by taking an imaginary part $\mathrm{i}0_-$ instead of $\mathrm{i}0_+$ in the definition (17) of the Green operator. In what follows, we will omit the superscript "(+)" of $\hat{G}_0^{(+)}(E)$ when there is no ambiguity.

We can also introduce the Green operator of the total Hamiltonian $\hat{H} = \hat{H}_0 + \hat{V}$:

$$\hat{G}^{(+)}(E) = \frac{1}{E - \hat{H} + \mathrm{i}0_+}. \tag{20}$$

Unlike $\hat{G}_0$, it is generally not possible to compute explicitly the matrix elements of $\hat{G}$ in the position basis $|\boldsymbol{r}\rangle$. Nevertheless, this operator will play a central role in the following.

It is useful to establish a number of simple relationships between $\hat{G}$ and $\hat{G}_0$. Starting from :

$$E - \hat{H} + \mathrm{i}0_+ = E - \hat{H}_0 + \mathrm{i}0_+ \; - \; \hat{V}, \tag{21}$$

we immediately obtain

$$\frac{1}{\hat{G}} = \frac{1}{\hat{G}_0} - \hat{V}, \tag{22}$$

and by multiplying (22) on the left by $\hat{G}$ and on the right by $\hat{G}_0$:

$$\hat{G}_0 = \hat{G} - \hat{G}\hat{V}\hat{G}_0 \tag{23}$$

what we will write in the following:

$$\hat{G} = \hat{G}_0 + \hat{G}V\hat{G}_0. \tag{24}$$

Of course, we can also multiply (22) on the right by $\hat{G}$ and on the left by $\hat{G}_0$ to obtain:

$$\hat{G} = \hat{G}_0 + \hat{G}_0\hat{V}\hat{G}. \tag{25}$$

We can then iterate the relations (23) and (24) by substituting G with its expression :

$$\begin{aligned} \hat{G} &= \hat{G}_0 + \hat{G}_0\hat{V}\hat{G}_0 + \hat{G}_0\hat{V}\hat{G}_0\hat{V}\hat{G} && (26)\\ &= \hat{G}_0 + \hat{G}_0\hat{V}\hat{G}_0 + \hat{G}_0\hat{V}\hat{G}\hat{V}\hat{G}_0 && (27)\\ &= \hat{G}_0 + \hat{G}_0\hat{V}\hat{G}_0 + \hat{G}\hat{V}\hat{G}_0\hat{V}\hat{G}_0 && (28) \end{aligned}$$

and so on, the important thing being that there is one and only one $\hat{G}$ in the last term of the sum.

By iterating this procedure to infinity, we can also express $\hat{G}$ as a series of products involving only $\hat{G}_0$ and $\hat{V}$:

$$\hat{G} = \hat{G}_0 + \hat{G}_0\hat{V}\hat{G}_0 + \hat{G}_0(\hat{V}\hat{G}_0)^2 + \dots \tag{29}$$

2-2 The transition matrix $\hat{T}$

The Born approximation to order 1 in $\hat{V}$ given in (13) is written with these notations:

$$|\psi_{\boldsymbol{k}}\rangle \approx |\boldsymbol{k}\rangle + \hat{G}_0\hat{V}|\boldsymbol{k}\rangle, \tag{30}$$

where we have set[1] $\langle \boldsymbol{r}|\psi_{\boldsymbol{k}}\rangle = \psi_{\boldsymbol{k}}(\boldsymbol{r})$ and $\langle \boldsymbol{r}|\boldsymbol{k}\rangle = \mathrm{e}^{\mathrm{i}\boldsymbol{k}\cdot\boldsymbol{r}}$. The infinite Born expansion (14) gives:

$$|\psi_{\boldsymbol{k}}\rangle = |\boldsymbol{k}\rangle + \hat{G}_0\hat{V}|\boldsymbol{k}\rangle + (\hat{G}_0\hat{V})^2|\boldsymbol{k}\rangle + \dots \tag{33}$$

For the following, it will be convenient to introduce the transition operator (or matrix) $\hat{T}(E)$ defined by

$$\hat{T} = \hat{V} + \hat{V}G_0\hat{V} + \hat{V}(\hat{G}_0\hat{V})^2 + \dots \tag{34}$$

which provides another form of the Lippmann–Schwinger equation:

$$\hat{T} = \hat{V} + \hat{V}\hat{G}_0\hat{T}. \tag{35}$$

The operator $\hat{T}$ provides a compact writing for the scattering state (33):

$$|\psi_{\boldsymbol{k}}\rangle = |\boldsymbol{k}\rangle + \hat{G}_0\hat{T}|\boldsymbol{k}\rangle. \tag{36}$$

We thus switch from the approximate Born expression (30) to the exact expression (36) by replacing the operator $\hat{V}$ by the operator $\hat{T}$. Of course, the formal simplicity of this result should not be misleading: all the difficulty has been transferred to the explicit calculation of $\hat{T}$.

The matrix element of $\hat{T}(E)$ between two states $|\boldsymbol{k}_i\rangle$ and $|\boldsymbol{k}_f\rangle$ computed from (34) takes into account all the "paths" allowing to couple these two states by the potential $\hat{V}$, starting at order 1 (direct coupling), then with a relay state $|\boldsymbol{k}_r\rangle$, etc:

$$\langle \boldsymbol{k}_f|\hat{T}|\boldsymbol{k}_i\rangle = \langle \boldsymbol{k}_f|\hat{V}|\boldsymbol{k}_i\rangle + \sum_{\boldsymbol{k}_r} \frac{\langle \boldsymbol{k}_f|\hat{V}|\boldsymbol{k}_r\rangle\langle \boldsymbol{k}_r|\hat{V}|\boldsymbol{k}_i\rangle}{E - E_r + \mathrm{i}0_+} + \dots \tag{37}$$

with for each relay state a denominator involving the difference between its energy E_r and the energy E considered.

[1] We will pose in all this course:

$$\langle \boldsymbol{r}|\boldsymbol{q}\rangle = \mathrm{e}^{\mathrm{i}\boldsymbol{q}\cdot\boldsymbol{r}}, \qquad \langle \boldsymbol{r}|\boldsymbol{r}'\rangle = \delta(\boldsymbol{r} - \boldsymbol{r}'), \qquad \langle \boldsymbol{q}|\boldsymbol{q}'\rangle = (2\pi)^3\,\delta(\boldsymbol{q} - \boldsymbol{q}'), \tag{31}$$

so that the closure relations in momentum and position representations can be written:

$$\hat{1} = \frac{1}{(2\pi)^3}\int |\boldsymbol{q}\rangle\langle \boldsymbol{q}|\,\mathrm{d}^3q = \int |\boldsymbol{r}\rangle\langle \boldsymbol{r}|\,\mathrm{d}^3r. \tag{32}$$

It is interesting to note the identity

$$\hat{V}|\psi_{\boldsymbol{k}}\rangle = \hat{T}|\boldsymbol{k}\rangle \tag{38}$$

which is simply proved by combining (15) and (36):

$$\hat{V}|\psi_{\boldsymbol{k}}\rangle = \left(E-\hat{H}_0\right)\left[|\boldsymbol{k}\rangle + \hat{G}_0\hat{T}|\boldsymbol{k}\rangle\right] = 0 \; + \; \left(E-\hat{H}_0\right)\left(E-\hat{H}_0\right)^{-1}\hat{T}|\boldsymbol{k}\rangle. \tag{39}$$

It is possible to express the series (34) defining the operator $\hat{T}$ in terms of the Green operator $\hat{G}$ of the total Hamiltonian. We have indeed:

$$\begin{aligned}\hat{T} &= \hat{V} + \hat{V}\left[\hat{G}_0 + \hat{G}_0\hat{V}\hat{G}_0 + \ldots\right]\hat{V} \\ &= \hat{V} + \hat{V}\hat{G}\hat{V}. \end{aligned} \tag{40}$$

This result is also rather formal, in the sense that the explicit calculation of $\hat{G}(E)$ is generally impossible to do, unlike the calculation of $\hat{G}_0(E)$. Nevertheless, it presents a very interesting point: if we take for the energy E a negative value corresponding to a bound state of $\hat{H}$, then we find a divergence in the expression of the scattering state. Anticipating slightly what follows, we deduce from this expression that the poles of the scattering amplitude (directly related to $\psi_{\boldsymbol{k}}$) give the energies of the bound states.

Finally, the relation $\hat{G} = \hat{G}_0 \; + \hat{G}_0\hat{V}\hat{G}$ between the two Green operators and its iterations allow to rewrite the scattering state (36):

$$\begin{aligned}|\psi_{\boldsymbol{k}}\rangle &= |\boldsymbol{k}\rangle + \hat{G}_0(\hat{V} + \hat{V}\hat{G}\hat{V})|\boldsymbol{k}\rangle \\ &= |\boldsymbol{k}\rangle + (\hat{G}_0 + \hat{G}_0\hat{V}\hat{G})\hat{V}|\boldsymbol{k}\rangle \\ &= |\boldsymbol{k}\rangle + \hat{G}\hat{V}|\boldsymbol{k}\rangle. \end{aligned} \tag{41}$$

We thus have a series of expressions allowing to link explicitly or implicitly the plane wave $|\boldsymbol{k}\rangle$ (eigenstate of $\hat{H}_0$) and the scattering state $|\psi_{\boldsymbol{k}}\rangle$ (eigenstate of $\hat{H}$):

$$|\psi_{\boldsymbol{k}}\rangle = |\boldsymbol{k}\rangle + \hat{G}_0\hat{T}|\boldsymbol{k}\rangle \tag{42}$$

$$= |\boldsymbol{k}\rangle + \hat{G}_0\hat{V}|\psi_{\boldsymbol{k}}\rangle \tag{43}$$

$$= |\boldsymbol{k}\rangle + \hat{G}\hat{V}|\boldsymbol{k}\rangle. \tag{44}$$

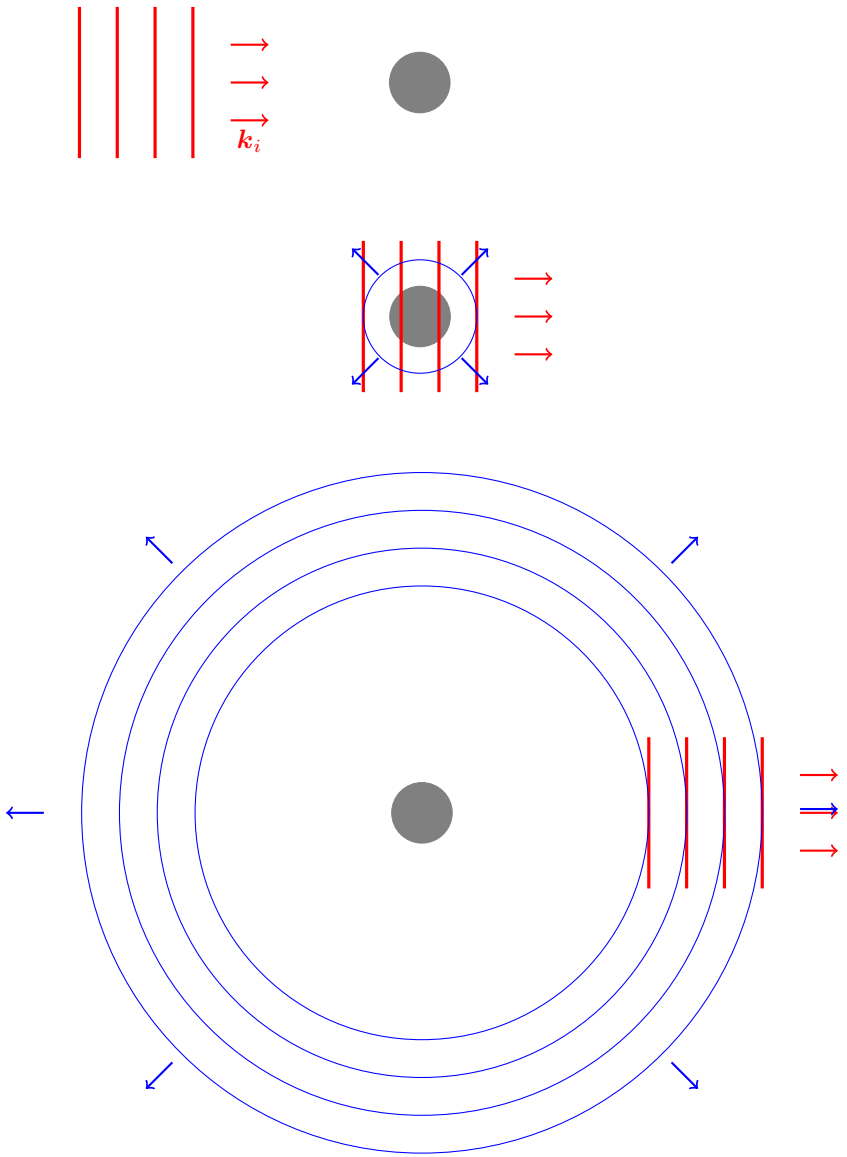

Figure 1. *Incident wave packet of wave vector $\boldsymbol{k}_i$ (in red) and scattered wave packet (in blue).*

2-3 The scattering matrix $\hat{S}$

In practice, we study a scattering process by preparing at the initial time t_i a wave packet of average energy E_i and average wave vector $\boldsymbol{k}_i$ known with a good precision, not covering the zone where $V(\boldsymbol{r})$ takes significant values. The wave packet propagates, arrives in the area where $V(\boldsymbol{r})$ plays a role, then leaves this zone as a scattered wave and a transmitted wave. We are then interested in the probability amplitude to find the scattered particle with a wave vector $\boldsymbol{k}_f$ at a later time t_f.

The quantity we want to evaluate is therefore of the type

$$\langle \boldsymbol{k}_f|\hat{U}(t_f,t_i)|\boldsymbol{k}_i\rangle, \qquad t_i \to -\infty,\ t_f \to +\infty, \tag{45}$$

where $\hat{U}(t_f,t_i) = \mathrm{e}^{-\mathrm{i}\hat{H}(t_f-t_i)/\hbar}$ is the evolution operator associated to the Hamiltonian $\hat{H}$, but we have to work a bit to give an unambiguous meaning to this expression. As a first step, we rewrite the previous expression as:

$$\langle \boldsymbol{k}_f|\hat{U}(t_f,0)\hat{U}(0,t_i)|\boldsymbol{k}_i\rangle \tag{46}$$

which we interpret as the scalar product of two vectors of the Hilbert space:

$$\hat{U}(0,t_i)|\boldsymbol{k}_i\rangle \quad \text{and} \quad \hat{U}^\dagger(t_f,0)|\boldsymbol{k}_f\rangle, \tag{47}$$

where the instant 0 can be seen as the one where the wave packet has arrived on the scattering center and where the interaction is maximal (the precise value of this instant is not important).

Since we want to make sense of the limit of these quantities when $t_i, t_f \to \pm\infty$, we must eliminate their "trivial" oscillations. Let us consider for example the first of these two terms. A first step in this direction is to eliminate the free evolution of $|\boldsymbol{k}_i\rangle$ described by the oscillatory term $\mathrm{e}^{\mathrm{i}E_it_i/\hbar}$ which would be present even if V were zero. So we take instead:

$$\mathrm{e}^{-\mathrm{i}E_it_i/\hbar}\hat{U}(0,t_i)|\boldsymbol{k}_i\rangle, \tag{48}$$

which corresponds to the *interaction representation*. Moreover, in order to simulate the progressive arrival of the wave packet on the scattering center, we will not consider a sudden branching of the coupling $\hat{V}$ at time t_i, as it could create an irrelevant transient regime. We rather take an adiabatic branching of this coupling and consider:

$$\lim_{\eta\to 0_+}\int_{-\infty}^{0}\mathrm{e}^{\eta t}\,\mathrm{e}^{-\mathrm{i}E_it/\hbar}\hat{U}(0,t)|\boldsymbol{k}_i\rangle\mathrm{d}t. \tag{49}$$

This vector is none other than the stationary scattering state $|\psi^{(+)}\rangle$. To show it, we just have to use the expression of the evolution operator $\hat{U}(0,t) = \mathrm{e}^{\mathrm{i}\hat{H}t/\hbar}$ and to perform the integration over time:

$$\begin{aligned}
(49) &= \eta\left[\int_{-\infty}^{0}\mathrm{e}^{-\mathrm{i}(E_i-\hat{H}+\mathrm{i}\eta\hbar)t/\hbar}\,\mathrm{d}t\right]|\boldsymbol{k}_i\rangle \\
&= \frac{\mathrm{i}\eta\hbar}{E_i-\hat{H}+\mathrm{i}\eta\hbar}|\boldsymbol{k}_i\rangle \\
&= \left[1+\frac{1}{E_i-\hat{H}+\mathrm{i}\eta\hbar}(\hat{H}-\hat{H}_0)\right]|\boldsymbol{k}_i\rangle \\
&= |\boldsymbol{k}_i\rangle+\hat{G}^{(+)}(E_i)\hat{V}|\boldsymbol{k}_i\rangle = |\psi^{(+)}_{\boldsymbol{k}_i}\rangle
\end{aligned} \tag{50}$$

where the limit $\eta \to 0_+$ is implicit. Note that we put here the explicit mention $^{(+)}$ of the advanced Green operator, because we will also need the retarded Green operator in what follows.

Similarly, we have to modify the other vector involved in the matrix element as follows:

$$\begin{aligned}
\hat{U}^\dagger(t_f,0)|\boldsymbol{k}_f\rangle \quad &\longrightarrow \quad \eta\int_0^{+\infty}\mathrm{e}^{-\eta t}\mathrm{e}^{-\mathrm{i}E_ft/\hbar}\hat{U}^\dagger(t,0)|\boldsymbol{k}_f\rangle \\
&\longrightarrow \quad \left[1+\frac{1}{E_f-\hat{H}-\mathrm{i}\eta\hbar}(\hat{H}-\hat{H}_0)\right]|\boldsymbol{k}_f\rangle \\
&\longrightarrow \quad |\boldsymbol{k}_f\rangle+\hat{G}^{(-)}(E_f)\hat{V}|\boldsymbol{k}_f\rangle = |\psi^{(-)}_{\boldsymbol{k}_f}\rangle.
\end{aligned} \tag{51}$$

Now that the notion of limit $t_i, t_f \to \pm\infty$ is well established, we can define the amplitude of probability we are looking for:

$$S_{fi} = \langle\psi^{(-)}_{\boldsymbol{k}_f}|\psi^{(+)}_{\boldsymbol{k}_i}\rangle \equiv \langle\boldsymbol{k}_f|\hat{S}|\boldsymbol{k}_i\rangle. \tag{52}$$

The explicit calculation of this matrix element is done without difficulty and we find:

$$S_{fi} = \delta_{\boldsymbol{k}_i,\boldsymbol{k}_f} - 2\mathrm{i}\pi\ \delta(E_i-E_f)\langle\boldsymbol{k}_f|\hat{T}(E_i)|\boldsymbol{k}_i\rangle. \tag{53}$$

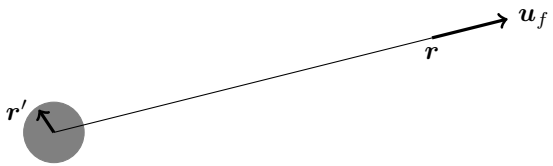

Figure 2. *Location of the points $\boldsymbol{r}$ and $\boldsymbol{r}'$ for the calculation of the scattering amplitude. The shaded area represents the range b of the potential.*

The knowledge of the transition matrix $\hat{T}$ is thus sufficient to determine all the relevant transition amplitudes in a scattering process. We will explore this notion more concretely in the next paragraph.

3 The scattering amplitude

We now give a physical meaning to the expression (12) found above for the stationary scattering states. We will be interested in their asymptotic behavior, i.e. their value at a point well outside the range of the potential. This will allow us to derive the notions of scattering amplitude and collision cross-section, which will be very useful in the following.

3-1 Definition

To exploit (12), let us consider a point $\boldsymbol{r}$ located in a region far from the area where V takes significant values (figure 2). We can expand the Green function $\mathcal{G}_0^{(+)}(\boldsymbol{r}-\boldsymbol{r}')$ in the form:

$$\frac{\mathrm{e}^{\mathrm{i}k|\boldsymbol{r}-\boldsymbol{r}'|}}{|\boldsymbol{r}-\boldsymbol{r}'|} \underset{r\to\infty}{\sim} \frac{\mathrm{e}^{\mathrm{i}kr}}{r}\,\mathrm{e}^{-\mathrm{i}k\boldsymbol{u}_f\cdot\boldsymbol{r}'} \tag{54}$$

where $\boldsymbol{u}_f = \boldsymbol{r}/r$ is the unit vector giving the direction where we look at the final product of the scattering. The Lippmann–Schwinger equation becomes

$$\psi_{\boldsymbol{k}}(\boldsymbol{r}) \underset{r\to\infty}{\sim} \mathrm{e}^{\mathrm{i}\boldsymbol{k}\cdot\boldsymbol{r}} + f(k,\boldsymbol{u}_i,\boldsymbol{u}_f)\frac{\mathrm{e}^{\mathrm{i}kr}}{r} \tag{55}$$

where $\boldsymbol{u}_i = \boldsymbol{k}/k$ is the unit vector parallel to the initial wave vector $\boldsymbol{k}_i$ and where we defined *the scattering amplitude*

$$f(k,\boldsymbol{u}_i,\boldsymbol{u}_f) = -\frac{m_\mathrm{r}}{2\pi\hbar^2}\int \mathrm{e}^{-\mathrm{i}k\boldsymbol{u}_f\cdot\boldsymbol{r}'}\,V(r')\,\psi_{\boldsymbol{k}_i}(\boldsymbol{r}')\,\mathrm{d}^3r', \tag{56}$$

which is a complex function of the energy $E = \hbar^2k^2/2m_\mathrm{r}$. Using the operator formulation developed in § 2, this definition can be written

$$f(k,\boldsymbol{u}_i,\boldsymbol{u}_f) = -\frac{m_\mathrm{r}}{2\pi\hbar^2}\,\langle\boldsymbol{k}_f|\hat{V}|\psi_{\boldsymbol{k}_i}\rangle \tag{57}$$

with $\boldsymbol{k}_f = k\boldsymbol{u}_f$, or using (38):

$$f(k,\boldsymbol{u}_i,\boldsymbol{u}_f) = -\frac{m_\mathrm{r}}{2\pi\hbar^2}\,\langle\boldsymbol{k}_f|\hat{T}|\boldsymbol{k}_i\rangle. \tag{58}$$

Let us assume for simplicity that the potential $V(\boldsymbol{r})$ is rotationally invariant. This implies that the scattering amplitude only depends on k and the angle θ between $\boldsymbol{u}_i$ and $\boldsymbol{u}_f$:

$$f(k,\boldsymbol{u}_i,\boldsymbol{u}_f) = f(k,\theta). \tag{59}$$

Like the scattering integral equation, the form (55) is implicit since the calculation of $f(k,\theta)$ requires the knowledge of $\psi_{\boldsymbol{k}}$, at least in some regions of space. It is nevertheless very meaningful; a scattering state can be seen as the superposition of an incident plane wave $\psi_{\boldsymbol{k}}^{(\mathrm{inc})}$ and a scattered wave $\psi_{\boldsymbol{k}}^{(\mathrm{scat})}$:

$$\psi_{\boldsymbol{k}} = \psi_{\boldsymbol{k}}^{(\mathrm{inc})} + \psi_{\boldsymbol{k}}^{(\mathrm{scat})}, \tag{60}$$

with the incident wave

$$\psi_{\boldsymbol{k}}^{(\mathrm{inc})}(\boldsymbol{r}) = \mathrm{e}^{\mathrm{i}\boldsymbol{k}\cdot\boldsymbol{r}} \tag{61}$$

and the scattered wave characterized by its amplitude $f(k,\theta)$ in a given direction θ:

$$\psi_{\boldsymbol{k}}^{(\mathrm{scat})}(\boldsymbol{r}) \underset{r\to\infty}{\sim} f(k,\theta)\frac{\mathrm{e}^{\mathrm{i}kr}}{r} \tag{62}$$

Note that if we had used the incoming Green function $\mathcal{G}_0^{(-)}$ instead of $\mathcal{G}_0^{(+)}$, we would have ended up with a scattering state composed of a plane wave and an incoming spherical wave. As a proper state of H_rel, this state is just as legitimate as (55), but it corresponds to a physical situation that is difficult to realize in practice. It would correspond to waves incoming from all directions of space with the adequate amplitude so that after collision, one obtains the plane wave $\mathrm{e}^{\mathrm{i}\boldsymbol{k}\cdot\boldsymbol{r}}$.

Born approximation. Recall that this approximation consists in replacing the stationary scattering state (*a priori* unknown) by its zeroth order approximation, $\mathrm{e}^{\mathrm{i}\boldsymbol{k}\cdot\boldsymbol{r}}$, in the integral of (12) or (56). The scattering amplitude at order 1 in V is thus written:

$$\text{Born's approximation:} \qquad f(k,\theta) \approx -\frac{m_\mathrm{r}}{2\pi\hbar^2}\int \mathrm{e}^{\mathrm{i}\boldsymbol{q}\cdot\boldsymbol{r}'}\, V(r')\,\mathrm{d}^3r' \qquad (63)$$
$$\approx -\frac{2m_\mathrm{r}}{q\hbar^2}\int_0^{+\infty}\sin(qr')\,V(r')\,r'\,\mathrm{d}r',$$

where we recall that θ is the angle between the two unit vectors $\boldsymbol{u}_i = \boldsymbol{k}/k$ and $\boldsymbol{u}_f = \boldsymbol{r}/r$, and $\boldsymbol{q} = k(\boldsymbol{u}_i - \boldsymbol{u}_f)$ with $q = 2k\sin(\theta/2)$. At this order of calculation, the scattering amplitude is therefore simply proportional to the Fourier transform of the scattering potential.

3-2 The collision cross-section

To make the interpretation of the scattering state even more concrete, it is useful to introduce the notion of collision cross-section. We define the differential cross-section $\frac{\mathrm{d}\sigma}{\mathrm{d}\Omega}(\Omega)$ using

$$\delta^2\mathcal{A} = \frac{\mathrm{d}\sigma}{\mathrm{d}\Omega}(\Omega)\;\delta^2\Omega. \qquad (64)$$

In this definition, $\delta^2\mathcal{A}$ (which has the dimension of a surface) is equal to the ratio between two fluxes:

- The outgoing flux in the solid angle $\delta\Omega$ around the mean direction defined by Ω (unit: s^{-1})
- the incoming flux for a well-defined incident direction $\boldsymbol{k}_i$ (unit: $\mathrm{s}^{-1}\mathrm{m}^{-2}$).

The quantity $\frac{\mathrm{d}\sigma}{\mathrm{d}\Omega}(\Omega)$ is an intrinsic property of the potential V and does not depend on the incident flux, since the outgoing flux is proportional to it.

To relate the differential cross-section to the scattering amplitude, the simplest way is to calculate the probability currents corresponding to the incident wave and the scattered wave. Let us recall the general definition of the probability current associated with a wave function $\psi(\boldsymbol{r})$:

$$\boldsymbol{J}(r) = \frac{\hbar}{m}\,\mathrm{Im}\left\{\psi^*(\boldsymbol{r})\;\boldsymbol{\nabla}\left[\psi(\boldsymbol{r})\right]\right\}. \qquad (65)$$

We find for the probability current associated with the incident wave (61)

$$\boldsymbol{J}^{(\mathrm{inc})}(\boldsymbol{r}) = \frac{\hbar}{m_\mathrm{r}}\,\mathrm{Im}\left\{\psi_{\boldsymbol{k}}^{(\mathrm{inc})*}\;\boldsymbol{\nabla}\left[\psi_{\boldsymbol{k}}^{(\mathrm{inc})}\right]\right\} = \frac{\hbar k}{m_\mathrm{r}}\boldsymbol{u}_i \qquad (66)$$

and for the probability current associated with the scattered wave (62):

$$\boldsymbol{J}^{(\mathrm{scat})}(\boldsymbol{r}) \underset{r\to\infty}{\sim} \frac{\hbar}{m_\mathrm{r}}\,\mathrm{Im}\left\{\psi_{\boldsymbol{k}}^{(\mathrm{scat})*}\;\boldsymbol{\nabla}\left[\psi_{\boldsymbol{k}}^{(\mathrm{scat})}\right]\right\} = \frac{\hbar k}{m_\mathrm{r}}\,|f(k,\theta)|^2\frac{\boldsymbol{u}_f}{r^2} \qquad (67)$$

Note that we have limited ourselves here to the dominant term at large r, which varies as $1/r^2$. This is indeed the only term that contributes to the outflow asymptotically. Note also that there is a third contribution to the probability current, coming from the crossed term between $\psi_{\boldsymbol{k}}^{(\mathrm{inc})}$ and $\psi_{\boldsymbol{k}}^{(\mathrm{scat})}$ in (65). We do not take this term into account for the moment. We will see in our discussion of the optical theorem that it has a zero contribution to the scattered flux outside the forward direction, i.e. for $\theta \neq 0$.

The ratio between the two currents in the definition (64) then gives the very simple result

$$\frac{\mathrm{d}\sigma}{\mathrm{d}\Omega}(\Omega) = |f(k,\theta)|^2. \qquad (68)$$

Note that in our reasoning based on probability currents, we have implicitly assumed that we are able, at least in principle, to distinguish between the final state corresponding to a scattering with angle θ and a scattering with angle $\pi - \theta$ (figure 3). When we look at the scattering of a "real" particle by a potential $V(r)$, it is obvious. When we are interested in the collision between two identical particles, it is more subtle: the two processes represented in figure 3 must not be equivalent, which imposes that the colliding particles are discernible, for example via their spin state. When the particles are indistinguishable, the result (68) must be modified, as we will see in § 4-3.

The total cross-section is defined as

$$\sigma_\mathrm{tot} = \int \frac{\mathrm{d}\sigma}{\mathrm{d}\Omega}\,\mathrm{d}^2\Omega = 2\pi\int_0^\pi |f(k,\theta)|^2\;\sin\theta\,\mathrm{d}\theta. \qquad (69)$$

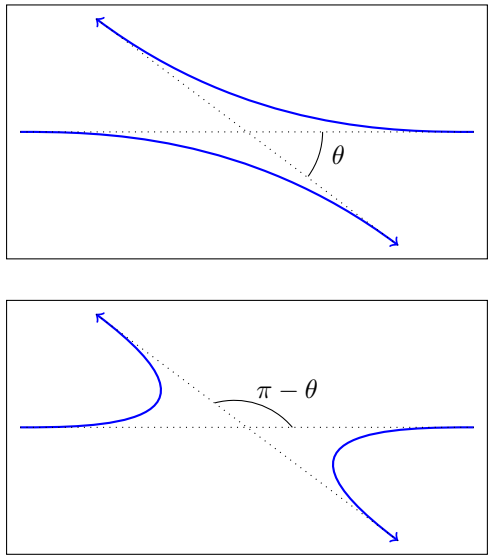

Figure 3. *Two collision processes leading to relative particle scattering of angle θ (top) and $\pi - \theta$ (bottom). If the particles are discernible, via their spin state for example, one can in principle distinguish these two processes and the result (68) applies. The case of indistinguishable particles is treated in § 4-3.*

By construction, this quantity is equal to the area of the surface that would have to be put in front of the incident beam to block a number of particles equivalent to that taken from the beam by the scattering process.

3-3 The optical theorem

In the preceding paragraphs, we arrived at the following asymptotic form for a stationary scattering state, i.e. an eigenstate of the Hamiltonian with energy $E = \hbar^2 k^2 / 2m_{\rm r}$:

$$\psi_{\boldsymbol{k}}(\boldsymbol{r}) \underset{r\to\infty}{\sim} \mathrm{e}^{\mathrm{i}\boldsymbol{k}\cdot\boldsymbol{r}} + f(k,\theta)\frac{\mathrm{e}^{\mathrm{i}kr}}{r}. \tag{70}$$

It should not be inferred from this simple form that any complex function $f(k,\theta)$ is eligible as a scattering amplitude. There are in fact several constraints on this function. The purpose of this paragraph is to present one of the most important ones,

$$2\,\mathrm{Im}\,[f(k,\theta=0)] = k\int_0^\pi |f(k,\theta)|^2\,\sin\theta, \tag{71}$$

which can also be written

$$\mathrm{Im}\,[f(k,\theta=0)] = \frac{k}{4\pi}\sigma_{\rm tot}, \tag{72}$$

and which is called the *optical theorem*. For a general review of the properties that the scattering amplitude f must satisfy, one can consult for example Goldberger & Watson (2004), Landau & Lifshitz (1975) or Joachain (1975).

The optical theorem finds its origin in the continuity equation verified by any solution $\psi(\boldsymbol{r},t)$ of the Schrödinger equation,

$$\boldsymbol{\nabla}\cdot\boldsymbol{J} + \frac{\partial\rho}{\partial t} = 0, \tag{73}$$

where the probability current $\boldsymbol{J}$ has been defined in (65) and where $\rho = |\psi|^2$. This relation is itself a consequence of the fact that the evolution governed by the Schrödinger equation is unitary. For a state of fixed energy E, the temporal evolution of ψ is given by $\psi(\boldsymbol{r},t) = \psi(\boldsymbol{r},0)\,\mathrm{e}^{-\mathrm{i}Et/\hbar}$ so that ρ is constant over time. We must therefore have:

$$\text{Stationary state:} \qquad \boldsymbol{\nabla}\cdot\boldsymbol{J} = 0. \tag{74}$$

As announced, this relation puts a strong constraint on the eligible functions $f(k,\theta)$.

The condition $\boldsymbol{\nabla}\cdot\boldsymbol{J} = 0$ leads to the fact that the flux of $\boldsymbol{J}$ through a sphere is zero. Let us therefore take a sphere $\mathcal{S}$ centered at 0, with an arbitrarily large radius r and impose the constraint

$$\int_{\mathcal{S}} \boldsymbol{u}_f\cdot\boldsymbol{J}\,\mathrm{d}^2\Omega = 0, \tag{75}$$

where $\boldsymbol{u}_f$ is as before the unit vector $\boldsymbol{r}/r$. The probability current is a quadratic function of the state (70) and is thus composed of three terms:

$$\boldsymbol{J} = \boldsymbol{J}^{(\rm inc)} + \boldsymbol{J}^{(\rm scat)} + \boldsymbol{J}^{(\rm interf)}. \tag{76}$$

The first two terms have already been calculated in the previous paragraph. The current $\boldsymbol{J}^{(\mathrm{inc})}$ given in (66) is uniform in space and therefore has a zero flux through the sphere $\mathcal{S}$:

$$\int_{\mathcal{S}} \boldsymbol{u}_f \cdot \boldsymbol{J}^{(\mathrm{inc})} \, \mathrm{d}^2\Omega = 0. \tag{77}$$

The current $\boldsymbol{J}^{(\mathrm{scat})}$ given in (67) is normal to the sphere and its flux is just the total cross-section, with a multiplicative coefficient:

$$\int_{\mathcal{S}} \boldsymbol{u}_f \cdot \boldsymbol{J}^{(\mathrm{scat})} \, \mathrm{d}^2\Omega = \frac{\hbar k}{m_{\mathrm{r}}} \sigma_{\mathrm{tot}}. \tag{78}$$

We still have to evaluate the contribution of the "interference" term $\boldsymbol{J}^{(\mathrm{interf})}$, involving both the contribution of $\psi_{\boldsymbol{k}}^{(\mathrm{inc})}$ and that of $\psi_{\boldsymbol{k}}^{(\mathrm{diff})}$:

$$\boldsymbol{J}^{(\mathrm{interf})} = \frac{\hbar}{m_{\mathrm{r}}} \mathrm{Im} \left\{ \psi_{\boldsymbol{k}}^{(\mathrm{inc})*} \, \boldsymbol{\nabla} \left[\psi_{\boldsymbol{k}}^{(\mathrm{scat})} \right] + \psi_{\boldsymbol{k}}^{(\mathrm{scat})*} \, \boldsymbol{\nabla} \left[\psi_{\boldsymbol{k}}^{(\mathrm{inc})} \right] \right\} \tag{79}$$

For r large, the asymptotic form of $\psi_{\boldsymbol{k}}^{(\mathrm{scat})}$ leads to:

$$\boldsymbol{J}^{(\mathrm{interf})} = \frac{\hbar}{m_{\mathrm{r}}} \, \mathrm{Im} \left\{ \mathrm{i}k(\boldsymbol{u}_i + \boldsymbol{u}_f) \, \frac{f(k,\theta)}{r} \, \mathrm{e}^{\mathrm{i}(kr - \boldsymbol{k}\cdot\boldsymbol{r})} \right\}. \tag{80}$$

Its flow through the sphere $\mathcal{S}$ reads:

$$\int_{\mathcal{S}} \boldsymbol{u}_f \cdot \boldsymbol{J}^{(\mathrm{interf})} \, \mathrm{d}^2\Omega = \frac{2\pi\hbar}{m_{\mathrm{r}}} \, \mathrm{Im} \left\{ \int_0^\pi \mathrm{i}kr \, (1+\cos\theta) \, \mathrm{e}^{\mathrm{i}kr(1-\cos\theta)} \, f(k,\theta) \, \sin\theta \, \mathrm{d}\theta \right\}. \tag{81}$$

When we take the limit $r \to \infty$, the exponential $\mathrm{e}^{\mathrm{i}kr(1-\cos\theta)}$ oscillates very fast around 0 and cancels the contribution of the different members of the integral, except if θ is chosen very close to 0 to "soften" the variation of the phase $kr(1-\cos\theta)$. By expanding the different terms in the neighborhood of $\theta = 0$, we arrive at:

$$\int_{\mathcal{S}} \boldsymbol{u}_f \cdot \boldsymbol{J}^{(\mathrm{interf})} \, \mathrm{d}^2\Omega = \frac{4\pi\hbar}{m_{\mathrm{r}}} \, \mathrm{Im} \left\{ f(k,0) \, \int_0^\pi \mathrm{i}kr \, \mathrm{e}^{\mathrm{i}kr\theta^2/2} \, \theta \, \mathrm{d}\theta \right\} \tag{82}$$

and the remaining integral is equal to -1 (to within a term oscillating infinitely fast).

In the end, we find that the total flux of J through the sphere S is equal to 0 if and only if the sum of the three contributions (77), (78) and (82) cancels out:

$$0 + \frac{\hbar k}{m_{\mathrm{r}}} \sigma_{\mathrm{tot}} - \frac{4\pi\hbar}{m_{\mathrm{r}}} \, \mathrm{Im} \{ f(k,0) \} = 0 \tag{83}$$

which corresponds to the announced "optical theorem".

The lesson of this theorem is a variant of "nothing is lost, nothing is created, everything is transformed": the particles that are scattered in the solid angle of 4π steradians are taken from the incident beam, which is therefore attenuated. This attenuation does not appear explicitly on the expression (70) of the scattering steady state, but it is nevertheless present in the form of a forward (destructive) interference between the incident and scattered waves.

3-4 The optical theorem in the isotropic case

The following chapters will be essentially devoted to the case of isotropic scattering, i.e. a scattering amplitude independent of the angle θ. The optical theorem takes a very simple form in this case. The total cross-section is:

$$\sigma_{\mathrm{tot}} = 2\pi \int_0^\pi |f(k)|^2 \, \sin\theta = 4\pi |f(k)|^2 \tag{84}$$

so that this theorem imposes

$$\mathrm{Im}\,[f(k)] = k \, |f(k)|^2 \tag{85}$$

which can also be written

$$\mathrm{Im} \left[\frac{1}{f(k)} \right] = -k. \tag{86}$$

The imaginary part of $1/f$ is thus completely fixed by the optical theorem, while there is no constraint at this stage on its real part. We will therefore frequently have to check that the result of an isotropic collision model leads to:

$$\frac{1}{f(k)} = \text{real function}(k) \; - \mathrm{i}k. \tag{87}$$

Note that the optical theorem imposes an upper bound on $|f(k)|$. It is indeed clear on (87) that

$$\frac{1}{|f(k)|} \geq k \qquad \Rightarrow \qquad \sigma = 4\pi |f(k)|^2 \leq \frac{4\pi}{k^2}. \tag{88}$$

When this inequality is saturated, we say that we have reached the *unitary regime*, i.e. the largest value allowed for the cross-section given the unitarity of quantum physics.

4 Rotational symmetry and Pauli principle

The dominant terms of the interaction between two neutral atoms – van der Waals potential at long range, exchange potential at short range – are generally rotationally invariant. This invariance can be broken if the interaction between the magnetic dipoles of the atoms becomes significant, as is the case for some species[2] such as dysprosium, erbium or chromium: their magnetic moment μ in the ground state is indeed equal to several times the Bohr magneton and the magnetic interaction energy $\sim \mu^2/r^3$ can become significant at very low temperatures. For the other species, it is generally reasonable to neglect this magnetic interaction, which brings us back to a rotation invariant potential.

We have already taken advantage of this invariance by writing the scattering amplitude in the form $f(k,\theta)$, which assumes that this amplitude depends only on the angle between the vectors $\boldsymbol{u}$ and $\boldsymbol{u}'$, and not on their particular orientation. But the consequences of rotation invariance go far beyond this simplification, as we will see in this section.

4-1 Taking into account the rotational symmetry

For a rotationally invariant Hamiltonian $H_{\rm rel}$, one can look for a basis of eigenstates common to $H_{\rm rel}$ and to the orbital angular momentum, more precisely the square of the angular momentum $\boldsymbol{L}^2$ and its projection on a given axis, z for example. By working with this eigenstate basis, one can make a partial wave expansion of the collision process, which greatly simplifies its analysis and allows to characterize it completely.

Consider a wave function $\psi(\boldsymbol{r}) = \psi(r,\theta,\varphi)$ eigenstate of $\boldsymbol{L}^2$ and L_z. We know from the general theory of orbital angular momentum that the θ and φ dependence of $\psi(\boldsymbol{r})$ is fixed as a spherical harmonic:

$$\psi(r,\theta,\varphi) = \chi(r)\, Y_{\ell,m}(\theta,\varphi) \tag{89}$$

with

$$\hat{L}^2\psi = \hbar^2\ell(\ell+1)\,\psi, \qquad \hat{L}_z\psi = \hbar m\,\psi, \tag{90}$$

ℓ being a positive or zero integer and m another integer of the set $\{-\ell, -\ell+1, \ldots, +\ell\}$. The radial dependence $\chi(r)$ is at this stage arbitrary because the operators $\boldsymbol{L}^2$ and L_z act only on the angular variables θ and φ.

Using the expression of the operator $\hat{\boldsymbol{p}}^2 = -\hbar^2\boldsymbol{\nabla}^2$ in spherical coordinates

$$\hat{\boldsymbol{p}}^2\psi = -\frac{\hbar^2}{r}\frac{\partial^2}{\partial r^2}(r\psi) + \frac{1}{r^2}\hat{\boldsymbol{L}}^2\psi \tag{91}$$

we deduce that the reduced function $u(r) = r\,\chi(r)$ is a solution of the one-dimensional differential equation

$$-\frac{\hbar^2}{2m_{\rm r}}\frac{{\rm d}^2}{{\rm d}r^2}u(r) + \left[V(r) + \frac{\hbar^2\ell(\ell+1)}{2m_{\rm r}r^2}\right]\,u(r) = E\,u(r) \tag{92}$$

on the ray $r \geq 0$, with the boundary condition $u(0) = 0$.

The physical interpretation of (92) is simple: thanks to the invariance by rotation, the 3D eigenvalue problem reduces to a series of independent 1D problems. Each value of ℓ corresponds to a "scattering channel" for a particle of mass $m_{\rm r}$ moving along the ray $r \geq 0$ with the effective potential:

$$V_{\rm eff}(r) = V(r) + \frac{\hbar^2\ell(\ell+1)}{2m_{\rm r}r^2}, \tag{93}$$

i.e. the sum of the interatomic potential discussed in the previous chapter and the centrifugal potential associated with the angular momentum $\hbar^2\ell(\ell+1)/2m_{\rm r}r^2$. In this point of view, the scattering process is described by considering a particle of mass $m_{\rm r}$ which arrives from $r = +\infty$ moving

[2] For the lanthanides, another element breaks the rotational invariance: the orbital angular momentum of the electrons in the ground state of the atom is not zero and the van der Waals interaction acquires a significant anisotropic component (of the order of 10 % of the isotropic part for Dy).

in the direction of decreasing r, penetrates in the zone where the potential $V(r)$ is appreciable, bounces on this zone to leave again towards $r = +\infty$. All the information about the scattering process is contained in the phase shift accumulated during the interaction with the potential V.

To obtain the value of this phase shift, it is sufficient to compare the coefficients of $\mathrm{e}^{\pm \mathrm{i}kr}$ in the solution $u(r)$ of the radial equation (92) according to whether $V(r)$ is present or not. The asymptotic form of the solution of the radial equation (92) for a given value of ℓ is traditionally written as:

$$u_\ell(r) \underset{r\to\infty}{\sim} (-1)^{\ell+1}\mathrm{e}^{-\mathrm{i}kr} + \mathrm{e}^{2\mathrm{i}\delta_\ell}\mathrm{e}^{\mathrm{i}kr} \;\propto\; \sin\left(kr - \ell\pi/2 \,+\, \delta_\ell\right) \qquad (94)$$

and solving the radial equation (92) will provide the phase $\delta_\ell(E)$. The reason for the coefficient $(-1)^{\ell+1}$ in (94) will become apparent later [eq. (99)], when we use the expansion of the plane wave $\mathrm{e}^{\mathrm{i}\boldsymbol{k}\cdot\boldsymbol{r}}$ on states with a well-defined angular momentum.

Note on the optical theorem. The optical theorem that we established in §3-3 expresses the conservation of the number of particles during the scattering process. Here, we have implicitly taken into account this conservation in each channel ℓ by assuming that the effect of the potential $V(r)$ can be described by the phase shift $\delta_\ell(k)$ of the outgoing wave, without changing its amplitude. We therefore expect the optical theorem to be automatically satisfied in this case. We will see later that this is indeed the case for each channel [*cf.* (105)].

4-2 The phase shifts δ_ℓ

For a given energy $\hbar^2k^2/2m_{\mathrm{r}}$, the set of states $\{Y_{\ell,m}(\theta,\varphi)\,u_\ell(r)/r\}$ that we have just introduced (completed by the possible bound states in the potential $V(r)$) constitutes a basis of the Hilbert space. We can then decompose the scattering state $\psi_{\boldsymbol{k}}(\boldsymbol{r})$ on this basis. Let us choose the z axis used for the quantization of $\hat{L}_z$ parallel to the incident $\boldsymbol{k}$ wave vector. Given the rotation invariance of the potential, the state $\psi_{\boldsymbol{k}}(\boldsymbol{r})$ is independent of the azimuthal angle φ and depends only on r and θ; it will therefore decompose on the $Y_{\ell,m=0}(\theta)\,u_\ell(r)/r$ states:

$$\psi_{\boldsymbol{k}}(\boldsymbol{r}) = \sum_\ell c_\ell\,\frac{u_\ell(r)}{r}\,Y_{l,0}(\theta) \qquad (95)$$

with by definition of spherical harmonics :

$$Y_{\ell,0}(\theta) = \sqrt{\frac{2\ell+1}{4\pi}}\,P_\ell(\cos\theta), \qquad (96)$$

where $P_\ell(x)$ is the Legendre polynomial of degree ℓ with the value $P_\ell(1) = 1$ for $\theta = 0$. Using the asymptotic expression (94) of the functions u_ℓ, we thus obtain the expected behavior for $\psi_{\boldsymbol{k}}(\boldsymbol{r})$ at large r:

$$\begin{aligned}\psi_{\boldsymbol{k}}(\boldsymbol{r}) \quad &\underset{r\to\infty}{\sim} \quad \frac{\mathrm{e}^{-\mathrm{i}kr}}{r}\sum_\ell (-1)^{\ell+1}\,c_\ell\sqrt{\frac{2\ell+1}{4\pi}}\,P_\ell(\cos\theta)\\ &+ \quad \frac{\mathrm{e}^{\mathrm{i}kr}}{r}\sum_\ell \mathrm{e}^{2\mathrm{i}\delta_\ell}\,c_\ell\sqrt{\frac{2\ell+1}{4\pi}}\,P_\ell(\cos\theta)\end{aligned} \qquad (97)$$

To relate the scattering amplitude to the phase shifts, it is sufficient to match (97) to the asymptotic expression of $\psi_{\boldsymbol{k}}$

$$\psi_{\boldsymbol{k}}(\boldsymbol{r}) \underset{r\to\infty}{\sim} \mathrm{e}^{\mathrm{i}kz} + f(k,\theta)\frac{\mathrm{e}^{\mathrm{i}kr}}{r}. \qquad (98)$$

A classical mathematical formula gives the expansion of the plane wave $\mathrm{e}^{\mathrm{i}kz}$ [see for example Landau & Lifshitz (1975)]:

$$\mathrm{e}^{\mathrm{i}kz} \underset{r\to\infty}{\sim} \frac{1}{2\mathrm{i}kr}\sum_\ell (2\ell+1)\,P_\ell(\cos\theta)\,\left[(-1)^{\ell+1}\mathrm{e}^{-\mathrm{i}kr} + \mathrm{e}^{\mathrm{i}kr}\right], \qquad (99)$$

which leads to

$$\begin{aligned}\psi_{\boldsymbol{k}}(\boldsymbol{r}) \quad &\underset{r\to\infty}{\sim} \quad \frac{\mathrm{e}^{-\mathrm{i}kr}}{r}\,\frac{1}{2\mathrm{i}k}\sum_\ell (-1)^{\ell+1}\,(2\ell+1)\,P_\ell(\cos\theta)\\ &+ \quad \frac{\mathrm{e}^{\mathrm{i}kr}}{r}\left[f(k,\theta) + \frac{1}{2\mathrm{i}k}\sum_\ell (2\ell+1)\,P_\ell(\cos\theta)\right]\end{aligned} \qquad (100)$$

The term-by-term comparison of (97) and (100) of the $\mathrm{e}^{-\mathrm{i}kr}/r$ component results in

$$c_\ell \sqrt{\frac{2\ell+1}{4\pi}} = 2\ell+1 \tag{101}$$

and thus for the component in $\mathrm{e}^{\mathrm{i}kr}/r$:

$$f(k,\theta) = \frac{1}{2\mathrm{i}k} \sum_\ell (2\ell+1)\ P_\ell(\cos\theta)\ \left(\mathrm{e}^{2\mathrm{i}\delta_\ell} - 1\right). \tag{102}$$

This amplitude is null if and only if all the phases δ_ℓ are null (modulo π).

It is convenient to write this amplitude as

$$f(k,\theta) = \sum_\ell (2\ell+1)\ P_\ell(\cos\theta)\ f_\ell(k) \tag{103}$$

where we have introduced the scattering amplitude of the ℓ channel:

$$f_\ell(k) = \frac{1}{2\mathrm{i}k}\left(\mathrm{e}^{2\mathrm{i}\delta_\ell} - 1\right) \tag{104}$$

or equivalently

$$\frac{1}{f_\ell(k)} = \frac{k}{\tan\delta_\ell(k)} - \mathrm{i}k. \tag{105}$$

The imaginary part of the scattering amplitude of each channel ℓ is thus equal to $-k$, whatever the scattering potential.

Because of the orthonormality properties of spherical harmonics[3], the total cross-section, obtained by integrating $|f(k,\theta)|^2$ over the solid angle, is written:

$$\sigma_{\mathrm{tot}} = \sum_\ell \sigma_\ell \qquad \text{with} \quad \sigma_\ell = \frac{4\pi}{k^2}(2\ell+1)\sin^2\left[\delta_\ell(k)\right]. \tag{107}$$

Each partial wave contributes positively to the total cross-section with an upper limit $4\pi(2\ell+1)/k^2$ for the ℓ-channel. We can verify from these expressions the optical theorem announced above.

[3]We use the fact that $P_\ell(1) = 1$ and

$$\int_0^\pi P_\ell(\cos\theta) P_{\ell'}(\cos\theta)\ \sin\theta\ \mathrm{d}\theta = \frac{2\delta_{\ell,\ell'}}{2\ell+1}. \tag{106}$$

4-3 Collision of indistinguishable particles

Let us now consider the case of a collision between two identical particles, which can be bosons or fermions. For simplicity, we assume that these two particles are prepared in the same spin state. Pauli principle thus imposes the symmetry or antisymmetry of the orbital part of the wave function:

$$\Psi(\boldsymbol{r}_A, \boldsymbol{r}_B) = \epsilon\, \Psi(\boldsymbol{r}_B, \boldsymbol{r}_A), \tag{108}$$

with the sign $\epsilon = +$ for bosons and $\epsilon = -$ for fermions. When using the center-of-mass and relative variables, the exchange $\boldsymbol{r}_A \leftrightarrow \boldsymbol{r}_B$ is transcribed into:

$$\boldsymbol{R} \leftrightarrow \boldsymbol{R}, \qquad \boldsymbol{r} \leftrightarrow -\boldsymbol{r}. \tag{109}$$

The Pauli principle does not constrain the state of the center-of-mass, but it does require that the wave function of the relative variable verifies

$$\psi(-\boldsymbol{r}) = \epsilon\, \psi(\boldsymbol{r}). \tag{110}$$

For spherical coordinates, the transformation $\boldsymbol{r} \to -\boldsymbol{r}$ is written:

$$r \to r, \quad \theta \to \pi - \theta, \quad \varphi \to \varphi + \pi \tag{111}$$

Now the spherical harmonics verify the property

$$Y_{\ell,m}(\pi-\theta, \varphi+\pi) = (-1)^\ell\, Y_{\ell,m}(\theta,\varphi). \tag{112}$$

Pauli principle thus comes down to the necessary and sufficient condition:

- The quantum number ℓ can only take even values ($\ell = 0, 2, 4, \ldots$) if the particles are bosons in the same spin state.
- The quantum number ℓ can only take odd values ($\ell = 1, 3, \ldots$) if the particles are fermions in the same spin state.

After this identification of the allowed collision channels, the characterization of the radial wave function in each channel is unchanged [*cf.* (92)]. Nevertheless, there is an additional modification to be made, which concerns the link between scattering amplitude and cross-section. After symmetrization or antisymmetrization, the asymptotic part of the scattering state is indeed written

$$\psi_{\boldsymbol{k}}(\boldsymbol{r}) \underset{r\to\infty}{\sim} \frac{1}{\sqrt{2}}\left[\mathrm{e}^{\mathrm{i}\boldsymbol{k}\cdot\boldsymbol{r}} + \epsilon\, \mathrm{e}^{-\mathrm{i}\boldsymbol{k}\cdot\boldsymbol{r}}\right] + \frac{1}{\sqrt{2}}\left[f(k,\theta) + \epsilon\, f(k,\pi-\theta)\right]\frac{\mathrm{e}^{\mathrm{i}kr}}{r}. \tag{113}$$

The differential cross-section is then

$$\frac{\mathrm{d}\sigma}{\mathrm{d}\Omega} = \frac{1}{2}\left|f(k,\theta) + \epsilon f(k,\pi-\theta)\right|^2 . \tag{114}$$

When we develop this expression, we find the sum of the cross-sections in θ and in $\pi - \theta$, plus an interference term. The latter can have spectacular consequences: for example, for polarized fermions, we find that the cross-section always vanishes for $\theta = \pi/2$, whatever the energy of the collision partners.

The expression (107) of the total cross-section becomes

$$\text{Bosons:} \qquad \sigma_{\mathrm{tot}} = 2\sum_{\ell \text{ pair}} \sigma_\ell \tag{115}$$

$$\text{Fermions:} \qquad \sigma_{\mathrm{tot}} = 2\sum_{\ell \text{ impair}} \sigma_\ell \tag{116}$$

with $\sigma_\ell = (4\pi/k^2)\,(2\ell+1)\sin^2\delta_\ell(k)$ as above. In other words, only half of the ℓ's contribute to each sum (even or odd ℓ depending on the statistical nature of the particles), but their contribution is doubled compared to the case of discernible particles.

A nice illustration of this effect of quantum statistics on the collisional cross-section is provided by Plattner & Sick (1981). These authors studied the Coulomb scattering between ^{12}C (a spinless boson) and ^{13}C (a spin $1/2$ fermion) carbon nuclei. A beam of C^{2+} ions is accelerated to an energy of the order of 4 MeV and sent on a target composed of carbon. The main results of this study are shown in figure 4. If the nuclei are discernible (^{12}C + ^{13}C), the differential cross-section does not show a marked structure: it decreases with the angle as expected for Rutherford scattering:

$$\frac{\mathrm{d}\sigma}{\mathrm{d}\Omega} \propto \frac{1}{\sin^4(\theta/2)}. \tag{117}$$

On the other hand, when the two nuclei are identical, marked oscillations are visible. The differential cross-section presents a local maximum at $\theta = \pi/2$ for bosons, because of the constructive interference between the two processes in figure 3. For fermions, this differential cross-section is on the contrary minimal in $\theta = \pi/2$. This minimum is not strictly zero, contrary to what one would expect from (114). This is due to the fact that the spins

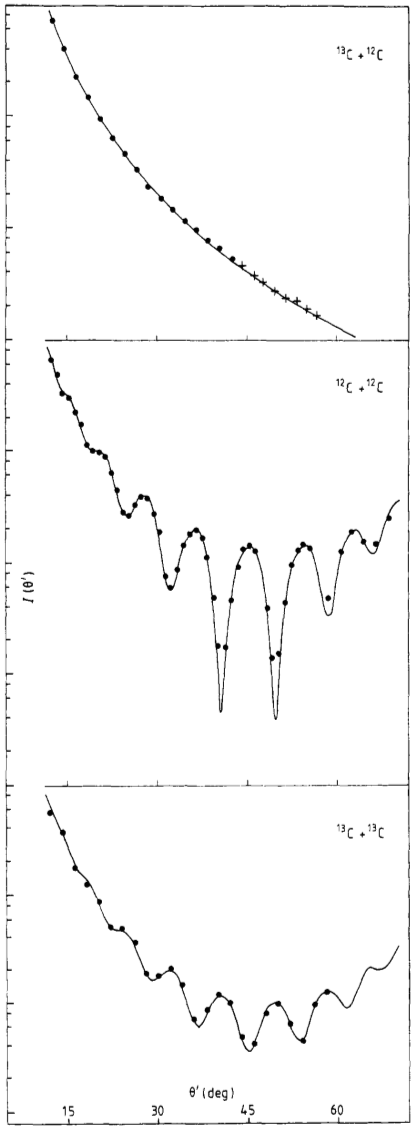

Figure 4. *Coulomb scattering between two carbon nuclei. ^{12}C is a spinless boson and ^{13}C is a spin 1/2 fermion. The angle θ' is approximately equal to $\theta/2$. Figure extracted from Plattner & Sick (1981).*

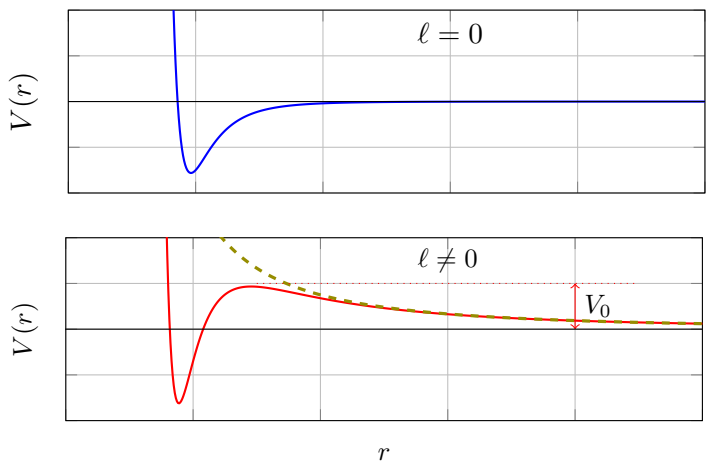

Figure 5. *Effective potential obtained by summing a Lennard–Jones potential in $C_{12}/r^{12} - C_6/r^6$ and the centrifugal potential proportional to $1/r^2$. Top: $\ell = 0$, bottom $\ell \neq 0$. The green dashed curve represents the centrifugal potential alone. For quantum gases, the barrier height for $\ell \neq 0$ is generally much larger than the thermal energies.*

of the ^{13}C nuclei were not polarized in the experiment: only a fraction of the collisions in this case involve indistinguishable particles.

4-4 Centrifugal barrier and cold atoms

We can distinguish two cases in the partial wave expansion we have just carried out (*cf.* figure 5):

- The zero angular momentum $\ell = 0$ (s wave regime), in which case the equation to solve involves only $V(r)$:

$$\ell = 0 \ : \qquad u''(r) + \left[k^2 - \frac{2m_\mathrm{r}}{\hbar^2} V(r)\right] u(r) = 0. \tag{118}$$

  Since the spherical harmonic $Y_{0,0}$ is independent of θ and φ, the wave function in this channel is isotropic.

- The non-zero angular momenta $\ell = 1, 2, \ldots$:

$$\ell \neq 0 \ : \qquad u''(r) + \left[k^2 - \frac{\ell(\ell+1)}{r^2} - \frac{2m_\mathrm{r}}{\hbar^2} V(r)\right] u(r) = 0 \tag{119}$$

  in which case the dominant term in $V_\mathrm{eff}(r)$ when $r \to \infty$ is the centrifugal potential which decreases as $1/r^2$, thus much slower than $V(r)$ which decreases as $1/r^6$. The effective potential then always presents a strictly positive barrier at large r.

The centrifugal barrier plays a particularly important role in the case of collisions between cold atoms. It is interesting to estimate the height of the potential bump V_0 resulting from the sum of the van der Waals potential and the centrifugal potential for the smallest possible non-zero angular momentum[4], $\ell = 1$:

$$\text{for } r \text{ large:} \qquad V_\mathrm{eff}(r) \approx -\frac{C_6}{r^6} + \frac{\hbar^2}{m_\mathrm{r} r^2}. \tag{120}$$

The maximum is found in $r = \left(3m_\mathrm{r}C_6/\hbar^2\right)^{1/4}$ and leads to

$$V_0 = \frac{2}{3\sqrt{3}} \frac{\hbar^3}{\sqrt{m_\mathrm{r}^3 C_6}}. \tag{121}$$

For rubidium atoms, this corresponds to an energy $V_0 \approx k_\mathrm{B} \times 30\,\mu\mathrm{K}$. The thermal energies of quantum gases are generally lower than this barrier by one or two orders of magnitude.

4-5 Power law potential and convergence criteria

In the following chapters, we will frequently use power-law potentials, $V(r) \propto r^{-n}$, with in particular $n = 6$ for van der Waals interaction. It is useful to keep in mind the convergence of the quantities introduced so far depending on the value of n. Here, we only give the main results and we refer the reader interested in their proofs to specialized works:

[4] In fact, as we have seen in §4-3, the angular momentum must be even for indiscernible bosons and the barrier should rather be estimated for $\ell = 2$. Its effect would only be increased.

- For $n \leq 1$, the phases $\delta_\ell(k)$ are infinite. They are well defined only for $n > 1$.
- For $n \leq 2$, the total cross-section diverges. This is in particular the case for Coulomb scattering, as can be seen from the differential cross-section given in (117), which behaves like $1/\theta^4$ in the neighborhood of $\theta = 0$.
- The convergence of the forward scattering amplitude $\theta = 0$, i.e. $f(k, 0)$, is obtained only for $n > 3$.

Chapter III

Low-Energy Collisions

The previous chapter was devoted to the presentation of the formalism allowing to treat a collision between two particles. We also explained how one can take advantage of the rotation invariance of the interaction potential to simplify the problem. It allowed us to describe the collision in terms of the phase shifts $\delta_\ell(k)$ associated to the various angular momenta ℓ. We now turn to the case of a low-energy collision, such as $kb \ll 1$, where $\boldsymbol{k}$ is the relative wave vector of the two collision partners and b the range of the interaction potential.

This problem is of great importance for the physics of cold atoms. It will bring a considerable simplification on the mathematical level: only the lowest partial waves (essentially $\ell = 0$ or 1) contribute significantly, and when they play a role, they can be characterized by only one or two physical parameters like the scattering length or the effective range. This simplification allows in particular to replace the real potential between atoms, which can be complicated to determine as we have seen in chapter I, by a much simpler potential leading to the same set of physical parameters. Here, we will discuss the examples of the square well and the pseudo-potential.

The origin of this simplification is well known in all fields of wave physics, optics or acoustics for example: if one observes a system of size b with a wave whose wavelength is such that $\lambda \sim 1/k \gg b$, one cannot distinguish the details of this system, which thus appears as a point object. We can then model the scattering of the wave by this system by replacing it by a simpler one.

1 The low energy radial equation

1-1 The range of the scattering potential

The notion of low-energy expansion is intimately related to the range b of the scattering potential, i.e. the range of distances around $\boldsymbol{r} = 0$ on which the potential $V(r)$ has an effect. For a potential such as a square well, which we will study in detail in § 3, the range is just equal to the width of the well. For a potential behaving like a power law at large r:

$$V(r) \sim -\frac{C_n}{r^n}, \tag{1}$$

this notion is more subtle. In fact, it only makes sense in quantum physics: if we consider a wave packet localized at an average distance σ from the center and with an extension also $\sim \sigma$, the potential energy $\sim -C_n/\sigma^n$ will be significant compared to the kinetic energy related to the localization $\sim \hbar^2/m\sigma^2$ when

$$\frac{C_n}{\sigma^n} \gtrsim \frac{\hbar^2}{m\sigma^2} \qquad \Leftrightarrow \qquad \sigma \lesssim \left(\frac{mC_n}{\hbar^2}\right)^{1/(n-2)}, \tag{2}$$

which defines, to within an arbitrary multiplicative coefficient, the range of the potential $-C_n/r^n$. Note that this reasoning only makes sense for $n > 2$. The Coulomb potential ($n = 1$) is of infinite range in both quantum

and classical mechanics. For the van der Waals potential $-C_6/r^6$, we will define throughout this course[1]

$$R_{\rm vdW} = \frac{1}{2}\left(\frac{2m_{\rm r}C_6}{\hbar^2}\right)^{1/4}. \tag{3}$$

The energy scale associated to this length scale is

$$E_{\rm vdW} = \frac{\hbar^2}{2m_{\rm r}R_{\rm vdW}^2}. \tag{4}$$

1-2 The different spatial areas to consider

In the previous chapter, we established the radial equation verified by the reduced wave function $u(r) = r\,\psi(r)$ for a given value ℓ of angular momentum:

$$-\frac{\hbar^2}{2m_{\rm r}}\frac{{\rm d}^2u}{{\rm d}r^2} + \left(\frac{\hbar^2\ell(\ell+1)}{2m_{\rm r}} + V(r)\right)u(r) = E\,u(r) \tag{5}$$

which can be written

$$u'' + \left(k^2 - \frac{\ell(\ell+1)}{r^2} - \frac{2m_{\rm r}V(r)}{\hbar^2}\right)u = 0 \tag{6}$$

with $E \equiv \hbar^2k^2/2m_{\rm r}$ and $u''(r) \equiv {\rm d}^2u/{\rm d}r^2$. In what follows, we characterize the solutions of this equation, taking advantage of the existence of two well-separated length scales for the low energy problem:

- The "short distance" scale given by the range of the potential b (i.e. $R_{\rm vdW}$ for the van der Waals potential). For $r \gg b$, we can neglect the influence of $V(r)$ in (6).
- The "long distance" scale given by $1/k$, i.e. the reduced de Broglie wavelength associated to the incident particle. For $r \ll 1/k$, one can neglect the influence of k^2 in (6).

[1] When defining scales of length, energy, etc. from dimensional considerations, it is generally preferable not to incorporate numerical factors (2, π, e,...) because these cannot be restored at the end of the calculation by simple homogeneity considerations. However, for the definition of the length scale $R_{\rm vdW}$, the weight of traditions is such that we preferred not to adopt a definition different from the one most common in the literature.

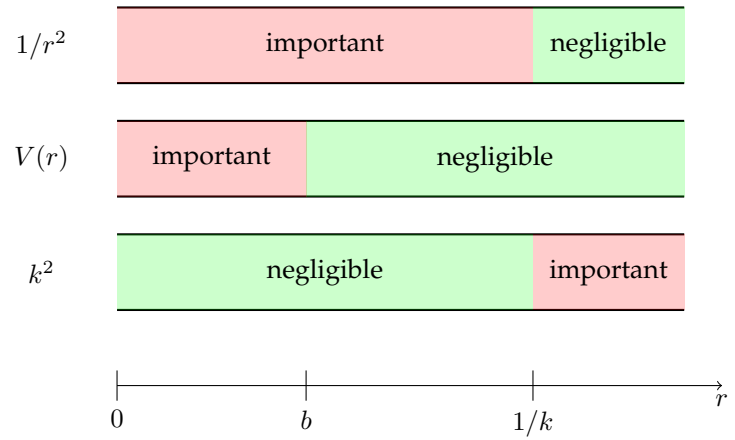

Figure 1. *The three spatial zones to consider when analyzing the behavior of the solutions of (6) for $\ell = 1$. For $\ell = 0$, the first line is not useful.*

There are therefore three zones of space to be considered, represented in figure 1:

- The inner area where the action of V is significant:

$$r < b: \qquad u'' - \left(\frac{\ell(\ell+1)}{r^2} + \frac{2m_{\rm r}V(r)}{\hbar^2}\right)u = 0 \tag{7}$$

  Solving exactly this equation requires the precise knowledge of the potential $V(r)$. The solution is independent of k, and thus of the energy, in this low-energy limit. As it is a second-order differential equation, there are two independent solutions, but we keep only the physically acceptable solution canceling at $r = 0$, since $u(r) = r\,\psi(r)$.

- The intermediate zone where we can neglect both the contribution of $V(r)$ and k^2:

$$b \ll r \ll 1/k: \quad u'' - \frac{\ell(\ell+1)}{r^2}u = 0. \tag{8}$$

  Two independent solutions of this equation are $r^{\ell+1}$ and $1/r^\ell$. The

physically interesting solution is written in this zone:

$$u(r) \propto \alpha\, r^{\ell+1} + \frac{\beta}{r^\ell}. \tag{9}$$

or $u(r) = \alpha r + \beta$ for $\ell = 0$.

- The outer region where k^2 dominates in front of $\ell(\ell+1)/r^2$ and $V(r)$, i.e. $r \gg 1/k$ for ℓ of the order of unity (or $r \gg \ell/k$ otherwise):

$$k \ll r : \qquad u'' + k^2 u = 0. \tag{10}$$

The solutions are $\sin kr$ and $\cos kr$ and we saw in the previous chapter that it is interesting to put the physically relevant linear combination in the form

$$\begin{aligned} u(r) &\propto \sin(kr - \ell\pi/2 + \delta_\ell), \\ &\propto \sin(kr - \ell\pi/2) \,+\, \tan(\delta_\ell)\, \cos(kr - \ell\pi/2), \end{aligned} \tag{11}$$

where the action of the scattering potential $V(r)$ is characterized by the phase shift $\delta_\ell(k)$.

1-3 The connection between zones

The goal of the theoretical study of a scattering problem is the determination of the phase shift $\delta_\ell(k)$ for a given potential $V(r)$. This determination amounts to connecting the solution in the outer region $r \gg 1/k$ to that found in the inner region $r < b$.

The connection at the level of $r \sim b$ between the inner and the intermediate zone is done on a case-by-case basis. According to the expression of the potential $V(r)$, an analytical or numerical resolution allows to determine the ratio α/β to be taken to connect to the solution verifying $u(0) = 0$.

The connection at the level of $r \sim 1/k$ between the intermediate and the external zone is done thanks to the exact solutions of the equation

$$u'' + \left(k^2 - \frac{\ell(\ell+1)}{r^2}\right) u = 0. \tag{12}$$

These solutions are linear combinations of :

$$\sqrt{kr}\; J_{\ell+1/2}(kr) \quad \text{and} \quad \sqrt{kr}\; Y_{\ell+1/2}(kr) \tag{13}$$

where $J_\alpha(x)$ and $Y_\alpha(x)$ are the Bessel functions of first and second kind. Let us give here some relevant properties of these Bessel functions:

- For $kr \ll 1$, we have

$$\sqrt{kr}\; J_{\ell+1/2}(kr) \;\sim\; c_J\; (kr)^{\ell+1}, \tag{14}$$

$$\sqrt{kr}\; Y_{\ell+1/2}(kr) \;\sim\; -c_Y\; (kr)^{-\ell} \tag{15}$$

which gives the expected behavior in (9). We will not specify here the proportionality coefficients c_J and c_Y, which are simple numbers involving $\Gamma(\ell+1/2)$ and $\Gamma(\ell+3/2)$.

- For $kr \gg 1$, we have

$$\sqrt{kr}\; J_{\ell+1/2}(kr) \;\sim\; \sqrt{2/\pi}\; \sin(kr - \ell\pi/2), \tag{16}$$

$$\sqrt{kr}\; Y_{\ell+1/2}(kr) \;\sim\; -\sqrt{2/\pi}\; \cos(kr - \ell\pi/2) \tag{17}$$

which gives the behavior expected from (11). More precisely, $\tan\delta_\ell$ characterizes the relative weight of $Y_{\ell+1/2}$ compared to $J_{\ell+1/2}$:

$$u(r) \propto \left[\sqrt{kr}\; J_{\ell+1/2}(kr)\right] - \tan\delta_\ell \left[\sqrt{kr}\; Y_{\ell+1/2}(kr)\right]. \tag{18}$$

We can therefore deduce from the above the behavior of the phase shift δ_ℓ with k. The extension of (18) in the intermediate zone gives:

$$u(r) \propto \left[c_J\; (kr)^{-\ell+1}\right] + \tan\delta_\ell \left[c_Y\; (kr)^{-\ell}\right] \tag{19}$$

i.e. by comparing with (9):

$$\frac{\beta}{\alpha} = \frac{c_Y}{c_J}\; \frac{\tan\delta_\ell}{k^{2\ell+1}}. \tag{20}$$

We have already mentioned that the ratio β/α, obtained by connecting the intermediate zone with the inner zone, is independent of k. Therefore, we deduce the scaling law at low energy:

$$\tan\left[\delta_\ell(k)\right] \propto k^{2\ell+1}. \tag{21}$$

This result is important for the following. It shows that for a given energy, the effect of the potential $V(r)$ – characterized by a non-zero value of $\tan\delta_\ell$ – will be weaker the larger ℓ is. In practice, the smallest value $\ell = 0$ will play a dominant role or, for polarized fermions for which only odd values of ℓ are allowed, the value $\ell = 1$.

The central role played by s-wave scattering ($\ell = 0$) is easily understood when we examine the effective potential formed by the real potential $V(r)$ and the centrifugal barrier $\hbar^2\ell(\ell+1)/2m_{\rm r}$. This potential, plotted in figure 2 for $V(r)$ of the Lennard-Jones form, comprises:

- a long-distance wing dominated by the centrifugal term,
- a local maximum for $r \sim R_{\rm vdW}$ with a barrier height $r \sim E_{\rm vdW}$.
- a short-distance behavior dominated by $V(r)$.

We have already mentioned in chapter II that in a quantum gas, the thermal energy of an atom is much lower than $E_{\rm vdW}$. Therefore, as soon as $\ell \neq 0$, the relative particle incident from $r = +\infty$ has an energy E much smaller than the height of the centrifugal barrier. Except in very specific cases (the shape resonances investigated in Chapter V), the particle will bounce back around the classical turning point $r_\ell(E)$, whose position is almost the same as in the absence of the scattering potential (figure 2). The scattering channels in the non-zero angular momentum waves are thus "inoperative", and everything happens for them as if the particles did not interact. Only the scattering in the s-wave ($\ell = 0$) remains.

1-4 Validity of the low-energy expansion

The above treatment consisted in completely neglecting the effect of $V(r)$ in the region $r > b$. When $V(r)$ is a square potential, which is strictly zero beyond b, this is obviously correct. On the other hand, this approximation can be problematic for a power-law potential $-C_n/r^n$. To assess the validity of this treatment, we need to compare the effect of the centrifugal term in $1/r^2$ with that of $1/r^n$ on the solution considered for $b \ll r \ll 1/k$:

$$u(r) \propto \alpha\, r^{\ell+1} + \frac{\beta}{r^\ell}. \tag{22}$$

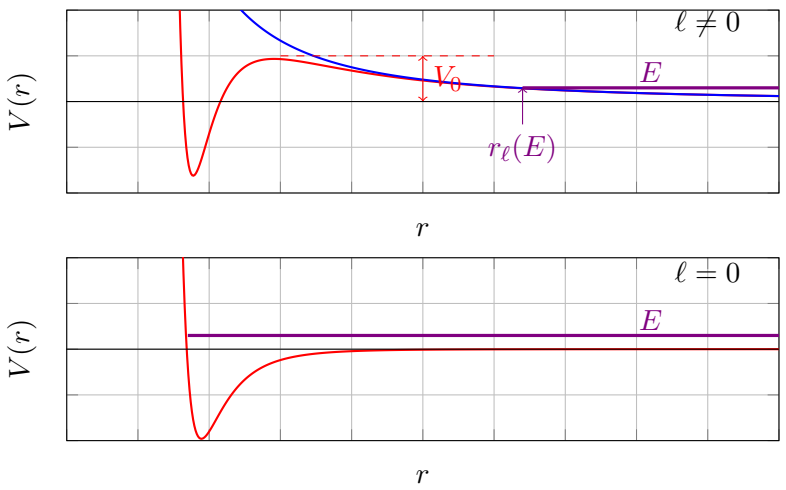

Figure 2. *Top figure, angular momentum $\ell \neq 0$. Red: Lennard-Jones potential superimposed on the centrifugal potential; blue: centrifugal potential alone. In a quantum gas, an atomic collision is generally done at an energy $E \ll V_0$ so that the atoms explore only the region dominated by the centrifugal barrier. The channels corresponding to $\ell \neq 0$ therefore give rise to a much weaker scattering than the $\ell = 0$ channel (bottom figure), at least when s-wave scattering is allowed (this excludes polarized fermions).*

More precisely, we have to make sure that $V(r) \times (\alpha\, r^{\ell+1})$ always remains small in front of $(\hbar^2\ell(\ell+1)/2m_{\rm r}r^2) \times (\beta/r^\ell)$ over this whole area. A priori, we expect these two terms to be comparable at the boundary $r = b$, and so the first term must decrease faster than the second when we take $r \gg b$. This imposes

$$n - \ell - 1 > 2 + \ell \qquad \Leftrightarrow \qquad n > 2\ell + 3. \tag{23}$$

This is a very restrictive condition. For a van der Waals potential $n = 6$, we see that the above, in particular the scaling law (21), is only valid for $\ell = 0$ (s wave) or $\ell = 1$ (p wave). For partial waves of higher angular momentum, the phase shift $\delta_\ell(k)$ decreases less rapidly with k than the law (21) indicates [Landau & Lifshitz (1975), § 132].

2 The s-wave and p-wave scattering

We have shown in the previous section that at low energy, scattering occurs mainly in channels of low angular momentum, starting with the s-wave, $\ell = 0$. We will therefore concentrate first on this channel, and then we will say a few words about the next channel $\ell = 1$.

Let us recall some important results established in the previous chapter from the partial wave expansion. The scattering amplitude $f(k,\theta)$ is written in the general form

$$f(k,\theta) = \sum_\ell (2\ell+1)\ P_\ell(\cos\theta)\ f_\ell(k), \tag{24}$$

which gives when restricted to the channel $\ell = 0$:

$$f(k,\theta) = f_0(k), \tag{25}$$

i.e. an isotropic scattering, as expected for a zero-angular momentum state. Furthermore, we related each amplitude $f_\ell(k)$ to the phase shift $\delta_\ell(k)$ by:

$$\frac{1}{f_\ell(k)} = \frac{k}{\tan\delta_\ell(k)} - \mathrm{i}k. \tag{26}$$

where the imaginary part of $1/f(k)$, i.e. the $-\mathrm{i}k$ term, comes from the optical theorem and is essential to ensure the unitarity of the scattering process: the outgoing flux must be equal to the incoming flux.

In this low-energy limit, the differential cross-section is isotropic, which leads to a very simple expression for the total cross-section:

$$\text{Low energy:} \qquad \frac{\mathrm{d}\sigma}{\mathrm{d}\Omega}(\Omega) = |f(k)|^2, \qquad \sigma_{\mathrm{tot}} = 4\pi|f(k)|^2. \tag{27}$$

2-1 Scattering length and effective range

For s-wave scattering, the general result (21) is written as:

$$k \to 0 : \qquad \tan[\delta_0(k)] \propto k. \tag{28}$$

The proportionality coefficient has the dimension of a length and we thus define the *scattering length*:

$$a = -\lim_{k\to 0} \frac{\tan[\delta_0(k)]}{k}. \tag{29}$$

Taking for the moment $\tan[\delta_0(k)] = -ak$ (the first corrective term will be discussed below), we obtain the low energy s-wave scattering amplitude:

$$\frac{1}{f(k)} \approx -\frac{1}{a} - \mathrm{i}k \qquad \Leftrightarrow \qquad f(k) \approx -\frac{a}{1+\mathrm{i}ka}. \tag{30}$$

The scattering length can be positive, negative, zero or infinite.

Next order of expansion of $f(k)$: the effective range. It can be shown [*cf.* Messiah (1962) and Landau & Lifshitz (1975)] that the expansion of the real part of $1/f$ involves only even powers of k, up to an order determined by the rapidity of the decay of $V(r)$. For the van der Waals potential decaying as r^{-6}, we get to order 2 in k:

$$\text{order 2 in } k: \qquad \frac{1}{f(k)} \approx -\frac{1}{a} - \mathrm{i}k + \frac{1}{2}r_e k^2, \tag{31}$$

where we have introduced the *effective range* r_e, a real quantity which also has the dimension of a length. For the energy domain of quantum gases, the knowledge of the scattering length a and of the effective range r_e is largely sufficient to describe correctly the whole physics of s-wave collisions. In fact, in this course, we will often limit ourselves to (30), i.e. a scattering with zero effective range ($r_e = 0$). This limit corresponds in particular to the pseudo-potential that we will introduce later.

"Unitary" regime. When we consider in a situation where $1/a = 0$ ($a = \pm\infty$), the scattering amplitude at low energy is equal to i/k and the cross-section to $4\pi/k^2$ (for discernible particles). These two quantities thus reach (in modulus) their maximum value allowed by the optical theorem and the unitarity of quantum mechanics. We will come back in the following chapters on the means to reach this regime and on its physical consequences.

Distinguishable vs. indistinguishable particles The results given above were established for discernible particles and they lead to the total effective cross-section:

$$\text{Discernible particles, low energy:} \quad \sigma_{\rm tot} \approx \frac{4\pi a^2}{1+k^2a^2}. \tag{32}$$

We have established in the previous chapter how to take into account the indistinguishability of particles, bosons or fermions. For polarized bosons, this indistinguishability doubles the contribution of even waves and cancels the contribution of odd waves; for fermions, the contributions are reversed. We deduce that in the s-wave regime of interest here, we have:

$$\text{Polarized bosons, low energy:} \quad \sigma_{\rm tot} \approx \frac{8\pi a^2}{1+k^2a^2}, \tag{33}$$

$$\text{Polarized fermions, low energy:} \quad \sigma_{\rm tot} \approx 0. \tag{34}$$

For polarized fermions, the dominant term is p-wave scattering, as we will see in §2-4.

2-2 Scattering length and last bound state

We mentioned in the previous chapter that the transition matrix $\hat{T}$ and the scattering amplitude f diverge when evaluated for an energy E equal to the energy of a bound state of the Hamiltonian $\boldsymbol{p}^2/2m_{\rm r} + V(r)$. If the scattering amplitude $f(E)$ is known precisely, it is therefore interesting to look at its poles to deduce the energy of the bound states without calculation. We will see an example of this for the square well in §3-3.

When one has only an approximate value of $f(k)$, this connection between the scattering amplitude and the bound states is of variable interest. When we use the expression of $f(k)$ given in (30), we find a single pole in $k = {\rm i}/a$ corresponding to the bound state:

$$\frac{{\rm e}^{{\rm i}kr}}{r} \longrightarrow \frac{{\rm e}^{-r/a}}{r} \quad \text{with} \quad E = \frac{\hbar^2k^2}{2m_{\rm r}} = -\frac{\hbar^2}{2m_{\rm r}a^2}. \tag{35}$$

This expression is acceptable only for $a > 0$, so that the state can be normalized. We will see in the rest of the course, in particular in §3-3 for the square well, that it provides a good estimate of the energy of the last bound state when $a \gg b$.

2-3 How to calculate a scattering length

We have given in (11) the general expression of the reduced wave function $u(r)$ for a state of angular momentum ℓ. For s-wave scattering, this expression simplifies into

$$u(r) \propto \sin(kr) + \tan(\delta_0)\cos(kr). \tag{36}$$

Let us take the limit $k \to 0$ of this expression using $\tan[\delta_0(k)] \approx -ka$. For a given r, we have $\sin kr \approx kr$, $\cos kr \approx 1$, so that

$$k \to 0: \quad u(r) \propto k(r-a). \tag{37}$$

To determine a, it is therefore sufficient to look for the zero-energy solution of the radial equation (6) for $\ell = 0$:

$$u''(r) + \frac{2m_{\rm r}V(r)}{\hbar^2}u(r) = 0. \tag{38}$$

Only the physically acceptable solution leading to $u(0) = 0$ must be retained. In the outer region where $V(r)$ is negligible, the radial equation (38) is written $u''(r) = 0$ and the solution retained is therefore of the form $u(r) = \alpha r + \beta$. The comparison of this form with (37) allows to deduce the scattering length $a = -\beta/\alpha$.

2-4 p-wave Scattering

For p-wave scattering ($\ell = 1$), the general result (21) becomes

$$k \to 0: \qquad \tan[\delta_1(k)] \propto k^3. \tag{39}$$

We are therefore led to introduce the *scattering volume*:

$$v = -\lim_{k\to 0}\frac{\tan[\delta_1(k)]}{k^3}. \tag{40}$$

Moreover, the Legendre polynomial $P_1(x) = x$ so that the scattering amplitude is

$$f(k,\theta) = 3\cos\theta\ f_1(k) \tag{41}$$

with

$$\frac{1}{f_1(k)} = \frac{k}{\tan[\delta_1(k)]} - \mathrm{i}k \approx -\frac{1}{k^2 v} - \mathrm{i}k. \tag{42}$$

At small k, the dominant term of the scattering amplitude is therefore the real part $f_1(k) \propto k^2$, the differential cross-section varies as

$$\frac{\mathrm{d}\sigma}{\mathrm{d}\Omega} = |f(k,\theta)|^2 \propto k^4 \cos^2\theta \tag{43}$$

and the total cross-section as $\sigma \propto k^4$.

The expression (42) above gives the dominant term of the real part for k small, as well as the exact value of the imaginary part. However, since these two terms differ by a factor k^3, it is important to specify whether other terms (in k^{-1} or in k^0) can contribute significantly to the real part of $1/f(k)$, with an amplitude that could exceed that of the imaginary part.

In an "effective range" type of expansion, similar to that carried out for the s-wave regime in (31), one indeed finds a correction of order k^2 with respect to the dominant term:

$$\frac{k^3}{\tan[\delta_1(k)]} \approx -\frac{1}{v} + \frac{k_e}{2}k^2, \tag{44}$$

where k_e has the dimension of a wave number. This additional term provides a correction to the scattering amplitude given in (42):

$$\frac{1}{f_1(k)} \approx -\frac{1}{k^2 v} + \frac{k_e}{2} - \mathrm{i}k. \tag{45}$$

This correction plays a more important role than its s-wave equivalent. Indeed, in the presence of a Fano–Feshbach resonance which provides $v = \infty$ and thus cancels the dominant term, it is the effective range term which becomes preponderant, and not the universal term $\mathrm{i}k$ as it is the case for s-wave scattering when $a = \infty$. Thus the description of a p-wave resonance leads to the introduction of two Tan's contacts, one associated with the volume v and the other associated with k_e (Yu, Thywissen, et al. 2015).

What we have just described applies well for potentials decreasing very fast at infinity (faster than $1/r^7$), but is strictly speaking incorrect for the van der Waals potential decaying as $1/r^6$ (Mott & Massey 1949). In this case, it can be shown that an additional term, of order $1/k$, contributes to the expression (45) giving the scattering amplitude (Gao 1998a). However, this term can generally be neglected in the case where the p-wave scattering is induced by a Fano–Feshbach resonance (Yoshida & Ueda 2015).

2-5 Examples of cold collision experiments

We now illustrate the above results with two experiments conducted on quantum gases.

s-wave collisions for bosons. Our first example concerns the observation of s-wave collisions, therefore isotropic, with bosons all prepared in the same spin state. The experiment was carried out at the Laboratoire Charles Fabry of the Institut d'Optique by Jaskula, Bonneau, et al. (2010) (see also Perrin, Chang, et al. (2007) for an earlier experiment carried out by the same group). The starting point is a Bose–Einstein condensate of metastable helium atoms, in which the particles have a negligible velocity. A light pulse with two pairs of laser beams induces a stimulated Raman transition to another internal state of the atom. This pulse creates two groups of atoms propagating in opposite directions with velocities $v = \pm 2v_{\mathrm{rec}}$, and a third group is constituted by the atoms remaining at rest. The velocity v_{rec} is the recoil velocity associated with the absorption or emission of a single resonant photon, that is 9.2 cm/s for metastable helium. Once collisions occurred, an image of the atomic cloud is taken after a ballistic expansion, which allows to determine its velocity distribution.

An example of result is shown in figure 3. Here, the product of the collision between the group of atoms at $v = 2v_{\mathrm{rec}}$ and the group of atoms at $v = 0$ was selected. It corresponds to a center-of-mass velocity equal to v_{rec}. We observe what remains of the two initial groups of atoms (bright spots at the top and bottom of the picture) and a spherical halo corresponding to the product of s-wave collisions. Since collisions are elastic, the final velocities of the atoms are equal in modulus to the initial velocity. The isotropy of the scattering amplitude results in a uniform density over the whole sphere.

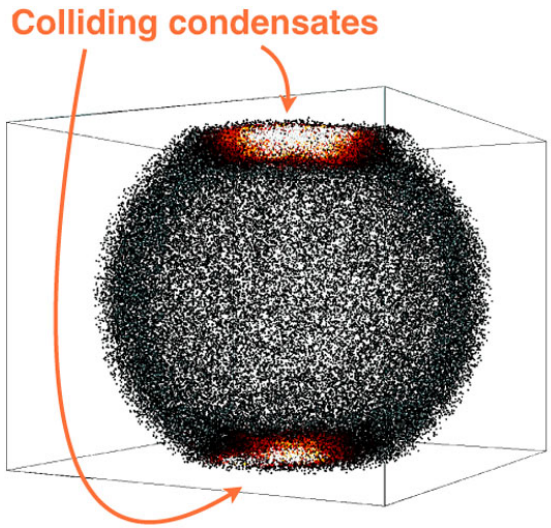

Figure 3. *Collision between two Bose-Einstein condensates of metastable helium. The spherical halo is in agreement with the prediction for s-wave scattering. Each point corresponds to the detection of an atom. Figure extracted from Jaskula, Bonneau, et al. (2010).*

Collision inhibition for polarized fermions. For polarized fermions, the allowed scattering channels are the odd ℓ partial waves, in particular $\ell = 1$ at low temperature. To highlight this phenomenon, DeMarco, Bohn, et al. (1999) studied the thermalization rate of a fermion cloud (^{40}K) in a harmonic trap. They started from a gas of 10^7 atoms at equilibrium in an anisotropic trap, so that the sizes of the gas along the three axes $\alpha = x, y, z$ of the trap verify the equipartition law of the energy $\frac{1}{2}m\omega_\alpha^2 r_\alpha^2 = \frac{1}{2}k_B T$. At a given time, one of the three eigenfrequencies of the trap is modified and one looks at the time necessary for the shape of the cloud to adapt to this new configuration under the effect of elastic collisions (Guéry-Odelin, Zambelli, et al. 1999). An example of relaxation to equilibrium is shown in figure 4 (left).

When the same experiment is repeated for lower temperatures, one observes a spectacular lengthening of the relaxation time, which is explained

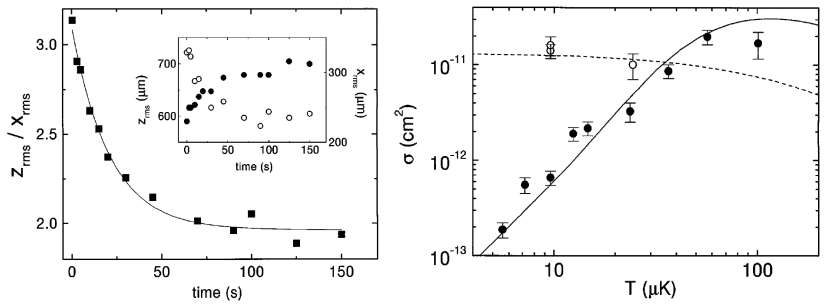

Figure 4. *Left: measurement of the relaxation towards equilibrium for an atomic cloud of ^{40}K (fermions) confined in a harmonic trap. This relaxation is the result of elastic collisions, in a cloud having initially an aspect ratio different from the one expected for the harmonic trap. Right: variation of the cross-section with the temperature of the cloud, for polarized atoms (closed symbols) and for a mixture of two spin states (open symbols). Figures extracted from DeMarco, Bohn, et al. (1999).*

by a decrease of the cross-section for polarized fermions (figure 4, right, closed symbols). This decay follows the law expected for the p-wave, $\sigma \propto k^4 \propto T^2$ between 5 and 50 μK. A control experiment consists in doing the same experiment with a mixture of two spin states (figure 4, right, open symbols). One then finds a cross-section that is approximately independent of temperature, as expected for s-wave collisions.

3 The example of the square well

A square-well potential is probably the simplest system on which to apply the concepts we have just outlined, in order to test and understand the main predictions. We consider in this section the attractive potential shown in figure 5, of depth $V_0 > 0$ and range b. We start by calculating the scattering length for this well. Then we study the stationary scattering states (positive energies) and the bound states (negative energies).

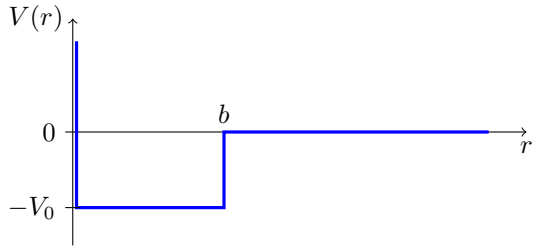

Figure 5. *Square potential well of depth V_0 and width b.*

3-1 The scattering length for a square well

As we wrote in §2-3, the simplest method to determine the scattering length is to look for the eigenstate of the Schrödinger equation of zero energy. The reduced wave function $u(r)$ of this state verifies

$$r < b \quad : \quad u''(r) + k_0^2 u(r) = 0 \tag{46}$$
$$r > b \quad : \quad u''(r) = 0 \tag{47}$$

with $V_0 = \hbar^2 k_0^2 / 2m_\mathrm{r}$. The solution is written

$$r < b \quad : \quad u(r) = A \sin(k_0 r) \tag{48}$$
$$r > b \quad : \quad u(r) = \alpha r + \beta \tag{49}$$

The continuity of u and its derivative in $r = b$ imposes:

$$\frac{k_0 \cos(k_0 b)}{\sin(k_0 b)} = \frac{\alpha}{\alpha b + \beta} \tag{50}$$

from which we deduce the scattering length via $a = -\beta/\alpha$:

$$a = b - \frac{\tan(k_0 b)}{k_0}. \tag{51}$$

The scattering length is plotted in figure 6 as a function of the depth of the potential well. When the well is shallow ($k_0 b \ll 1$), this scattering length is small and negative. This is easily understood by the Born approximation:

$$k \to 0 : \qquad f(k) \approx -\frac{m_\mathrm{r}}{2\pi\hbar^2} \int V(\boldsymbol{r}) \, \mathrm{d}^3 r = \frac{k_0^2 b^3}{3} \tag{52}$$

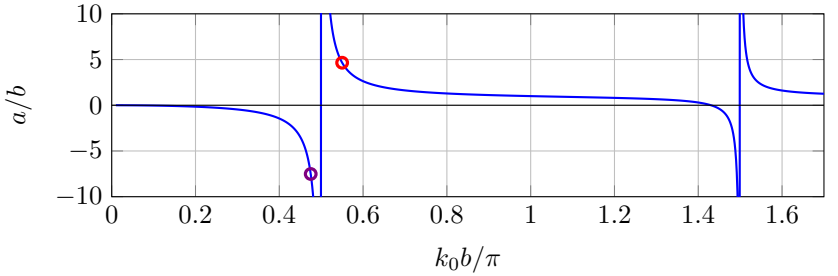

Figure 6. *Variation of the scattering length of a square well as a function of its depth $V_0 = \hbar^2 k_0^2 / 2m_\mathrm{r}$.*

which corresponds to the first non-zero term of the low-k_0 expansion of (51). When k_0 increases and becomes of the order of $1/b$, the scattering length (51) diverges[2] tending towards $-\infty$ when $k_0 b \to \pi/2$ by negative values, then switches to $+\infty$ to decrease again, then meets a second divergence in $k_0 b = 3\pi/2$, etc.

In order to understand these divergences, we will search for the bound states in this square well in §3-3. We will show that each divergence is associated with the appearance of a new bound state (Levinson's theorem). Before that, in order to get an intuition of the physical meaning of the scattering length, we will study the eigenstates of the Schrödinger equation with a slightly positive energy.

3-2 The square well: scattering states

The reduced wave function of a scattering state with positive energy $E = \hbar^2 k^2 / 2m_\mathrm{r}$ verifies

$$r < b \quad : \quad u''(r) + k_1^2 u(r) = 0, \qquad k_1^2 = k_0^2 + k^2, \tag{53}$$
$$r > b \quad : \quad u''(r) + k^2 u(r) = 0, \tag{54}$$

[2] It is also possible to compute analytically the effective range for this square model (Castin 2007). The behavior of this parameter also presents a succession of divergences.

whose solution is written:

$$r < b \quad : \quad u(r) = A \sin(k_1 r) \tag{55}$$
$$r > b \quad : \quad u(r) = B \sin(kr + \delta_0) \tag{56}$$

The connection of u and its derivative at the point $r = b$ gives the value of the phase shift $\delta_0(k)$:

$$\frac{1}{k_1} \tan(k_1 b) = \frac{1}{k} \tan(kb + \delta_0) \tag{57}$$

which can be written

$$\delta_0(k) = -kb + \arctan\left[\frac{k}{k_1} \tan(k_1 b)\right] \qquad \mod [\pi]. \tag{58}$$

We check on this expression that the scattering length found above [*cf.* (51)] is obtained as $-\lim_{k\to 0} \tan[\delta_0(k)]/k$.

Let us start by examining the case of a positive scattering length by taking as an example the point marked by a red circle in figure 6 ($k_0 b = 0.55\pi$). Let us look at the behavior of three low-energy eigenstates: $k/k_0 = 0.02, 0.03, 0.05$ (figure 7). The long-range variation (figure 7, top) is a sinusoid of period $2\pi/k$, as expected. When we zoom in on the central part (figure 7, bottom), we see that these states all share the same node, located to a very good approximation at the level of the scattering length. They therefore all behave like

$$u(r) \propto \sin[k(r - a)]] \tag{59}$$

for $r \gtrsim a$, as expected from (56) and from $\delta_0(k) \approx -ka$.

The physical interpretation of the scattering length is therefore simple in the case $a > 0$: the behavior of the scattering states for $r > a$ is identical to the one we would have if we were working with a hard-core potential, of radius equal to the scattering length. Of course, here the $u(r)$ functions are non-zero for $r < a$, contrary to the case of a hard-core potential. This would play a role if we were interested in inelastic collisions leading to dimer formation. But for elastic processes, a positive scattering length is equivalent to a hard-core potential and therefore tends to keep the particles away from each other by forcing the relative wave function to cancel at $r = a$.

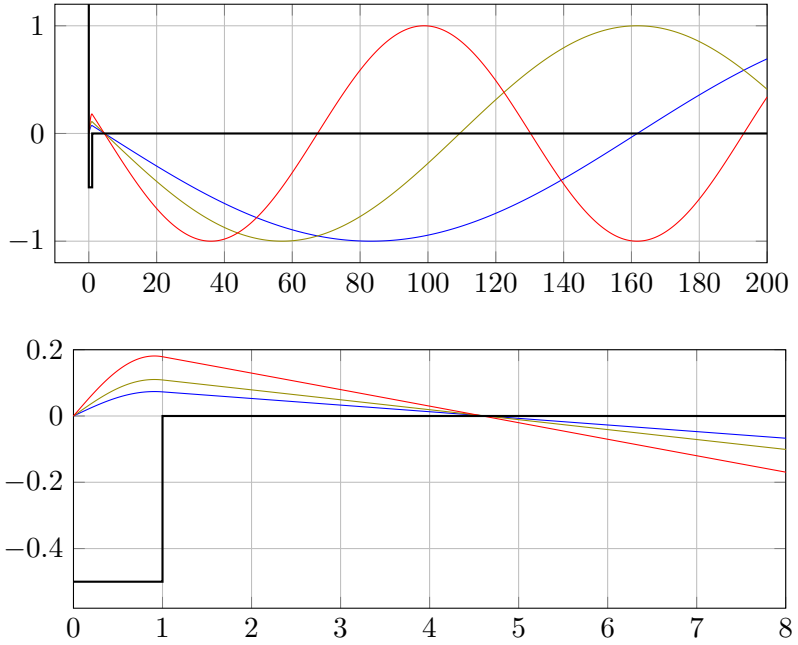

Figure 7. *Scattering states for a square well, in the case $a > 0$ (red point in figure 6). The wave numbers are $k/k_0 = 0.02, 0.03, 0.05$ and the scattering length is $a = 4.7\, b$.*

Let's move on to the case of a negative scattering length, with the purple point of figure 6, corresponding to $k_0 b = 0.475\pi$. We still consider the three low-energy states: $k/k_0 = 0.02, 0.03, 0.05$ (figure 8). We now see that the long-range sinusoidal behavior corresponds to curves that would intersect at the $r = a$ (negative) point if extended into the non-physical region $r < 0$. Such a behavior is also in agreement with the expected variation in $\sin[k(r - a)]$ and it leads to an *increased* probability of finding the two particles close to each other, compared to what one would have if they did not interact.

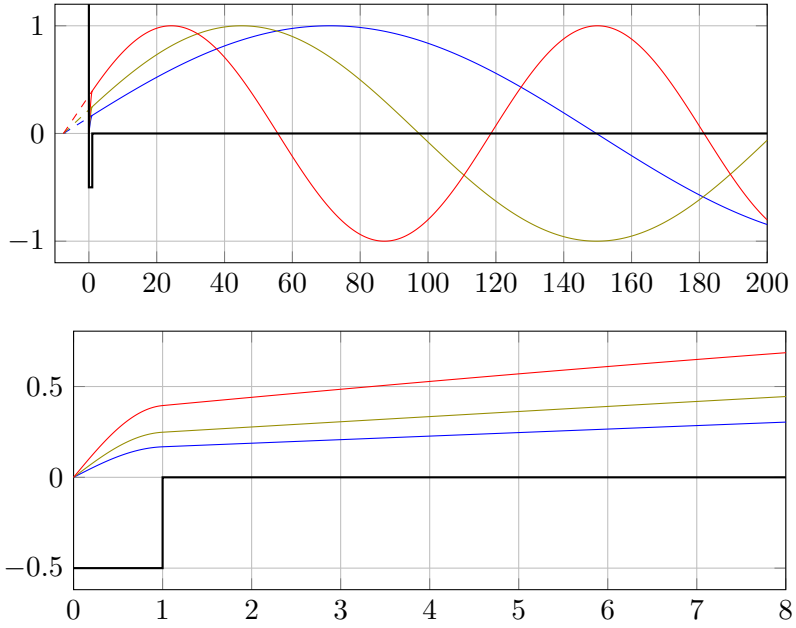

Figure 8. *Scattering states for a square well in the case $a < 0$ (purple point in figure 6). The wave numbers are $k/k_0 = 0.02, 0.03, 0.05$ and the scattering length is $a = -7.5\,b$.*

3-3 The square well: bound states

We now relate the divergences found for the scattering length to the appearance of bound states in the square well. Let us start by recalling that in three dimensions, such a well does not always admit bound states. To prove this, we start from the reduced radial wave function expected for a bound state. Since $E < 0$, we introduce κ and k_1 such that

$$\frac{\hbar^2\kappa^2}{2m_r} = |E|, \qquad k_1^2 = k_0^2 - \kappa^2. \tag{60}$$

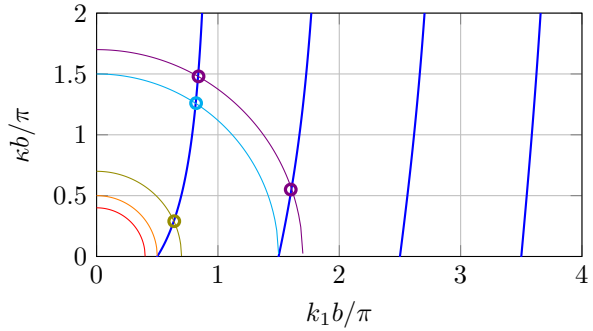

Figure 9. *Principle of the graphical solution allowing to find the bound states in a 3D square well [cf. (65) and (66)]. We have to find the intersection between the curve $y = -x\cot(\pi x)$ (with $x = k_1 b/\pi$ and $y = \kappa b/\pi$) and the circle of radius $k_0 b/\pi$. The threshold of the first (resp. second) bound state corresponds to the orange (resp. cyan) circle of radius $k_0 b/\pi = 1/2$ (resp. $3/2$). There is no bound state for $k_0 b/\pi = 0.4$ (red circle), only one bound state for $k_0 b/\pi = 0.7$ (green circle) and two bound states for $k_0 b/\pi = 1.7$ (purple circle).*

The reduced radial wave function of a bound state must verify

$$r < b \quad : \quad u''(r) + k_1^2 u(r) = 0 \tag{61}$$
$$r > b \quad : \quad u''(r) - \kappa^2 u(r) = 0 \tag{62}$$

with the boundary condition $u(0) = 0$. The physically acceptable solution is therefore written, to within a multiplicative factor:

$$r < b \quad : \quad u(r) = A\,\sin(k_1 r) \tag{63}$$
$$r > b \quad : \quad u(r) = B\,\mathrm{e}^{-\kappa r} \tag{64}$$

and we need to connect the $\sin(k_1 r)$ inside the well with the decreasing exponential outside the well, by equating the left and right values of the function and its first derivative in $r = b$.

If the well is too shallow, the sine will be a strictly increasing function inside the well, even for the maximum possible value $k_1 = k_0$ (see for example figure 8). When this is the case, it cannot then be smoothly connected

to the decreasing exponential for $r > b$. More precisely, the condition for connecting u and u' in $r = b$ imposes

$$k_1 \cot(k_1 b) = -\kappa \tag{65}$$

that we link to the relationship

$$k_1^2 + \kappa^2 = k_0^2 \tag{66}$$

to make a graphical resolution (figure 9). In the region ($k_1 > 0$, $\kappa > 0$), we have to find the intersection between the curve defined by (65), drawn in blue in figure 9 and the circle (66). We can see that the first bound state appears for $k_0 b = \pi/2$, the second bound state for $k_0 b = 3\pi/2$, etc. These thresholds of existence of the bound states match the divergences of the scattering length found above.

We can also check on this completely solvable case the link between the energies of the bound states and the poles of the scattering amplitude. The latter is calculated here from the phase shift $\delta_0(k)$ given in (58) and the relation (26). The energies of the first bound states are plotted in figure 10, as a function of the parameter k_0 controlling the well depth. We also show the approximate prediction $-\hbar^2/(2m_r a^2)$, giving the energy of the last bound state when it is close to the dissociation limit. This prediction is useful when a is very large, but we find that it quickly becomes inaccurate when we move away from this limit.

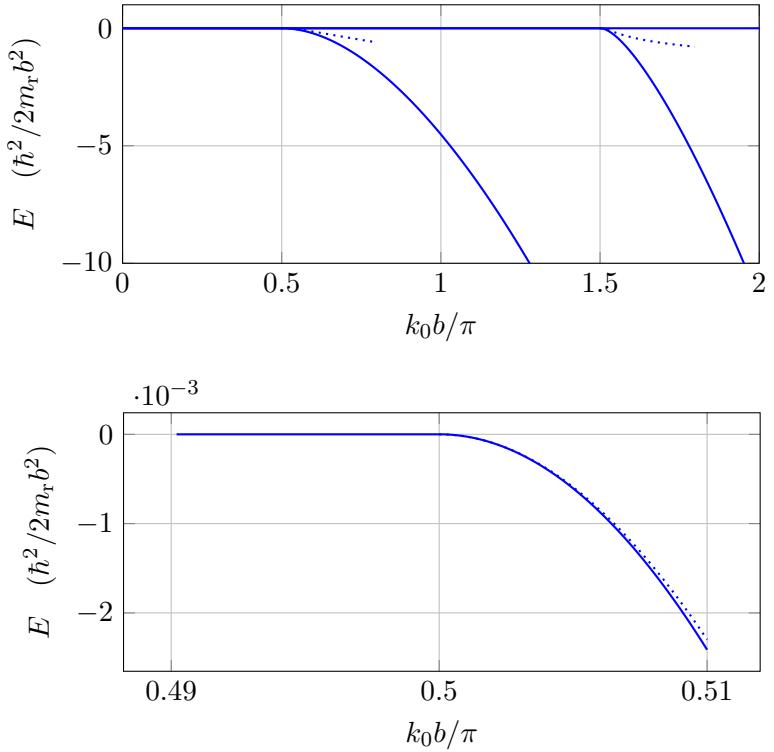

Figure 10. *Energies of the first bound states in a square potential well. The dotted curve indicates the approximate prediction $-\hbar^2/(2m_r a^2)$, valid near the dissociation threshold. The lower figure is an enlargement of the upper one near the threshold for the first bound state.*

4 Pseudo-potential and Bethe–Peierls condition

In what precedes, we have established the laws which govern the interactions between particles at low energy. This low-energy domain corresponds to the regime where the thermal wavelength of the particles $\lambda = 2\pi/k$ is large compared to the range b of the potential. Equivalently, the kinetic energy of the particles must be small in front of $\hbar^2/mb^2$. When this condition is fulfilled, the collisions occur mostly in the s-wave regime, at least when it is not forbidden by Pauli principle.

The scattering amplitude is then written:

$$\text{Low energy:} \qquad \frac{1}{f(k)} \approx -\frac{1}{a} - \mathrm{i}k + \frac{1}{2} r_e k^2 + \dots \tag{67}$$

The imaginary part of $f(k)$ in $\mathrm{i}k$ is imposed by the unitarity of quantum mechanics. The scattering length a and the effective range r_e are real quantities with the dimension of a length, characterizing the potential. In general, out of the vicinity of a resonance, a and r_e are of the order of b, i.e. of the order of R_{vdW} for the van der Waals potential. Thus, since the relevant k are such that $kb \ll 1$, the three contributions to $f(k)$ rank according to:

$$\frac{1}{|a|} \gg |\mathrm{i}k| \gg |r_e k^2|. \tag{68}$$

and it is then sufficient to know a, the correction in $r_e k^2$ having only a minor influence.

The scattering length thus plays a central role in the description of quantum gases. In most cases, knowing its value is sufficient to determine the collective properties of the fluid, whether static (e.g. equation of state) or dynamic: collective excitations such as phonons, solitons, vortices, or even demixing phenomena in multicomponent systems. Since it is the only relevant parameter, it is legitimate to replace the real potential by a model potential leading to the same scattering length.

The aim of this paragraph is to propose a simple model potential of zero range, leading to a purely isotropic scattering $f(k,\theta) = f(k)$ and whose expansion in k stops at order 1:

$$\frac{1}{f(k)} = -\frac{1}{a} - \mathrm{i}k, \tag{69}$$

so that the effective range will be zero. Note that this type of model potential admits at most one bound state, since we know that the energies of the bound states correspond to the poles of the scattering amplitude. More precisely if (69) is exact, there is only one pole $k = \mathrm{i}/a$ and the wave function $\propto \mathrm{e}^{\mathrm{i}kr} = \mathrm{e}^{-r/a}$ corresponds to a bound state if $a > 0$; the energy of this state is $-\hbar^2/(2m_{\mathrm{r}}a^2)$. There is no bound state if $a < 0$.

Satisfying this requirement is not obvious; we will start from a contact potential, proportional to the Dirac distribution $\delta(\boldsymbol{r})$, which seems the most natural choice, but we will almost immediately encounter mathematical difficulties related to the action of $\delta(\boldsymbol{r})$ on wave functions which behave like $1/r$ in the neighborhood of the origin. We will then switch to a regularized contact potential, the pseudo-potential, and show its equivalence with the Bethe–Peierls boundary condition.

4-1 Contact potential in position representation

We begin our analysis by explaining why a contact potential $\hat{V} = \bar{g}\,\delta(\boldsymbol{r})$ is not suitable, whereas its one-dimensional equivalent is quite legitimate. The contact potential is defined by its action on a wave function by

$$\hat{V}\,[\psi(\boldsymbol{r})] = \bar{g}\,\psi(0)\,\delta(\boldsymbol{r}), \quad \bar{g} \text{ real, positive or negative.} \tag{70}$$

A difficulty arises when we consider the wave function $\psi_{\boldsymbol{k}}(\boldsymbol{r})$ of a scattering state, calculated for example from the Born expansion.

Let us recall the principle of this expansion. We start from the Lippmann-Schwinger equation

$$\psi_{\boldsymbol{k}}(\boldsymbol{r}) = \mathrm{e}^{\mathrm{i}\boldsymbol{k}\cdot\boldsymbol{r}} + \int \mathcal{G}_0(\boldsymbol{r}-\boldsymbol{r}')\,\hat{V}\,[\psi_{\boldsymbol{k}}(\boldsymbol{r}')]\;\mathrm{d}^3r', \tag{71}$$

with the Green function associated to the Hamiltonian of a free particle:

$$\mathcal{G}_0(\boldsymbol{r}) = -\frac{m_{\mathrm{r}}}{2\pi\hbar^2}\,\frac{\mathrm{e}^{\mathrm{i}kr}}{r}. \tag{72}$$

We look for the solution of this equation in powers of the scattering potential, so here of the parameter $\bar{g}$:

$$\psi_{\boldsymbol{k}} = \psi_{\boldsymbol{k}}^{(0)} + \psi_{\boldsymbol{k}}^{(1)} + \psi_{\boldsymbol{k}}^{(2)} + \dots \tag{73}$$

We have $\psi_{\boldsymbol{k}}^{(0)}(\boldsymbol{r}) = \mathrm{e}^{\mathrm{i}\boldsymbol{k}\cdot\boldsymbol{r}}$ and the recurrence relation

$$\psi_{\boldsymbol{k}}^{(n+1)}(\boldsymbol{r}) = \int \mathcal{G}_0(\boldsymbol{r}-\boldsymbol{r}')\,\hat{V}\left[\psi_{\boldsymbol{k}}^{(n)}(\boldsymbol{r}')\right]\;\mathrm{d}^3r'. \tag{74}$$

The calculation of the first order term is straightforward:

$$\begin{aligned}\psi_{\boldsymbol{k}}^{(1)}(\boldsymbol{r}) &= \int \mathcal{G}_0(\boldsymbol{r}-\boldsymbol{r}')\,\hat{V}\left[\mathrm{e}^{\mathrm{i}\boldsymbol{k}\cdot\boldsymbol{r}'}\right]\;\mathrm{d}^3r' = \bar{g}\int \mathcal{G}_0(\boldsymbol{r}-\boldsymbol{r}')\,\delta(\boldsymbol{r}')\,\mathrm{d}^3r' \\ &= \bar{g}\,\mathcal{G}_0(\boldsymbol{r}) = -\frac{\bar{g}m_{\mathrm{r}}}{2\pi\hbar^2}\,\frac{\mathrm{e}^{\mathrm{i}kr}}{r}.\end{aligned} \tag{75}$$

However, a problem arises when we try to calculate the second order term in the expansion of $\psi_{\boldsymbol{k}}(\boldsymbol{r})$:

$$\begin{aligned}\psi_{\boldsymbol{k}}^{(2)}(\boldsymbol{r}) &= \int \mathcal{G}_0(\boldsymbol{r}-\boldsymbol{r}')\,\hat{V}\left[\psi_{\boldsymbol{k}}^{(1)}(\boldsymbol{r}')\right]\;\mathrm{d}^3r' \\ &= -\frac{\bar{g}m_{\mathrm{r}}}{2\pi\hbar^2}\int \mathcal{G}_0(\boldsymbol{r}-\boldsymbol{r}')\,\hat{V}\left[\frac{\mathrm{e}^{\mathrm{i}kr'}}{r'}\right]\;\mathrm{d}^3r'\end{aligned} \tag{76}$$

where we used the result (75) giving $\psi_{\boldsymbol{k}}$ at order 1 in V. We are led to act with the potential $\hat{V}$, thus the Dirac distribution, on a function which diverges in $\boldsymbol{r}' = 0$!

The action of $\delta(\boldsymbol{r})$ on the $1/r$ function has no well-defined mathematical meaning and we cannot use this $\delta(\boldsymbol{r})$ distribution as it is: we will have to regularize it and this will be the subject of § 4-3 and § 4-4. Before doing so, it is nevertheless useful to take up the problem of the "real" Dirac distribution in the momentum representation, i.e. to study the behavior of the elements of the scattering matrix $\hat{T}(E)$ between two plane waves.

4-2 Contact potential in momentum representation

In the preceding paragraph, we looked at the scattering states in the position representation and we were stuck at order 2 of the Born expansion, when we had to act with $\delta(\boldsymbol{r})$ on the function $\mathrm{e}^{\mathrm{i}kr}/r$. We now take up the same problem again, but in the momentum representation.

We again use the Born expansion, this time written in terms of the transition matrix $\hat{T}(E)$ introduced in Chapter II:

$$\hat{T}(E) \;= \hat{V} \;+ \hat{V}\frac{1}{E - \hat{H}_0 + \mathrm{i}0_+}\hat{V} \;+ \;\ldots, \qquad E = \frac{\hbar^2 k^2}{2m_{\mathrm{r}}}. \tag{77}$$

At order 1 in $\bar{g}$, computing the matrix element of $\hat{T}$ between any two momentum states $\boldsymbol{q}_1$ and $\boldsymbol{q}_2$ poses no problem[3] :

$$\text{Order 1}: \quad \langle \boldsymbol{q}_1|\hat{T}|\boldsymbol{q}_2\rangle = \langle \boldsymbol{q}_1|\hat{V}|\boldsymbol{q}_2\rangle = \bar{g}\int \mathrm{e}^{-\mathrm{i}\boldsymbol{q}_1\cdot\boldsymbol{r}}\;\delta(\boldsymbol{r})\;\mathrm{e}^{\mathrm{i}\boldsymbol{q}_2\cdot\boldsymbol{r}}\;\mathrm{d}^3r = \bar{g}. \tag{80}$$

Difficulties arise at order 2. By inserting the closure relation (79) for the momentum at the level of the free propagator $1/(E - \hat{H}_0 + \mathrm{i}0_+)$, we find:

$$\text{Order 2}: \quad \langle \boldsymbol{q}_1|\hat{T}|\boldsymbol{q}_2\rangle = \bar{g} + \frac{\bar{g}^2}{(2\pi)^3}\int \frac{1}{E - \varepsilon(q) + \mathrm{i}0_+}\,\mathrm{d}^3q, \tag{81}$$

with $\varepsilon(q) = \hbar^2 q^2/2m_{\mathrm{r}}$. Now the quantity

$$\mathcal{I}(E) = \frac{1}{(2\pi)^3}\int \frac{1}{E - \varepsilon(q) + \mathrm{i}0_+}\,\mathrm{d}^3q \tag{82}$$

is divergent when the integral is performed on q up to infinity. This problem is of course the same as the one encountered in the position representation, with the action of $\delta(\boldsymbol{r})$ on the function $1/r$.

Nevertheless, let us forget momentarily that $\mathcal{I}(E)$ is divergent. All orders of the Born series can be treated as we did above for order 1 and we end up with a geometric series which we can sum:

$$\begin{aligned}\langle \boldsymbol{q}_1|\hat{T}(E)|\boldsymbol{q}_2\rangle &= \bar{g}\Big\{1 \;+\; \bar{g}\,\mathcal{I}(E) \;+\; [\bar{g}\,\mathcal{I}(E)]^2 \;+\; \ldots\Big\} \\ &= \frac{\bar{g}}{1 - \bar{g}\,\mathcal{I}(E)}.\end{aligned} \tag{83}$$

We now see how to make sense of this formal summation by introducing a cutoff in the momentum space. We assume that the integral over the moments q does not extend to infinity, but stops at a cutoff value noted $q_{\max}$. The integral is then easily computed and we find (up to a term in $1/q_{\max}$):

$$\begin{aligned}\mathcal{I}(E) &= -\frac{m_{\mathrm{r}}}{\pi^2\hbar^2}\int_0^{q_{\max}} \frac{q^2}{q^2 - k^2 - i0_+}\,\mathrm{d}q \\ &= -\frac{m_{\mathrm{r}}}{\pi^2\hbar^2}\left(q_{\max} + \mathrm{i}\frac{\pi k}{2}\right).\end{aligned} \tag{84}$$

Generally, the scattering amplitude from the wave vector $\boldsymbol{k}$ to the wave vector $\boldsymbol{k}'$ is written as a function of the $\hat{T}$ matrix element (see chapter II):

$$f(\boldsymbol{k}, \boldsymbol{k}') = -\frac{m_{\mathrm{r}}}{2\pi\hbar^2}\langle \boldsymbol{k}'|\hat{T}|\boldsymbol{k}\rangle \tag{85}$$

which gives using (83) and (84):

$$\frac{1}{f(k)} = -\frac{2\pi\hbar^2}{m_{\mathrm{r}}}\left[\frac{1}{\bar{g}} - \mathcal{I}(E)\right] = -\frac{2\pi\hbar^2}{m_{\mathrm{r}}\bar{g}} - \frac{2q_{\max}}{\pi} - \mathrm{i}k. \tag{86}$$

[3] Recall that we set throughout this course (*cf.* chapter II):

$$\langle \boldsymbol{r}|\boldsymbol{q}\rangle = \mathrm{e}^{\mathrm{i}\boldsymbol{q}\cdot\boldsymbol{r}}, \qquad \langle \boldsymbol{r}|\boldsymbol{r}'\rangle = \delta(\boldsymbol{r} - \boldsymbol{r}'), \qquad \langle \boldsymbol{q}|\boldsymbol{q}'\rangle = (2\pi)^3\,\delta(\boldsymbol{q} - \boldsymbol{q}'), \tag{78}$$

so that the closure relations in momentum and position representation are written:

$$\hat{1} = \frac{1}{(2\pi)^3}\int |\boldsymbol{q}\rangle\langle \boldsymbol{q}|\,\mathrm{d}^3q = \int |\boldsymbol{r}\rangle\langle \boldsymbol{r}|\,\mathrm{d}^3r. \tag{79}$$

Let us first notice that we find the form requested in (69), in particular the imaginary part imposed by unitarity. Then, we can assign a scattering length to this problem thanks to the cut in momentum space:

$$\frac{1}{a} = \frac{2\pi\hbar^2}{m_{\rm r}\bar{g}} + \frac{2q_{\max}}{\pi}. \tag{87}$$

This expression is the basis of an approach to the problem in terms of renormalization. It is used for example to calculate the Lee-Huang-Yang correction to the energy of a weakly interacting Bose gas using the following steps (Pethick & Smith 2008a; Pitaevskii & Stringari 2016):

- The real (physical) scattering length a and the associated coupling g are assumed to be known:
$$g = \frac{2\pi\hbar^2 a}{m_{\rm r}} = \frac{4\pi\hbar^2 a}{m}. \tag{88}$$
- We give ourselves a bare coupling $\bar{g}$ and a cutoff $q_{\max}$ verifying (87), which is rewritten:
$$\frac{1}{g} = \frac{1}{\bar{g}} + Q_{\max} \qquad \text{with} \quad Q_{\max} = \frac{m_{\rm r} q_{\max}}{\pi^2\hbar^2} \tag{89}$$
or equivalently
$$\bar{g} = \frac{g}{1 - gQ_{\max}} \approx g(1 + gQ_{\max} + \ldots). \tag{90}$$
- The calculations are carried out for the contact potential $\bar{g}\,\delta(\boldsymbol{r})$, written in momentum representation within the second quantization formalism:
$$\frac{\bar{g}}{2L^3} \sum_{\boldsymbol{q}_1,\boldsymbol{q}_2,\boldsymbol{q}} \hat{a}^\dagger_{\boldsymbol{q}_1+\boldsymbol{q}} \hat{a}^\dagger_{\boldsymbol{q}_2-\boldsymbol{q}} \hat{a}_{\boldsymbol{q}_2} \hat{a}_{\boldsymbol{q}_1}, \tag{91}$$
with the parameters $\bar{g}$ and $Q_{\max}$. Finally, the result is expressed as a function of g. If the result is of order 1 in $\bar{g}$, we simply replace $\bar{g}$ by g, using (90) at order 0 in $Q_{\max}$. If the result contains terms going to a higher order in $\bar{g}$, as for the Lee-Huang-Yang correction, one performs a systematic expansion of each term using again (90). The final result for a physical quantity must be expressed in terms of g only, the $Q_{\max}$ terms having been eliminated.

For a more complete and rigorous implementation of this renormalization procedure, see Braaten, Kusunoki, et al. (2008).

4-3 The pseudo-potential

We now turn to the study of an interaction potential $\hat{V}$ of zero range which does not exhibit the singularities of the Dirac distribution. The lesson of the previous study is that we must "erase" the divergence in $\boldsymbol{r} = 0$ of the $\mathrm{e}^{\mathrm{i}kr}/r$ function. We wish to achieve this result without modifying the action of $\delta(\boldsymbol{r})$ when it acts on a regular function in $\boldsymbol{r} = 0$. There are many ways to achieve this goal [see Olshanii & Pricoupenko (2001)]. The simplest one was proposed by Huang & Yang (1957) [see also Breit (1947)], which consists in taking

$$\hat{V}_{\rm pp}\left[\psi(\boldsymbol{r})\right] = g\,\delta(\boldsymbol{r})\,\frac{\partial}{\partial r}\left[r\psi(\boldsymbol{r})\right]\Big|_{r=0}. \tag{92}$$

With this definition, any function $\psi(\boldsymbol{r})$ that diverges in 0 as

$$\psi(\boldsymbol{r}) = \frac{\alpha}{r} + \psi_{\rm reg}(\boldsymbol{r}) \tag{93}$$

with $\psi_{\rm reg}$ regular in 0, leads to a well-defined value for $\hat{V}_{\rm pp}\psi(\boldsymbol{r})$:

$$\hat{V}_{\rm pp}\left[\psi(\boldsymbol{r})\right] = g\,\psi_{\rm reg}(0) \tag{94}$$

whatever the value of α which is simply "erased". In particular, for the function $\mathrm{e}^{\mathrm{i}kr}/r$ which comes from the first order of Born expansion, we write

$$\frac{\mathrm{e}^{\mathrm{i}kr}}{r} = \frac{1}{r} + \psi_{\rm reg}(\boldsymbol{r}) \qquad \text{with} \quad \psi_{\rm reg}(\boldsymbol{r}) = \frac{\mathrm{e}^{\mathrm{i}kr} - 1}{r} \to \mathrm{i}k \ \text{ when } r \to 0, \tag{95}$$

and we obtain

$$\hat{V}_{\rm pp}\left[\frac{\mathrm{e}^{\mathrm{i}kr}}{r}\right] = \mathrm{i}gk\,\delta(\boldsymbol{r}). \tag{96}$$

It is remarkable that this simple prescription is sufficient to allow the calculation of all terms of the Born expansion giving the scattering states of the Hamiltonian

$$\hat{H} = -\frac{\hbar^2}{2m_{\rm r}}\nabla^2 + \hat{V}_{\rm pp}. \tag{97}$$

One could have feared that the terms of order 2,3,... lead to stronger divergences as $r^{-2}, r^{-3}, \ldots$, which would have required regularization procedures with increasing complexity. Fortunately, this is not the case, as can be seen by examining the second order term. Taking its expression from where we left it [cf. (76)] and using (96), we obtain:

$$\psi_{\boldsymbol{k}}^{(2)}(\boldsymbol{r}) = \frac{-gm_{\rm r}}{2\pi\hbar^2}(\mathrm{i}gk)\int \mathcal{G}_0(\boldsymbol{r}-\boldsymbol{r}')\,\delta(\boldsymbol{r}')\,\mathrm{d}^3r' = \mathrm{i}k\left(\frac{-gm_{\rm r}}{2\pi\hbar^2}\right)^2\frac{\mathrm{e}^{\mathrm{i}kr}}{r}. \quad (98)$$

Order 2 has therefore the same mathematical structure in $\mathrm{e}^{\mathrm{i}kr}/r$ as order 1, and it differs from it only by its prefactor independent of r.

The quantity $gm_{\rm r}/2\pi\hbar^2$ has the dimension of a length and (anticipating a little) we will note it

$$a \equiv \frac{gm_{\rm r}}{2\pi\hbar^2}. \quad (99)$$

We will indeed see that a is equal to the scattering length for this pseudo-potential.

Scattering state for the pseudo-potential. The result of the calculation of the scattering state at order 2 reads

$$\psi_{\boldsymbol{k}}(\boldsymbol{r}) = \mathrm{e}^{\mathrm{i}\boldsymbol{k}\cdot\boldsymbol{r}} - a\frac{\mathrm{e}^{\mathrm{i}kr}}{r} + \mathrm{i}a^2k\frac{\mathrm{e}^{\mathrm{i}kr}}{r} + \ldots \quad (100)$$

The calculation of the following orders is then not a problem. The recurrence relation (74) allows to express the order $n+1$ as a function of the order n:

$$\psi_{\boldsymbol{k}}^{(n+1)}(\boldsymbol{r}) = \int \mathcal{G}_0(\boldsymbol{r}-\boldsymbol{r}')\,\hat{V}_{\rm pp}\left[\psi_{\boldsymbol{k}}^{(n)}(\boldsymbol{r}')\right]\,\mathrm{d}^3r', \quad (101)$$

which gives

$$\psi_{\boldsymbol{k}}^{(n+1)}(\boldsymbol{r}) = -\mathrm{i}ka\;\psi_{\boldsymbol{k}}^{(n)}(\boldsymbol{r}) = (-\mathrm{i}ka)^n\,\psi_{\boldsymbol{k}}^{(1)}(\boldsymbol{r}). \quad (102)$$

Thanks to this recurrence relation, the scattering state is obtained from the geometric series

$$\sum_{n=0}^{\infty}(-\mathrm{i}ka)^n = \frac{1}{1+\mathrm{i}ka} \quad (103)$$

hence the result:

$$\psi_{\boldsymbol{k}}(\boldsymbol{r}) = \mathrm{e}^{\mathrm{i}\boldsymbol{k}\cdot\boldsymbol{r}} + \frac{1}{1+\mathrm{i}ka}\psi_{\boldsymbol{k}}^{(1)}(\boldsymbol{r}) \quad (104)$$

or

$$\psi_{\boldsymbol{k}}(\boldsymbol{r}) = \mathrm{e}^{\mathrm{i}\boldsymbol{k}\cdot\boldsymbol{r}} - \frac{a}{1+\mathrm{i}ka}\frac{\mathrm{e}^{\mathrm{i}kr}}{r}. \quad (105)$$

This state is associated with the scattering amplitude

$$f(k) = -\frac{a}{1+\mathrm{i}ka} \qquad \Leftrightarrow \qquad \frac{1}{f(k)} = -\frac{1}{a} - \mathrm{i}k. \quad (106)$$

As an exercise, we can check directly that $\psi_{\boldsymbol{k}}$ is a solution of the Schrödinger equation

$$-\frac{\hbar^2}{2m_{\rm r}}\nabla^2\psi(\boldsymbol{r}) + \hat{V}_{\rm pp}\left[\psi(\boldsymbol{r})\right] = E\,\psi(\boldsymbol{r}) \qquad \text{with} \quad E = \frac{\hbar^2k^2}{2m_{\rm r}}. \quad (107)$$

For this we use

$$\nabla^2\left(\frac{\mathrm{e}^{\mathrm{i}kr}}{r}\right) = \nabla^2\left(\frac{1}{r}\right) + \nabla^2\left(\frac{\mathrm{e}^{\mathrm{i}kr}-1}{r}\right) \qquad \text{with} \quad \nabla^2\left(\frac{1}{r}\right) = -4\pi\,\delta(\boldsymbol{r}) \quad (108)$$

and for the radially symmetric regular function $f(r) = (\mathrm{e}^{\mathrm{i}kr}-1)/r$:

$$\nabla^2 f = \frac{1}{r}\frac{\mathrm{d}^2}{\mathrm{d}r^2}(rf) = (\mathrm{i}k)^2\frac{\mathrm{e}^{\mathrm{i}kr}}{r}. \quad (109)$$

This verification shows that the validity of the expression of $\psi_{\boldsymbol{k}}$ is not linked to the convergence of the geometric series (103).

There are several important points to make about this result:

- The scattering amplitude does not depend on the angle θ, while we did not make the assumption that k was small. The pseudo-potential has the peculiarity to scatter only in the s-wave, whatever the collision energy.
- The expression (105) of the scattering state is not only asymptotic as for a non-zero range potential: it is valid at any point $\boldsymbol{r}$ different from the origin.

- The quantity that we have noted a corresponds indeed to the scattering length, defined as $-\lim_{k\to 0} f(k)$.
- The imaginary part of $1/f(k)$ is indeed equal to $-\mathrm{i}k$, as required from unitarity.
- The expression on the right-hand side of (106), which holds regardless of k, shows that the effective range r_e of the pseudopotential is zero.
- All scattering states behave identically in the neighborhood of $r = 0$:

$$r \to 0 : \qquad \psi_{\boldsymbol{k}}(\boldsymbol{r}) \propto \frac{1}{r} - \frac{1}{a} + \mathcal{O}(r). \tag{110}$$

  This point will play a central role in deriving the Bethe-Peierls boundary condition.

Bound state of the pseudo-potential. In a one-dimensional contact potential, $V(x) = g\,\delta(x)$, we find one (and only one) bound state if and only if the coefficient g is negative. It is almost the same for the 3D case, with one major difference: the potential $\hat{V}_{\rm pp}\left[\psi(\boldsymbol{r})\right] = g\,\delta(\boldsymbol{r})\frac{\partial}{\partial r}\left[r\psi(\boldsymbol{r})\right]$ admits one (and only one) bound state if and only if g is positive !

To show this result, the quickest way is to use the fact (already mentioned several times) that the bound states, when they exist, correspond to the poles of the scattering amplitude. In the present case, we know the exact expression of the scattering amplitude [*cf.* (106)]. It has a single pole

$$1 + \mathrm{i}ka = 0 \quad \Rightarrow \quad k = \frac{\mathrm{i}}{a}, \quad E = -\frac{\hbar^2}{2m_{\rm r}a^2} \tag{111}$$

and this pole corresponds to an acceptable physical bound state if and only if the corresponding state $\sim \mathrm{e}^{\mathrm{i}kr}/r = \mathrm{e}^{-r/a}/r$ is normalizable. It is therefore necessary that a and consequently g are positive.

More precisely, we can check explicitly that the state

$$\psi_{\rm bound}(\boldsymbol{r}) = \frac{\mathrm{e}^{-r/a}}{r} \tag{112}$$

is a solution of the Schrödinger equation (107) for the energy $E = -\hbar^2/(2m_{\rm r}a^2)$. We use for that [*cf.* (108) and (109)]

$$\nabla^2\left[\frac{\mathrm{e}^{-r/a}}{r}\right] = -4\pi\delta(\boldsymbol{r}) + \frac{1}{a^2}\frac{\mathrm{e}^{-r/a}}{r} \tag{113}$$

and

$$\hat{V}_{\rm pp}\left[\frac{\mathrm{e}^{-r/a}}{r}\right] = g\,\delta(\boldsymbol{r})\frac{\mathrm{d}}{\mathrm{d}r}\left(r\frac{\mathrm{e}^{-r/a}}{r}\right) = -\frac{g}{a}\delta(\boldsymbol{r}), \tag{114}$$

hence the result since $g = 2\pi\hbar^2 a/m_{\rm r}$. We notice that the variation around $r = 0$ of this bound state is identical to that of the scattering states [*cf.* (110)]:

$$r \to 0 : \qquad \psi_{\rm bound}(\boldsymbol{r}) \propto \frac{1}{r} - \frac{1}{a} + \mathcal{O}(r). \tag{115}$$

4-4 The Bethe-Peierls boundary condition

When looking for the eigenstates of the Hamiltonian in the presence of the pseudo-potential, we have found wave functions varying like $1/r$ in the neighborhood of the origin. This kind of variation is unusual[4]: when $V(\boldsymbol{r})$ is a continuous function of r, possibly divergent in $r = 0$ like the Coulomb potential, the eigenstates in the vicinity of $r = 0$ vary as $\psi(\boldsymbol{r}) = \beta_0 + \mathcal{O}(r)$, where $\mathcal{O}(r)$ represents a term tending to 0 at least linearly when $r \to 0$. The appearance of a $1/r$ term in the eigenstates calls for several remarks:

- The variation in $1/r$ near the origin remains compatible with the fact that the function is square-integrable. Indeed, the integral

$$\int \left(\frac{1}{r}\right)^2 \mathrm{d}^3r = \int \left(\frac{1}{r}\right)^2 4\pi r^2\,\mathrm{d}r \tag{116}$$

  is convergent in $r = 0$. This would not be the case if the divergence were more violent (like $1/r^2$ for example).
- In the presence of the pseudo-potential $\hat{V}_{\rm pp}$, the eigenstates are written in the neighborhood of $r = 0$

$$\psi(\boldsymbol{r}) = \frac{\beta_{-1}}{r} + \beta_0 + \mathcal{O}(r), \tag{117}$$

[4] This variation cannot show up for the eigenstates of the Hamiltonian in a regular potential, as shown by the following reasoning. Suppose that ψ contains such a term, $\psi(\boldsymbol{r}) = \alpha_1/r + \psi_{\rm reg}(\boldsymbol{r})$ where $\psi_{\rm reg}$ is non-divergent in $r = 0$. When we apply $H = -\frac{\hbar^2}{2m_{\rm r}}\nabla^2 + V(\boldsymbol{r})$ on ψ, the Laplacian of the kinetic energy acting on the term in $1/r$ gives $\nabla^2\,(1/r) = -4\pi\,\delta(\boldsymbol{r})$. If the potential $V(\boldsymbol{r})$ does not itself contain a term proportional to the Dirac distribution to compensate for this $\delta(\boldsymbol{r})$ coming from the kinetic energy, the function ψ will not satisfy $\hat{H}\psi(\boldsymbol{r}) = E\,\psi(\boldsymbol{r})$.

where the term in $\mathcal{O}(r)$ can be expanded into a series $\sum_{n\geq 1}\beta_n(\theta,\varphi)\,r^n$. The fact that an additional β_{-1}/r term appears in this expansion could lead one to think that the set of functions accessible through the pseudo-potential has been "enlarged": the β_{-1} coefficient seems to provide an additional degree of freedom with respect to the $\{\beta_0,\beta_1,\beta_2,\ldots\}$ coefficients. This is not the case; indeed, for a pseudopotential of fixed scattering length a, we found that all eigenstates of H , whether free or bound, behave as

$$\psi(\boldsymbol{r}) \propto \frac{1}{r} - \frac{1}{a} + \mathcal{O}(r). \tag{118}$$

The coefficients β_{-1} and β_0 are therefore not independent, but related by $\beta_{-1} = -a\beta_0$.

This discussion suggests the equivalence between the following two points of view:

- The strategy adopted in 4-3 consists in adding the pseudo-potential $\hat{V}_{\rm pp}$ to the kinetic energy term. We then compute the eigenstates (bound or free) of the Hamiltonian

$$\hat{H} = -\frac{\hbar^2}{2m_{\rm r}}\nabla^2 + \hat{V}_{\rm pp}. \tag{119}$$

  We deduce that all these eigenstates behave as (118) and so does any physically acceptable wave function of the system, which must be written as a linear combination of the eigenstates of $\hat{H}$.

- We "forget" $\hat{V}_{\rm pp}$ and we work with the Hamiltonian of a free particle for the relative motion:

$$\hat{H}_0 = -\frac{\hbar^2}{2m_{\rm r}}\boldsymbol{\nabla}^2, \tag{120}$$

  but any physically acceptable wave function of the system is required to behave as

$$\psi(\boldsymbol{r}) \propto \frac{1}{r} - \frac{1}{a} \;+\; \mathcal{O}(r) \tag{121}$$

  in the vicinity of $\boldsymbol{r}=0$ or equivalently

$$\left.\frac{\mathrm{d}}{\mathrm{d}r}[r\psi(r)]\right|_{r=0} = -\frac{1}{a}[r\psi(r)]_{r=0}. \tag{122}$$

This point of view, introduced by Bethe & Peierls (1935) [see also Wigner (1933)], is often favored when one wishes to deal with systems with more than two particles. One takes into account the interactions between particles by imposing that the N-body wave function verifies for any pair (i,j) [see for example Werner & Castin (2012) for bosons]:

$$r_{ij}\to 0: \qquad \Psi(\boldsymbol{r}_1,\ldots,\boldsymbol{r}_N) = \left(\frac{1}{r_{ij}} - \frac{1}{a}\right) A_{ij}\left[\boldsymbol{R}_{ij},\{r_k\}_{k\neq i,j}\right] \;+\; \mathcal{O}(r_{ij}) \tag{123}$$

where A_{ij} is a regular function of the coordinates of the $N-2$ other particles and of $R_{ij} = (\boldsymbol{r}_i+\boldsymbol{r}_j)/2$.

The action of $\hat{H}_0$ on the eigenstates of $\hat{H}$ found in (105) and (112) is

$$\hat{H}_0\psi_{\boldsymbol{k}}(\boldsymbol{r}) = \frac{\hbar^2k^2}{2m_{\rm r}}\,\psi_{\boldsymbol{k}}(\boldsymbol{r}) \;-\; \frac{a}{1+\mathrm{i}ka}\,\frac{2\pi\hbar^2}{m_{\rm r}}\,\delta(\boldsymbol{r}) \tag{124}$$

for the scattering states and

$$\hat{H}_0\psi_{\rm bound}(\boldsymbol{r}) = -\frac{\hbar^2}{2m_{\rm r}a^2}\,\psi_{\rm bound}(\boldsymbol{r}) \;+\; \frac{2\pi\hbar^2}{2m_{\rm r}}2m_{\rm r}\,\delta(\boldsymbol{r}) \tag{125}$$

for the bound state. In this point of view, $\boldsymbol{r}=0$ is singular since all the wave functions are infinite at this point and it is simpler to write

$$\text{At any point } \boldsymbol{r}\neq 0: \qquad \hat{H}_0\psi_{\boldsymbol{k}} = \frac{\hbar^2k^2}{2m_{\rm r}}\psi_{\boldsymbol{k}}, \tag{126}$$

and for $a>0$:

$$\text{At any point } \boldsymbol{r}\neq 0: \qquad \hat{H}_0\psi_{\rm bound} = -\frac{\hbar^2}{2m_{\rm r}a^2}\psi_{\rm bound}, \tag{127}$$

and then modify slightly the definition of the scalar product of two functions

$$\langle\psi_2|\psi_1\rangle = \int' \psi_2^*(\boldsymbol{r})\,\psi_1(\boldsymbol{r})\,\mathrm{d}^3r \tag{128}$$

where the symbol $\int'$ means that we take the integral over the whole space except a ball centered in 0, whose radius is made to tend to 0. With this definition, we have $\int'\delta(\boldsymbol{r})f(\boldsymbol{r}) = 0$ for any function f. This redefinition of the scalar product allows us to state that the $\psi_{\boldsymbol{k}}$ (completed by $\psi_{\rm bound}$ when $a>0$) form an orthogonal basis of the space of wave functions of a system of scattering length a, this basis being an eigenbasis of the kinetic energy Hamiltonian in the sense of (126) and (127).

Domain of the Hamiltonian. The boundary condition (121), which must be satisfied by any physically acceptable wave function, defines the *domain of the Hamiltonian*. It can be compared to the treatment of the 1D infinite square well in the introductory courses to quantum physics: to describe the motion of a particle on the segment $x \in [0, L]$, we take a purely kinetic Hamiltonian, $\hat{H}_0 = -\frac{\hbar^2}{2m}\frac{\mathrm{d}^2}{\mathrm{d}x^2}$, and we impose on any physically acceptable wave function to cancel out at $x = 0$ and $x = L$, which constitutes the domain of the Hamiltonian in this case.

It is essential to work only with functions in this domain, in order to avoid inconsistencies in the results. In the case of the 1D infinite square well, Castin & Werner (2012) provide the very simple example of the constant function $1/\sqrt{L}$, which has zero kinetic energy while the energies of the eigenstates, satisfying the boundary conditions $\psi(0) = \psi(L) = 0$, are strictly positive: $E_n = n^2 E_1$ with n strictly positive integer and the ground state energy $E_1 = \pi^2\hbar^2/(2mL^2)$. This apparent violation of the theorem

$$\forall \psi : \qquad \langle\psi|\hat{H}_0|\psi\rangle \geq E_1 \tag{129}$$

is simply due to the fact that $\psi(x) = 1/\sqrt{L}$ has been chosen outside the domain of $\hat{H}_0$, thus not allowed.

In the 3D case of interest here, a simple example of the importance of respecting the domain of the Hamiltonian is obtained for the $g < 0$ case. We know that there is no bound state in this case, and that a basis of eigenfunctions is provided by the scattering states, which all have a positive energy. We deduce that for any physical state of the system, the average energy $E(\psi) = \langle\psi|\hat{H}|\psi\rangle$ must also be positive. Nevertheless, if we consider a Gaussian function $\psi(\boldsymbol{r}) \propto \exp(-r^2/4\sigma^2)$, we can find values of σ leading to $E(\psi) < 0$. The reason is simple: this Gaussian function does not verify the boundary condition (121) and is therefore not eligible as a possible state of the system. One can consult the lecture notes by Castin (2007) for a more detailed discussion of this point.

What is the value of the kinetic energy? The answer to this question is tricky for potentials of zero range, whether one uses $\hat{V}_{\mathrm{pp}}$ or the Bethe–Peierls boundary condition. Let us start by recalling that for sufficiently regular wave functions in $r = 0$, the kinetic energy term can be computed indifferently from both members of the equality

$$-\frac{\hbar^2}{2m_{\mathrm{r}}}\int \psi^*(\boldsymbol{r})\,\boldsymbol{\nabla}^2\psi(\boldsymbol{r})\,\mathrm{d}^3r = +\frac{\hbar^2}{2m_{\mathrm{r}}}\int \boldsymbol{\nabla}\left(\psi^*(\boldsymbol{r})\right)\cdot\boldsymbol{\nabla}\left(\psi(\boldsymbol{r})\right)\,\mathrm{d}^3r. \tag{130}$$

which is obtained by an integration by parts, assuming that the wave function decreases sufficiently fast at infinity.

The problem becomes more complicated when we handle functions that vary like $1/r$ in the neighborhood of $\boldsymbol{r} = 0$. In the left-hand side, $\boldsymbol{\nabla}^2\psi(\boldsymbol{r})$ contains $\delta(\boldsymbol{r})$ and the quantity $\int \psi^*(\boldsymbol{r})\delta(\boldsymbol{r})\mathrm{d}^3r$ is not defined. In the right-hand side, $\boldsymbol{\nabla}\psi$ and $\boldsymbol{\nabla}\psi^*$ each vary as $1/r^2$, so that we end up with an integral of type $\int_0 r^{-2}\,\mathrm{d}r$, which is divergent.

When we take the option of using the Bethe-Peierls boundary condition, we can make sense of the left-hand side member, provided we replace $\int$ by $\int'$ as we saw above. But the result is then the total energy, for example $-\hbar^2/2m_{\mathrm{r}}a^2$ for the bound state. It is obviously not the kinetic energy which must always be positive.

We therefore arrive at the following conclusion for eigenstates in a zero-range potential: whether one uses $\hat{V}_{\mathrm{pp}}$ or the Bethe–Peierls boundary condition, the average kinetic energy, computed thanks to the right-hand side of (130), is infinite (and positive) and the interaction energy is infinite (and negative); only the sum of the two is a finite quantity, equal to $+\hbar^2k^2/2m_{\mathrm{r}}$ for a scattering state and $-\hbar^2/2m_{\mathrm{r}}a^2$ for the bound state. To give a precise meaning to each of the two components of the energy, we have to go back to a potential of non-zero range b.

The fact that the kinetic energy is infinite in the case studied here can be understood simply by looking at the behavior of the momentum distribution of the states for large values of $\boldsymbol{q}$. For a wave function $\psi(\boldsymbol{r})$, the momentum distribution is given by $n(\boldsymbol{q}) = |\tilde{\psi}(\boldsymbol{q})|^2$, where $\tilde{\psi}(\boldsymbol{q})$ is the Fourier transform of $\psi(\boldsymbol{r})$. Now, we know that the Fourier transform of $1/r$ is, to within one numerical coefficient, $1/q^2$:

$$2\pi^2\frac{1}{r} = \int \frac{1}{q^2}\mathrm{e}^{\mathrm{i}\boldsymbol{q}\cdot\boldsymbol{r}}\,\mathrm{d}^3q. \tag{131}$$

Since a function $\psi(\boldsymbol{r})$ satisfying the Bethe-Peierls boundary condition diverges as $1/r$ at the origin (except if $a = 0$), the dominant term of the momentum distribution of this function for large moments is $n(\boldsymbol{q}) \propto |1/q^2|^2 =$

$1/q^4$. We then immediately understand that the 3D integral giving the kinetic energy

$$E_{\mathrm{kin}} = \int \frac{\hbar^2 q^2}{2m_{\mathrm{r}}}\, n(\boldsymbol{q})\ \mathrm{d}^3 q \tag{132}$$

is divergent. This divergence plays a central role in the formalism of the Tan contact.

Chapter IV

Van der Waals Interaction and Low-Energy Universality

The previous chapters were devoted to the general formalism allowing to study the interaction between two particles. Among the main results, we have established that at low energy and for a potential $V(r)$ decreasing fast enough when $r \to \infty$, the interaction can be characterized by a single number, the scattering length. The goal of this chapter is to apply these results to a realistic atomic potential, varying as $-1/r^6$ at large distances.

For the species commonly used in cold atom experiments, the potential $V(r)$ describing the interaction between two atoms contains many vibrational states. It follows that the theoretical study of the problem can be performed using a semi-classical approach, based on the WKB (Wentzel–Kramers–Brillouin) method, with some subtleties that we will describe. The WKB approach leads to a remarkable universality of the result, linking the value of the scattering length to the energy of the weakly bound states in the interatomic potential[1].

We will also present the most accurate experimental method currently available to determine the position of the last bound states. This method, called *two-color photo-association*, allows to deduce the scattering length thanks to the universality mentioned above. It consists in measuring the rate of formation of weakly bound dimers in a gas of ultra-cold atoms illuminated by a pair of resonant light beams.

[1] I thank Raphaël Lopes and Sylvain Nascimbene for several enlightening discussions on this subject.

1 The semi-classical approximation

The square well studied at the end of the previous chapter is one of the rare examples of potentials where we have an exact analytical solution to the scattering problem. In the general case, one must resort to numerical calculations or approximate methods. Among these, the WKB method is particularly well adapted to the situation we are interested in. It requires a potential which varies continuously with distance and which has many bound states. These two conditions are fulfilled for the case of the interaction potential between neutral atoms.

In this first section we will recall the main ingredients of the semi-classical approximation. For more details, we refer the reader to the book by Schiff (1968) and to the review article by Berry & Mount (1972).

1-1 Principle of the approximation

The semi-classical method consists in searching for the solutions of the one-dimensional Schrödinger equation

$$-\frac{\hbar^2}{2m_{\mathrm{r}}}V(x) + V(x) = E(x) \tag{1}$$

in the form $\psi(x) = \exp(\mathrm{i}S(x)/\hbar)$ and expand $S(x)$ in "powers of $\hbar$":

$$S(x) = S_0(x) + \hbar S_1(x) + \hbar^2 S_2(x) + \dots , \tag{2}$$

$\hbar$ being formally treated as a small parameter. This is of course an abuse of language since the small parameter of a perturbative expansion must in principle be dimensionless. We will give a more precise criterion of the validity of the approximation later on.

The Schrödinger equation is written as a function of $S(x)$.

$$S'^2 - \mathrm{i}\hbar S'' = 2m_\mathrm{r}\left[E - V(x)\right]. \tag{3}$$

At order 0 in $\hbar$, we obtain

$$\text{Order 0:} \qquad S_0'^2 = 2m_\mathrm{r}\left[E - V(x)\right], \tag{4}$$

whose solution is written according to the relative value of the energy E and the potential $V(x)$:

- allowed region $E > V(x)$:

$$S_0'(x) = \pm p(x) \qquad \text{with} \quad p(x) = \sqrt{2m_\mathrm{r}(E - V(x))}, \tag{5}$$

- forbidden region $E < V(x)$:

$$S_0'(x) = \pm \mathrm{i}p(x) \qquad \text{with} \quad p(x) = \sqrt{2m_\mathrm{r}(V(x) - E)}. \tag{6}$$

At order 1, we find

$$\text{Order 1:} \qquad 2S_0'S_1' - \mathrm{i}S_0'' = 0 \quad \Rightarrow \quad S_1' = \mathrm{i}\frac{S_0''}{2S_0'}, \tag{7}$$

whose solution is $\frac{\mathrm{i}}{2}\log(p(x))$.

By limiting ourselves to this order of calculation, we have the approximate solutions:

$$\text{allowed region:} \qquad \psi(x) = \frac{C}{\sqrt{k(x)}}\exp\left(\pm\mathrm{i}\int^x k(x')\,\mathrm{d}x'\right) \tag{8}$$

$$\text{forbidden region:} \qquad \psi(x) = \frac{C}{\sqrt{\kappa(x)}}\exp\left(\pm\int^x \kappa(x')\,\mathrm{d}x'\right), \tag{9}$$

where $p(x) = \hbar k(x)$ in the allowed region and $p(x) = \hbar\kappa(x)$ in the forbidden region.

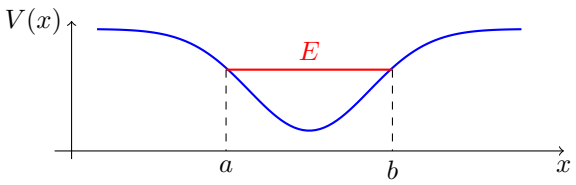

Figure 1. *Semi-classical approximation in a potential well. The connection at the turning points a and b is made using the conditions (12,13).*

The physical interpretation of this semi-classical expression is interesting. At least in the allowed region, it is a mixture of wave physics, with the oscillating phase which can give rise to an interference phenomenon, and corpuscular physics, with the prefactor whose square modulus $\propto 1/p(x)$ expresses the fact that the density of a fluid is inversely proportional to its velocity, for a given flux[2].

1-2 First condition of validity: continuity

A necessary condition for the validity of the above expansion is related to the hypothesis $S'^2 \gg \hbar|S''|$, i.e.

$$\left|\frac{\mathrm{d}}{\mathrm{d}x}\left(\frac{\hbar}{S'}\right)\right| \ll 1. \tag{10}$$

Let us consider for example the allowed region. The quantity $\hbar/S' = 1/k(x)$ represents, to within a factor of $1/2\pi$, the de Broglie wavelength $\lambda(x)$ of the particle. The validity criterion is therefore written:

$$\frac{1}{2\pi}\left|\frac{\mathrm{d}\lambda}{\mathrm{d}x}\right| \ll 1. \tag{11}$$

which is indeed a condition on a dimensionless parameter.

The criterion of validity (11) consists in imposing that the wavelength and thus the potential $V(x)$ vary little on the length scale λ. This excludes in particular:

[2] a phenomenon well known to all drivers who have experienced accordion-like traffic on a congested road...

- Any discontinuous potential, since λ does not then have the same value on each side of the discontinuity; the square well studied in the previous chapter cannot be treated by the semi-classical method.

- The "classical turning points" in a regular potential well like the one in figure 1, i.e. the points where $E = V(x)$; indeed, the de Broglie wavelength diverges at these points since the classical velocity cancels out there, and the constraint (11) cannot be satisfied. We will see in the next paragraph how to handle such points.

- For a continuous potential and outside the turning points, some areas can also be excluded. This is precisely the case for the potential in $1/r^6$, as we will see when we deal with the *quantum reflection* phenomenon.

1-3 Quantification of energy in a well

Let us consider the problem represented in figure 1, where a particle of energy E is confined in a potential well. To derive a quantization condition on the energy, we need to start from the constraint on the wave function in the two forbidden regions to the left and to the right of the well. In both cases, we want the wave function to tend to 0 when $|x| \to \infty$. This imposes the choice $\exp\left(-\int_x^a \kappa(x')\mathrm{d}x'\right)$ in the left forbidden region and $\exp\left(-\int_b^x \kappa(x')\mathrm{d}x'\right)$ in the right forbidden region

Then, we must analyze the consequences of these conditions on the wave function in the allowed region. To do this, we have to get around the difficulty mentioned at the end of the previous paragraph, which indicates that the semi-classical approximation is not valid around a turning point. The standard method to connect the allowed and forbidden regions is to linearize the potential in the neighborhood of this point. We can then take advantage of the fact that we know the exact solutions of the Schrödinger equation in a linear potential (they are Airy functions) and we can use their asymptotic form on both sides of the turning point to connect to the WKB wave functions. We will come back to the validity of this connection in the next paragraph.

All calculations done, we arrive at the following rule at the turning point a:

$$\frac{1}{\sqrt{\kappa(x)}}\exp\left(-\int_x^a \kappa\,\mathrm{d}x'\right) \longrightarrow \frac{2}{\sqrt{k(x)}}\sin\left(\int_a^x k\,\mathrm{d}x' + \frac{\pi}{4}\right) \tag{12}$$

and at the turning point b:

$$\frac{1}{\sqrt{\kappa(x)}}\exp\left(-\int_b^x \kappa\,\mathrm{d}x'\right) \longrightarrow \frac{2}{\sqrt{k(x)}}\sin\left(\int_x^b k\,\mathrm{d}x' + \frac{\pi}{4}\right). \tag{13}$$

A little algebra then allows us to show that the two expressions (12,13) for the allowed region are compatible with each other if and only if

$$\int_a^b k(x',E)\,\mathrm{d}x' = \left(j - \frac{1}{2}\right)\pi. \tag{14}$$

with j non-zero integer: $j = 1, 2, \ldots$.

For a harmonic potential, we can check that this condition leads to the exact quantization of the energy levels. Note that in general, the semi-classical approximation is not intended to give precisely the least excited states because the validity criterion (11) is generally not satisfied for these states.

The result (14) is obtained by assuming a smooth potential at the two turning points a and b. If there is a hard-core potential on one side and a smooth one on the other side, this result is slightly modified. If we take for example a hard core in a, the WKB function must be $\frac{2}{\sqrt{k}}\sin\left(\int_a^x k\,\mathrm{d}x'\right)$ instead of (12). The quantization condition then becomes

With a hard core on one side: $$\int_a^b k(x',E)\,\mathrm{d}x' = \left(j - \frac{1}{4}\right)\pi. \tag{15}$$

Finally, if we assume that there is a hard core in both a and b, the additional term $1/4$ disappears and we get:

With a hard core on each side: $$\int_a^b k(x',E)\,\mathrm{d}x' = j\,\pi. \tag{16}$$

1-4 Second condition of validity: connection

In the previous paragraph we described the connection procedure at a point $x = b$ at the boundary between permitted and forbidden regions.

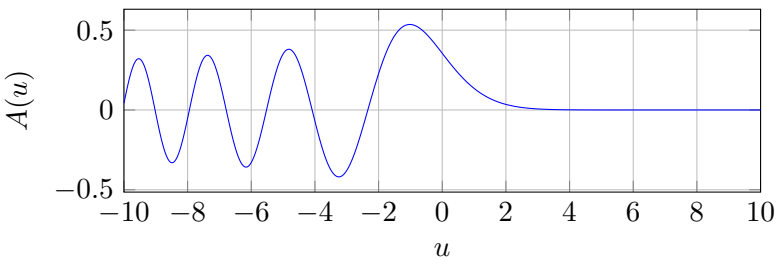

Figure 2. *Airy function, solution of (18).*

We have indicated that we replace the potential $V(x)$ in this region by its linear approximation:

$$V(x) \approx V(b) + (x-b)V'(b) \tag{17}$$

We then use the exact solution in this linear potential, which is an Airy function. Recall that the generic Airy function $\mathrm{A}(u)$ is defined as a solution of

$$-\frac{\mathrm{d}^2\mathrm{A}}{\mathrm{d}u^2} + u\mathrm{A}(u) = 0, \tag{18}$$

which is effectively a 1D Schrödinger equation by taking $\hbar = 1$, $2m_\mathrm{r} = 1$, a linear potential $V(u) = u$ and the energy $E = 0$.

This function is plotted in figure 2. Its asymptotic regime on either side of $u = 0$ is written:

$$u \gg 1 \quad : \qquad \mathrm{A}(u) \sim \frac{1}{2\sqrt{\pi}}, \frac{\exp\left(-\frac{2}{3}u^{3/2}\right)}{u^{1/4}} \tag{19}$$

$$u \ll -1 \quad : \qquad \mathrm{A}(u) \sim \frac{1}{\sqrt{\pi}} \frac{\sin\left(\frac{2}{3}|u|^{3/2} + \frac{\pi}{4}\right)}{|u|^{1/4}}. \tag{20}$$

We recognize in these asymptotic expressions the behaviors of the WKB functions given in (8) and (9), taking:

$$k(u) = \sqrt{|u|} \quad \Rightarrow \quad \int_0^{|u|} k(u)\,\mathrm{d}u = \frac{2}{3}|u|^{3/2}. \tag{21}$$

For the energy $E = V(b)$, the Schrödinger equation in the linearized potential (17) reduces to (18) by

$$u = \frac{x-b}{\ell_\mathrm{Airy}} \qquad \text{where} \qquad \ell_\mathrm{Airy} = \left(\frac{\hbar^2}{2m_\mathrm{r}V'(b)}\right)^{1/3} \tag{22}$$

and its solution is therefore:

$$\psi(x) = \mathrm{A}\left(\frac{x-b}{\ell_\mathrm{Airy}}\right). \tag{23}$$

In order to allow for the connection of the asymptotic expressions of the Airy function with the WKB solutions, the approximation (17) should be at least valid on the range $[b-\ell_\mathrm{Airy}, b+\ell_\mathrm{Airy}]$. In other words, the second-order correction to $V(x)$ must be small over this range:

$$\frac{1}{2}\,\ell_\mathrm{Airy}^2\,|V''(b)| \lesssim \ell_\mathrm{Airy}|V'(b)|. \tag{24}$$

We will see that this constraint is not always satisfied for the van der Waals potential.

2 Bound states in a vdW potential

Having established these few general results regarding the semi-classical method, we now use them to estimate the energies of bound states in a potential well behaving at large distances as $V(r) = -C_6/r^6$. Before moving on to a quantitative study, let us recall the length and energy scales associated with the van der Waals potential (*cf.* chapter 3):

$$R_\mathrm{vdW} = \frac{1}{2}\left(\frac{2m_\mathrm{r}C_6}{\hbar^2}\right)^{1/4}, \qquad E_\mathrm{vdW} = \frac{\hbar^2}{2m_\mathrm{r}R_\mathrm{vdW}^2}. \tag{25}$$

2-1 The binding energies

To begin our study, we will treat the slightly more general case of a power-law potential $V(r) = -C_n/r^n$. We start from the equation verified by the

reduced radial wave function:

$$-\frac{\hbar^2}{2m_{\rm r}}u''(r)+V(r)\,u(r)=E\,u(r). \tag{26}$$

We are of course mainly interested in the case $n=6$, but it is equally simple to treat the case of an arbitrary exponent. The results we are going to find were obtained by LeRoy & Bernstein (1970).

Here we consider weakly bound states in this potential well, which are essentially localized in the region where the van der Waals potential dominates over the short-range potential. Therefore, the results that we will obtain depend very little on the exact shape of this short-distance potential. To simplify the notations, we will model it as a hard core at the R_a point. One can consult the articles of Comparat (2004) and Jelassi, Lesegno, et al. (2008) for an improvement of this simple approximation.

Our starting point will be Eq. (15) that we will use to find the variation with j of the energy E_j of the weakly bound states (recall that we take here the zero energy at the atomic dissociation limit so that $E_j<E_{j+1}<0$). For this, we rewrite this formula

$$j=\frac{1}{4}+\frac{1}{\pi}\int_{R_a}^{R_b}k(r,E)\;\mathrm{d}r, \tag{27}$$

and we will derive this formula with respect to the energy E by formally treating j as a real number for a moment. Then, we will of course be interested in the particular values of E which give an integer value of j.

The left turning point is set to the position R_a of the hard core, as shown above. The right turning point, R_b, is defined by $E=-C_n/R_b^n$. The derivative of (27) with respect to E gives

$$\frac{\mathrm{d}j}{\mathrm{d}E}=\frac{1}{\pi}\int_{R_a}^{R_b}\frac{\partial k}{\partial E}\,\mathrm{d}r\;+\;\frac{1}{\pi}\frac{\partial R_b}{\partial E}\,k(R_b,E) \tag{28}$$

and the second term of the right-hand side cancels out since $k(R_b,E)=0$. We thus find after the change of variable $x=(r/R_b)^n$:

$$\frac{\mathrm{d}j}{\mathrm{d}E}=\frac{\sqrt{2m_{\rm r}}\,C_n^{1/n}}{2\pi n\hbar\,|E|^{(n+2)/2n}}\int_{(R_a/R_b)^n}^{1}x^{(2-n)/2n}\,(1-x)^{-1/2}\;\mathrm{d}x. \tag{29}$$

This integral can be computed analytically by taking the limit $R_a/R_b\to 0$ and we find finally[3] the differential equation:

$$\frac{\mathrm{d}E}{\mathrm{d}j}\approx K_n|E|^{(n+2)/2n}\qquad\text{with}\quad K_n=\frac{2\hbar\sqrt{\pi}}{\sqrt{2m_{\rm r}}\,C_n^{1/n}}\,\frac{n\,\Gamma(1+1/n)}{\Gamma(1/2+1/n)}. \tag{30}$$

The integration of this differential equation is simple:

$$\frac{\mathrm{d}E}{|E|^{(n+2)/2n}}=K_n\,\mathrm{d}j\qquad\Rightarrow\qquad\frac{2n}{n-2}|E|^{(n-2)/2n}=K_n\,[j(0)-j(E)] \tag{31}$$

For energy $E=0$, (27) gives:

$$j(0)\equiv j_d=\frac{1}{4}+\frac{\Phi}{\pi}\qquad\text{with}\quad\Phi=\int_{R_a}^{+\infty}k(r,E=0)\;\mathrm{d}r. \tag{32}$$

The integral is computed at the dissociation limit of the dimer: the turning point R_b is then rejected at infinity and the result depends on the position of the hard core R_a (the integral diverges if we take $R_a\to 0$). Note that j_d is generally not an integer. Moreover, a necessary condition for the validity of the semi-classical approximation is $j_d\gg 1$.

Once the value of j_d is known, we see that the energy of a bound state $j\le j_d$ is such that (with j integer):

$$E_j=-\tilde{K}_n(j_d-j)^{2n/(n-2)}\qquad\text{with}\quad\tilde{K}_n=\left(\frac{n-2}{2n}K_n\right)^{2n/(n-2)}. \tag{33}$$

If we trust the semi-classical approximation even for the deepest levels, then we find that there are $j_{\max}=E(j_d)$ bound states, where $E(j_d)$ denotes the integer part of j_d.

In the particular case of the van der Waals potential ($n=6$) truncated at R_a, this relation becomes

$$E_j\approx -28.65\;(j_d-j)^3\;E_{\rm vdW} \tag{34}$$

and the value of j_d deduced from (32) is:

$$\Phi=2\left(\frac{R_{\rm vdW}}{R_a}\right)^2\quad\Rightarrow\quad j_d=\frac{1}{4}+\frac{2}{\pi}\left(\frac{R_{\rm vdW}}{R_a}\right)^2. \tag{35}$$

[3] The result can be expressed in terms of the special function $B(p,q)=\int_0^1 x^{p-1}(1-x)^{q-1}\,\mathrm{d}x=\Gamma(p)\Gamma(q)/\Gamma(p+q)$, with $\Gamma(1/2)=\sqrt{\pi}$.

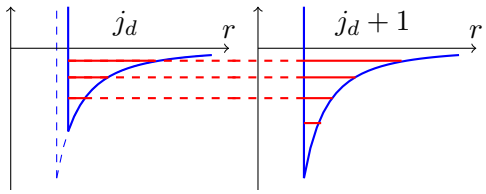

Figure 3. *Variation of the position of the bound states in a truncated van der Waals potential, when we move the position of the hard core towards $r = 0$ in order to increase j_d by 1. The number of levels is also increased by 1, and we recover the energies already present plus a new eigenvalue corresponding to the energy of the ground state in the new well. Note that this is a schematic diagram and that the energies are not to scale.*

When we vary the position of the hard core and thus the value of j_d, we find the following result: there is a perfect periodicity of the position of the last bound states: the passage $j_d \to j_d + 1$ gives back exactly the same values of the bound energies provided that we make the substitution $E_j \to E_{j+1}$. In other words, the potential well obtained for $j_d + 1$, deeper than the one for j_d, will contain exactly one more state, its ground state located at the bottom of the well. All the other eigenenergies for $j_d + 1$ will be identical to the energies found for j_d (figure 3).

Finally, let us return to the value of the parameter j_d whose integer part gives the number of bound states in the potential $V(r)$. The value given in (35) was obtained for a short-range potential and by trusting the semi-classical approximation even for energies extremely close to the dissociation limit. Two corrections must be made to this value:

- If the short-range potential is not a hard core, but a regular potential, the $1/4$ term in (32) must be replaced by $1/2$, as we have seen for the passage from (14) to (15).
- Moreover, we will see in § 2-3 and § 4-3 that the semi-classical approximation must be corrected for an energy E very close to the dissociation limit. This leads to replace the $1/2$ term by $3/8$.

Thus, for a regular short-range potential and taking into account the corrections to the WKB approximation near the dissociation limit, we have (Flambaum, Gribakin, et al. 1999):

$$\text{Number of bound states : integer part of } \frac{3}{8} + \frac{1}{\pi}\int_{R_a}^{+\infty} k(r, E = 0)\, \mathrm{d}r. \quad (36)$$

2-2 A first universality: weakly bound states

The relation (34) is a first example of universality for our problem: if we give ourselves the atomic parameters (m_{r}, C_6) and if the experiment provides the energy E_j of the j-th level, we can deduce the value of j_d and thus the energies of the other levels, at least those weakly bound for which the van der Waals potential plays a dominant role. Two questions can nevertheless be raised in front of this statement:

- The universality found here relies on the semi-classical approximation, but is this correct for weakly bound states?
- Universality has been obtained for a potential strictly equal to $-C_6/r^6$ up to the hard-core point R_a. Does it hold for another type of short-range repulsive potential?

To answer the first question and to study the validity of the semi-classical approximation for the determination of bound states, let us start by comparing the predictions (34,35) with the results of a numerical calculation of the bound states. We consider in both cases a van der Waals potential $-C_6/r^6$, truncated by a hard core potential in R_a, and we plot in figure 4 the position of the last bound states as a function of R_a, for two ranges of variation of R_a. We see that the agreement is excellent in both cases, except for the very last bound state, when it approaches the dissociation limit (Boisseau, Audouard, et al. 1998). We will come back to this problem related to the last bound state in the next paragraph (§ 2-3), but the answer to the first question raised above is clearly positive: the universality found above is not an artifact of the semi-classical approximation.

For completeness, we have plotted the wave functions of these bound states in figure 5 (top). We can distinguish two zones in this plot:

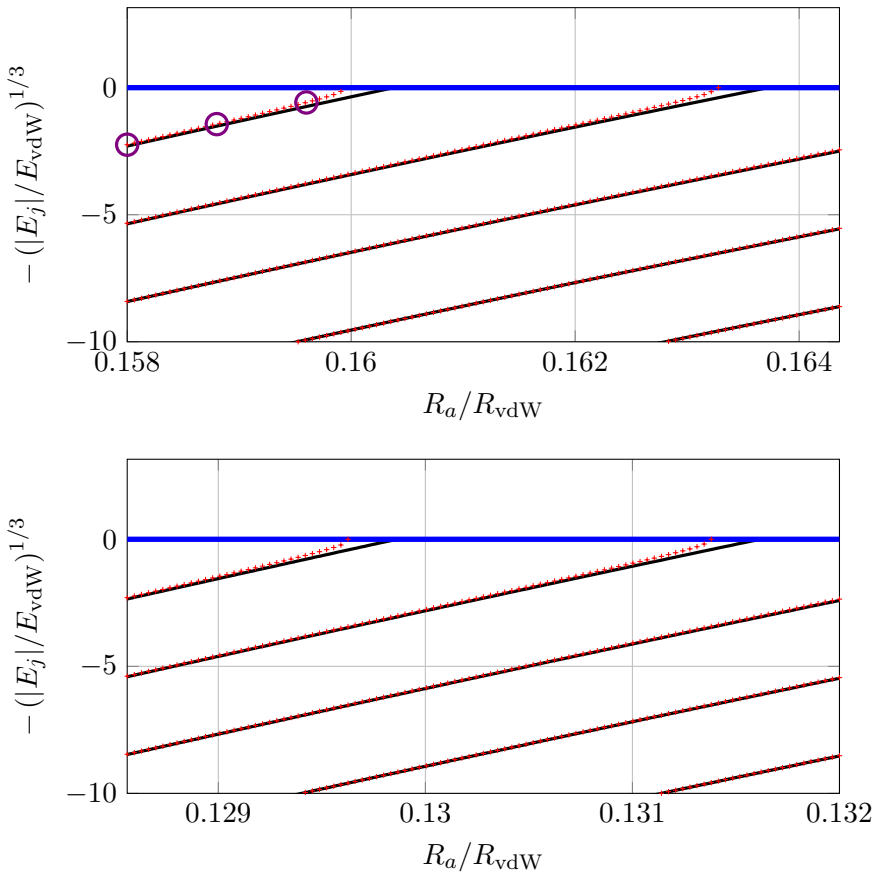

Figure 4. *The last bound states in a van der Waals potential truncated at $r = R_a$. Comparison of the semi-classical result (34, in black) and a numerical calculation (in red). The number of bound states is 25, 24 or 23 in the top graph (resp. 38, 37 or 36 in the bottom graph) for this range of R_a values. On the top figure, the three energies marked by a purple circle will be studied in more detail in figure 7, where we plot the wave functions of the corresponding states.*

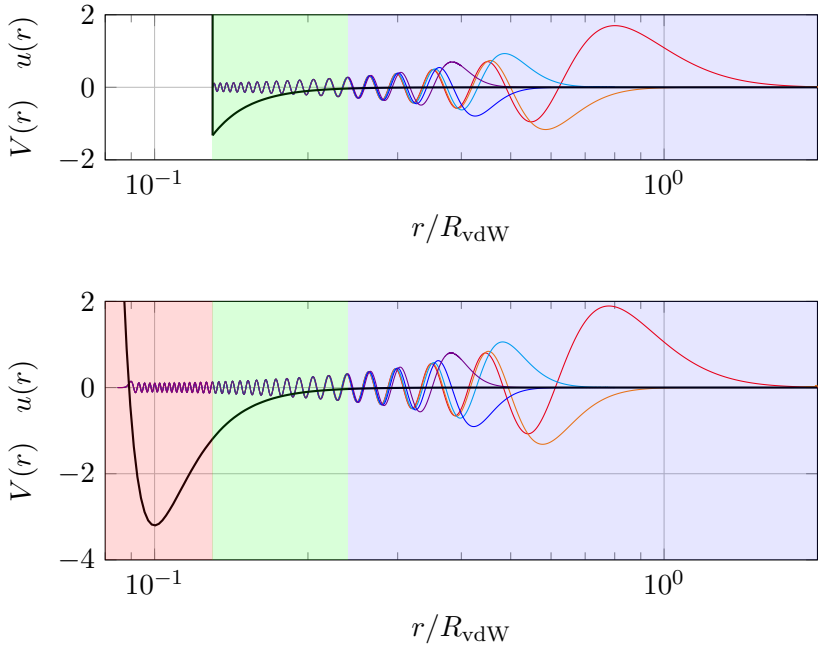

Figure 5. *Top: the last 5 bound states for a hard core potential in $R_a = 0.13\, R_{\mathrm{vdW}}$. Bottom: the last 5 bound states for a Lennard-Jones potential with a minimum in $0.10\, R_{\mathrm{vdW}}$.*

- In the small r area, colored in green, all wave functions oscillate in phase. This is well understood from the semi-classical approximation: the wave functions all start with a node at the hard core in R_a and the local wave numbers $k(r, E_j)$ for r small are almost all equal. In this region, the van der Waals potential C_6/r^6 is indeed much larger than the energy differences $E_j - E_{j'}$ for weakly bound states.

- In the region of large r, colored in blue, the value of C_6/r^6 is reduced, the difference between wave numbers becomes appreciable, and the wave functions are out of phase with each other; in particular, they have different turning points R_b.

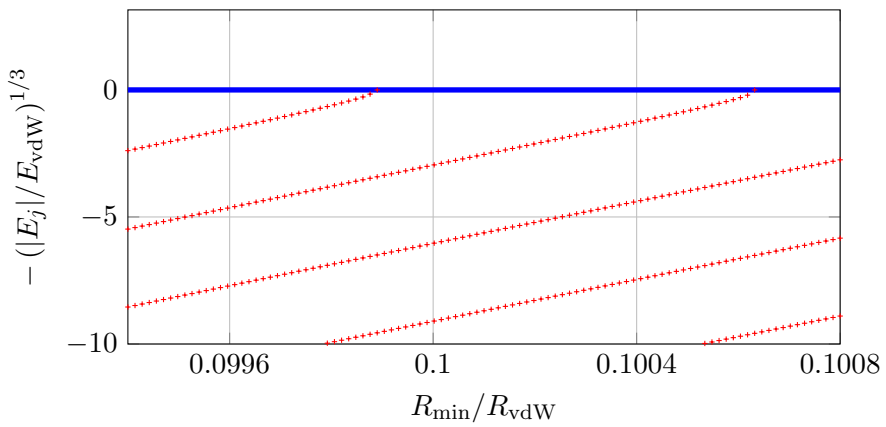

Figure 6. *Positions of the last bound states for a Lennard-Jones potential. There are 68,67 or 66 bound states in the potential for this range of values of* $r_{\rm min}$.

Let us now turn to the second question, concerning the modification of the result when considering another type of short-range repulsive potential. We have plotted in figure 6 the result obtained for the energies of the last bound states for a Lennard-Jones potential:

$$V(r) = \frac{C_{12}}{r^{12}} - \frac{C_6}{r^6}, \tag{37}$$

by adjusting the coefficient C_{12} of the repulsive term so that the minimum of the potential $R_{\rm min}$ is at a given location, here $\approx 0.10\,R_{\rm vdW}$. The result obtained here is almost identical to the result obtained for a truncated van der Waals potential, except for a translation of the abscissae, which depends on the precise link between $R_{\rm min}$ and R_a. Here again, the knowledge of the energy of a weakly bound state is sufficient to determine the position of all the others, with a law identical to that obtained for the truncated van der Waals potential.

To understand the origin of this universality in the behavior of the last bound states, it is useful to look at the shape of the wave functions of these states. We have plotted them in figure 5 (bottom) for the Lennard-Jones potential with $R_{\rm min} = 0.10\,R_{\rm vdW}$. We can distinguish three regions of r values on this graph:

- The inner zone, colored in red, corresponds to values of r where the repulsive potential C_{12}/r^{12} plays a significant role, insofar as its value is at least equal to 10% of the absolute value of the van der Waals potential C_6/r^6. The behavior of the states in this region is therefore not universal and depends on the precise form adopted for the repulsive potential. Let us simply note that (i) the inner turning point is almost identical for all states and (ii) the wave functions oscillate in phase: indeed, the wave numbers $k(r, E_j)$ are almost all equal due to the value of the potential $C_{12}/r^{12} - C_6/r^6$, much larger than the differences in energies $|E_j - E_{j'}|$.

- The intermediate zone, colored in green, is the important part for our discussion. In this zone, the repulsive potential is negligible and the dynamics is entirely controlled by the van der Waals potential. In this zone, the local wave numbers $k(r, E_j)$ remain almost equal because the van der Waals potential C_6/r^6 is much larger than the energy differences $|E_j - E_{j'}|$: therefore, the wave functions still oscillate in phase.

- In the external area, colored in blue, the different eigenstates have different behaviors, linked to the fact that they have different energies and therefore different turning points.

In conclusion, due to the "locking" of the phases of the wave functions in the intermediate (green) region, we infer that the evolution of the wave functions in the outer (blue) region will be the same as for a truncated van der Waals potential (figure 5, top), provided that we adjust the position of the hard core to reproduce the phase found in the central part. The role of the repulsive potential for weakly bound states is simply to fix the value of this global phase of the wave functions. Even if the precise characteristics of this repulsive potential are not known, the experimental measurement of the energy of a single weakly bound state is sufficient to assign the value of this phase, to then deduce the position of all other weakly bound states.

2-3 The problem of the last bound state

Since our study of the square well in the previous chapter, we know that this domain of parameters leading to a very weakly bound state corresponds to a divergence of the scattering length (Levinson's theorem). It can therefore play an important role in the experiments and we will investigate further the discrepancy between the WKB prediction and the numerical calculation visible in figure 4.

The key to understanding this discrepancy lies in the validity condition (24) associated with the connection between the allowed and forbidden regions of the classical motion. Recall that this condition relates to the curvature of the potential $V(r)$, which must be sufficiently small for the linear approximation of this potential to be valid over an adequate range of values of r.

When we transpose this condition to the van der Waals potential with a turning point in R_b, we find

$$R_b \lesssim R_{\mathrm{vdW}}. \tag{38}$$

For the energy $E_j = -C_6/R_b^6$ given by (34), the turning point $R_{b,j}$ is

$$\frac{R_{b,j}}{R_{\mathrm{vdW}}} \approx \frac{1}{\sqrt{j_d - j}}. \tag{39}$$

The validity condition (38) will thus be satisfied essentially for all values of j except $j_{\max}$, since $j_d - j_{\max}$ can become notably smaller than 1 when the last level is very close to the dissociation limit. In this case, the turning point exceeds the value R_{vdW}, the validity condition (38) is violated and this explains the observed discrepancy between WKB prediction and numerical calculation for this last level (Boisseau, Audouard, et al. 1998; Gao 1999)

As an example, we have plotted in figure 7 the variation of the probability density $|u_{j_{\max}}(r)|^2$ of the last bound state $j_{\max}$ for three neighboring positions of the hard core corresponding to significantly different energies of the last bound state: -11.3,-2.95,-0.20 E_{vdW}. It can be seen that for the first two, the relative particle is located relatively close to the origin ($r \lesssim R_{\mathrm{vdW}}$) while in the third case, weakly bound, the particle is mostly beyond this point. According to the criterion (38), one expects the semi-classical prediction to be correct in the first two cases, and less so in the third. This is indeed what we see when we return to figure 4 for these values of the hard core position (each point is marked by a purple circle).

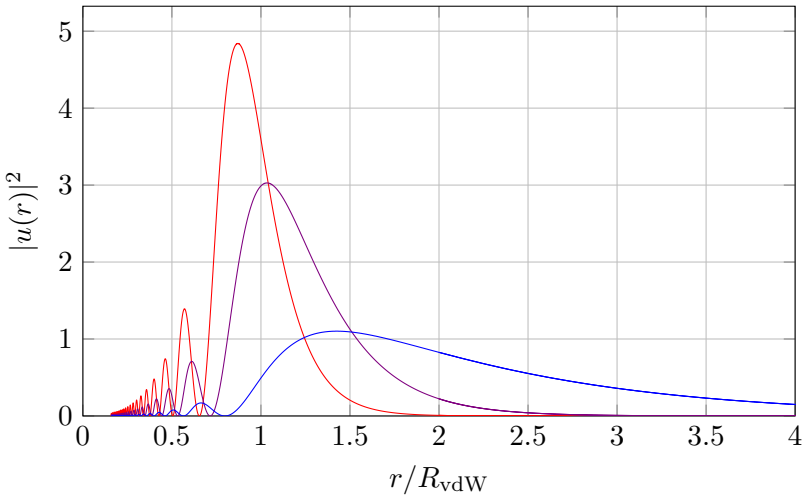

Figure 7. *Probability distribution of the last bound state ($j_{\max} = 25$) for different positions of the hard core, 0.1580, 0.1588 and 0.1596 R_{vdW}, corresponding to significantly different binding energies: -11.3,-2.95,-0.20 E_{vdW} (red, purple, blue).*

Let us note finally that this failure of the semi-classical approximation for the last bound state does not call into question the universality of the relative positions of weakly bound states. Simply the position of the last state must be calculated numerically as a function of the position of the hard core, as we have done in figure 4. Once this calculation is done, the experimental knowledge of the position of a weakly bound state allows to predict the position of the others.

2-4 Bound states of angular momentum $\ell = 2$

In all the above, we have been interested in states of angular momentum $\ell = 0$; indeed, because of the very low temperatures involved in the experiments, the s-wave regime dominates the collisions between atoms. However, we will see that experimentalists can produce, from collisions in the s-wave, bound states of angular momentum $\ell = 2$; this is possible because the free-bound transition is done by passing through an excited state that is itself a quantum superposition of states with different angular momenta.

The calculation of the bound states of angular momentum $\ell = 2$ is done as for $\ell = 0$, by making the substitution

$$-\frac{C_6}{r^6} \quad \longrightarrow \quad -\frac{C_6}{r^6} + \frac{\hbar^2 \ell(\ell+1)}{2m_{\rm r} r^2} \qquad \text{with} \quad \ell = 2. \tag{40}$$

The introduction of the centrifugal potential does not introduce any length scale (a manifestation of *scale invariance*) as can be seen by writing the Schrödinger equation with the units of length and energy $R_{\rm vdW}$ and $E_{\rm vdW}$ for a truncated potential:

$$-\frac{{\rm d}^2 u}{{\rm d}r^2} + \left(-\frac{16}{r^6} + \frac{\ell(\ell+1)}{r^2}\right) u = Eu \qquad \text{with} \quad u(R_a) = 0 \quad \text{and } \ell = 2. \tag{41}$$

Using the parameters of figure 4, we have plotted in figure 8 the energies of the last bound states for the two angular momenta $\ell = 0$ (in red) and $\ell = 2$ (in green). We see that the energy $E_j^{\ell=2}$ is generally close to $E_j^{\ell=0}$. This is easily understood from the Schrödinger equation (41): if the bound state occupies only the region $r \ll R_{\rm vdW}$, the centrifugal potential $1/r^2$ is a small perturbation of the van der Waals potential $1/r^6$, the energy $E_j^{\ell=2}$ being just slightly higher than $E_j^{\ell=0}$. On the other hand when the last bound state is close to the dissociation limit, the $1/r^2$ term cannot be treated perturbatively. The link between the behaviors of weakly bound states of various angular momenta ℓ is studied in detail by Gao (2000) and Gao (2001).

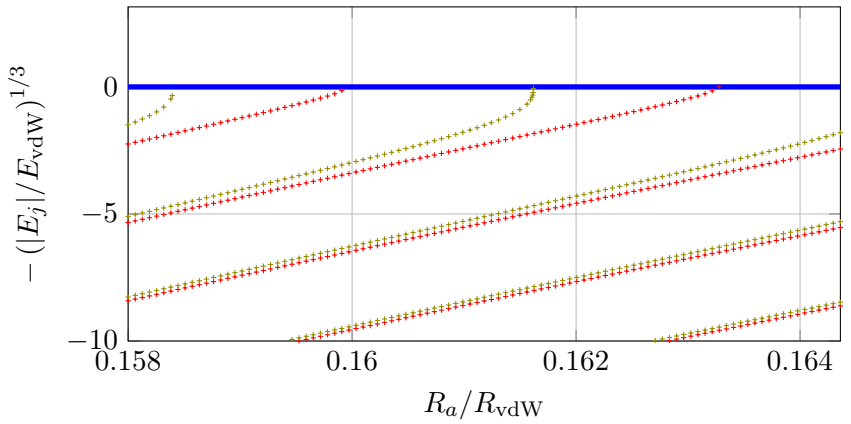

Figure 8. *The last bound states in a van der Waals potential truncated in R_a, for angular momentum $\ell = 0$ (red dots, identical to those in figure 4) and $\ell = 2$ (green dots). An almost identical figure (except for a global translation) is obtained for any other type of short-range potential, such as the C_{12}/r^{12} term of the Lennard-Jones potential.*

3 Observation of weakly bound states

The predictions we have just made about the energies of weakly bound states are extremely constraining. If we assume the value of C_6 to be known, the position of these states is determined by a single parameter, the position of the hard core for a truncated van der Waals potential or more generally the global phase imposed on the different wave functions by the short-range potential. For a given atomic species, the energies of the different bound states must therefore be positioned on a vertical line in the plots of figures 6 or 8. We will show that this is indeed the case, by taking the example of recent experiments on the ytterbium atom. These experiments use a very precise experimental technique, the two-color photoassociation.

We will not give here an exhaustive bibliography on the subject of photoassociation of cold atoms. In France, the researchers of the Aimé Cotton laboratory have played a pioneering role in the development of this

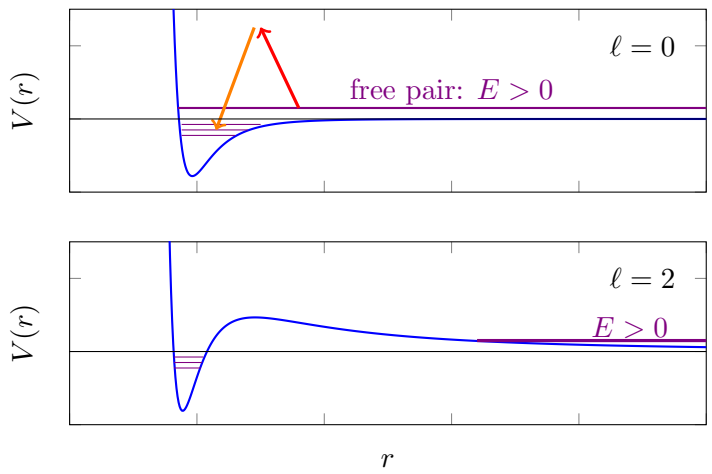

Figure 9. *Top: principle of a two-color photoassociation experiment in a gas of cold atoms. Bottom : if the incident angular momentum of the pair of atoms is not zero, the centrifugal barrier prevents the atoms from getting close enough to make the transition to a bound state.*

technique and we refer the interested reader to the review article of Pillet, Vanhaecke, et al. (2003), as well as to Thorsheim, Weiner, et al. (1987), Weiner, Bagnato, et al. (1999), Stwalley & Wang (1999), Abeelen & Verhaar (1999), Kostrun, Mackie, et al. (2000), Bahns, Gould, et al. (2000), Araujo, Weinstein, et al. (2003), and Dulieu, Raoult, et al. (2006).

3-1 Two-color photoassociation

Starting from a very cold gas, one illuminates the atoms with a light beam containing two frequencies ω_1 and ω_2 and one tries to induce transitions from the asymptotically free state of a pair of atoms to a weakly bound dimer (figure 9, top). If we neglect the incident kinetic energy, which is very low, the transition will take place with a maximum rate when the resonance condition is reached:

$$\hbar(\omega_1 - \omega_2) = |E_j| \tag{42}$$

is satisfied. To be efficient, we must choose frequencies ω_1 and ω_2 close to a resonance with an excited electronic state.

Let us consider a pair of bosonic atoms. The incident collisional state corresponds to $\ell = 0$. Otherwise, the centrifugal barrier prevents the atoms from getting close enough for the overlap with the targeted bound state to be appreciable (figure 9, bottom). As explained by Ciuryło, Tiesinga, et al. (2004) and Borkowski, Ciuryło, et al. (2009) for the case of alkaline earth atoms, one can thus form, after passage in the excited electronic state, dimers of angular momentum in the electronic ground state $\ell = 0$ and $\ell = 2$.

3-2 An example : the ytterbium atom

To illustrate this technique, let us consider the recent experiments conducted on the Ytterbium atom by Borkowski, Buchachenko, et al. (2017) in the group of Y. Takahashi at Kyoto University [see also Kitagawa, Enomoto, et al. (2008)]. The experiments were performed on a Bose-Einstein condensate, which allows to eliminate the contribution of the initial kinetic energy to the shift and broadening of the photoassociation line.

The experimental scheme is shown in figure 10. The two wavelengths necessary for the photoassociation are generated from the same light beam thanks to two acousto-optic modulators (AOM). The photoassociation signal consists of a loss of atoms when the "free-bound" Raman resonance is reached (figure 11). The measurement is made for several light intensities and atomic densities, and then extrapolated to zero intensity and density to remove associated systematic effects.

The measurements of Borkowski, Buchachenko, et al. (2017) have been made for several isotopes of ytterbium (168, 170,174) which allows to test the variation of theoretical predictions for several reduced masses. Let us concentrate here on the isotope ^{170}Yb: Borkowski, Buchachenko, et al. (2017) measured six lines corresponding to the weakest bound states, three being assigned to a $\ell = 0$ state and the other three to $\ell = 2$ state (see table 1).

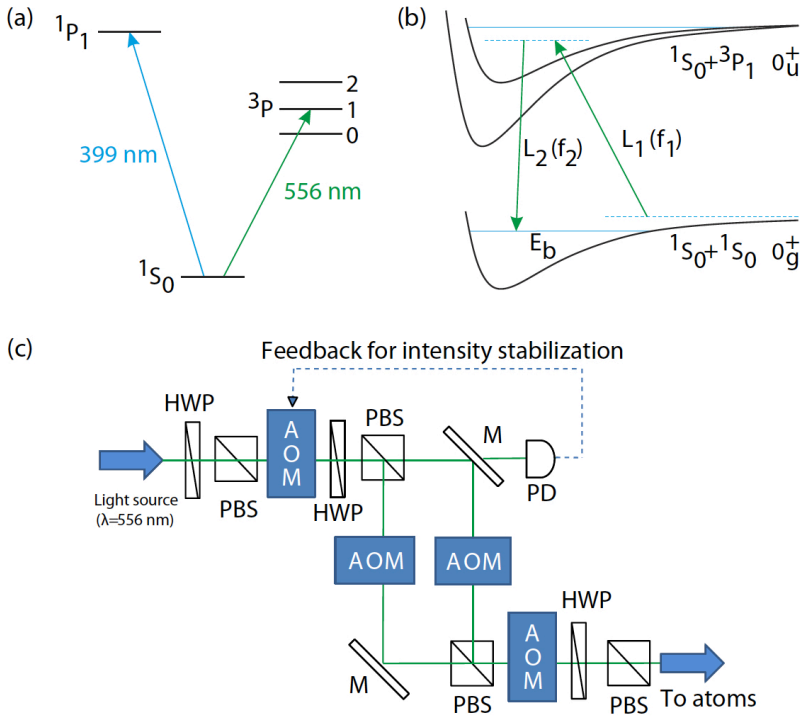

Figure 10. *Schematic diagram of the two-color photo-association experiment conducted in Y. Takahashi's group on Ytterbium atoms. Figure extracted from Borkowski, Buchachenko, et al. (2017).*

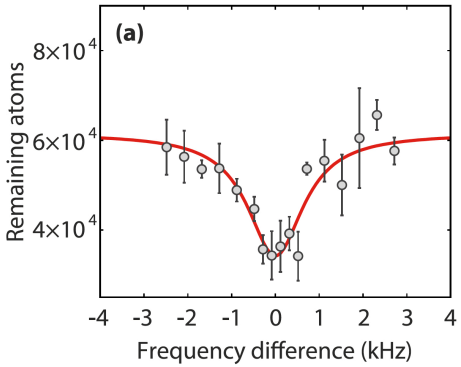

Figure 11. *A typical photo-association signal in a ^{170}Yb condensate. A significant fraction of the atoms are lost when the resonance from the incident (free) state to one of the bound states of the molecular potential is reached. Figure extracted from Borkowski, Buchachenko, et al. (2017).*

$\ell = 0$	$\ell = 2$
27.70024 (44)	3.66831 (32)
463.72552 (80)	398.05626 (46)
1922.01467 (505)	1817.14074 (80)

Table 1. *Photo-association resonances (in MHz) measured by Borkowski, Buchachenko, et al. (2017) for the isotope ^{170}Yb, for which $E_{\rm vdW}/h = 3.5\,MHz$.*

3-3 Comparison with the theoretical model

To verify that the model described above does indeed account for these results, let us repeat in figure 12 the plot of figure 8 made for a truncated van der Waals potential. We now restrict the plot to a variation interval of $R_a/R_{\rm vdW}$ corresponding to a period for the sequence of appearance of the new states. Let us also plot the six levels of table 1 as horizontal lines, taking the value of C_6 given in Chapter I: $C_6 = 1929$ atomic units ($E_{\rm vdW}/h = 3.5\,$MHz), and let us look when the energies of these 6 levels intersect the theoretical predictions. We see that the six intersections occur almost all for the same value of $R_a/R_{\rm vdW} \approx 0.1614$, which is a remarkable confirmation of the simple theoretical model developed here.

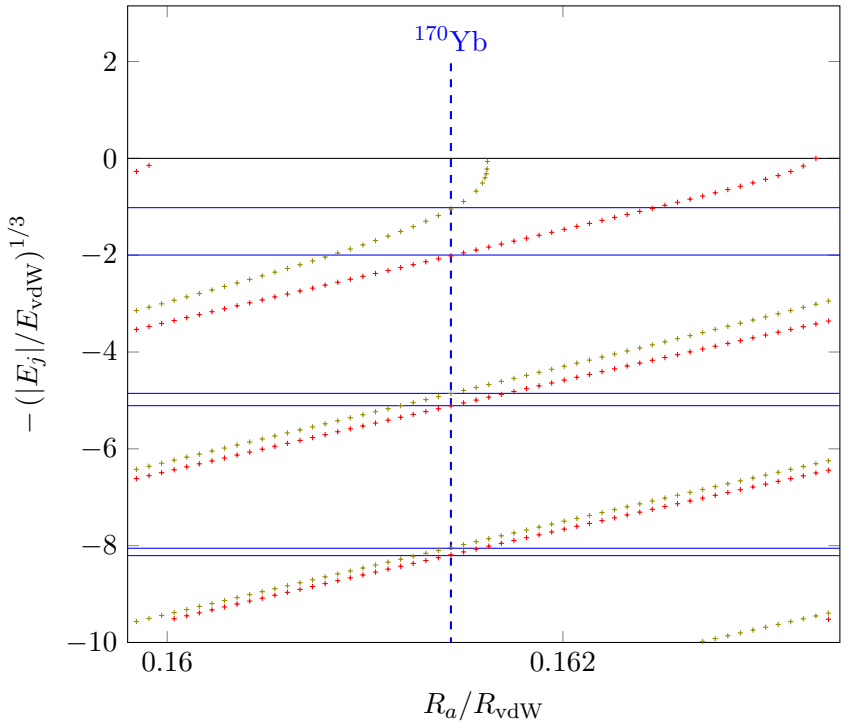

Figure 12. *Validation of the previously developed model: the horizontal lines represent the experimentally measured energies for the last 6 bound states of the dimer $^{170}Yb_2$. The intersections of these lines with the calculated positions of the energy levels ($\ell = 0$ in red and $\ell = 2$ in green) are done for one and the same value of the only free parameter of the model, the ratio R_a/R_{vdW}, which is therefore completely determined (modulo the period of the model).*

The fact that the value $R_a/R_{\mathrm{vdW}} \approx 0.1614$ is determined only modulo the period of appearance of the new bound states is not a problem if we are aiming at determining the scattering length. Indeed, we will see that its value is governed by the same laws as these last bound states.

In practice, the extreme accuracy of the measurements of Borkowski, Buchachenko, et al. (2017), better than 1 kHz, allows considerable refinement of the model presented here. One can add corrective terms concerning the long-range attraction, in $-C_8/r^8$ and $-C_{10}/r^{10}$. One can also test (weak) corrections to the Born–Oppenheimer approximation (Lutz & Hutson 2016).

4 Scattering length for vdW interaction

There are many methods for estimating the scattering length of a gas of atoms, from measuring the elastic collision cross-section $\sigma = 8\pi a^2$ in a thermalization experiment to using the mean-field energy $2\pi\hbar^2 a\rho/m_{\mathrm{r}}$ in a Bose–Einstein condensate of density ρ. We will not review all these methods here, but focus on the most accurate technique, based on its link with the positions of the last bound states that we have studied in the previous sections.

4-1 Scattering states and quantum reflection

Since we have at our disposal both the WKB approximation and the numerical solution of the Schrödinger equation, it is interesting to start our study by comparing the positive energy solutions, corresponding to the stationary scattering states. The WKB solution for the reduced wave function $u(r)$ of energy E is written for the van der Waals potential truncated by a hard core at the point R_a:

$$u(r) = \frac{1}{\sqrt{k(r)}} \sin\left(\int_{R_a}^{r} k(r')\,\mathrm{d}r'\right) \qquad \text{with} \quad \frac{\hbar^2 k^2(r)}{2m_{\mathrm{r}}} = E + \frac{C_6}{r^6}. \tag{43}$$

When $r \to \infty$, this solution behaves as a superposition of $\mathrm{e}^{\pm \mathrm{i}k_0 r}/\sqrt{k_0}$ with $E = \hbar^2 k_0^2/2m_{\mathrm{r}}$, which corresponds to a normalization ensuring a probability flux independent of E. We will take here the same normalization

convention for the solutions of the Schrödinger equation found numerically.

We show in figure 13 three solutions corresponding to the three energies[4] $E/E_{\mathrm{vdW}} = 0.0025, 0.025, 0.25$ for a given hard core ($R_a/R_{\mathrm{vdW}} = 0.1588$). The red plots correspond to the numerically calculated solutions and the blue plots to the WKB approximation. On this large scale plot (r/R_{vdW} between 0 and 200), no major difference appears between the two sets of predictions.

Now let's enlarge the area to small r (figure 14). We can see that the WKB solution has a notably larger amplitude in the inner region ($r \lesssim R_{\mathrm{vdW}}$) than the exact solution (note the difference in vertical scale between the two plots). More precisely, the three WKB solutions are almost identical in this area for the three considered energies. On the contrary, the amplitudes of the exact solutions decrease when E decreases : more precisely, the probability for finding the relative particle in this zone decreases approximately as $\sqrt{E}$.

This important difference in magnitudes between the exact numerical result and the WKB approximation is even more evident in figure 15, where the probability density of presence $|u(r)|^2$ has been plotted in the lowest energy case, $E/E_{\mathrm{vdW}} = 0.0025$. We can see that the probability found numerically is reduced by a factor of 20 compared to the WKB prediction.

To understand this major flaw in the WKB approximation for very low energy scattering states, one must return to the validity condition (11), expressing that the wavelength must vary slowly on its own scale. Let us take a particle arriving from $r = +\infty$ with a kinetic energy E. At a point r, its kinetic energy is equal to $E + C_6/r^6$ and a simple calculation gives

$$\frac{1}{2\pi}\left|\frac{\mathrm{d}\lambda}{\mathrm{d}r}\right| = \frac{3r^2/4}{(1 + Er^6/16)^{3/2}} \tag{44}$$

where lengths and energies are expressed in units of R_{vdW} and E_{vdW}. This function, which must be small in front of 1 for the WKB approximation to be good, is plotted in figure 16. We see that the approximation is just marginal for the largest of the energies considered here, $E/E_{\mathrm{vdW}} = 0.25$

[4]For rubidium, $E_{\mathrm{vdW}}/h = 6$ MHz (or equivalently $E_{\mathrm{vdW}}/k_{\mathrm{B}} = 300\,\mu$K). The energies considered here correspond to temperatures of 750 nK, 7.5 μK and 75 μK, which is representative of the parameters encountered in a cold atom experiment.

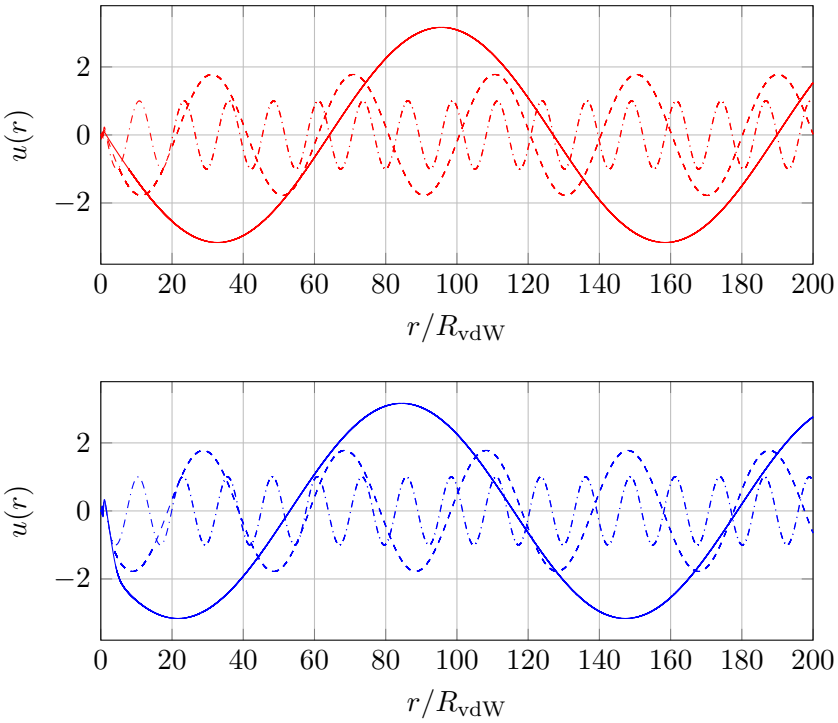

Figure 13. *Reduced wave functions for low and positive energies $E/E_{\mathrm{vdW}} = 0.0025, 0.025, 0.25$ for a van der Waals potential $-C_6/r^6$ truncated in $R_a/R_{\mathrm{vdW}} = 0.1588$. Top: numerical solution of the Schrödinger equation. Bottom: solution obtained in the semi-classical approximation. The normalization chosen here leads to a probability flux independent of E.*

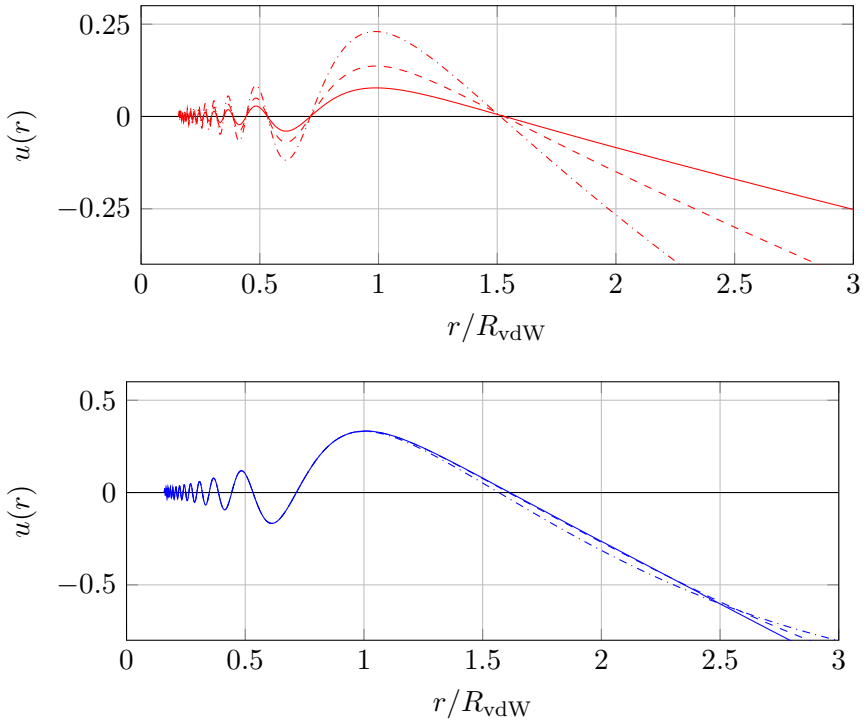

Figure 14. *Same wave functions as in figure 13, with a zoom on the central part. We see that the probability density in the vicinity of the origin is strongly reduced for the exact solution, compared to the semi-classical approximation. More precisely, the probability density for the exact solution varies as $\sqrt{E}$ and thus tends to 0 when $E \to 0$.*

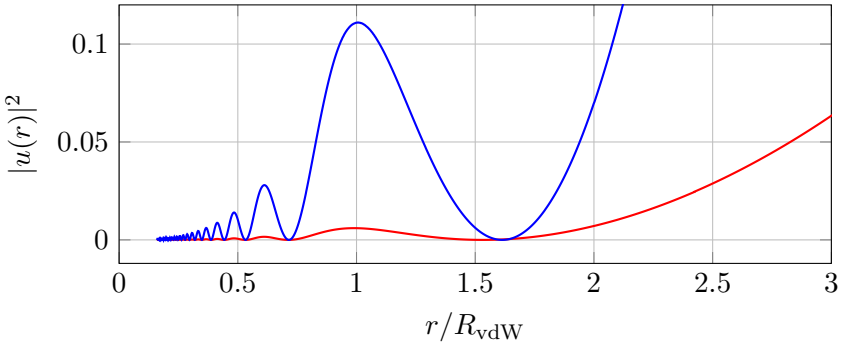

Figure 15. *Probability density for the lowest of the energies considered in figures 13 and 14, $E/E_{\mathrm{vdW}} = 0.0025$. We see that the semi-classical approximation (in blue) overestimates this probability of presence by a factor ~ 20 with respect to the exact result (in red).*

and becomes really poor for the lowest energies, at least for distances r of the order of R_{vdW}.

The physical meaning of this failure of the WKB approximation is related to the fact that the van der Waals potential actually varies too fast for the wavelength to "adiabatically adapt" as the relative particle, arriving from $r = +\infty$, approaches $r = 0$ and is accelerated by the potential. The situation we encounter here is called *quantum reflection*, the simplest illustration of which consists of a simple potential step, like the one shown in figure 17. Let us consider a particle arriving from the right with an energy $E \ll V_0$; instead of going down this step as one would classically expect, the quantum particle can make a half-turn, and the probability for this non-intuitive behavior tends to 1 when $E/V_0 \to 0$: the transmitted flux tends to 0 as $E/V_0 \to 0$, and the reflected flux is then almost equal to the incident flux.

The quantum reflection phenomenon has been observed for atoms on a liquid helium surface (Nayak, Edwards, et al. 1983; Berkhout, Luiten, et al. 1989) or on a solid surface (Shimizu 2001; Druzhinina & DeKieviet 2003; Pasquini, Shin, et al. 2004). Its role in cold atom collisions has been mentioned by Côté, Heller, et al. (1996), but it remains nevertheless not so

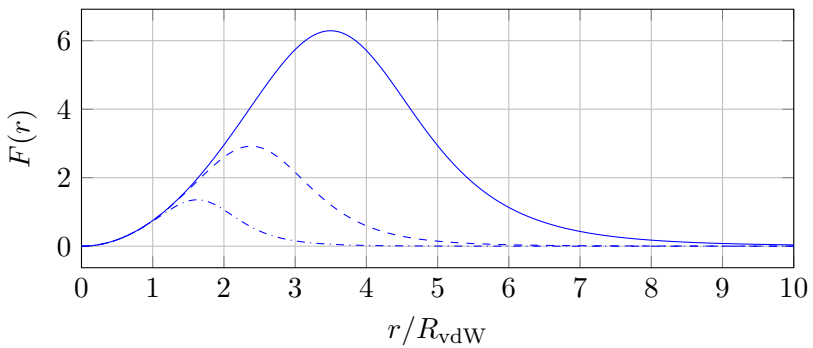

Figure 16. *Variation of $\frac{1}{2\pi}\left|\frac{\mathrm{d}\lambda}{\mathrm{d}r}\right|$ with r, for the three energies considered in the text, $E/E_{\rm vdW} = 0.0025, 0.025, 0.25$ (solid, dashed, and dotted-dotted).*

well known. However, it is essential for the success of experiments with quantum gases: the considerable reduction of the probability of finding the two atoms close to each other, compared to what would be expected semi-classically, leads to a drastic reduction of losses in cold and dense gases.

4-2 The exact solution for a truncated vdW potential

It is clear from the above that the semi-classical approximation is not suitable for the quantitative description of very low energy collisions in the van der Waals potential. Its validity condition $\frac{\mathrm{d}\lambda}{\mathrm{d}r} \ll 1$ is not satisfied and it cannot provide the value of the scattering length. In order to progress, we will present in this paragraph an exact treatment for the case of a van der Waals potential truncated by a hard core in R_a, as we did for the search for bound states. Once this particular case is understood, we will move on in the next paragraph (§4-3) to the case of any short-range repulsive potential.

We start from the equation verified by the reduced wave function for $E = 0$:

$$\frac{\mathrm{d}^2u}{\mathrm{d}r^2} + \frac{16}{r^6}u(r) = 0 \qquad \text{with} \quad r \le R_a : \ u(r) = 0, \tag{45}$$

where distances are expressed in units of $R_{\rm vdW}$, and thus $R_a \ll 1$. Following Landau & Lifshitz (1975), §132 [see also Gribakin & Flambaum (1993)], we can make the following change of variable and function:

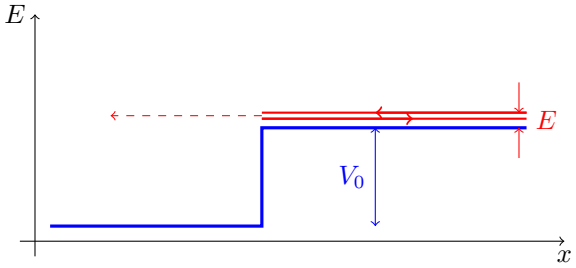

Figure 17. *Quantum reflection on a potential step; a particle arriving from $x = +\infty$ with an energy $E \ll V_0$ turns back with a probability close to 1, while a classical particle would continue towards $-\infty$.*

$$r = \sqrt{\frac{2}{x}}, \qquad u(r) = \frac{1}{x^{1/4}}\,\phi(x) \tag{46}$$

to arrive at the following equation

$$x^2\frac{\mathrm{d}^2\phi}{\mathrm{d}x^2} + x\frac{\mathrm{d}\phi}{\mathrm{d}x} + (x^2 - \alpha^2)\,\phi(x) = 0 \qquad \text{with} \quad \alpha = \frac{1}{4} \text{ and } x \ge x_a : \ \phi(x) = 0, \tag{47}$$

where the point $x_a = 1/2R_a^2 \gg 1$ corresponds to the position of the hard core.

This equation is well known in mathematics since it is used to define the Bessel functions. For a given value of α, the solutions form a space of dimension 2, generated by the functions $J_\alpha(x)$ and $Y_\alpha(x)$, the Bessel functions of first and second kind. We will use here the asymptotic behavior of these functions (*cf.* Wikipedia):

- when $r \to \infty$, so when $x \to 0$:

$$J_{1/4}(x) \approx \frac{1}{\Gamma(5/4)}\left(\frac{x}{2}\right)^{1/4}, \tag{48}$$

$$Y_{1/4}(x) \approx -\frac{\Gamma(1/4)}{\pi}\left(\frac{2}{x}\right)^{1/4} + \frac{1}{\Gamma(5/4)}\left(\frac{x}{2}\right)^{1/4}; \tag{49}$$

- when $r \to R_a \ll 1$, so when $x \to x_a \gg 1$:

$$J_{1/4}(x) \approx \sqrt{\frac{2}{\pi x}} \cos\left(x - \frac{3\pi}{8}\right), \qquad Y_{1/4}(x) \approx \sqrt{\frac{2}{\pi x}} \sin\left(x - \frac{3\pi}{8}\right). \tag{50}$$

Let's write the solution of (47) in the form

$$\phi(x) = A\, J_{1/4}(x) + B\, Y_{1/4}(x). \tag{51}$$

The condition $\phi(x_a) = 0$ with $x_a \gg 1$ imposes

$$\frac{A}{B} = -\frac{Y_{1/4}(x_a)}{J_{1/4}(x_a)} \approx \tan\left(x_a - \frac{3\pi}{8}\right). \tag{52}$$

Examining the solution for $x \ll 1$ then gives:

$$\phi(x) \approx \frac{A+B}{\Gamma(5/4)} \left(\frac{x}{2}\right)^{1/4} - \frac{B\Gamma(1/4)}{\pi} \left(\frac{2}{x}\right)^{1/4}, \tag{53}$$

which gives for the function $u(r)$:

$$u(r) \propto r - a \qquad \text{with} \quad a = \bar{a}\left[1 - \tan\left(x_a - \frac{3\pi}{8}\right)\right] \tag{54}$$

By reintroducing the natural unit of length $R_{\rm vdW} = \frac{1}{2}\left(2m_{\rm r}C_6/\hbar^2\right)^{1/4}$, we find that the quantity $\bar{a}$ introduced above is defined by [5].

$$\frac{\bar{a}}{R_{\rm vdW}} = \frac{\pi}{\Gamma(1/4)\Gamma(5/4)} \approx 0.9560. \tag{55}$$

Finally, let us note that the quantity x_a which plays the role of a phase in (54) has a simple interpretation. By reintroducing here also the unit of length $R_{\rm vdW}$, we have

$$x_a = 2\frac{R_{\rm vdW}^2}{R_a^2} = \int_{R_a}^{+\infty} k(r, E=0)\, {\rm d}r. \tag{56}$$

This phase x_a is therefore equal to the phase accumulated between $r = R_a$ and $r = +\infty$ calculated in the WKB approximation. We said above that the WKB approximation alone does not allow us to calculate the scattering length, but it is nevertheless not totally absent from the correct result.

[5] This definition is found in different forms in the literature, these forms being linked together by $\Gamma(x)\Gamma(1-x) = \pi/\sin(\pi x)$.

4-3 The Gribakin and Flambaum approach

Gribakin & Flambaum (1993) have given a very elegant generalization of the above discussion for the case of a potential behaving like $-C_6/r^6$ at infinity, but with an arbitrary short-range repulsive potential. We will not repeat here the details of their approach, but we will summarize it with the help of figure 18. The top diagram shows what we discussed in the previous paragraph. In the case of a truncated $-C_6/r^6$ potential, the solution written as a linear combination of the Bessel functions $J_{1/4}(x)$ and $Y_{1/4}(x)$ is valid for all r and provides the desired result. It is therefore useless to use the WKB solution, which in any case would only be valid at relatively short distances (green zone), but would become incorrect around $r = R_{\rm vdW}$.

In the case of an arbitrary short-range repulsive potential, the solution in terms of Bessel functions is only correct for large r, when this short-range potential is negligible in front of the van der Waals potential. This range of values for r corresponds to the green and the blue zones in the bottom diagram of figure 18. The WKB solution is valid for relatively small r ($r < R_{\rm vdW}$, red and green zones on this same diagram). The idea of Gribakin & Flambaum (1993) is therefore to:

- choose a point r_* inside the green zone;
- use the WKB solution to the left of this point, for $r < r_*$;
- use a linear combination of $J_{1/4}(x)$ and $Y_{1/4}(x)$ to the right of this point, for $r > r_*$;
- connect these two solutions in r_*, and check that the result for a does not depend on the precise value chosen for r_*.

The implementation of this method does not pose any practical problem. The final result takes a form almost identical to (54-56):

$$a = \bar{a}\left[1 - \tan\left(\Phi - \frac{\pi}{8}\right)\right] \qquad \text{with} \quad \Phi = \int_{R_a}^{+\infty} k(r, E=0)\, {\rm d}r, \tag{57}$$

where R_a is the interior turning point for $E = 0$. We thus find again the WKB phase accumulated on the whole accessible domain which was already involved in the definition of x_a in (56). The only difference between (54) and (57) is the additional term $\pi/4$ in the tangent argument. This term

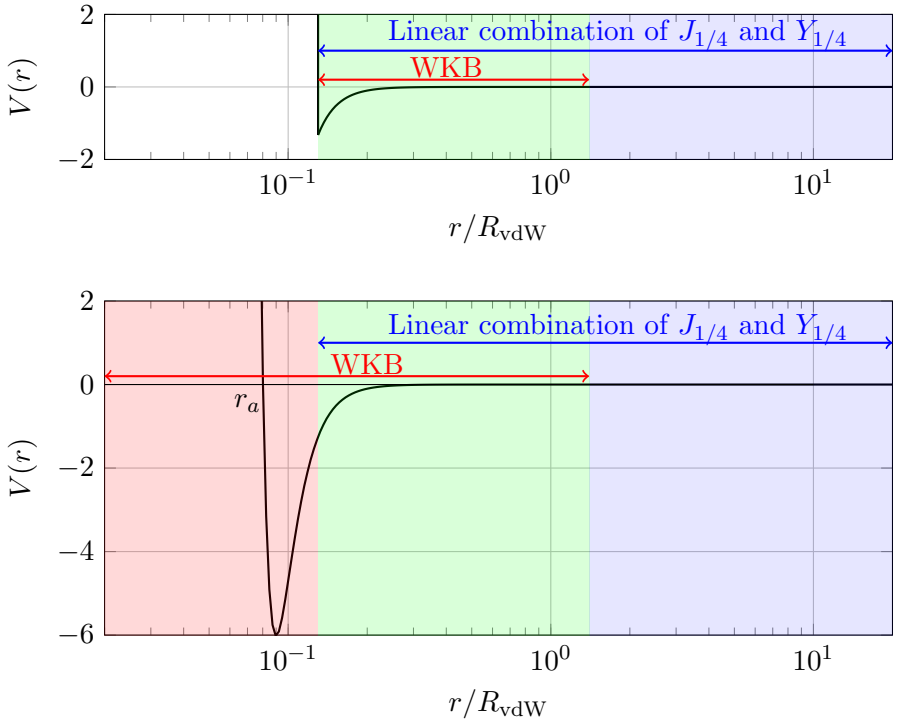

Figure 18. *Top: for a truncated van der Waals potential, the solution in terms of Bessel functions $J_{1/4}$ and $Y_{1/4}$ is valid over the whole range $r > R_a$ (green and blue areas). The semi-classical solution, on the other hand, can only be used for $R_a < r < R_{\rm vdW}$ (green zone). Bottom: for a regular short-range potential, the semi-classical solution is valid from the internal turning point to $R_{\rm vdW}$ (green zone and red zone). The solution in terms of Bessel functions is valid when the short-range potential is negligible (green and blue zones). It is therefore possible to connect the two types of solution at a point in the green zone, the final result not depending on the point chosen.*

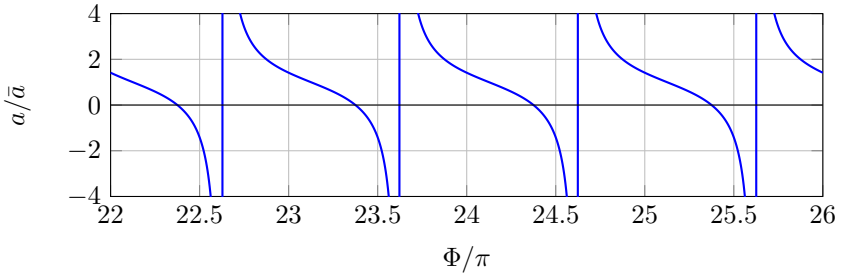

Figure 19. *Variation of the scattering length with the phase Φ.*

is not surprising: it simply comes from the semi-classical phase difference between a steep edge and a regular edge, a difference that we had already pointed out in (14–15).

We plotted the variation of a with the phase Φ in figure 19. This variation shows successive divergences of a, each time the argument of the tangent is $\pi/2$ modulo π, that is:

$$\Phi = \frac{5\pi}{8} \mod [\pi]. \tag{58}$$

According to Levinson's theorem, this condition corresponds to the threshold for the appearance of a new bound state in the potential $V(r)$, when we vary for example the amplitude of the short-range potential [cf. the result already announced in (36)]. Note that we find here the fact already studied in (14): the semi-classical approximation is inaccurate to describe this last bound state, since the formula (14) would predict a threshold of appearance at $\Phi = \frac{\pi}{2} \mod [\pi]$. One can check that the shift of $\frac{\pi}{8}$ between the two predictions is directly observable in the plots of figure 4.

Note that the scattering length that we find here is "mostly" positive; if we assume that the phase Φ is random and uniformly distributed between 0 and π, we obtain a positive value of a with a probability of $3/4$ and a negative one for a probability of $1/4$.

Effective range. It is also possible to calculate the effective range r_e using this approach (Gao 1998a; Flambaum, Gribakin, et al. 1999):

$$r_e = C\,\bar{a}\left[1 - 2\frac{\bar{a}}{a} + 2\left(\frac{\bar{a}}{a}\right)^2\right] \qquad \text{with} \quad C = \frac{[\Gamma(1/4)]^4}{6\pi^2} \approx 2.918. \tag{59}$$

In this case, this quantity is positive and diverges whenever a vanishes.

4-4 Universality in the van der Waals problem

We now turn to the last point of our study which concerns the universality of the energy spectrum associated with the van der Waals potential, including the value of the scattering length and the position of the last bound states. Various facets of this universality have been discussed, not always explicitly, by different authors and in particular by Gao (1998b), Crubellier, Dulieu, et al. (1999), Flambaum, Gribakin, et al. (1999), and Boisseau, Audouard, et al. (2000). We will summarize the main results here and present them in a graphic form [see figure 21].

To begin with, let us recall the result already obtained for the bound states. We started from the "phasing" of the wave functions $u_j(r)$ of these different states in the intermediate (green) region of the figure 7. This intermediate region corresponds to the positions r for which the short-range repulsive potential is negligible in front of C_6/r^6; the phasing is due to the following two elements: (i) The left turning point is almost the same for all these states; (ii) In this region where the semiclassical approximation is valid, the wave numbers $k(r, E_j)$ (at a given point r) are almost the same for all E_j energies of weakly bound states. Therefore, it is not necessary to know the details of the short-range potential. All that matters is the common phase it imposes on these wave functions. One could also replace this short-range potential by a hard core located at a point R_a equal to one of the nodes common to all functions $u_j(r)$ in the intermediate region: the E_j's would not be modified in this substitution.

Let us now consider the zero-energy state, whose asymptotic behavior $u_0(r) \propto r - a$ determines the scattering length. The previous "phasing" also occurs for this state because its left turning point is almost the same as that of a weakly bound state and its wave number in the intermediate region

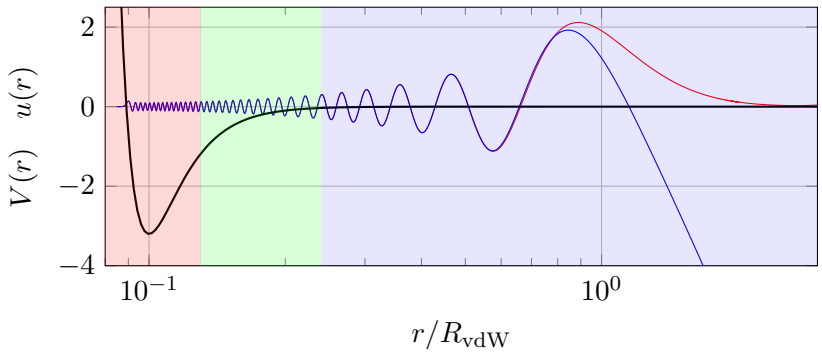

Figure 20. *Wave function $u_{j_{\max}}(r)$ of the last bound state (red) and of the $u_0(r)$ state of zero energy (blue) in a Lennard-Jones potential with a minimum in $R_{\min} = 0.1002\,R_{\rm vdW}$.*

$k(r, E = 0)$ is also very close to the wave number $k(r, E_j)$ of the last bound states. This point is illustrated by an example in figure 20.

The universality found for the bound states thus immediately extends to the scattering length a, whose value is a function only of $\int k(r, E = 0)\,\mathrm{d}r$ modulo π [Eq. (57)]. As for E_j, the value of a would not be modified if we substituted the short-range potential with a hard core located at any of the nodes common to $u_j(r)$ and $u_0(r)$ in the intermediate region colored in green in figures 7 and 20. Therefore, for the problem of interest here, the only role of the short-range repulsive potential is to fix the common phase of the oscillation of $u_j(r)$ and $u_0(r)$ in the intermediate region. Once this phase is fixed, the set

$$\{a, E_{j_{\max}}, E_{j_{\max}-1}, E_{j_{\max}-2}, \ldots\} \tag{60}$$

is fully determined.

Ideally, the knowledge of only one element of this set allows to go back to the common phase and thus to all the other elements. This is the announced universality. In practice, it is often useful to measure two or three energies E_j of bound states to refine the determination of C_6 and other possible long-range corrections ($-C_8/r^8$ for example), and then to deduce the scattering length with an excellent accuracy. Moreover, let us recall that

the relevant energies E_j must be sufficiently close to zero to reach the zone colored in green.

Once we know that all the numbers (60) depend on only one variable (the common phase of u_j and u_0), it becomes possible to use one of them as a parameter and plot all the others according to this parameter. This is what we have done in figure 21. This is a plot in polar coordinates (θ, ρ), where the angle θ is defined as

$$\frac{\theta}{2} = \Phi - \frac{\pi}{8} \quad \Rightarrow \quad a = \bar{a}\,[1 - \tan(\theta/2)] \tag{61}$$

with as in (55) $\bar{a} = 0.956\, R_{\rm vdW}$. The polar angle $\theta = 0$ thus corresponds to $a = \bar{a}$, the angle $\theta = \pi$ to a scattering length $a = \pm\infty$. The sector $a < 0$ corresponds to the quarter plane between $\theta = \pi/2$ and $\theta = \pi$. Along the ray of angle θ, we have marked in blue (resp. red) the value of the energies of the last bound states of $\ell = 0$ (resp. $\ell = 2$), plotted at the points

$$\rho_j = \left(\frac{-E_j}{E_{\rm vdW}}\right)^{1/3} \tag{62}$$

The choice of the power $1/3$ allows to obtain a curve close to an Archimedean spiral $\rho \propto \theta$, taking into account the relations (34-57)

We have checked that this plot remains almost unchanged when we take a hard-core potential, a Lennard-Jones potential or another type of short-range repulsive potential. The only important point is to have enough bound states so that the intermediate region dominated by the $-C_6/r6$ van der Waals potential has an appreciable size.

Finally, we have plotted the known experimental parameters for some atomic species in figure 22, superimposed on the theoretical prediction already shown in figure 21. We see that the agreement with the simple model used in this chapter is excellent. The data presented in this plot are extracted from the following articles:

- Metastable helium : Moal, Portier, et al. (2006)
- Lithium 7: Abraham, McAlexander, et al. (1995)
- Calcium 40: Pachomow, Dahlke, et al. (2017)

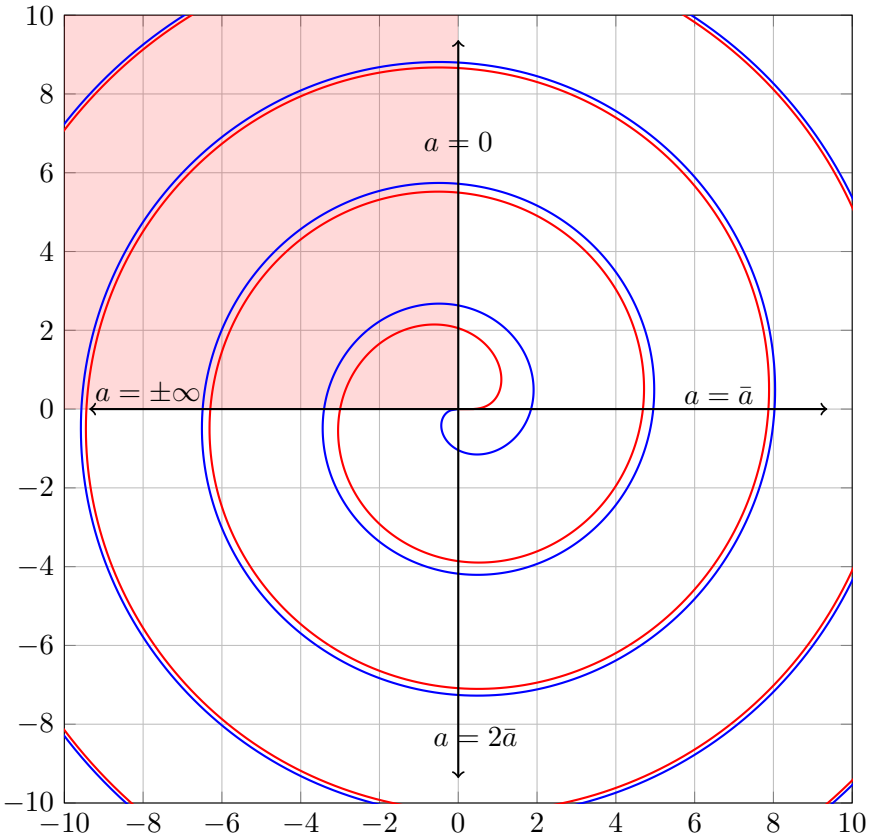

Figure 21. *Plot in polar coordinates of the universal relation linking the set $\{a, E_{j_{\max}}, E_{j_{\max}-1}, E_{j_{\max}-2}, \ldots\}$ where the E_j are the energies of the bound states of angular momentum $\ell = 0$ (blue) or $\ell = 2$ (red). The polar angle parametrizes the scattering length according to the law (61) and the distance to the origin represents the value of the energies of the bound states according to (62). The area colored in red corresponds to a negative scattering length.*

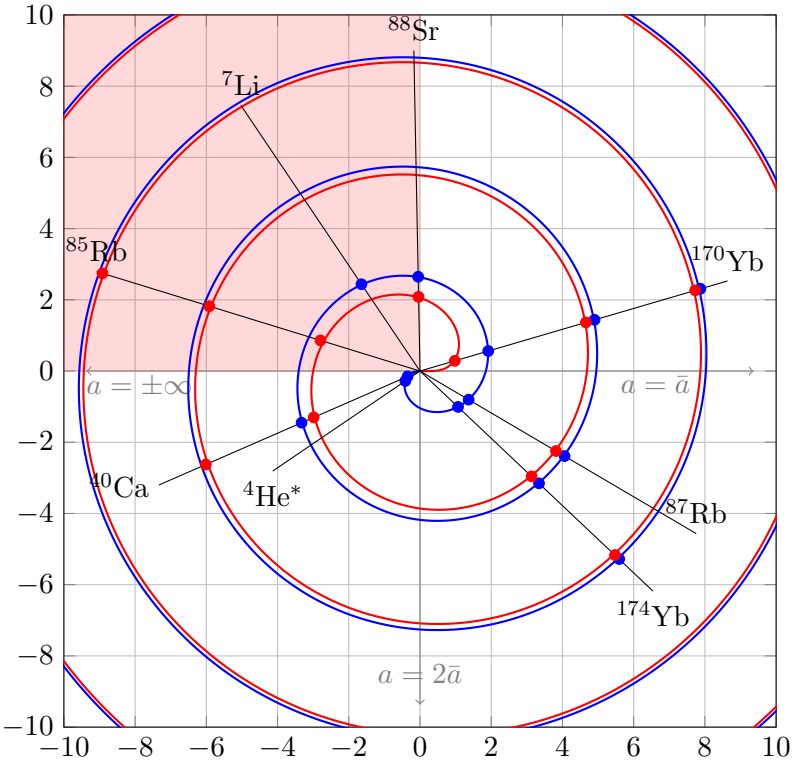

Figure 22. *Same plot as for figure 21, with a set of atomic data. The model developed in this chapter accounts very well for the universal link between the scattering length and the energies of the last bound states.*

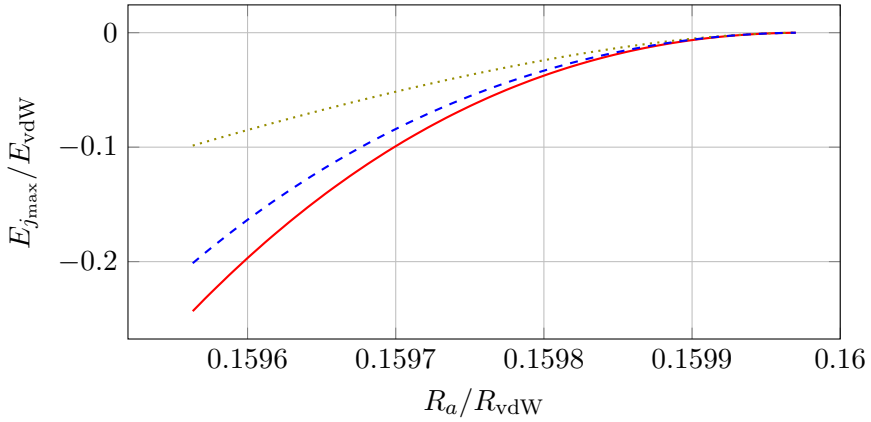

Figure 23. *Comparison between the exact value of the energy of the last bound state (solid red line) and the approximations (63) in dashed green and (64) in dashed blue. The calculation is done for a van der Waals potential truncated in R_a in the vicinity of the resonance, with the scattering length a varying from $3.2\,R_{\mathrm{vdW}}$ to $+\infty$.*

- Rubidium 85: Tsai, Freeland, et al. (1997)
- Rubidium 87: Wynar, Freeland, et al. (2000)
- Strontium 88: Escobar, Mickelson, et al. (2008)
- Ytterbium 170 and 174: Borkowski, Buchachenko, et al. (2017). For this atomic species, it is possible to perform measurements on several isotopes and thus verify the atomic mass scaling laws as well as the corrections to the Born–Oppenheimer approximation (Verhaar, Kempen, et al. 2009).

For alkali metal atoms, we have essentially restricted ourselves to the case where we could find reliable data for collisions in the triplet state, for which only one channel contributes. For other types of collisions, the multi-channel description complicates the laws found here.

To conclude, let us insist on the fact that the universality found here that links the scattering length and the energies of the last bound states goes far

beyond the relation

$$E_{\text{bound}} \approx -\frac{\hbar^2}{2m_{\text{r}}a^2} \tag{63}$$

which gives (whatever the potential is) the energy of the last bound state when $a \to \infty$. The universality highlighted here is valid whatever the value of a provided that the potential well is deep enough to contain many bound states. Let us also point out without proof an improvement of the approximation (63) as an expansion in powers of $1/(a - \bar{a})$ with the dominant term (Gao 2004):

$$E_{\text{lie}} \approx -\frac{\hbar^2}{2m_{\text{r}}(a - \bar{a})^2}. \tag{64}$$

The two approximations (63) and (64) are plotted together in figure 23; we can see that the second approximation is indeed more accurate than the first one.

Chapter V

Scattering Resonances

In the following two chapters, we will discuss scattering resonances and more precisely, Fano–Feshbach resonances. This is an essential tool in quantum gas physics; it has opened the way to the regime of strong interactions, which is reached when the scattering length becomes on the order of the distance between particles in the gas. Fano–Feshbach resonances also allow the preparation of gases with almost zero interaction ($a = 0$), thus realizing the ideal gas model. They are a source of very precise data on the structure of dimers and thus on the interatomic potentials. Finally, they have allowed the development of a very original research on few-body systems, including the study of Efimov states.

We will start by situating the Fano–Feshbach resonances in the general framework of scattering resonances which, for an s-wave collision, lead to a divergence of the scattering length. We will show the originality of the Fano–Feshbach resonances which involve two collision channels, one open, the other closed, whose relative energies can be controlled, allowing one to scan through the resonance. We will also investigate the meaning of an infinite scattering length and we will study for that purpose a very instructive model proposed by Busch, Englert, et al. (1998), which gives the eigenstates of a two-particle system confined in a harmonic trap. We will then develop a simple two-channel resonance model, for which an analytical treatment can be conducted. This model will use the notion of separable potential that we will specify beforehand in the single channel case. In the next chapter, we will deepen this model to bring out the important notion of resonance width and clarify the contribution of the closed channel. We will then describe more quantitative treatments of these resonances, and finish by presenting some recent experiments. We will examine the main tools available in the laboratory to characterize these resonances and we will see that they can have unexpected extensions, in connection for example with quantum chaos.

In the last twenty years, the literature dealing with Fano–Feshbach resonances in atomic gases has become extremely vast and it is not possible to cite here all the important work that has been done. We refer the reader to the review articles of Köhler, Góral, et al. (2006) and Chin, Grimm, et al. (2010) which presented at the time of their publication a complete overview of the field.

1 Examples of scattering resonances

In this chapter and the next one, we will be mainly interested in Fano-Feshbach resonances, obtained by coupling two scattering channels, one open, the other closed. To put these resonances in perspective, we will briefly review in this first section some types of resonances encountered in cold atom physics.

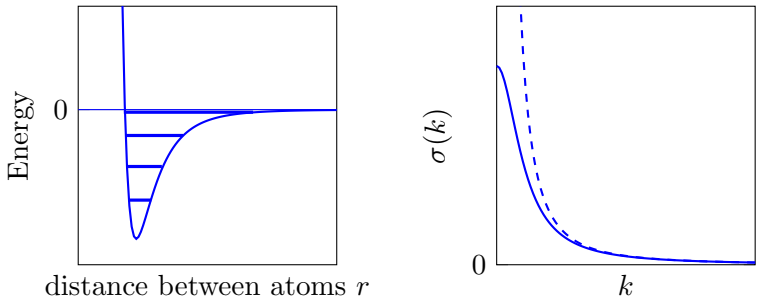

Figure 1. *Zero-energy resonance. Left: This type of resonance occurs when the last bound state of the potential $V(r)$ is very close to the dissociation limit or if a new bound state is about to appear for a small variation of $V(r)$ (N.B. Here, the position of the energy levels is purely indicative). Right: the solid line represents the variation of the scattering cross-section according to (2). When the bound state is exactly at the dissociation limit, the cross-section varies as $8\pi/k^2$ and thus diverges in $k = 0$ (dashed curve).*

1-1 Zero-energy resonance

The zero-energy resonance is a process that we have already met in the previous chapters. It occurs for s-wave collisions, when a new bound state is about to appear or when it has just appeared, following the variation of one of the parameters of the interatomic potential $V(r)$, the coefficient C_6 for example (figure 1, left).

The scattering amplitude can be written in this case:

$$f(k) \approx -\frac{a}{1 + \mathrm{i}ka} \tag{1}$$

which corresponds to a cross-section for polarized bosons varying as (*cf.* figure 1, right):

$$\sigma(k) = 8\pi|f(k)|^2 = \frac{8\pi a^2}{1 + k^2a^2} \qquad \text{with} \quad E = \frac{\hbar^2k^2}{2m_\mathrm{r}}. \tag{2}$$

At the precise point where the resonance occurs ($a = \infty$), the cross-section

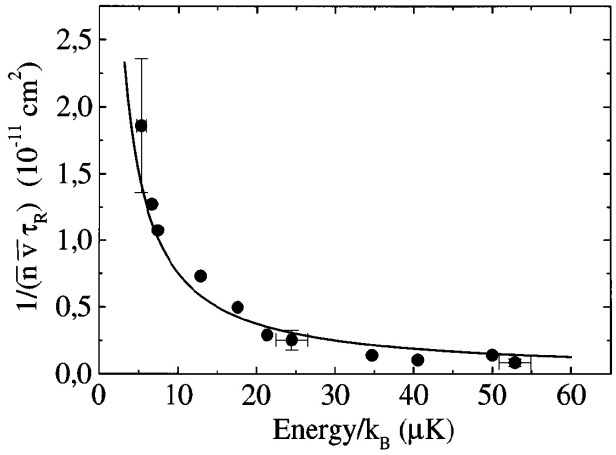

Figure 2. *Measurement of the elastic collision cross-section for a gas of polarized cesium atoms. This measurement is based on the relaxation time to thermal equilibrium τ_R, for a known density n and root-mean-square velocity $\bar{v}$. The solid line represents the prediction obtained by molecular dynamics for a gas of the same density and temperature, and placed in the unitary regime (3). Figure extracted from Arndt, Dahan, et al. (1997).*

reaches its largest value allowed by the unitarity of quantum mechanics:

$$\text{Unitary regime for polarized bosons:} \qquad \sigma(k) = \frac{8\pi}{k^2}. \tag{3}$$

Cesium in zero magnetic field has the particularity to be naturally in this regime (Arndt, Dahan, et al. 1997). We show in figure 2 the measurement of the cross-section for elastic collisions as a function of temperature for a gas of polarized cesium atoms (triplet state $|f = m_f = 4\rangle$ for which the spins of the external electron and the nucleus are aligned). We see that the cross-section varies as $\sigma(T) \propto 1/T$, in agreement with the prediction of the unitary regime (3).

A precise analysis of these results and of the position of the last bound states allowed Kerman, Chin, et al. (2001) to determine the scattering length for this triplet state and they found $a = 2400 \pm 100\, a_0 = 130\,\mathrm{nm}$. It

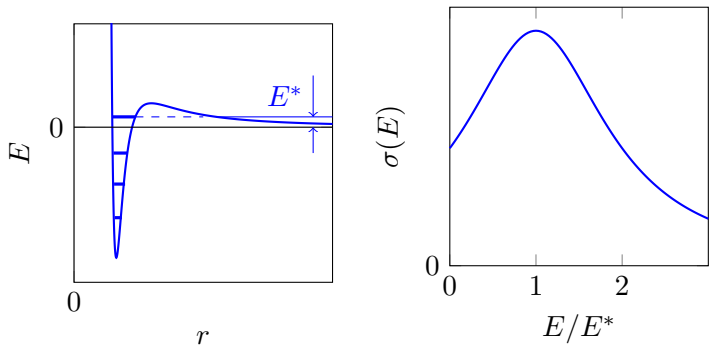

Figure 3. *Shape resonance. Left: interaction potential in the presence of a centrifugal barrier for a non-zero angular momentum. A quasibound state of energy E^* can exist at small distances from r, its lifetime being limited by the tunneling effect through the barrier. Right: resonance of the scattering cross-section for an incident energy close to E^*.*

is not strictly speaking infinite, but it is 25 times larger than the most probable value $\bar{a}$ (i.e. an cross-section 625 times larger than naively expected!). At first sight, such a large scattering length seems to be good news for obtaining a Bose–Einstein condensate, as it allows to carry out the evaporative cooling extremely quickly. Unfortunately, this scattering resonance is accompanied (as almost always for bosons) by important losses due to inelastic collisions, which prevent the condensation in a weak magnetic field (Söding, Guery-Odelin, et al. 1998). The judicious use of Fano–Feshbach resonances in a higher magnetic field and of an internal state different from the triplet state allowed Weber, Herbig, et al. (2003) to circumvent this difficulty and to finally condense this atomic species.

1-2 Shape Resonance

A shape resonance occurs when the interatomic potential behaves repulsively at infinity, as is the case for partial-wave collisions of non-zero angular momentum. In this case, the centrifugal potential varying as $1/r^2$ is dominant at long range compared to the van der Waals potential in $-1/r^6$.

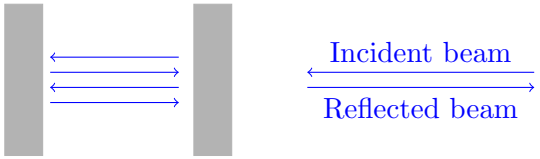

Figure 4. *Fabry-Perot cavity formed by two mirrors with high reflection coefficient. The variation of the phase shift of the reflected beam with respect to the incident beam is similar to that found for a shape resonance.*

The situation is then analogous to that of a Fabry–Perot cavity in optics. There may be one (or more) positive energy state E^* confined inside the potential well located in the vicinity of $r = 0$ (figure 3). This state is equivalent to the light field trapped in a cavity formed by two mirrors (figure 4). A dimer prepared in this state is unstable and eventually dissociates, just as the light field eventually escapes from the Fabry–Perot cavity since the mirrors are not perfectly reflecting. The lifetime of the dimer can be large when compared to the typical period of molecular oscillations.

Let us now consider a collision between two initially free atoms of energy close to E^*. The relative particle can of course bounce back outside the potential barrier, but the dimer can also be formed temporarily. The interference between these two processes causes a rapid variation of the phase shift associated to this partial wave, and thus a peak in the collision cross-section. This peak is all the more narrow as the lifetime of the quasi-bound state is large.

Several cold atom experiments have demonstrated this type of resonance. Volz, Dürr, et al. (2005) have observed it for the d-wave on a rubidium 87 condensate, with a rather subtle detection method, since it uses molecules themselves formed from a Fano–Feshbach resonance. Very recently, Yao, Qi, et al. (2019) have observed such a d-wave resonance in a potassium 41 Bose–Einstein condensate.

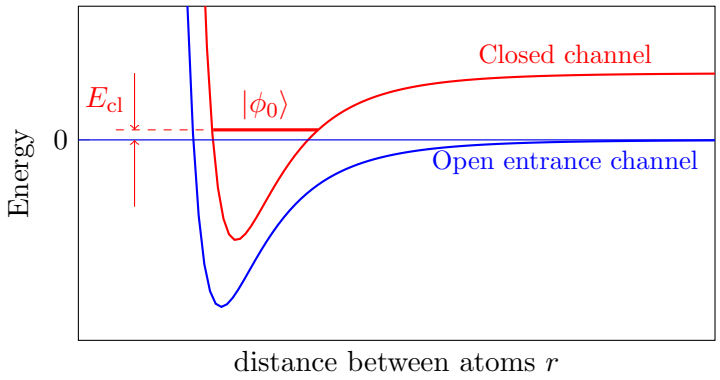

Figure 5. *Fano–Feshbach resonance: the incident particles are prepared in an internal state corresponding to the open channel. During the collision, the quasi-resonant coupling to a bound state $|\phi_0\rangle$ of the closed channel causes a significant change in the collisional phase shift, and thus a resonance of the scattering amplitude and the corresponding cross-section.*

1-3 Fano–Feshbach resonance

Unlike the two processes described above, a Fano–Feshbach resonance involves at least two collision channels (figure 5). This type of multi-channel resonance was introduced in nuclear physics by Feshbach (1958) [see also Feshbach (1962)] and in the context of atomic physics by Fano (1961). The early historical developments around these ideas are described in detail in the review article of Chin, Grimm, et al. (2010).

In the context of quantum gas physics, the first mentions of this type of resonance came from the physics of atomic hydrogen, which was the only system available before the advent of laser cooling of other atomic species. It was the Dutch team around B. Verhaar who transposed these ideas to alkali collisions (Tiesinga, Verhaar, et al. 1993; Moerdijk, Verhaar, et al. 1995). The first experimental demonstrations of these resonances were made at MIT by Inouye, Andrews, et al. (1998), at the University of Austin by Courteille, Freeland, et al. (1998), in Boulder (Roberts, Claussen, et al. 1998) and in Stanford (Vuletic, Kerman, et al. 1999).

We are interested here in the case of collisions between cold atoms and will therefore describe this process for s-wave interactions, which are the most relevant in practice. Channel 1, called *open channel* and described by the interatomic potential $V_1(r)$, is the one in which the two colliding particles arrive. This channel corresponds to a certain spin state of the incident atoms. The channel 2 described by $V_2(r)$ corresponds to another spin state of the atoms. It is a closed channel: the value of $V_2(r)$ at infinity is well above the incident energy of the particles and its population after the collision is negligible. On the other hand, the coupling between the two channels during the collision is significant; it can induce a variation of the phase shift δ_0, and thus modify the scattering amplitude and the corresponding cross-section.

The analogy with the Fabry–Perot cavity given above is also interesting in this case. One naively expects (and this will be confirmed by a quantitative analysis) that the influence of the closed channel is important when the latter presents a bound state $|\phi_0\rangle$ whose energy $E_{\rm cl}$ is close to the energy of the incident particles, i.e. $E_{\rm cl} \approx V_1(\infty)$.

An essential aspect of these resonances is that it is possible to finely tune the energy difference $E_{\rm cl} - V_1(\infty)$. It is sufficient that the magnetic moments of the spin states of the two channels are different. The variation of the ambient magnetic field will shift the $V_2(r)$ curve with respect to $V_1(r)$, and thus of varying the gap $E_{\rm cl} - V_1(\infty)$.

The variation of the scattering length in the vicinity of a Fano–Feshbach resonance controlled by a magnetic field is traditionally written in the form

$$a = a_{\rm bg}\left(1 - \frac{B_1}{B - B_0}\right), \tag{4}$$

and thus depends on three parameters: $a_{\rm bg}$ represents the background scattering length; this is essentially the value associated with the open channel far from the resonance. The field B_0 gives the position of the resonance where the scattering length diverges, and the parameter B_1 gives the "width in magnetic field" of the resonance. Let's assume for the sake of argument that B_1 is positive; to the left of the resonance, when we go from $B = B_0$ to $B = B_0 - B_1$, the value of a falls from infinity to $2a_{\rm bg}$; to the right of the resonance, for $B = B_0 + B_1$, the scattering length cancels out (figure 6).

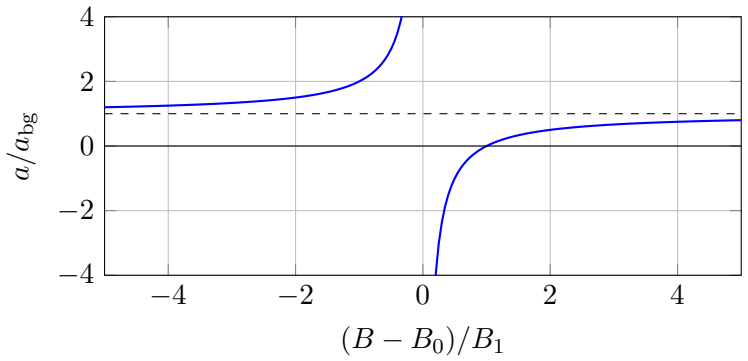

Figure 6. *Variation of the scattering length with the magnetic field, according to the law (4), plotted here for $B_1 > 0$. The dashed line indicates the value of the background scattering length $a_{\rm bg}$.*

Let's anticipate a bit on the results that will follow: we will show that the Fano–Feshbach resonance does not occur exactly for $E_{\rm cl} = 0$, but for $\tilde{E_{\rm cl}} \equiv E_{\rm cl} - \Delta = 0$ where Δ is an energy shift that we will calculate. The link between the magnetic field B and the energy $E_{\rm cl}$ of the bound state $|\phi_0\rangle$ of the closed channel (measured with respect to the dissociation limit of the free channel) is thus done by

$$E_{\rm cl} - \Delta = \delta\mu\,(B - B_0) \tag{5}$$

where $\delta\mu$ is the difference between the magnetic moment of the pair of atoms in the free channel and the magnetic moment of the bound dimer in the $|\phi_0\rangle$ state.

Let us also point out an important point concerning the expression (4). We will see in the next chapter that the main characteristic of a Fano–Feshbach resonance is its *width*, which determines the relative weights of the open and closed channels in the states that may appear. It would be tempting to assume that this width is given solely by $|B_1|$. We will see that the reality is more complex: the equation (4) is a convenient parameterization, but it partially hides the important physical quantities that really characterize the resonance.

We will present at the end of the next chapter some recent experiments which illustrate the diversity of situations where a Fano–Feshbach resonance can occur. Here, we show in figure 7 the result of one of the first experiments where these resonances have been seen in the framework of cold atomic gases (Inouye, Andrews, et al. 1998). This experiment was conducted on a condensate of sodium atoms, for which the resonance is around 900 Gauss (0.09 T). The resonance manifests itself both by an increased loss of atoms due to inelastic collisions and by a variation of the interaction energy, measured by ballistic expansion of the gas. In the same period, Fano–Feshbach resonances were observed for ^{85}Rb (Roberts, Claussen, et al. 1998; Courteille, Freeland, et al. 1998) and for ^{133}Cs (Vuletic, Kerman, et al. 1999).

1-4 Confinement Induced Resonance

These resonances, initially predicted by Olshanii (1998), then physically interpreted by Bergeman, Moore, et al. (2003), occur when atoms are strongly trapped along one or two directions in space. Consider for example atoms moving freely along a tube of axis z, with a strong confinement in the xy plane characterized by the oscillation frequency $\omega_\perp$. Starting from atoms interacting with a scattering length a in 3 dimensions, Olshanii (1998) and Bergeman, Moore, et al. (2003) show that the interaction between two confined atoms can be modeled by a Dirac distribution, $g_{\rm 1D}\,\delta(z_1 - z_2)$, with

$$g_{\rm 1D} = \frac{2\hbar^2 a}{m_{\rm r} a_\perp^2}\,\frac{1}{1 - Ca/a_\perp} \qquad \text{with} \quad C = 1.4603, \tag{6}$$

where $a_\perp^2 = \hbar/m_{\rm r}\omega$. A scattering resonance occurs when $a_\perp = Ca$.

The interpretation of this phenomenon is in fact very close to a Fano–Feshbach resonance. The different channels are the different states of excitation of the transverse atomic motion. The open channel corresponds to the ground state of energy $\hbar\omega_\perp$. The closed channel of interest is the excited level of the transverse motion of energy $3\hbar\omega_\perp$, which contains a state of orbital angular momentum $\ell_z = 0$ and which can thus couple resonantly to the ground state during a collision. Bergeman, Moore, et al. (2003) show that this channel always contains a bound state, and that the resonance

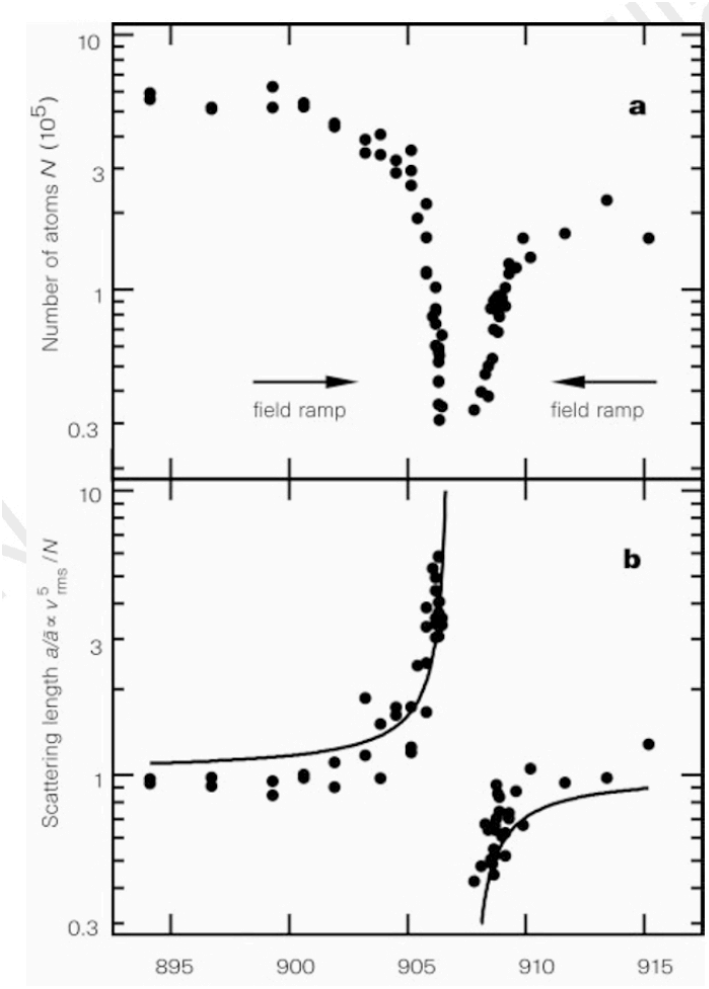

Figure 7. *Fano–Feshbach resonance in a sodium atom condensate. The top graph shows the loss of atoms in the vicinity of the resonance. The lower graph shows the variation of the scattering length, deduced from the measurement of the interaction energy of the gas, itself deduced from the ballistic expansion of the atomic cloud when it is released from the trap. Figure extracted from Inouye, Andrews, et al. (1998).*

condition $a_\perp = Ca$ corresponds precisely to the point where the energy of this bound state is equal to $\hbar\omega_\perp$, the dissociation limit of the open channel. A similar phenomenon occurs with a confinement along one direction of space, the collisions being then two-dimensional (Petrov, Holzmann, et al. 2000).

This type of resonance was observed in Innsbruck by Haller, Gustavsson, et al. (2009). Starting from a Bose-Einstein condensate of cesium atoms, the Innsbruck researchers placed this gas in a series of tubes formed by a two-dimensional optical lattice. A Fano–Feshbach resonance is then used to adjust the ratio $a/a_\perp$. Thanks to this confinement-induced resonance, Haller, Gustavsson, et al. (2009) succeeded in producing a one-dimensional gas in strong interaction (a phase called *super Tonks–Girardeau*).

Finally, it should be noted that Massignan & Castin (2006) and Nishida & Tan (2008) (see also Xiao, Zhang, et al. (2019)) have shown that this type of resonance can be extended to interactions between atoms of different species, one of which is strongly confined along certain directions in space and the other not at all. A first experimental study of this phenomenon was conducted by Lamporesi, Catani, et al. (2010).

2 Is the limit $a = \pm\infty$ singular?

The scattering resonances we will be interested in the following, namely the Fano–Feshbach resonances, are characterized by a scattering length that tends to $\pm\infty$ while the range of the potential remains finite. In a mean-field approach, where the interaction energy of a particle is proportional to an where n is the density of the gas, a singularity appears when a diverges. We show in the following that this singularity is only an artifact of the mean-field approach.

We will present here the model developed by Busch, Englert, et al. (1998), who considered two particles interacting through the pseudo-potential $\hat{V}_{\rm pp}$ (thus of zero range). These two particles are placed in an isotropic harmonic potential of frequency ω. We will see that there is a perfect continuity of the energy levels of this binary system through the $a = \pm\infty$ resonance. On the other hand, we will see that there is no conti-

nuity around $a = 0$: for the pseudopotential, the limits $a \to 0_+$ and $a \to 0_-$ are not equivalent.

We are therefore interested in the Hamiltonian

$$\hat{H}_{\rm tot} = \left(\frac{\hat{p}_A^2}{2m} + \frac{1}{2}m\omega^2 r_A^2\right) + \left(\frac{\hat{p}_B^2}{2m} + \frac{1}{2}m\omega^2 r_B^2\right) + \hat{V}_{\rm pp}(\boldsymbol{r}_A - \boldsymbol{r}_B). \quad (7)$$

We will take here the definition of the pseudo-potential based on the Bethe–Peierls boundary condition (see chapter 3).

2-1 Center-of-mass and relative variable

The interest of the choice of a harmonic confinement potential is that it preserves the separation between center-of-mass and relative variables. We have indeed

$$\boldsymbol{R} = \frac{1}{2}(\boldsymbol{r}_A + \boldsymbol{r}_B) \quad \boldsymbol{r} = \boldsymbol{r}_A - \boldsymbol{r}_B \quad \Rightarrow \qquad 2R^2 + \frac{r^2}{2} = r_A^2 + r_B^2 \quad (8)$$

which leads to

$$\frac{1}{2}m\omega^2 r_A^2 + \frac{1}{2}m\omega^2 r_B^2 = \frac{1}{2}M\omega^2 R^2 + \frac{1}{2}m\omega^2 r^2 \quad (9)$$

with $M = 2m$ for the total mass and $m_{\rm r} = m/2$ for the reduced mass.

The motion of the center-of-mass is that of a particle of mass M confined in a harmonic potential. The corresponding energy levels are unchanged by the interaction between particles and are therefore $(n + 3/2)\,\hbar\omega$, with $n = 0, 1, \ldots$. In the following, we concentrate on the motion of the relative particle which is governed by the Hamiltonian

$$\hat{H} = \frac{\hat{p}^2}{2m_{\rm r}} + \frac{1}{2}m_{\rm r}\omega^2 r^2 + \hat{V}_{\rm pp}(r). \quad (10)$$

Let us note that Chen, Xiao, et al. (2020) have recently extended this study to the case of an anisotropic harmonic potential.

2-2 The one-dimensional case

Before tackling the 3D case, it is interesting to consider the one-dimensional case for which the simple contact potential $V(x) = g\,\delta(x)$ is legitimate. The eigenvalue equation for the relative variable is then written

$$-\frac{\hbar^2}{2m_{\rm r}}\frac{{\rm d}^2\psi}{{\rm d}x^2} + \frac{1}{2}m_r\omega^2 x^2\psi(x) + g\,\delta(x)\,\psi(x) = E\,\psi(x). \quad (11)$$

Let us use the natural energy and length scales[1] for the harmonic oscillator, i.e. $\hbar\omega$ and $a_{\rm ho} = \sqrt{\hbar/m_{\rm r}\omega}$. This eigenvalue equation is simplified to

$$-\frac{1}{2}\psi''(x) + \frac{x^2}{2}\psi(x) + G\,\delta(x)\,\psi(x) = E\,\psi(x) \qquad \text{with} \quad G = g/(a_{\rm ho}\hbar\omega). \quad (12)$$

The problem is parity invariant (change $x \leftrightarrow -x$). We can therefore look for solutions in the form of even or odd functions $\psi(x)$. For an odd function, $\psi(0) = 0$ so that the contact potential does not contribute. We thus find the same eigenfunctions (Hermite functions) and the same spectrum as in the absence of interaction:

$$\text{Energies of odd functions :} \qquad E_n = n + \frac{1}{2}, \quad n = 1, 3, \ldots \quad (13)$$

These energies are plotted in red in figure 9.

We now focus on the even functions. For these, the presence of $\delta(x)$ creates a singularity at $x = 0$: the first derivative of $\psi(x)$ is discontinuous at this point with a jump obtained by integrating (12) on an arbitrarily small interval centered in 0:

$$-\frac{1}{2}\left[\psi'(0_+) - \psi'(0_-)\right] + G\psi(0) = 0. \quad (14)$$

The parity of ψ implies that $\psi'(0_-) = -\psi'(0_+)$ hence the boundary condition:

$$\text{Even functions :} \qquad \psi'(0_+) = G\,\psi(0). \quad (15)$$

Two examples of even functions with this type of angular point in $x = 0$ are plotted in figure 8.

To solve the problem completely, it is now sufficient to find out under which condition on the energy E there exists on the open interval $x \in (0, +\infty)$ a solution of

$$-\frac{1}{2}\psi''(x) + \frac{x^2}{2}\psi(x) = E\,\psi(x) \quad (16)$$

[1] We define here $a_{\rm ho}$ from the reduced mass $m_{\rm r}$ and not from the mass of each atom m. This introduces a factor $\sqrt{2}$ with respect to Busch, Englert, et al. (1998).

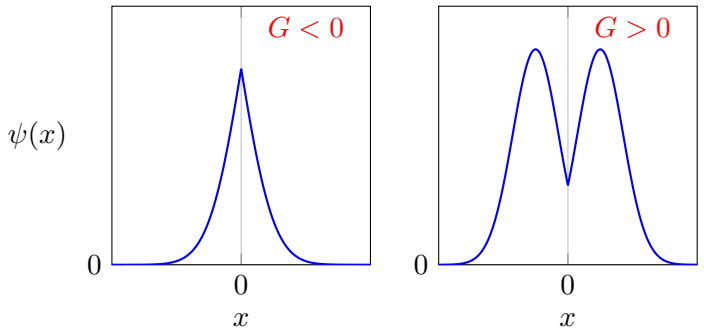

Figure 8. *Examples of angular points at $x = 0$ for even eigenfunctions, resulting from the presence of the potential $G\,\delta(x)$ in the Schrödinger equation.*

which

- satisfies the boundary condition (15),
- tends to 0 when $x \to +\infty$.

The general solution of (16) is written[2] in terms of the Kummer function $M(a, b, z)$.

$$\psi(x) \propto \left[\alpha M\left(\frac{1}{4} - \frac{E}{2}, \frac{1}{2}, x^2\right) + \beta x M\left(\frac{3}{4} - \frac{E}{2}, \frac{3}{2}, x^2\right)\right] \mathrm{e}^{-x^2/2}. \qquad (19)$$

In the vicinity of the origin, we find $M(a, b, x^2) = 1 + \mathcal{O}(x^2)$ so that the boundary condition (15) imposes $\beta = \alpha G$. When $x \to +\infty$, the Kummer function diverges as:

$$M(a, b, z) \sim \frac{\Gamma(b)}{\Gamma(a)}\, \mathrm{e}^z\, z^{a-b}. \qquad (20)$$

To prevent $\psi(x)$ from diverging as $\mathrm{e}^{x^2/2}$ at infinity, the divergences of the two contributions to (19) must cancel each other and we have to impose:

$$\frac{\Gamma(1/2)}{\Gamma(1/4 - E/2)} + G\frac{\Gamma(3/2)}{\Gamma(3/4 - E/2)} = 0 \qquad (21)$$

or by using $\Gamma(1/2) = 2\Gamma(3/2)$:

$$G = -2\,\frac{\Gamma(3/4 - E/2)}{\Gamma(1/4 - E/2)}. \qquad (22)$$

For each value of G, this relation selects an (infinite) series of discrete values of E. These values are plotted in blue in figure 9.

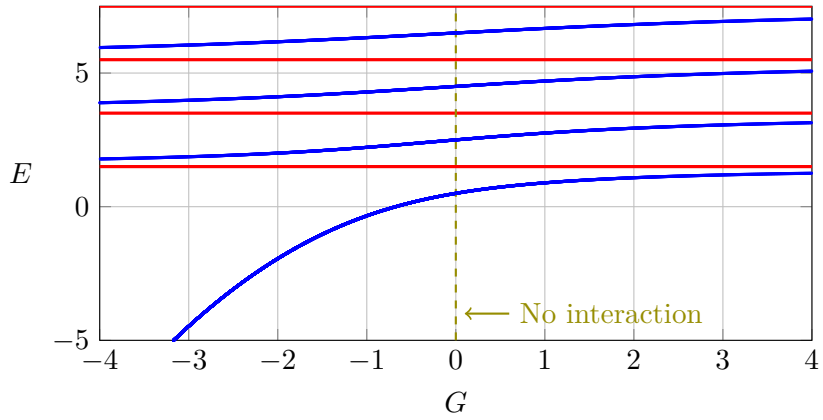

Figure 9. *1D Case. Blue: variation of the energies of even wave functions for the relative variable of two trapped particles. Red: energies of the odd wave functions.*

Let's comment on a few elements regarding this figure:

- For G large and negative, the potential $G\,\delta(\boldsymbol{r})$ simulates a deep attractive well, with a strongly bound state corresponding to an even wave

[2] To show this result, we make the changes of variable and function $z = x^2$ and $\phi(z) = \psi(x)$, which allows to rewrite (16) in the form of Kummer equation:

$$z\phi'' + (b - z)\,\phi' - a\phi = 0, \qquad (17)$$

with

$$a = \frac{1}{4} - \frac{E}{2} \qquad b = \frac{1}{2}, \qquad (18)$$

whose solutions are the Kummer functions $M(a, b, z)$ and $z^{1-b}M(a + 1 - b, 2 - b, z)$ (*cf.* Wikipedia page *Confluent hypergeometric function*).

function. The other even states must be orthogonal to this localized state. This almost amounts to impose a node in $x = 0$ to these states, as for the odd states. The energy of an excited even state is then close to that of the immediately lower odd state.

- In $G = 0$, there is no interaction and we find the unperturbed energies, $1/2$, $5/2$, $9/2$ for the even states. We find this result on (22) since the function $\Gamma(x)$ is infinite for all values $x = 0, -1, -2, \ldots$ of the argument.
- For G large and positive, we have the equivalent of a hard core potential in the neighborhood of $x = 0$, which practically imposes on the even wave functions to have a node at this point (*cf.* figure 8, right). Their energy is then very close to the odd wave function of n immediately above.

The interpretation of the one-dimensional results is therefore consistent with intuition.

2-3 The three-dimensional case

The pseudo-potential has an effect only on wave functions with zero angular momentum. Therefore, we will restrict ourselves to this class of isotropic states in what follows. We continue to use the energy scales $\hbar\omega$ and $a_{\rm ho} = \sqrt{\hbar/m_{\rm r}\omega}$ for energy and position. We thus look for the solutions of the radial Schrödinger equation for the wave function $u(r) = r\psi(r)$

$$-\frac{1}{2}u''(r) + \frac{r^2}{2}u(r) = E\,u(r) \tag{23}$$

with the Bethe–Peierls boundary condition:

$$u(r) \propto r - a \qquad \Leftrightarrow \qquad u'(0) = -\frac{1}{a}\,u(0). \tag{24}$$

Recall that in the absence of interaction or for a regular potential, the boundary condition for the reduced radial wave function is $u(0) = 0$.

The problem is thus formally identical to the one we solved in 1D, provided that we make the substitution

$$G \quad \longrightarrow \quad -\frac{1}{a}. \tag{25}$$

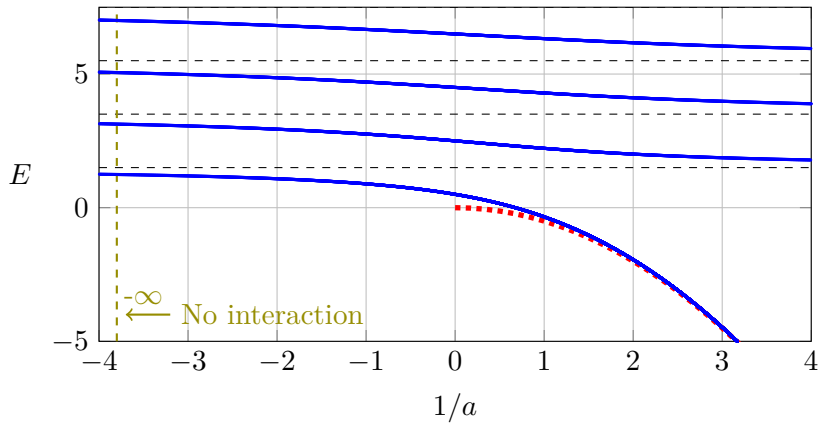

Figure 10. *3D Case. Energies of the $\ell = 0$ states for the relative variable of two trapped particles. The red dashed line gives the $-\hbar^2/2m_{\rm r}a^2$ energy of the bound state that appears for $a > 0$ in the absence of a harmonic trap. The black dashed lines show the energies of the $\ell = 0$ states in the absence of interaction.*

Therefore, we simply take the results of figure 9 as they are, and plot them in figure 10 as a function of $1/a$ (this simply means reversing the x-axis).

Despite this formal similarity in the calculations, the interpretation of the results is very different. The following points should be noted:

- In figure 10, we have drawn in black dashed lines the position of the energy levels for the states $\ell = 0$ in absence of interaction, $E_n = n+3/2$ with $n = 0, 2, 4, \ldots$. The first remark concerns the position of the ground state in the presence of interaction: it is always below the lowest of the dashed lines. This means that the pseudo-potential must be considered as attractive, in the sense that it lowers the energy of the ground state whatever the sign of a. This result is obviously very different from the one found at 1D, where the position of the ground state can be above or below the non-interacting value, depending on the sign of G.
- When $1/a \to -\infty$, i.e. $a \to 0_-$, the energy levels in the presence of interaction approach the unperturbed energy levels. It is thus this limit

(and only it) which allows to find with certainty the case without interaction.

- When we place ourselves exactly at $1/a = 0$, the Bethe-Peierls boundary condition (24) is written $u'(0) = 0$, i.e. a horizontal tangent in $r = 0$. This condition is equivalent to the one imposed on the even functions in the 1D case in the absence of interaction (§ 2-2). We thus find the $n + 1/2$ energy levels with $n = 0, 2, 4, \ldots$: in the unitary limit, the interactions lower each $\ell = 0$ state by 1 (i.e. $\hbar\omega$) with respect to the limit without interaction.

- When we cross the $1/a = 0$ region, i.e. $a = \pm\infty$, no singularity appears on the position of the energy levels. This result is of course very different from what one would expect in a mean-field theory, where the energy is proportional to a and therefore would diverge towards $\pm\infty$ at this point.

- When $1/a \to +\infty$, i.e. $a \to 0_+$, the energy of the ground state tends towards $-\infty$. This can be explained simply by the existence of a dimer in this region with an energy $-\hbar^2/(2m_r a^2)$ (red dotted line). Strictly speaking, this result for the dimer energy is only correct for free particles, but it is expected to approximately hold in the trapped case as soon as the corresponding energy becomes dominant with respect to $\hbar\omega$.

- In this region $1/a$ large and positive, one can recover the non-interacting limit, but one has to prepare the system on its first excited state. The energy of this state tends towards $3/2\ \hbar\omega$ when $a \to 0_+$. As this energy is higher than the energy found for the ground state in the absence of interaction, one often uses the term *repulsive branch* to designate this state. In particular, its generalization to the N-body problem allows to describe the atomic condensates observed in the $a > 0$ regime. However, it should be noted that, as this is an excited state, it can be fragile if an energy dissipation channel allows its decay towards the true ground state, i.e. the dimer.

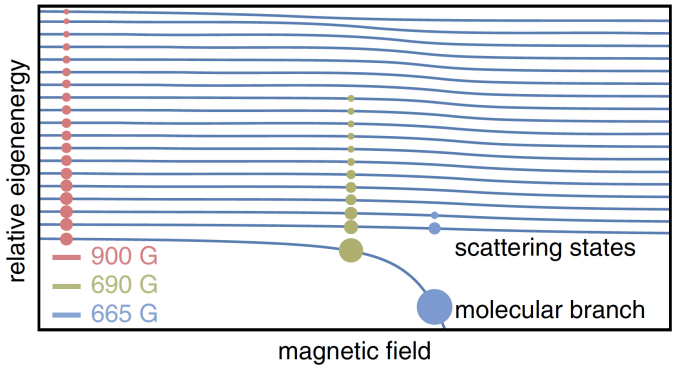

Figure 11. *Preparation of a wave packet in a system of two ^{6}Li atoms confined in an optical tweezer, thanks to a quench consisting in suddenly changing the stiffness of the trap. Figure extracted from Guan, Klinkhamer, et al. (2019).*

2-4 Experimental Study

Guan, Klinkhamer, et al. (2019) have conducted a detailed experimental study of this model by confining two ^{6}Li atoms in an optical tweezer. The atoms are prepared in two different spin states, so that s-wave interactions are allowed. Starting from the ground state of the two atoms in the optical tweezer for an adjustable scattering length, they perform a quench by abruptly changing the stiffness of the tweezer, which has the effect of preparing a coherent superposition of several eigenstates (figure 11).

The number of states contributing significantly to this superposition depends on the value of the scattering length, which is controlled by the magnetic field via a resonance:

- When a is small and negative (left of figure 11), a large number of states, close to those of the non-interacting case, are populated. Guan, Klinkhamer, et al. (2019) estimate that the population of the most populated state does not exceed $2\,\%$.

- When a is very large (unitary regime in the center of figure 11), only a few states are significantly populated.

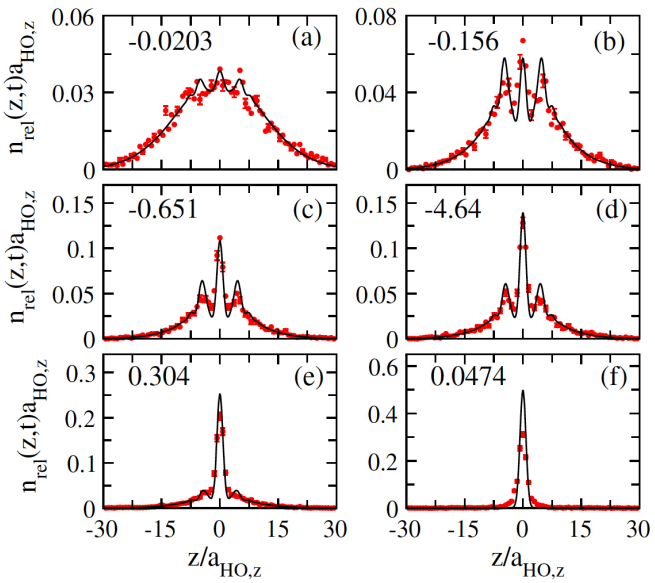

Figure 12. *Probability densities of the relative variable, measured and calculated at $t = 3.5$ ms after the quench. These measurements are made for different values of the scattering length, shown in units of $a_{\rm ho}$ (along the z axis). Figure extracted from Guan, Klinkhamer, et al. (2019).*

- When a is small and positive (right-hand side of figure 11), only the bound dimer is appreciably populated, both before and after the quench.

Once the quench is done, Guan, Klinkhamer, et al. (2019) let the system evolve freely for an adjustable time t before measuring the position of the two particles. This measurement is made with a resolution of $4\,\mu$m, which corresponds to $\sim 0.5\,a_{\rm ho}$. The results for the relative density after the delay $t = 3.5$ ms, corresponding to about 4 collisions between the two partners, are given in figure 12.

These results fully confirm the interpretation given above for this model:

- In the case $a < 0$ and small (left of figure 11), the large number of populated states leads to a rapid dephasing of the various amplitudes contributing to the wave packet and one observes a broad, almost unmodulated distribution of the relative variable, as for independent particles.
- In the intermediate regime ($|a|$ large, a situation close to the unitary regime), one can observe interference between a few amplitudes. These interferences allow to "follow" in real time the collisions between the two atoms by measuring the accumulated phase shifts.
- For $a > 0$ and small (right-hand side of figure 11), only the strongly bound dimer is significantly populated; the probability distribution for the relative variable is therefore strongly peaked around 0.

For completeness, it should be noted that these experiments were carried out in a non-isotropic harmonic trap and that the model developed above must be refined in order to make a quantitative treatment of the collision process (solid lines in figure 12).

3 A convenient tool: separable potentials

Before moving on to the modeling of a resonance of a two-channel scattering process, we will briefly study a very convenient tool for modeling a single-channel scattering process, the separable potentials. We will first explain how these potentials differ from the potentials considered so far, and then we will show that they lead to an analytical solution for the determination of the eigenstates of the Hamiltonian, both for the bound and the scattering states.

3-1 Local potential vs. separable potential

As we have seen several times in this course, the problem of the interaction between two particles can be reduced to a one-body problem evolving in a potential described by the operator $\hat{V}$. Among the possible $\hat{V}$ operators, we can distinguish (among many others) two remarkable classes:

- The most used one concerns the *local operators*[3]. A local operator is such that the action on a wave function $\psi(\boldsymbol{r}) \equiv \langle \boldsymbol{r}|\psi\rangle$ gives at the point $\boldsymbol{r}$ a result depending only on the value of the function ψ at that point, and not on the values $\psi(\boldsymbol{r}')$ at $\boldsymbol{r}' \neq \boldsymbol{r}$. The matrix elements of $\hat{V}$, which is Hermitian, are written in position representation:

$$\langle \boldsymbol{r}|\hat{V}|\boldsymbol{r}'\rangle = V(\boldsymbol{r})\ \delta(\boldsymbol{r}-\boldsymbol{r}') \tag{26}$$

so that

$$\langle \boldsymbol{r}|\hat{V}|\psi\rangle = \int \langle \boldsymbol{r}|\hat{V}|\boldsymbol{r}'\rangle\ \langle \boldsymbol{r}'|\psi\rangle \mathrm{d}^3 r' = V(\boldsymbol{r})\ \psi(\boldsymbol{r}). \tag{27}$$

- Another interesting class is the *separable operators* introduced by Yamaguchi (1954), whose matrix elements in position representation are such that

$$\langle \boldsymbol{r}|\hat{V}|\boldsymbol{r}'\rangle = V_0\, \phi_0(\boldsymbol{r})\, \phi_0(\boldsymbol{r}'), \tag{28}$$

where V_0 is a real coefficient having the dimension of an energy and where the function ϕ_0 is supposed to be real, normalized

$$\langle \phi_0|\phi_0\rangle = \int \phi_0^2(\boldsymbol{r})\ \mathrm{d}^3 r = 1, \tag{29}$$

and can be understood as the wave function of a localized state $|\phi_0\rangle$. The separable potential $\hat{V}$ is therefore proportional to the projector on $|\phi_0\rangle$:

$$\hat{V} = V_0\ |\phi_0\rangle\langle\phi_0|. \tag{30}$$

The action of $\hat{V}$ on a wave function $\psi(\boldsymbol{r})$ is written:

$$\langle \boldsymbol{r}|\hat{V}|\psi\rangle = V_0\ \phi_0(\boldsymbol{r}) \int \phi_0(\boldsymbol{r}')\, \psi(\boldsymbol{r}')\ \mathrm{d}^3 r', \tag{31}$$

which is generally non-local, in the sense defined above: the result at point $\boldsymbol{r}$ of the action of $\hat{V}$ on $|\psi\rangle$ involves the values $\psi(\boldsymbol{r}')$ over the whole area where ϕ_0 takes significant values. The range of the operator $\hat{V}$ is thus given by the size of this zone.

[3]This name does not assume anything about the range of the potential. A potential can be long-ranged, like the Coulomb potential, and verify the locality criterion defined in (26-27)

These separable potentials are not realized as such in nature, but they are very convenient models because they can be treated analytically in full. The simple model of a Fano–Feshbach resonance that we will discuss later will use this type of potential to describe the interaction between the atoms. Before tackling this two-channel problem, it is useful to look at the treatment of the one-channel problem:

$$\hat{H} = \frac{\hat{p}^2}{2m_{\mathrm{r}}} + \hat{V}, \tag{32}$$

both from the point of view of scattering states and bound states.

Note that the contact potential $\hat{V} = g\,\delta(\boldsymbol{r}-\boldsymbol{r}_0)$ (which has no singularity in 1D) can be seen as a separable potential for which the projector is on the well-defined position state $|\boldsymbol{r}_0\rangle$:

$$\hat{V} = g\,|\boldsymbol{r}_0\rangle\langle\boldsymbol{r}_0|. \tag{33}$$

The contact potential is therefore both local and separable.

3-2 Bound state in a separable potential

The eigenvalue equation of the Hamiltonian (32) for a bound state of energy $E = -\hbar^2\kappa^2/2m_{\mathrm{r}}$ is:

$$-\frac{\hbar^2}{2m_{\mathrm{r}}}\boldsymbol{\nabla}^2\psi(\boldsymbol{r}) + V_0 I\,\phi_0(\boldsymbol{r}) = -\frac{\hbar^2\kappa^2}{2m_{\mathrm{r}}}\psi(\boldsymbol{r}) \tag{34}$$

with

$$I = \langle\phi_0|\psi\rangle = \int \phi_0(\boldsymbol{r}')\,\psi(\boldsymbol{r}')\ \mathrm{d}^3 r' = \frac{1}{(2\pi)^3}\int \tilde{\phi_0}^*(\boldsymbol{q}')\,\tilde{\psi}(\boldsymbol{q}')\ \mathrm{d}^3 q'. \tag{35}$$

This equation is simpler to solve in Fourier space[4]:

$$\left(q^2+\kappa^2\right)\tilde{\psi}(\boldsymbol{q}) = \frac{I}{\sigma_0}\tilde{\phi_0}(\boldsymbol{q}), \tag{37}$$

[4]Recall the convention adopted in this course for the passage in Fourier space, i.e. from the continuous basis in position $|\boldsymbol{r}\rangle$ to the continuous basis in wave vector $|\boldsymbol{q}\rangle$:

$$\tilde{\psi}(\boldsymbol{q}) = \langle\boldsymbol{q}|\psi\rangle = \int \langle\boldsymbol{q}|\boldsymbol{r}\rangle\langle\boldsymbol{r}|\psi\rangle\ \mathrm{d}^3 r = \int \mathrm{e}^{-\mathrm{i}\boldsymbol{q}\cdot\boldsymbol{r}}\psi(\boldsymbol{r})\ \mathrm{d}^3 r, \tag{36}$$

and $\langle\boldsymbol{q}|\boldsymbol{q}'\rangle = (2\pi)^3\delta(\boldsymbol{q}-\boldsymbol{q}')$.

where we put

$$V_0 = -\frac{\hbar^2}{2m_{\rm r}\sigma_0}. \tag{38}$$

Here the real quantity σ_0 has the dimension of a surface and can be positive or negative. The solution of (37) is written :

$$\tilde{\psi}(\boldsymbol{q}) = \frac{I}{\sigma_0}\frac{\tilde{\phi_0}(\boldsymbol{q})}{q^2+\kappa^2}, \tag{39}$$

the value of κ being determined so as to satisfy the self-consistency condition imposed to the definition of I:

$$I = \frac{1}{(2\pi)^3}\int \tilde{\phi_0}^*(\boldsymbol{q})\,\tilde{\psi}(\boldsymbol{q})\,\mathrm{d}^3q = \frac{I}{\sigma_0\,(2\pi)^3}\int \frac{|\tilde{\phi_0}(\boldsymbol{q})|^2}{q^2+\kappa^2}\,\mathrm{d}^3q, \tag{40}$$

which entails

$$\frac{1}{(2\pi)^3}\int \frac{|\tilde{\phi_0}(\boldsymbol{q})|^2}{q^2+\kappa^2}\,\mathrm{d}^3q = \sigma_0. \tag{41}$$

The left-hand side is a decreasing function of κ and so there is, at σ_0 and ϕ_0 fixed, at most one value of κ that can be a solution of this equation. Note that there is no solution when σ_0 is negative.

Conversely, if one wishes to model a problem for which one knows (approximately) the energy of the bound state and the form of its wave function, the equation (41) gives the coupling V_0 to be used in the expression of the separable potential $\hat{V}$.

3-3 Scattering states in a separable potential

Let us now consider a scattering state of energy $E = \hbar^2k^2/2m_{\rm r}$, continuously connecting to the plane wave $\mathrm{e}^{\mathrm{i}\boldsymbol{k}\cdot\boldsymbol{r}}$ when the coupling g tends to 0. The eigenvalue (Lippmann–Schwinger) equation is:

$$(E-\hat{H}_0)|\psi\rangle = V_0 I\,|\phi_0\rangle \tag{42}$$

whose physically relevant solution is

$$|\psi_{\boldsymbol{k}}\rangle = |\boldsymbol{k}\rangle + \frac{V_0 I}{E-\hat{H}_0+\mathrm{i}0_+}|\phi_0\rangle. \tag{43}$$

This solution reads in position and momentum representations:

$$\psi_{\boldsymbol{k}}(\boldsymbol{r}) = \mathrm{e}^{\mathrm{i}\boldsymbol{k}\cdot\boldsymbol{r}} + V_0 I\int \mathcal{G}_0^{(+)}(\boldsymbol{r}-\boldsymbol{r}')\,\phi_0(\boldsymbol{r}')\,\mathrm{d}^3r' \tag{44}$$

$$\tilde{\psi}_{\boldsymbol{k}}(\boldsymbol{q}) = (2\pi)^3\delta(\boldsymbol{q}-\boldsymbol{k}) - \frac{I}{\sigma_0}\frac{\tilde{\phi_0}(\boldsymbol{q})}{k^2-q^2+\mathrm{i}0_+}. \tag{45}$$

For simplicity, we will restrict ourselves in what follows to the case where the real quantity $\phi_0(\boldsymbol{r})$ is spherically symmetric, which implies that $\tilde{\phi_0}(\boldsymbol{q})$ is also real and spherically symmetric. The scattered wave appearing in (43) is then isotropic, indicating that scattering occurs only in the s-wave. Using the asymptotic expression of $\mathcal{G}_0^{(+)}$ seen in chapter 2:

$$\mathcal{G}_0^{(+)}(\boldsymbol{r}-\boldsymbol{r}') = -\frac{m_{\rm r}}{2\pi\hbar^2}\,\frac{\mathrm{e}^{\mathrm{i}k|\boldsymbol{r}-\boldsymbol{r}'|}}{|\boldsymbol{r}-\boldsymbol{r}'|} \approx -\frac{m_{\rm r}}{2\pi\hbar^2}\,\frac{\mathrm{e}^{\mathrm{i}kr}}{r}\mathrm{e}^{-\mathrm{i}\boldsymbol{k}_f\cdot\boldsymbol{r}'}, \tag{46}$$

we arrive at the scattering amplitude

$$f(k) = \frac{I}{4\pi\sigma_0}\tilde{\phi_0}(k). \tag{47}$$

As for the search for a bound state, we still have to determine the value of the integral I, which is done from the self-consistency condition:

$$I = \frac{1}{(2\pi)^3}\int \tilde{\phi_0}(q)\,\tilde{\psi}_{\boldsymbol{k}}(\boldsymbol{q})\,\mathrm{d}^3q = \tilde{\phi_0}(k) - \frac{I}{\sigma_0\,(2\pi)^3}\int \frac{\tilde{\phi_0}^2(q)}{k^2-q^2+\mathrm{i}0_+}\,\mathrm{d}^3q, \tag{48}$$

which can be written

$$\begin{aligned} I &= \tilde{\phi_0}(k)\left[1+\frac{1}{\sigma_0\,(2\pi)^3}\int \frac{\tilde{\phi_0}^2(q)}{k^2-q^2+\mathrm{i}0_+}\,\mathrm{d}^3q\right]^{-1} \\ &= \tilde{\phi_0}(k)\left[1+\frac{1}{\sigma_0\,(2\pi)^3}\int \mathcal{PP}\left(\frac{\tilde{\phi_0}^2(q)}{k^2-q^2}\right)\mathrm{d}^3q - \mathrm{i}\frac{k}{4\pi\sigma_0}\,\tilde{\phi_0}^2(k)\right]^{-1} \end{aligned} \tag{49}$$

The scattering amplitude is then:

$$\frac{1}{f(k)} = \frac{1}{\tilde{\phi_0}^2(k)}\left[4\pi\sigma_0 + \frac{1}{2\pi^2}\int \mathcal{PP}\left(\frac{\tilde{\phi_0}^2(q)}{k^2-q^2}\right)\mathrm{d}^3q\right] - \mathrm{i}k. \tag{50}$$

We recover the imaginary part $-\mathrm{i}k$ imposed by the optical theorem and we have an exact analytical expression for the real part.

3-4 An example of separable potential

Yamaguchi (1954) proposed the following example, which can be treated entirely analytically[5]:

$$\phi_0(\boldsymbol{r}) = \frac{1}{\sqrt{2\pi b}} \frac{\mathrm{e}^{-r/b}}{r}, \qquad \tilde{\phi}_0(\boldsymbol{q}) = \sqrt{\frac{8\pi}{b}} \frac{1}{q^2 + \frac{1}{b^2}}, \tag{53}$$

where the length b represents the range of the potential.

A necessary condition for having a bound state is $V_0 < 0$, i.e. $\sigma_0 > 0$. More precisely, the condition of existence of a bound state (41) is

$$\frac{1}{(\kappa + \frac{1}{b})^2} = \sigma_0 \qquad \leftrightarrow \qquad \kappa = \frac{1}{\sqrt{\sigma_0}} - \frac{1}{b}. \tag{54}$$

So we must take $0 < \sigma_0 < b^2$ for the bound state to exist. When this is the case, its wave function is written:

$$\tilde{\psi}(\boldsymbol{q}) \propto \frac{1}{(q^2 + \kappa^2)(q^2 + \frac{1}{b^2})}, \qquad \psi(\boldsymbol{r}) \propto \frac{1}{r} \left(\mathrm{e}^{-\kappa r} - \mathrm{e}^{-r/b} \right). \tag{55}$$

In the same way, we can determine the scattering states and arrive in particular at the expression of the scattering length:

$$\frac{a}{b} = \frac{2b^2}{b^2 - \sigma_0}. \tag{56}$$

In particular, we find that the scattering length diverges at the threshold for the appearance of a bound state, $\sigma_0 = b^2$; it is positive when the bound state exists and negative otherwise.

[5] We recall the closure relations in position and momentum spaces:

$$\hat{1} = \int |\boldsymbol{r}\rangle\langle\boldsymbol{r}| \, \mathrm{d}^3 r = \frac{1}{(2\pi)^3} \int |\boldsymbol{q}\rangle\langle\boldsymbol{q}| \, \mathrm{d}^3 q \tag{51}$$

which lead to the following normalization for $\phi_0(\boldsymbol{r}) = \langle \boldsymbol{r} | \phi_0 \rangle$ and $\tilde{\phi}_0(\boldsymbol{q}) = \langle \boldsymbol{q} | \boldsymbol{\phi}_0 \rangle$:

$$1 = \langle \phi_0 | \phi_0 \rangle = \int |\phi_0(\boldsymbol{r})|^2 \, \mathrm{d}^3 r = \frac{1}{(2\pi)^3} \int |\tilde{\phi}_0(\boldsymbol{q})|^2 \, \mathrm{d}^3 q. \tag{52}$$

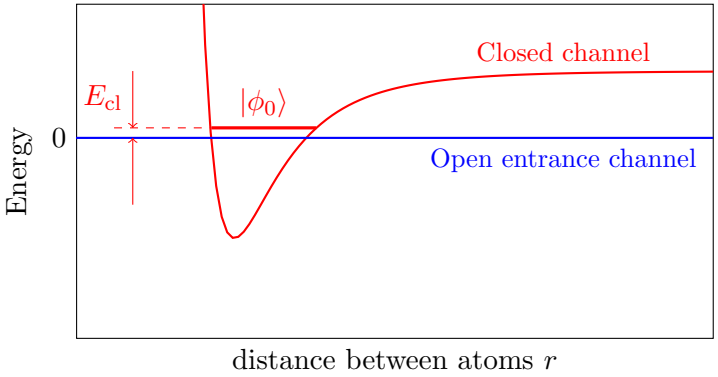

Figure 13. *Simplified model of a Fano–Feshbach resonance: we assume that there is no interaction in the entrance channel. Moreover, we make the approximation that only one bound state of the closed channel contributes significantly to the resonance.*

4 A simple model of Fano–Feshbach resonance

In this section, we develop a simplified model of a Fano–Feshbach resonance, which will allow us to calculate analytically all the properties of the system. In the next chapter, we will see that this model is in fact rich enough to identify the important parameters such as the width of the resonance and the contribution of the closed channel. Other analytical approaches based on simple model potentials can be found in the literature, see for example Kokkelmans, Milstein, et al. (2002), Duine & Stoof (2004), Gogolin, Mora, et al. (2008), and Chin, Grimm, et al. (2010).

4-1 The physical model

We assume that the two atoms collide in a channel for which there is no interaction (figure 13). The Hamiltonian of this open channel is

$$\hat{H}_0 = \frac{\hat{p}^2}{2m_{\mathrm{r}}} \tag{57}$$

for the relative variable. For the *closed channel* which will allow the resonance, we make the approximation that only a bound state contributes, in a way similar to what we saw in the previous paragraph in the framework of separable potentials. We will note this state $|\phi_0\rangle$ and its energy $E_{\rm cl}$.

The wave function $\phi_0(\boldsymbol{r})$ is assumed to be normalized, $\int |\phi_0(\boldsymbol{r})|^2 \, \mathrm{d}^3 r = 1$, and it is "rigid"; the only control parameter in all that follows is the energy $E_{\rm cl}$, which can be varied for example by changing the ambient magnetic field. This energy $E_{\rm cl}$ is referenced to the zero energy of the open channel, corresponding to zero incident kinetic energy.

In this model, a given state of the relative variable for our pair of atoms is therefore a two-component spinor, giving the probability amplitudes for the two channels:

$$\begin{pmatrix} \text{open} \\ \text{closed} \end{pmatrix} = \begin{pmatrix} |\psi\rangle \\ |\phi\rangle \end{pmatrix} \qquad \text{with} \quad |\phi\rangle = \alpha |\phi_0\rangle. \tag{58}$$

The unknowns are the wave function $\psi(\boldsymbol{r})$ and the proportionality coefficient α (a complex number), which must be determined according to the problem studied.

We will denote $\hat{W}$ the operator coupling the open and the closed channels. We will assume that this operator is local in position and thus characterized by a function $W(\boldsymbol{r})$. Just like the wave function of the bound state $\phi_0(\boldsymbol{r})$, the function $W(\boldsymbol{r})$ is localized in the neighborhood of the origin, where the inter-channel couplings mentioned in § 1 are significant. We will see very soon that the results depend only on the product $W(\boldsymbol{r})\, \phi_0(\boldsymbol{r})$. To simplify the notations, we will assume that this product is real, but our approach can be easily generalized to the complex case. Moreover, we will assume it to be isotropic so that its Fourier transform will also be isotropic. This assumption is correct if the bound state is formed in an s-wave channel. An eigenstate of energy E of the two-channel model must therefore satisfy the two coupled equations

$$\hat{H}_0 |\psi\rangle + \hat{W} |\phi\rangle = E\, |\psi\rangle \tag{59}$$

$$\hat{W} |\psi\rangle + E_{\rm cl} |\phi\rangle = E\, |\phi\rangle. \tag{60}$$

This system of two equations is valid both for the search of scattering states, asymptotically free and thus with energy $E > 0$, and of possible two-channel bound states, with energy $E < 0$.

4-2 Search for scattering states

Let us choose an energy $E > 0$ and solve the system (59-60). Look at the first of these equations in which we replace $|\phi\rangle$ by its value $\alpha|\phi_0\rangle$, without trying to determine the complex coefficient α for the moment. This equation is written

$$(E - \hat{H}_0)|\psi\rangle = \alpha \hat{W} |\phi_0\rangle \tag{61}$$

and can be solved by the usual technique of Green function that we used in chapter II. It is formally identical to the one found for a separable potential in the previous paragraph [eq. (42)] and we will therefore solve it in the same way. We use here the operator notation, which is a bit more compact. We introduce as in chapter 2

$$\hat{G}_0(E) = \frac{1}{E - \hat{H}_0 + \mathrm{i}0_+} \tag{62}$$

where we added as before an infinitesimal and positive imaginary part, corresponding to the advanced Green function (outgoing spherical wave). A particular solution of the equation (61) without a source term is a state with a well-defined momentum, $|\boldsymbol{k}\rangle$, i.e. the plane wave $\mathrm{e}^{\mathrm{i}\boldsymbol{k}\cdot\boldsymbol{r}}$, so that a physically relevant solution of (61) for our problem is

$$|\psi_{\boldsymbol{k}}\rangle = |\boldsymbol{k}\rangle + \alpha\, \hat{G}_0(E)\, \hat{W} |\phi_0\rangle. \tag{63}$$

This expression, similar to the equation (43) obtained for a separable potential, already constitutes a first element of answer to our scattering problem. The above expression has indeed the canonical form of a scattering state with an incident plane wave of wave vector $\boldsymbol{k}$ (with $E = \hbar^2 k^2 / 2m_{\rm r}$) and a scattered wave. An identical approach to that of chapter 2 based on the asymptotic expression of the Green function $\mathcal{G}_0(\boldsymbol{r} - \boldsymbol{r}') = \langle \boldsymbol{r}|\hat{G}_0(E)|\boldsymbol{r}'\rangle$ leads to the asymptotic wave function:

$$\psi_{\boldsymbol{k}}(\boldsymbol{r}) \underset{r\to\infty}{\sim} \mathrm{e}^{\mathrm{i}\boldsymbol{k}\cdot\boldsymbol{r}} - \alpha \frac{m_{\rm r}}{2\pi\hbar^2} \, \frac{\mathrm{e}^{\mathrm{i}kr}}{r} \int \mathrm{e}^{-\mathrm{i}\boldsymbol{k}_f\cdot\boldsymbol{r}'} \, W(\boldsymbol{r}')\, \phi_0(\boldsymbol{r}') \, \mathrm{d}^3 r'. \tag{64}$$

We recognize here the Fourier transform of the function $W(\boldsymbol{r})\phi_0(\boldsymbol{r})$, taken at the point $\boldsymbol{k}_f = k\boldsymbol{r}/r$. In the following, it will be useful to introduce the

function proportional to this Fourier transform:

$$g(\boldsymbol{k}) = \sqrt{\frac{m_{\rm r}}{2\pi\hbar^2}} \int \phi_0(\boldsymbol{r})\, W(\boldsymbol{r})\, {\rm e}^{-{\rm i}\boldsymbol{k}\cdot\boldsymbol{r}}\, {\rm d}^3r \tag{65}$$

$$= \sqrt{\frac{m_{\rm r}}{2\pi\hbar^2}}\, \langle \boldsymbol{k}|\hat{W}|\phi_0\rangle. \tag{66}$$

As we wrote above, the assumption of reality and isotropy for $\phi_0\, W$ entails that g is also real and isotropic: $g(\boldsymbol{k}) = g(k)$.

The scattering amplitude associated with the state (64) is written

$$f(k) = -\alpha \sqrt{\frac{m_{\rm r}}{2\pi\hbar^2}}\, g(k), \tag{67}$$

and we now need to determine the coefficient α to complete our study of the scattering problem.

To do this, we transfer the result (63) for $|\psi_{\boldsymbol{k}}\rangle$ into the second equation of the system (59-60) and we find

$$\hat{W}|\boldsymbol{k}\rangle + \alpha\, \hat{W}\, \hat{G}_0(E)\, \hat{W}|\phi_0\rangle + E_{\rm cl}\, \alpha\, |\phi_0\rangle = E\alpha\, |\phi_0\rangle. \tag{68}$$

We project this equation onto $|\phi_0\rangle$ and group the terms proportional to α to arrive at the explicit expression:

$$\alpha = \frac{\langle\phi_0|\hat{W}|\boldsymbol{k}\rangle}{E - E_{\rm cl} - \langle\phi_0|\hat{W}\, \hat{G}_0(E)\, \hat{W}|\phi_0\rangle}. \tag{69}$$

The numerator of (69) also involves the Fourier transform of the function $\phi_0(\boldsymbol{r})\, W(\boldsymbol{r})$ taken at point $\boldsymbol{k}$. The matrix element in the denominator can be written:

$$-\langle\phi_0|\hat{W}\, \hat{G}_0(E)\, \hat{W}|\phi_0\rangle = -\frac{1}{(2\pi)^3} \int \frac{|\langle\phi_0|\hat{W}|\boldsymbol{q}\rangle|^2}{E - \varepsilon(\boldsymbol{q}) + {\rm i}0_+}\, {\rm d}^3q, \tag{70}$$

where we have set as in the previous chapters $\varepsilon(\boldsymbol{q}) = \hbar^2q^2/2m_{\rm r}$. Here again, the result is expressed in terms of the Fourier transform of $\phi_0(\boldsymbol{r})\, W(\boldsymbol{r})$, this time taken at a generic point $\boldsymbol{q}$.

To evaluate (70), we use :

$$\frac{1}{E - \varepsilon(\boldsymbol{q}) + {\rm i}0_+} = \mathcal{P}\mathcal{P}\left(\frac{1}{E - \varepsilon(\boldsymbol{q})}\right) - {\rm i}\pi\, \delta(E - \varepsilon(\boldsymbol{q})). \tag{71}$$

Let us first look at the imaginary part of this expression. We have $\delta(E - \frac{\hbar^2q^2}{2m_{\rm r}}) = \delta(k-q)\, \frac{m_{\rm r}}{\hbar^2 q}$, which leads to the simple result:

$$\text{imaginary part of (70)}: \qquad {\rm i}k\, g^2(k). \tag{72}$$

As for the real part, it cannot be calculated explicitly at this stage and we will simply pose, once the angular integral is done:

$$\text{real part of (70)}: \qquad \delta E_{\rm cl}(k) = \frac{2}{\pi} \int_0^{+\infty} \frac{q^2}{q^2 - k^2}\, g^2(q)\, {\rm d}q. \tag{73}$$

The value of α is therefore:

$$\alpha = \frac{\sqrt{\frac{2\pi\hbar^2}{m_{\rm r}}}\, g(k)}{E - E_{\rm cl} + \delta E_{\rm cl}(k) + {\rm i}k\, g^2(k)} \tag{74}$$

from which we obtain the scattering amplitude using (67):

$$f(k) = \frac{g^2(k)}{E_{\rm cl} - \delta E_{\rm cl}(k) - E - {\rm i}kg^2(k)}, \quad E = \frac{\hbar^2k^2}{2m_{\rm r}}. \tag{75}$$

Let us insist on the fact that within the framework of the model, we have not made any approximation. The function $f(k)$ must therefore satisfy all the properties required for a scattering amplitude, in particular the optical theorem. We verify indeed that

$$\frac{1}{f(k)} = \frac{E_{\rm cl} - \delta E_{\rm cl}(k) - E}{g^2(k)} - {\rm i}k, \tag{76}$$

with the correct imaginary part.

4-3 Scattering length

The scattering length is defined as $a = -\lim_{k\to 0} f(k)$, which gives using (75):

$$a = -\frac{g_0^2}{E_{\rm cl} - \Delta} \qquad \text{with} \quad g_0 \equiv g(0) \tag{77}$$

and

$$\Delta \equiv \delta E_{\rm cl}(0) = \frac{2}{\pi} \int_0^{+\infty} g^2(q)\, {\rm d}q, \tag{78}$$

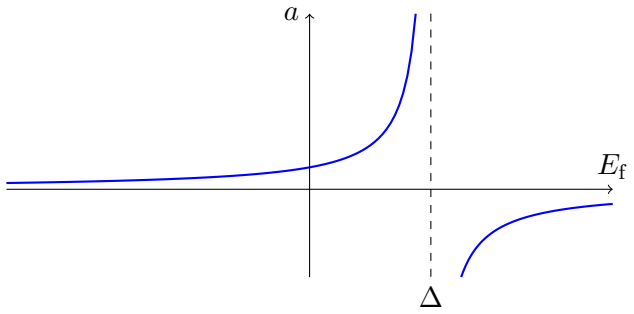

Figure 14. *Variation of the scattering length a with the energy $E_{\rm cl}$ of the state $|\phi_0\rangle$ for our simple model [Eq. (77)].*

the quantity Δ being obviously positive.

The result (77), plotted in Figure 14, is the first lesson of our study. Any value for the scattering length, positive or negative, can be obtained by properly adjusting the control parameter $E_{\rm cl}$. The resonance itself is obtained by taking

$$\text{resonance}: \quad E_{\rm cl} = \Delta. \tag{79}$$

The position of this resonance is not $E_{\rm cl} = 0$ as one could have naively expected: the maximum (infinite) scattering length is obtained by adjusting the position of the bound state above the $E = 0$ energy of the open channel, with the following formal expression for the shift Δ [see also (78)]

$$\Delta = -\langle\phi_0|\hat{W}\,\hat{G}_0(0)\,\hat{W}|\phi_0\rangle \;\geq 0. \tag{80}$$

In the context of our model, this result is exact. As we will show in the next chapter, its structure is reminiscent of the result of second-order perturbation theory for the $|\phi_0\rangle$ state, with the square of the matrix element of W in the numerator, and the energy of the free states in the denominator. In the next chapter, we will also study how to connect this simple model with the physical problem of two-atom interaction via a van der Waals potential.

Chapter VI

Characterization of a Fano–Feshbach resonance

We continue in this chapter our study of the Fano–Feshbach resonances. Let us recall that this is a process involving two collision channels, one open, the other closed, whose relative energies can be controlled which allows one to scan the resonance. Thanks to this remarkable tool, one can now use dilute quantum gases to approach the physics of strong interactions, with a scattering length that can reach, or even exceed, the average distance between particles.

In the previous chapter, we presented a simple model to describe a Fano–Feshbach resonance, with a non-interacting open entrance channel and a closed channel described by a separable potential associated to a function ϕ_0. We have shown that it leads to a resonant behavior of the scattering length when the energy $E_{\rm cl}$ of the closed channel approaches the zero energy of the open channel. We now wish to deepen the predictions of this model to reach the important notion of *resonance width* and to clarify the contribution of the closed channel. We will then move on to describe more quantitative treatments of these resonances, ending with the presentation of some recent experiments. We will examine the main tools available in the laboratory to characterize these resonances and we will see that they can have unexpected extensions, in connection for example with quantum chaos.

As we have already indicated in the previous chapter, the literature dealing with Fano–Feshbach resonances in atomic gases is extremely vast and it is not possible to cite here all the important work that has been done. We refer the interested reader to the review articles by Köhler, Góral, et al. (2006), Chin, Grimm, et al. (2010) and Naidon & Endo (2017).

1 A simple model (continued)

1-1 The ingredients of the model

The model introduced in the previous chapter is based on the following elements (figure 1):

- The particles do not interact in the open channel.
- In the closed channel, the interaction potential is separable, corresponding to the projector on the localized state $\phi_0(\boldsymbol{r})$.
- The coupling between open and closed channels is described by the potential $W(\boldsymbol{r})$.

In this model, a given state of the relative variable for our pair of atoms is a two-component spinor, giving the probability amplitudes for the two channels:

$$\begin{pmatrix} \text{open} \\ \text{closed} \end{pmatrix} = \begin{pmatrix} |\psi\rangle \\ |\phi\rangle \end{pmatrix} \qquad \text{with} \quad |\phi\rangle = \alpha|\phi_0\rangle. \tag{1}$$

The unknowns are the wave function $\psi(\boldsymbol{r})$ and the proportionality coefficient α, these unknowns being determined by solving the eigenvalue equa-

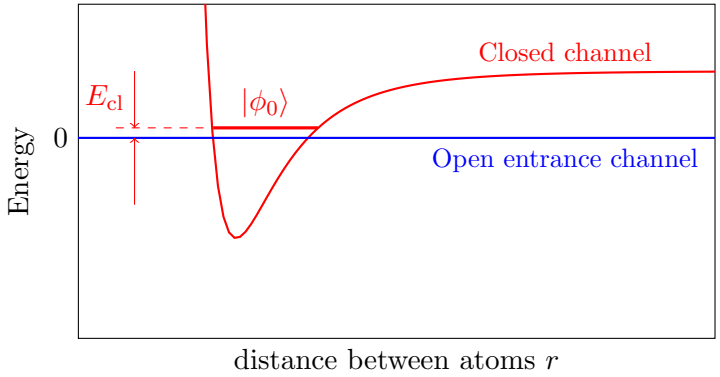

Figure 1. *Modeling of a Fano–Feshbach resonance. We assume that the particles do not interact in the input channel (open channel). Moreover, we assume that only one bound state of the closed channel contributes to the resonance.*

tion for the Hamiltonian. More precisely, an eigenstate of energy E in this two-channel model satisfies the two coupled equations

$$\hat{H}_0|\psi\rangle + \hat{W}|\phi\rangle = E\,|\psi\rangle \tag{2}$$
$$\hat{W}|\psi\rangle + E_{\rm cl}|\phi\rangle = E\,|\phi\rangle. \tag{3}$$

The main result of the analysis carried out in the previous chapter is the expression of the s-wave scattering amplitude $f(k)$:

$$f(k) = \frac{g^2(k)}{E_{\rm cl} - E + \langle\phi_0|\hat{W}\hat{G}_0(E)\hat{W}|\phi_0\rangle} \qquad \text{with} \quad E = \frac{\hbar^2k^2}{2m_{\rm r}}, \tag{4}$$
$$= \frac{g^2(k)}{E_{\rm cl} - \delta E_{\rm cl}(k) - E - {\rm i}kg^2(k)}, \tag{5}$$

where the coupling $g(k)$ is related to the Fourier transform of the product $W(\boldsymbol{r})\phi_0(\boldsymbol{r})$, which we assume to be real and isotropic:

$$g(k) = \sqrt{\frac{m_{\rm r}}{2\pi\hbar^2}} \int {\rm e}^{-{\rm i}\boldsymbol{k}\cdot\boldsymbol{r}}\, W(\boldsymbol{r})\,\phi_0(\boldsymbol{r})\,{\rm d}^3r = \sqrt{\frac{m_{\rm r}}{2\pi\hbar^2}}\,\langle\boldsymbol{k}|\hat{W}|\phi_0\rangle. \tag{6}$$

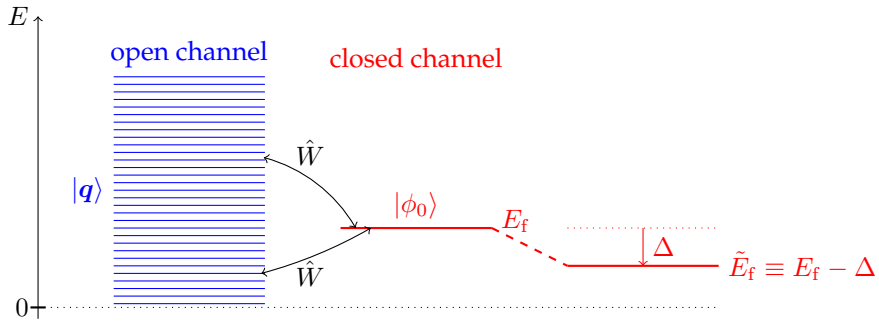

Figure 2. *The energy of the closed channel is displaced due to its coupling with the continuum formed by the open channel. The resonance occurs when this displacement brings the level $|\phi_0\rangle$ to zero energy [*cf. *eq. (10)].*

The energy shift $\delta E_{\rm cl}(k)$ is given by

$$\delta E_{\rm cl}(k) = \frac{2}{\pi}\int_0^{+\infty} \frac{q^2}{q^2-k^2}\,g^2(q)\,{\rm d}q. \tag{7}$$

The limit $k \to 0$ of the scattering amplitude $f(k)$ gives the value of scattering length

$$a = -\frac{g_0^2}{\tilde{E_{\rm cl}}} \qquad \text{with} \quad g_0 \equiv g(0), \quad \tilde{E_{\rm cl}} \equiv E_{\rm cl} - \Delta \tag{8}$$

and

$$\Delta \equiv \delta E_{\rm cl}(0) = -\langle\phi_0|\hat{W}\,\hat{G}_0(0)\,\hat{W}|\phi_0\rangle = \frac{2}{\pi}\int_0^{+\infty} g^2(q)\,{\rm d}q. \tag{9}$$

The expression (8) shows that the resonance $a = \pm\infty$ occurs when we adjust the energy of the closed channel to

$$\tilde{E_{\rm cl}} = E_{\rm cl} - \Delta = 0. \tag{10}$$

One could have naively expected that the resonance would occur when $E_{\rm cl} = 0$, i.e. when the energy of the state of the closed channel coincides with the asymptotic energy of the open channel, in this case $E = 0$. But this

would ignore the fact that the coupling between the two channels shifts the energy of the state of the closed channel.

The shift of the resonance to $E_{\rm cl} = \Delta$ can be explained simply by considering the energy shift of $|\phi_0\rangle$ at order 2 of the perturbation theory[1] (*cf.* figure 2):

$$\begin{aligned} E_{\rm cl}^{(2)} &= E_{\rm cl} + \sum_{\boldsymbol{q}} \frac{|\langle \boldsymbol{q}|\hat{W}|\phi_0\rangle|^2}{E_{\rm cl}-\epsilon_q} \qquad \text{with} \quad \epsilon_q = \frac{\hbar^2 q^2}{2m_{\rm r}}, \\ &= E_{\rm cl} + \frac{1}{(2\pi)^3}\int \frac{|\langle \boldsymbol{q}|\hat{W}|\phi_0\rangle|^2}{E_{\rm cl}-\epsilon_q}\,{\rm d}^3q. \end{aligned} \tag{11}$$

At this order of the perturbation theory, the resonance between the two channels is expected for $E_{\rm cl}^{(2)} = 0$, i.e.

$$0 = E_{\rm cl} + \frac{1}{(2\pi)^3}\int \frac{|\langle \boldsymbol{q}|\hat{W}|\phi_0\rangle|^2}{-\epsilon_q}\,{\rm d}^3q \tag{12}$$

where we have taken $E_{\rm cl} = 0$ in the integral of the right-hand side, since the numerator of this integral already involves the coupling to order 2. Using the relation (6) between the matrix element $\langle \boldsymbol{q}|\hat{W}|\phi_0\rangle$ and $g(q)$, we immediately verify that this resonance condition is equivalent to (10), i.e. $\tilde{E_{\rm cl}} = 0$.

In what follows, we will use the "renormalized" energy $\tilde{E_{\rm cl}} = E_{\rm cl} - \Delta$ rather than the "bare" energy $E_{\rm cl}$ to characterize the position of the state $|\phi_0\rangle$ in the vicinity of the resonance.

1-2 Is there a bound state?

As we have seen in the previous chapters, the problem of low-energy scattering is intimately related to the search for weakly bound states. More precisely, we know that for single channel scattering, the divergence of a is associated with the appearance of a new bound state: this state appears when a switches from large and negative values to large and positive values. Its energy in the regime of large a is given by

$$E_{\rm bound} \approx -\frac{\hbar^2}{2m_{\rm r}a^2}, \tag{13}$$

and its wave function is

$$\psi_{\rm bound}(\boldsymbol{r}) \approx \frac{{\rm e}^{-\kappa r}}{r} \qquad \text{with} \quad \frac{\hbar^2\kappa^2}{2m_{\rm r}} = |E_{\rm bound}|. \tag{14}$$

This result remains valid in our two-channel model, at least in the immediate vicinity of the resonance.

The explicit search for bound states is carried out in the appendix of this chapter. It is shown that there is at most one bound state and that its energy (when it exists) is given by the pole of the scattering amplitude (4), i.e. an energy E satisfying the equation :

$$E - \langle\phi_0|\hat{W}\,\hat{G}_0(E)\,\hat{W}|\phi_0\rangle = E_{\rm cl}. \tag{15}$$

It is also shown that this equation has a solution only if $\tilde{E_{\rm cl}} < 0$, corresponding to a positive scattering length. This is summarized in figure 3.

We can recover this result from the calculated scattering amplitude[2] to order 1 in k, so in the immediate vicinity of the resonance:

$$\text{order 1 in } k: \qquad f(k) \approx \frac{g_0^2}{\tilde{E_{\rm cl}} - {\rm i}kg_0^2} \tag{17}$$

At this order in k, the function $f(k)$ admits a single pole in $k = {\rm i}\kappa$ with $\kappa = -\tilde{E_{\rm cl}}/g_0^2 = 1/a$, so that the corresponding state[3] $\propto {\rm e}^{{\rm i}kr}/r = {\rm e}^{-\kappa r}/r$ is decreasing at infinity only if $\kappa > 0$, so $a > 0$. The energy of the bound state is then given by the "universal" law (13).

Let us note moreover that the extension $1/\kappa = a$ of the bound state wave function is very large in the near-resonant regime. It thus exceeds that of the $|\phi_0\rangle$ state of the closed channel, which is a fixed quantity. Therefore, we expect the bound state to be essentially carried by the open channel in this regime. We will verify and clarify this point in the next section.

[1] The shift at order 1 is null because we have assumed $\langle\phi_0|\hat{W}|\phi_0\rangle = 0$.

[2] Note that because of the spherical symmetry of the function $W\phi_0$, its Fourier transform

$$g(q) = \frac{2\pi}{q}\int_0^{+\infty} \sin(qr)\,W(r)\,\phi_0(r)\,r\,{\rm d}r \tag{16}$$

has a Taylor expansion including only even powers of q.

[3] Remember that we selected ${\rm e}^{{\rm i}kr}/r$ and not ${\rm e}^{-{\rm i}kr}/r$ by taking the advanced Green function.

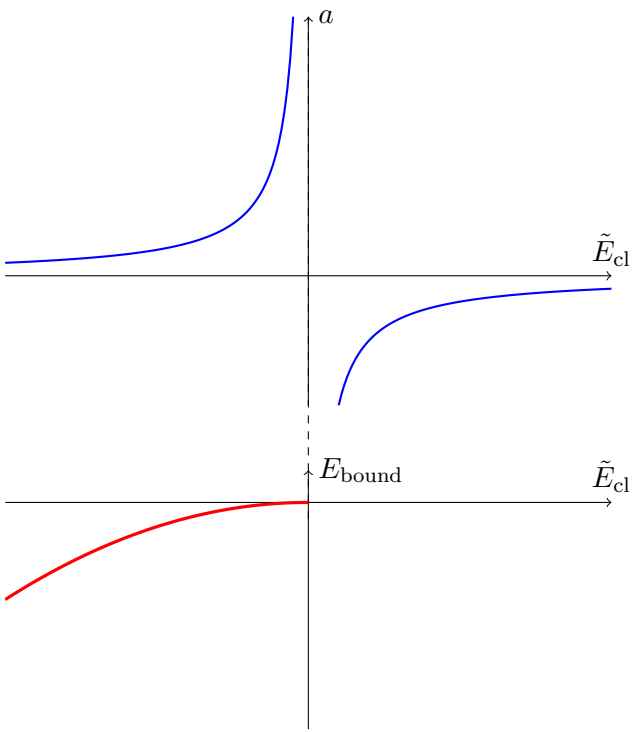

Figure 3. *Top: variation of the scattering length a with the renormalized energy $\tilde{E}_{\rm cl}$ of the $|\phi_0\rangle$ state [Eq. (8)]. Bottom: variation of the energy of the bound state according to the "universal" law (13). The bound state appears in the domain $\tilde{E}_{\rm cl} < 0$, corresponding to positive values of a. The limits of the region where this universal law is valid are discussed in § 2.*

1-3 Structure of the resonance

Before going further in the exploration of our model, it is useful to check that the form (5) found for the scattering amplitude corresponds to the canonical expressions given in the literature. Let us start with Landau & Lifshitz (1975), who propose the following expression in the vicinity of a scattering resonance [their eq. (134.17)]:

$$f(k) = -\alpha - \frac{\hbar\gamma}{\sqrt{2m_{\rm r}}\left(E - E_0 + {\rm i}\gamma\sqrt{E}\right)}, \tag{18}$$

where α represents the background scattering length taken equal to zero in our model. Our result (5) reduces to this expression when we take the small k limit: $g(k) \to g_0$, $\delta E_{\rm cl}(k) \to \Delta$; it is then sufficient to take $E_0 \equiv \tilde{E}_{\rm cl}$ and to define the width γ by:

$$\frac{\hbar\gamma}{\sqrt{2m_{\rm r}}} = g_0^2, \tag{19}$$

to identify (5) and (18).

Very recently, Naidon & Pricoupenko (2019) have made a critical analysis of the treatments used so far for Fano–Feshbach resonances in atomic physics. They use the following form for the scattering length [their eq. (17)]:

$$a = a_{\rm bg} - \frac{\lim_{k\to 0}\Gamma/2k}{E_m + \Delta}. \tag{20}$$

This corresponds to our expression (8) with the same definition of Δ (except for the sign), the identification $E_m \equiv E_{\rm cl}$ and the definition of the width Γ:

$$\Gamma = 2kg_0^2. \tag{21}$$

In the two cases mentioned above, the widths γ and Γ are proportional to our parameter g_0^2, and they are not dimensionless. To define unambiguously the notion of wide/narrow resonances, it is preferable to use a dimensionless number, i.e. to compare γ or Γ to a physically relevant quantity expressed in the same physical unit. This is what we will do in the following paragraph.

1-4 The width of the resonance

A Fano–Feshbach resonance leads to a divergence of the scattering length to positive or negative values, depending on the sign of $\tilde{E}_{\rm cl}$. Close to resonance, it coincides with the universal regime of a zero-energy resonance found in the single channel case, with a bound state of energy $\approx -\hbar^2/2m_{\rm r}a^2$ when $\tilde{E}_{\rm cl}$ is close enough to 0 and negative. To better characterize a Fano–Feshbach resonance, we must now specify its width, i.e. the domain over which the universal regime applies.

We start from a "reasonable" value for a, which we take equal to the length $R_{\rm vdW} = \frac{1}{2}\left(2m_{\rm r}C_6/\hbar^2\right)^{1/4}$ introduced in chapter IV for van der Waals interaction. We can assume that the open channel, which we have taken here without interaction to simplify the calculations, has in fact a scattering length of this order. The important question at this point is: Can the universal regime cover all values of $|a|$ from infinity up to $\sim R_{\rm vdW}$ or does it stop much earlier? We will see that the answer to this question depends on the strength of the coupling between the two channels.

To characterize the coupling strength in our model, we will use the energy Δ defined in (9), which gives the shift of the closed channel state induced by the coupling $\hat{W}$, at order two of perturbation theory. It will be useful to relate this energy Δ to the parameter g_0^2 which enters the expression of a [*cf.* (8)]; to do this, let us assume that the product $W(r)\phi_0(r)$ has itself a spatial extension of the order of $R_{\rm vdW}$, i.e. an extension $\sim 1/R_{\rm vdW}$ for its Fourier transform $g(q)$ defined in (6). Since the energy Δ defined in (9) involves the integral over q of $g^2(q)$, we find:

$$\Delta \sim \frac{g_0^2}{R_{\rm vdW}}. \tag{22}$$

In what follows, we will assume for simplicity that the above relationship is an equality. The introduction of a multiplicative factor of order 1 would not change our conclusions.

The van der Waals problem provides a natural energy scale, $E_{\rm vdW} = \hbar^2/(2m_{\rm r}R_{\rm vdW}^2)$, and it is therefore natural to measure the energy Δ using this scale. We will explain in detail in §2 why the ratio $\Delta/E_{\rm vdW}$ is decisive to characterize the nature of the resonance. More precisely, we will use the following classification:

$$\text{Large resonance :} \qquad \Delta \gg E_{\rm vdW}, \tag{23}$$

$$\text{Narrow resonance :} \qquad \Delta \ll E_{\rm vdW}. \tag{24}$$

We can already give a qualitative justification of this choice by returning to the expression (5) of the scattering amplitude $f(k)$. The physically interesting values of k are $\lesssim 1/R_{\rm vdW}$ since beyond this value, the contributions of the other partial waves become significant. At order 0 in k, we have $f(k) = -a$ which we have already commented. At order 1, $E_{\rm cl} - \delta E_{\rm cl}(k) = E_{\rm cl} - \Delta = \tilde{E}_{\rm cl}$, $g(k) = g_0$, $E = 0$ and we find

$$\text{order 1 in } k : \qquad f(k) = \frac{g_0^2}{\tilde{E}_{\rm cl} - {\rm i}kg_0^2} \tag{25}$$

which leads to the "universal" regime. Let us now look at the possible corrections to order 2 in k which are of two kinds:

- The Taylor expansion of $g^2(k)$ and $\delta E_{\rm cl}(k)$: if one takes a smoothly varying function $g(k)$ on the scale of $1/R_{\rm vdW}$, one does not expect these corrections, which are of the type *effective range*, to play a role different from that which they have for a single-channel scattering.
- The energy $E = \hbar^2k^2/2m_{\rm r}$ which is to be compared to the linear term ${\rm i}kg_0^2$ for k up to the value $1/R_{\rm vdW}$. Using (22), it is then immediately noticed that this term is negligible for a broad resonance, while it is dominant for a narrow resonance.

It is therefore expected – and this will be confirmed in §2 – that for a broad resonance, the properties of the resonance are similar to those of a single-channel zero-energy resonance. One can therefore stick to (25), which can be written

$$\text{Broad:} \qquad f(k) \approx \frac{-a}{1+{\rm i}ka} \qquad \text{with} \quad a = -\frac{g_0^2}{\tilde{E}_{\rm cl}} \tag{26}$$

for all values of k up to $R_{\rm vdW}^{-1}$.

On the contrary, for a narrow resonance, only the immediate vicinity of $\tilde{E}_{\rm cl} = 0$, with a very large scattering length, can be described with the formalism of a single channel resonance. As soon as one leaves this domain,

one must return to the description in terms of coupled channels; in particular, the contribution of the closed channel dominates that of the open channel for the bound state associated with the scattering resonance. Regarding the scattering amplitude, it reads (Petrov 2003):

$$\text{Narrow:} \qquad f(k) \approx \frac{-a}{1 + \mathrm{i}ka + k^2 R_* a} \qquad \text{with} \quad R_* \equiv \frac{\hbar^2}{2m_{\mathrm{r}} g_0^2}. \tag{27}$$

For a narrow resonance, the length R_* is much larger than R_{vdW} and the quadratic term in the denominator of (27) becomes dominant even for relatively small values of k. Note that (27) has the general structure that we derived in Chapter 3 for the s-wave scattering amplitude in terms of scattering length a and effective range r_e:

$$f(k) = \frac{-a}{1 + \mathrm{i}ka - \frac{1}{2}k^2 r_e a}, \tag{28}$$

with the effective range $r_e = -2R_*$ negative and large compared to its "usual" value $\sim R_{\mathrm{vdW}}$.

Link with other parameterizations. The dimensionless parameter Δ/E_{vdW} used here is equivalent to that introduced by Naidon & Endo (2017):

$$\frac{\Delta}{E_{\mathrm{vdW}}} \sim \frac{R_{\mathrm{vdW}}}{R_*}. \tag{29}$$

One can check that this parameter also coincides with the parameter s_{res} introduced by Chin, Grimm, et al. (2010) [their equation (35)], once references to the background scattering length a_{bg} and the magnetic moment of the atoms are removed. The table 1 gives the width of this parameter $s_{\mathrm{res}} \approx \Delta/E_{\mathrm{vdW}}$ for some known Fano–Feshbach resonances for alkali metal atoms.

1-5 Useful domain for the model parameters

Our treatment of the resonance is based on two dimensionless parameters

$$\frac{\Delta}{E_{\mathrm{vdW}}} \qquad \text{and} \qquad \frac{\tilde{E_{\mathrm{cl}}}}{E_{\mathrm{vdW}}}. \tag{30}$$

Atom	B [G]	a_{bg} [a_0]	s_{res}
^{6}Li	834.1	-1405	59
	690.4	-1727	29
	811.2	-1490	46
^{7}Li	736.8	-25	0.80
^{23}Na	907	63	0.09
^{39}K	402.4	-29	2.1
^{40}K	224.2	174	2.7
^{85}Rb	155.04	-443	28
^{87}Rb	1007.4	100	0.13
^{133}Cs	48.0	926	0.67

Table 1. *Width s_{res} of some Fano–Feshbach resonances for alkali metal atoms. We reproduce here the values given by Chin, Grimm, et al. (2010) for their dimensionless parameter s_{res} which practically coincides with our $g_0^2/(R_{\mathrm{vdW}}E_{\mathrm{vdW}}) \approx \Delta/E_{\mathrm{vdW}}$.*

The first one characterizes the strength of the coupling, the second the deviation from resonance. We will see that two constraints exist on the useful domain for these parameters.

Criterion 1: Our treatment is based on the assumption that the resonance described by the coupling to the bound state $|\phi_0\rangle$ is isolated. This assumption only makes sense if the displacement Δ of the considered bound state is small enough not to bring it to the neighborhood of other bound states. Now, this state is generally the last or the penultimate bound state of the closed channel and we have seen in chapter IV that the energy gap between the last two bound states varies between 40 and 200 E_{vdW} (this structure is recalled in figure 4). For security, we will take as a suitable range of variation of Δ

$$\frac{\Delta}{E_{\mathrm{vdW}}} \lesssim 100. \tag{31}$$

Beyond this value, it is possible that another bound state, not taken into account in the model, is closer to the threshold $E = 0$ of the open channel and our model would then lose its relevance. One can check that the values of $s_{\mathrm{res}} \approx \Delta/E_{\mathrm{vdW}}$ given in table 1 satisfy this inequality.

Criterion 2. Using the estimate (22) of the energy Δ, the value (8) of the

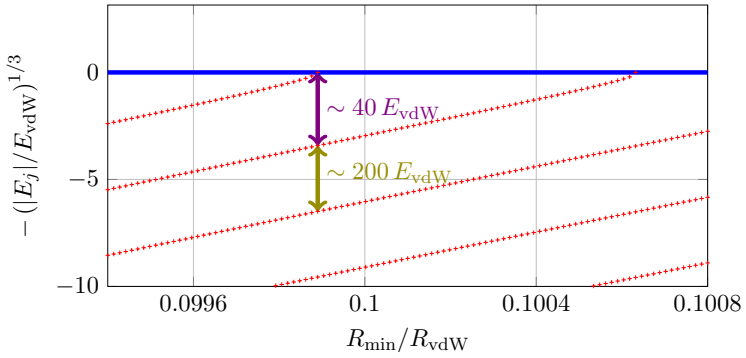

Figure 4. Criterion 1. *Energies of the last bound states in a van der Waals potential (see chapter 4). If we use the last bound state of the closed channel to induce the Fano–Feshbach resonance, the model used in this chapter only makes sense if we limit the displacement Δ to less than $\sim 100\ E_{\rm vdW}$.*

scattering length can be written:

$$\frac{a}{R_{\rm vdW}} \sim \frac{\Delta}{\tilde{E}_{\rm cl}}. \tag{32}$$

We recall that our model aims at describing a resonance of the scattering length, thus values of a higher than the typical value $R_{\rm vdW}$. We must therefore restrict the amplitude of variation of $|\tilde{E}_{\rm cl}|$ to the interval

$$|\tilde{E}_{\rm cl}| \lesssim \Delta. \tag{33}$$

Beyond this range, plotted in Figure 1, the values found for a would be anomalously low and probably not significant compared to the typical background scattering length.

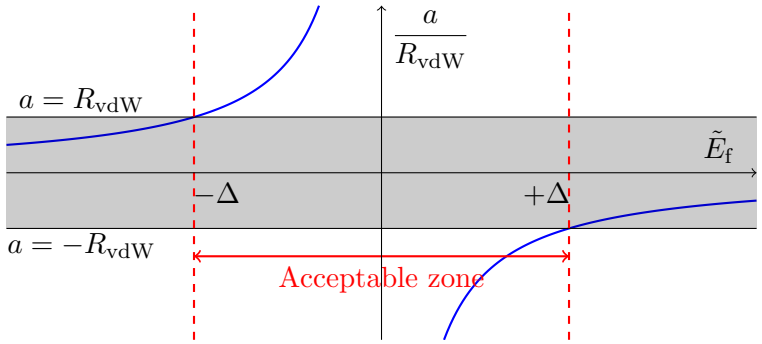

Figure 5. Criterion 2. *Validity domain $|E_f| \lesssim \Delta$ imposed by the condition $|a| \gtrsim R_{\rm vdW}$ [cf. (33)].*

2 Broad vs. narrow resonances

2-1 Side $a > 0$ and energy of the bound state

We focus in this paragraph on the case of positive scattering lengths, i.e. $\tilde{E}_{\rm cl} < 0$. Our starting point will be the scattering amplitude (5), which we rewrite after taking the limit at small k: $g(k) \to g_0$, $\delta E_{\rm cl}(k) \to \Delta$, as suggested by the comparison with the result of Landau & Lifshitz (1975) made in the previous paragraph:

$$f(k) \approx \frac{g_0^2}{\tilde{E}_{\rm cl} - E - {\rm i}kg_0^2}, \qquad E = \frac{\hbar^2 k^2}{2m_{\rm r}}. \tag{34}$$

Note that this expression does not result from a systematic expansion of $f(k)$ to order 2 in k since it would then be necessary to include also corrections to g_0 and Δ:

$$g(k) = g_0\left(1 + \nu k^2 + \ldots\right), \qquad \delta E_{\rm cl}(k) = \Delta\left(1 + \nu' k^2 + \ldots\right) \tag{35}$$

with $\nu, \nu' \sim R_{\rm vdW}^2$. However, we will be able to identify the main elements with this simplified version, the additional corrections related to the variations of $g(k)$ and $\delta E_{\rm cl}(k)$ being of the same nature as those induced by the effective range term in the single-channel case.

The (approximate) energies of the bound states are obtained by looking

for the poles of this scattering amplitude. We put $k = \mathrm{i}\kappa$ and look for the solutions with κ real positive, so that the wave function $\mathrm{e}^{\mathrm{i}kr}/r = \mathrm{e}^{-\kappa r}/r$ is physically acceptable (i.e. normalizable). We have to solve the second degree equation in κ:

$$\frac{\hbar^2\kappa^2}{2m_{\mathrm{r}}} + g_0^2\kappa + \tilde{E_{\mathrm{cl}}} = 0. \tag{36}$$

Let's introduce the dimensionless quantity $X = \kappa R_{\mathrm{vdW}}$ which allows to rewrite this equation in the form:

$$X^2 + \left(\frac{\Delta}{E_{\mathrm{vdW}}}\right) X + \left(\frac{\tilde{E_{\mathrm{cl}}}}{E_{\mathrm{vdW}}}\right) = 0, \tag{37}$$

where we assumed that (22) is exact to simplify the notations. The energy of the bound state is written as a function of X:

$$\frac{E_{\mathrm{bound}}}{E_{\mathrm{vdW}}} = -\kappa^2 R_{\mathrm{vdW}}^2 = -X^2. \tag{38}$$

Recall that we are interested in seeing how the parameter κ goes from the value 0 at resonance to the "typical" value $\sim 1/R_{\mathrm{vdW}}$: we are therefore interested in the values of the unknown X between 0 and 1.

The equation (37) has a positive (unique) solution if and only if $\tilde{E_{\mathrm{cl}}} < 0$:

$$2X = -\frac{\Delta}{E_{\mathrm{vdW}}} + \sqrt{\left(\frac{\Delta}{E_{\mathrm{vdW}}}\right)^2 - 4\frac{\tilde{E_{\mathrm{cl}}}}{E_{\mathrm{vdW}}}}, \tag{39}$$

whose variations we will now discuss. First of all, let us notice that in the immediate vicinity of the resonance, that is to say for $\tilde{E_{\mathrm{cl}}}$ small, this solution reads [*cf.* (8)]

$$4|\tilde{E_{\mathrm{cl}}}| \ll \frac{\Delta^2}{E_{\mathrm{vdW}}} : \qquad X \approx -\frac{\tilde{E_{\mathrm{cl}}}}{\Delta} \quad \Leftrightarrow \quad \kappa \approx \frac{1}{a}. \tag{40}$$

We recover the result

$$E_{\mathrm{bound}} \approx -\frac{\hbar^2}{2m_{\mathrm{r}}a^2}, \tag{41}$$

i.e. the universal law relating the scattering length and the energy of the last bound state when it is close to the dissociation limit.

To go further, we will distinguish the two cases of a broad resonance ($\Delta \gg E_{\mathrm{vdW}}$) and a narrow resonance ($\Delta \ll E_{\mathrm{vdW}}$).

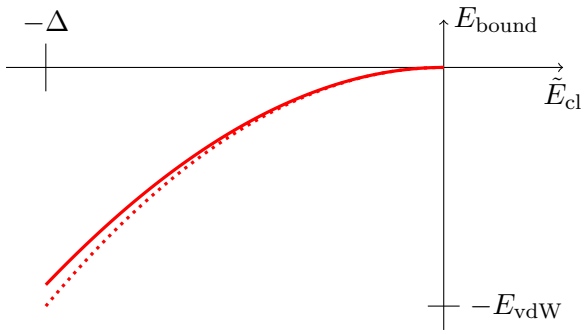

Figure 6. *Continuous curve: variation of the energy of the bound state with $\tilde{E}_{\mathrm{cl}}$ deduced from (38-39), for a large resonance ($\Delta = 20\, E_{\mathrm{vdW}}$). The approximation $E_{\mathrm{lie}} = -\hbar^2/2m_{\mathrm{r}}a^2$, plotted in dotted lines, is valid over the whole accessible range of $\tilde{E}_{\mathrm{cl}}$, i.e. for a varying between R_{vdW} and $+\infty$.*

Broad resonance $\Delta \gg E_{\mathrm{vdW}}$. In this case, the expansion (40) can be extended to the whole relevant energy range of $|\tilde{E_{\mathrm{cl}}}|$, between 0 and Δ. When $|\tilde{E_{\mathrm{cl}}}|$ reaches the value Δ, we have $X \sim 1$ and thus $\kappa \sim 1/R_{\mathrm{vdW}}$. The universal regime (41) thus extends to all values of the scattering length a, from R_{vdW} to $+\infty$ (*cf.* figure 6).

Narrow resonance $\Delta \ll E_{\mathrm{vdW}}$. In this case, the expansion (40) ceases to be valid for

$$|\tilde{E_{\mathrm{cl}}}| \sim \frac{\Delta^2}{E_{\mathrm{vdW}}} \qquad \Leftrightarrow \qquad \frac{a}{R_{\mathrm{vdW}}} \sim \frac{E_{\mathrm{vdW}}}{\Delta} \gg 1, \tag{42}$$

and then we switch to another non-universal regime:

$$\frac{\Delta^2}{E_{\mathrm{vdW}}} \ll |\tilde{E_{\mathrm{cl}}}| \lesssim \Delta : \qquad X \approx \sqrt{|\tilde{E_{\mathrm{cl}}}|/E_{\mathrm{vdW}}} \quad \Leftrightarrow \quad \hbar\kappa \approx \sqrt{2m_{\mathrm{r}}|\tilde{E_{\mathrm{cl}}}|}, \tag{43}$$

where we have taken into account the restriction (33) on $\tilde{E_{\mathrm{cl}}}$. This gives for the energy of the bound state (*cf.* figure 7):

$$E_{\mathrm{bound}} = -\frac{\hbar^2\kappa^2}{2m_{\mathrm{r}}} \approx \tilde{E_{\mathrm{cl}}}. \tag{44}$$

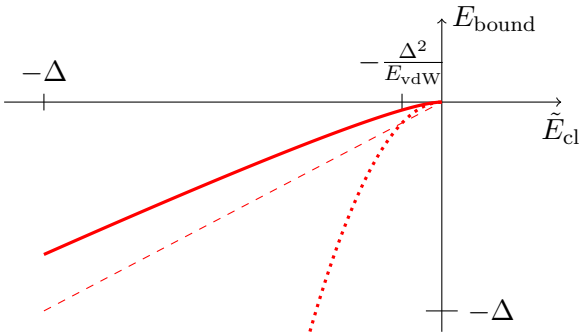

Figure 7. *Continuous curve: Energy of the bound state deduced from (38-39) for a narrow resonance ($\Delta = 0.1\ E_{\rm vdW}$). The approximation $E_{\rm bound} = -\hbar^2/2m_{\rm r}a^2$, plotted in dotted lines, is valid only over a small range around the resonance: $|\tilde{E}_{\rm cl}| < \Delta^2/E_{\rm vdW}$. Over the rest of the range accessible for $|\tilde{E}_{\rm cl}|$, the energy of the bound state varies approximately linearly, as predicted in (44) and plotted in dashed lines.*

The state is much less bound than one would expect if the universal prediction $\hbar^2/2m_{\rm r}a^2$ applied. In fact, the energy of the bound state found in (44) is equal to that of the closed channel state. In this regime, the predictions are very different from the single-channel result and the bound state is essentially concentrated in the closed channel, as we show below.

2-2 The population of the closed channel

We continue our study of the bound state to focus now on its composition: how are the probability amplitudes distributed between open and closed channel? We go back to the two-component spinor which defines this state:

$$\begin{pmatrix} \text{open} \\ \text{closed} \end{pmatrix} = \begin{pmatrix} |\psi\rangle \\ |\phi\rangle \end{pmatrix} = \alpha \begin{pmatrix} \hat{G}_0(E)\,\hat{W}|\phi_0\rangle \\ |\phi_0\rangle \end{pmatrix} \tag{45}$$

The α coefficient is unimportant here, since it is simply used to normalize the global state. Instead, we are interested in the weight of the closed channel:

$$\frac{\Pi_{\rm cl}}{\Pi_{\rm op}+\Pi_{\rm cl}} = \frac{1}{1+\langle\phi_0|\hat{W}\hat{G}_0^2(E)\hat{W}|\phi_0\rangle}, \tag{46}$$

with $E = -\hbar^2\kappa^2/2m_{\rm r}$.

The computation of the matrix element in the denominator of (46) is carried out in a similar way to what we did in the previous chapter. By inserting a closure relation on the $\boldsymbol{q}$ moments and expressing $\langle\phi_0|\hat{W}|\boldsymbol{q}\rangle$ as a function of $g(q)$, we arrive at

$$\langle\phi_0|\hat{W}\hat{G}_0^2(E)\hat{W}|\phi_0\rangle = \frac{8m_{\rm r}}{\pi\hbar^2}\int \frac{q^2\,g^2(q)}{(q^2+\kappa^2)^2}\,{\rm d}q. \tag{47}$$

The above integral is divergent in $q = 0$ if we take $\kappa = 0$. For small and non-zero κ, it is convergent and dominated by small values of q. So we can take in this integral $g(q) \approx g(0) \equiv g_0$ to arrive at:

$$\langle\phi_0|\hat{W}\hat{G}_0^2(E)\hat{W}|\phi_0\rangle = \frac{2m_{\rm r}g_0^2}{\hbar^2\kappa} = \frac{1}{X}\,\frac{\Delta}{E_{\rm vdW}}, \tag{48}$$

and therefore:

$$\frac{\Pi_{\rm cl}}{\Pi_{\rm op}+\Pi_{\rm cl}} = \frac{X}{\frac{\Delta}{E_{\rm vdW}}+X} = \frac{\sqrt{1+u}\,-\,1}{\sqrt{1+u}\,+\,1}, \qquad u = -4\frac{\tilde{E}_{\rm cl}E_{\rm vdW}}{\Delta^2} > 0. \tag{49}$$

Two examples of variation for $\Delta/E_{\rm vdW} = 0.1$ (narrow resonance) and $\Delta/E_{\rm vdW} = 20$ (broad resonance) are plotted in figure 8.

Let's take up the distinction between broad and narrow resonance established in the previous paragraph:

- For a large resonance, $\Delta/E_{\rm vdW} \gg 1$, this population of the closed channel remains small over the whole range $|\tilde{E}_{\rm cl}| \lesssim \Delta$. The resonance is thus dominated by the open channel.
- For a narrow resonance, $\Delta/E_{\rm vdW} \ll 1$, the open channel population is dominant only in the immediate vicinity of the resonance, $|\tilde{E}_{\rm cl}| \lesssim 2\Delta^2/E_{\rm vdW}$. The closed channel becomes dominant when $|\tilde{E}_{\rm cl}|$ exceeds this value, i.e. when we leave the universal regime for the variation of the energy of the bound state [*cf.* (42)].

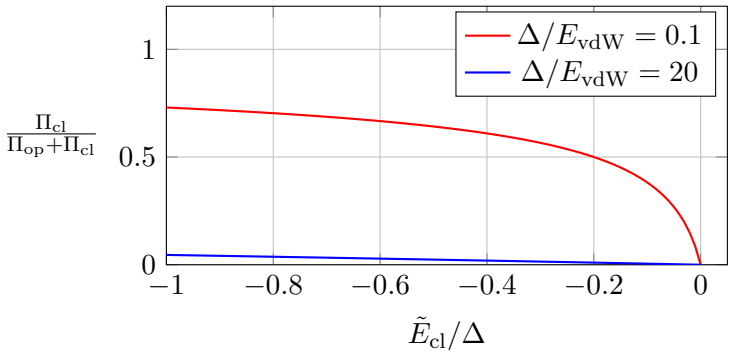

Figure 8. *Variation of the relative population of the closed channel for the bound state found when $\tilde{E}_{\rm cl} < 0$ [cf. (49)].*

The conclusion of this study is that there is a one-to-one correspondence between the fact that a resonance is entirely dominated by the open channel and the fact that it is broad in the sense of $\Delta \gg E_{\rm vdW}$. In practice, it is often easier to test the first criterion, i.e. to determine the dominant channel, as explained by Chin, Grimm, et al. (2010).

2-3 Side $a < 0$ and shape of the resonance

Let us now look at the $a < 0$ side of the resonance, for which no bound state is expected. This case corresponds to the situation where the "renormalized" energy $\tilde{E}_{\rm cl}$ of the $|\phi_0\rangle$ state is above the open channel threshold. The question we wish to answer concerns the variations with E of the collision cross-section $\sigma(E)$. Is it a decreasing function of E as in the case of a single channel, zero-energy resonance, or does it exhibit a peak for an energy E^* close to $\tilde{E}_{\rm cl}$? The answer to this question depends again on whether the resonance is broad or narrow.

Our starting point is the scattering amplitude (34) from which we deduce the cross-section (for polarized bosons):

$$\sigma(E) = 8\pi|f(E)|^2 = \frac{8\pi g_0^4}{(E-\tilde{E}_{\rm cl})^2 \;+\; (2m_{\rm r}g_0^4/\hbar^2)\,E}. \tag{50}$$

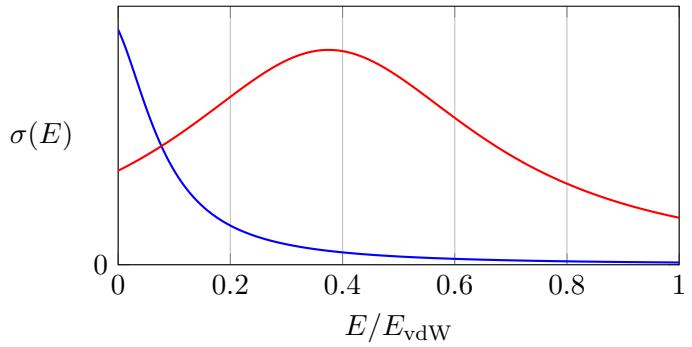

Figure 9. *The scattering cross-section for of a narrow resonance ($\Delta = 0.5\,E_{\rm vdW}$). For a small detuning $\tilde{E}_{\rm cl}$ (here $\tilde{E}_{\rm cl} = 0.1\,E_{\rm vdW}$ for the blue curve), the scattering cross-section is maximal at zero incident energy. For a larger detuning ($\tilde{E}_{\rm cl} = 0.5\,E_{\rm vdW}$ for the red curve), the cross-section presents a maximum for a non-zero incident energy E^*, close to $\tilde{E}_{\rm cl}$.*

The denominator is a quadratic function of E and is minimum in

$$E^* = \tilde{E}_{\rm cl} - \frac{\Delta^2}{2E_{\rm vdW}}, \tag{51}$$

a point that corresponds to a maximum of the cross-section.

Let's go back to our distinction between broad and narrow resonances.

- For a broad resonance, $\Delta \gg E_{\rm vdW}$ and for the physically relevant domain $|\tilde{E}_{\rm cl}| \lesssim \Delta$, the maximum is reached for negative energy. This means that in the region $E \geq 0$, the scattering cross-section $\sigma(E)$ is maximal in 0 and is a decreasing function of E. Again, this corresponds to the universal regime expected for a single-channel problem when a bound state is about to appear.
- For a narrow resonance, $\Delta \ll E_{\rm vdW}$, two cases are possible, as illustrated in figure 9:
  - In the domain very close to the resonance, $0 < \tilde{E}_{\rm cl} < \Delta^2/2E_{\rm vdW}$, we recover the universal behavior, with a cross-section which decreases when the collision energy E increases.

- Outside this domain, for $\Delta^2/2E_{\rm vdW} < \tilde{E_{\rm cl}} \lesssim \Delta$, the minimum E^* is located in the part $E > 0$, more precisely in a point close to $\tilde{E_{\rm cl}}$. The cross-section thus has a resonant behavior in $E^* \approx \tilde{E_{\rm cl}}$. This behavior is very different from the universal regime and is reminiscent of a shape resonance.

To conclude, let us mention an important point in connection with the commonly used formula:

$$a = a_{\rm bg}\left(1 - \frac{B_1}{B - B_0}\right) = a_{\rm bg} - \frac{a_{\rm bg}\, B_1\, \delta\mu}{\tilde{E_{\rm cl}}}, \tag{52}$$

which leads us to identify $a_{\rm bg}\, B_1\, \delta\mu$ with our parameter g_0^2. From the initial formula, it is tempting to say that a resonance will be large if B_1 is large (typically several Gauss). But the above study shows that the important parameter is not B_1, but the product $a_{\rm bg}B_1\, \delta\mu$, which is proportional to our parameter Δ. If $a_{\rm bg}$ is abnormally low, the field B_1 can be large although the Fano–Feshbach resonance has all the characteristics of a narrow resonance. This situation is encountered for the isotope 7 of lithium (boson) prepared in its lowest magnetic state. As shown in the table 1, this atomic species exhibits a resonance for $B_0 = 737\,$G; the corresponding B_1 field is $192\,$G, which is considerable (Khaykovich, Schreck, et al. 2002). But the scattering length $a_{\rm bg} = -1.3\,$nm is relatively small so that this resonance cannot be considered as large ($s_{\rm res} \approx \Delta/E_{\rm vdW} \approx 1$).

3 Quantitative approaches

The model we developed above assumed that the atoms did not interact in the open channel. This allowed us to conduct the calculations in a quasi-analytical manner and to derive the essential notions of universality and resonance width. In order to go further, it is of course necessary to enrich the description of the collision and first of all to take into account the interaction in the open channel. This leads, in the absence of coupling with the closed channel, to the background scattering length $a_{\rm bg}$. In a second step, it is also necessary to go beyond the isolated resonance approximation, which consisted in keeping only the state $|\phi_0\rangle$ in the closed channel.

3-1 The standard "isolated resonance" approach

This approach is described in several articles and books. In the context of cold atom physics, let us indicate for example Moerdijk, Verhaar, et al. (1995), Goral, Koehler, et al. (2004), and recently Naidon & Pricoupenko (2019). One can also consult the detailed and complete treatment of Pethick & Smith (2008b) and Cohen-Tannoudji & Guéry-Odelin (2011).

When one simply aims at taking into account the interaction in the open channel, the equations that served as a starting point for our simple model are barely modified. We keep the description of the collisional steady state in the form of the spinor:

$$\begin{pmatrix}\text{open}\\ \text{closed}\end{pmatrix} = \begin{pmatrix}|\psi\rangle\\ |\phi\rangle\end{pmatrix} \qquad \text{with} \quad |\phi\rangle = \alpha|\phi_0\rangle, \tag{53}$$

with a closed channel still reduced to the state $|\phi_0\rangle$. The eigenvalue equation for this spinor is written:

$$\left(\hat{H}_0 + \hat{V}\right)|\psi\rangle + \hat{W}|\phi\rangle = E\,|\psi\rangle \tag{54}$$

$$\hat{W}|\psi\rangle + E_{\rm cl}|\phi\rangle = E\,|\phi\rangle. \tag{55}$$

The method of solving remains formally unchanged, even though we no longer have analytical expressions for the different elements involved.

Let us take a positive energy $E = \hbar^2k^2/2m_{\rm r}$. For $\hat{W} = 0$, the solution of (54) is a scattering state of the open channel $|\psi_{\boldsymbol{k}}^{\rm op}\rangle$, leading to the scattering length $a_{\rm bg}$ when $k \to 0$. For $\hat{W} \neq 0$, the formal resolution of (54) is performed using the Green operator of the open channel:

$$\hat{G}^{\rm op}(E) = \frac{1}{E - (\hat{H}_0 + \hat{V}) + {\rm i}0_+}. \tag{56}$$

The general solution of (54) is written

$$|\psi_{\boldsymbol{k}}\rangle = |\psi_{\boldsymbol{k}}^{\rm op}\rangle + \hat{G}^{\rm op}(E)\hat{W}|\phi\rangle \tag{57}$$

This result reported in (55) allows to formally determine the value of the coefficient α:

$$\alpha = \frac{\langle\phi_0|\hat{W}|\psi_{\boldsymbol{k}}^{\rm op}\rangle}{E - E_{\rm cl} - \langle\phi_0|\hat{W}\,\hat{G}^{\rm op}(E)\,\hat{W}|\phi_0\rangle}. \tag{58}$$

The combination of (57) and (58) then gives

$$|\psi_{\boldsymbol{k}}\rangle = |\psi_{\boldsymbol{k}}^{\rm op}\rangle + \hat{G}^{\rm op}(E)\,\hat{T}(E)|\psi_{\boldsymbol{k}}^{\rm op}\rangle \tag{59}$$

with

$$\hat{T}(E) = \frac{\hat{W}|\phi_0\rangle\langle\hat{\phi}_0|\hat{W}}{E - E_{\rm cl} - \langle\phi_0|\hat{W}\,\hat{G}^{\rm op}(E)\,\hat{W}|\phi_0\rangle}. \tag{60}$$

The relation (59) has the same structure as the Lippmann–Schwinger equation obtained in chapter 2 for a single-channel scattering problem, expressing the scattering state $|\psi_{\boldsymbol{k}}\rangle$ in terms of the incident plane wave $|\boldsymbol{k}\rangle$ and the transition operator $\hat{T}$:

$$|\psi_{\boldsymbol{k}}\rangle = |\boldsymbol{k}\rangle + \hat{G}_0(E)\,\hat{T}(E)|\boldsymbol{k}\rangle. \tag{61}$$

We have thus formally reduced our two-channel problem to a single-channel problem with the transposition

$$|\boldsymbol{k}\rangle \to |\psi_{\boldsymbol{k}}^{\rm op}\rangle, \quad \hat{G}_0 \to \hat{G}^{\rm op}. \tag{62}$$

We deduce that the transition amplitude $f(\boldsymbol{k},\boldsymbol{k}')$ is proportional to $\langle\psi_{\boldsymbol{k}'}^{\rm ouv}|\hat{T}(E)|\psi_{\boldsymbol{k}}^{\rm ouv}\rangle$, which generalizes the result of chapter 2: $f(\boldsymbol{k},\boldsymbol{k}') \propto \langle\boldsymbol{k}'|\hat{T}(E)|\boldsymbol{k}\rangle$.

Let us examine what happens when we take the limit $E \to 0$ of (59):

- The first term $|\psi_{\boldsymbol{k}}^{\rm op}\rangle$ will show in its asymptotic part a behavior in $r - a_{\rm bg}$, corresponding to the scattering length $a_{\rm bg}$.
- The second term of (59) is resonant when the denominator of the operator $T(E)$ cancels. Let us write the limit $E \to 0$ of this denominator as
$$\lim_{E\to 0}\left[E - E_{\rm cl} - \langle\phi_0|\hat{W}\,\hat{G}^{\rm op}(E)\,\hat{W}|\phi_0\rangle\right] = -E_{\rm cl} + \Delta \tag{63}$$
with the real coefficient
$$\Delta = -\langle\phi_0|\hat{W}\,\hat{G}^{\rm op}(0)\,\hat{W}|\phi_0\rangle = \frac{1}{(2\pi)^3}\int \frac{\left|\langle\phi_0|\hat{W}|\psi_{\boldsymbol{k}}^{\rm op}\rangle\right|^2}{\hbar^2k^2/2m_{\rm r}}\,{\rm d}^3k \tag{64}$$
which generalizes (9). As in our simplified model, the imaginary part of this denominator shows the term proportional to k required by the optical theorem and which tends to 0 when $k \to 0$.

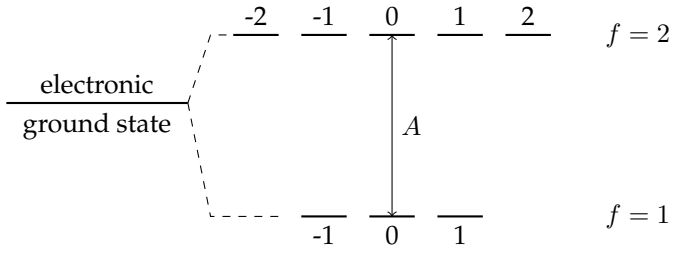

Figure 10. *Hyperfine structure of the electronic ground state of an alkali atom with nuclear spin $3/2$. The value of the quantum number m_f for each state is given.*

This leads to the following expression for the scattering length:

$$a = a_{\rm bg} - \frac{C}{\tilde{E_{\rm cl}}} \qquad \text{with} \quad \tilde{E_{\rm cl}} = E_{\rm cl} - \Delta \tag{65}$$

where the coefficient C (which generalizes g_0^2 and which we will not explain here) involves the matrix elements of the operator $\hat{W}$.

From this point on, the discussion of resonance width, possible bound state, etc. is similar to what we described earlier from our simplified model.

3-2 Coupled-channel modeling

In order to obtain an accurate modeling of a Fano–Feshbach resonance, it is necessary to go beyond the "isolated resonance" approach. For this, one must take into account in a quantitative way the degree of freedom associated with the closed channel, or rather with the closed channels because there are generally several potential curves which come into play in a collision.

Let us take the example of a bosonic alkali metal atom like lithium 7, sodium, potassium 39 or 41, or rubidium 87. All these atoms have an electronic ground state with orbital angular momentum $l = 0$ and an electron

spin $s = 1/2$. Their nucleus has a spin $i = 3/2$. The hyperfine coupling between the magnetic moment of the external electron and that of the nucleus is written $(A/4)\ \boldsymbol{s}\cdot\boldsymbol{i}$, where A depends on the atomic species. This coupling splits the electronic ground state into two hyperfine sublevels separated by A, of total angular momentum $f = 1$ and $f = 2$ (figure 10). In the following we will focus on the influence of this spin degree of freedom (electronic and nuclear) on the collision dynamics.

When the two atoms (marked by the index $\alpha = 1, 2$) are far apart, their interaction can be neglected. In the presence of a magnetic field $\boldsymbol{B}$ oriented along the z axis, the spin Hamiltonian is

$$\sum_{\alpha=1,2} -A\boldsymbol{s}_\alpha \cdot \boldsymbol{i}_\alpha + (\gamma_e s_{z,\alpha} - \gamma_n i_{z,\alpha})B, \tag{66}$$

to which we must add the kinetic energy Hamiltonian for the two atoms. A spin eigenstate of the pair of atoms is thus characterized by the four quantum numbers: $f_1, m_{f_1}, f_2, m_{f_2}$.

When the atoms are close, the dominant term is their mutual interaction. The van der Waals interaction, which has been studied in previous chapters, does not involve spin and we will not discuss it again here. The dominant interaction results from the exchange of electrons (see chapter I) and it depends on the total electronic spin S of the atom pair, with the singlet $V_S(r)$ and triplet $V_T(r)$ potentials associated respectively with $S = 0$ and $S = 1$. The dominant term of the Hamiltonian can then be written:

$$\frac{1}{4}\left[V_S(r) + 3V_T(r)\right] + \boldsymbol{s}_1 \cdot \boldsymbol{s}_2 \left[V_T(r) - V_S(r)\right]. \tag{67}$$

The short-range eigenstates are therefore characterized by the quantum numbers S, I, F, M_F.

We find that there is one quantity that is conserved for any distance between the two atoms: the projection of the total spin on the z axis. It is characterized by the quantum number $M_F = m_{f_1} + m_{f_2}$. For the other spin degrees of freedom, there is a continuous rotation of the eigenbasis as the atoms approach each other. This point is illustrated in figure 11 that we extracted from Moerdijk, Verhaar, et al. (1995). It focuses on the interaction between two sodium atoms, but would be unchanged (apart from a recalibration of the axes) for the other species mentioned above.

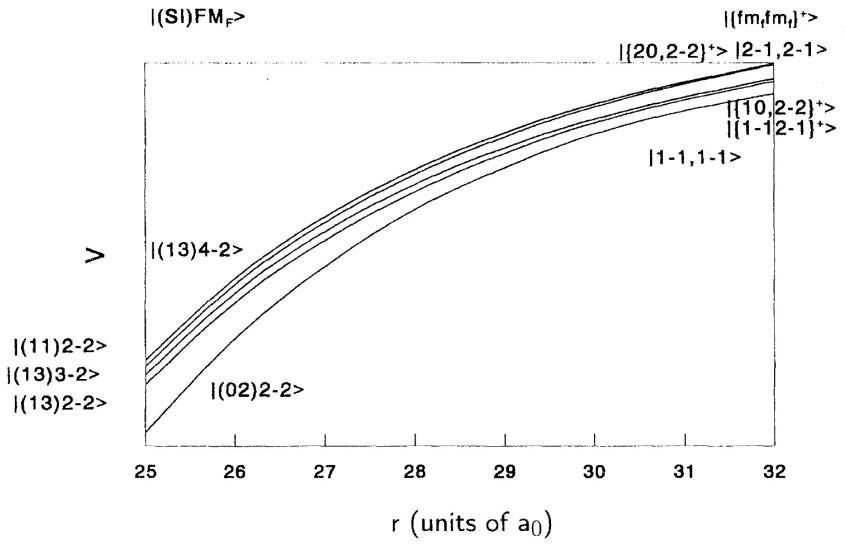

Figure 11. *Interaction potentials for the five coupled channels in a collision between two alkali atoms prepared in a state such that $M_F = m_{f_1} + m_{f_2} = -2$. The numerical data are for a pair of sodium atoms. Figure extracted from Moerdijk, Verhaar, et al. (1995).*

This figure shows the channels to be considered for a collision between two atoms prepared in the $|f = 1, m_f = -1\rangle$ state. From what we have just seen, the only quantum number that will be conserved during the collision is $M_F = m_{f_1} + m_{f_2} = -2$. This means that all the channels corresponding to this same value of M_F can be coupled together and we need to identify them.

When the atoms are far apart, there are five possible states with this value of M_F:

- The one we have taken as the input state of the collision, is noted $|f_1 m_{f_1}, f_2 m_{f_2}\rangle = |1\ -1, 1, -1\rangle$ in figure 11.
- The state obtained by taking one atom in $|f = 1, m_f = -1\rangle$ and the other in $|f = 2, m_f = -1\rangle$, and symmetrizing the result. This state

is noted $|\{1\ -1, 2\ -1\}^+\rangle$ in figure 11. It has an energy A above the incident state, and will therefore correspond to a closed channel.

- The state obtained by taking one atom in $|f = 1, m_f = 0\rangle$ and the other in $|f = 2, m_f = -2\rangle$, and by symmetrizing the result. This state also has an energy A above the incident state.
- The state obtained by taking an atom in $|f = 2, m_f = 0\rangle$ and the other in $|f = 2, m_f = -2\rangle$, and by symmetrizing the result. This state has an energy $2A$ above the incident state.
- The state obtained by taking the two atoms in $|f = 2, m_f = -1\rangle$. This state has an energy $2A$ above the incident state.

In the end, we find one open channel and four closed channels, two with energy A and two with energy $2A$. When the atoms come closer together, we see in figure 11 that the spin states of these five states mix to form four states in the triplet channel and one state in the singlet channel. The notation in figure 11 for these states is $|(SI)Fm_F\rangle$.

To treat this problem, one must therefore (i) choose a working basis, which can for example be the $|(SI)Fm_F\rangle$ basis, (ii) write the Hamiltonian at any point r in this basis, which will be represented by a 5×5 matrix, (iii) solve the five coupled Schrödinger equations to extract the scattering state corresponding to a given energy [see for example Moerdijk, Verhaar, et al. (1995), Mies & Raoult (2000), and Chin, Grimm, et al. (2010)]. This method, which proves to be very accurate (see §4-1), relies of course on a good knowledge of the interaction potentials.

3-3 The coupling $\hat{W}$

We discussed in the previous paragraph the nature of the different coupled channels, which allows us to give now some additional elements on the coupling $\hat{W}$ introduced in the discussion of our simple model. So far, we have indicated without further precision that $\hat{W}$ had a non-zero matrix element between the open channel and the state $|\phi_0\rangle$ of the closed channel.

The precise definition of the open channel requires to specify the basis of the spin space on which we choose to write the Hamiltonian (step (i) at the end of the previous paragraph). One can for example prefer the decoupled basis $|f_1 m_{f_1}, f_2 m_{f_2}\rangle$. In these conditions, the coupling $\hat{W}$ will be deduced from the expression (67): it will involve the matrix elements of $\vec{s}_1 \cdot \vec{s}_2$, with a prefactor proportional to $V_T(r) - V_S(r)$. With this choice, $W(r)$ is very large in the entire inner region of the potential well, where the difference between V_S and V_T is maximum. This approach is perfectly legitimate, but it can lead to large matrix elements of $\hat{W}$, which can make the isolated resonance approximation problematic.

Another approach, put forward in particular by Naidon & Pricoupenko (2019), consists in using a rotating basis for the spin, which diagonalizes at any point r the interaction Hamiltonian. By construction, the non-diagonal elements between channels vanish. But $\hat{W}$ is still not zero: one has to take into account the rotation of the basis vectors with r. Naidon & Pricoupenko (2019) develop this analysis and show that $\hat{W}$ is then no longer local (multiplication by a function of r), but also involves the operator $\frac{\mathrm{d}}{\mathrm{d}r}$. With this choice, $\hat{W}$ takes on important values in the "transition zone" defined in chapter 4. These are the r distances where the exchange potential becomes comparable to the van der Waals interaction; indeed the latter, independent of the spin, always admits the decoupled states $|f_1 m_{f_1}, f_2 m_{f_2}\rangle$ as its proper basis whereas the exchange interaction favors the $|(SI)Fm_F\rangle$ basis. Naidon & Pricoupenko (2019) show that this choice corresponds to a better controlled approximation, which leads them to modify the commonly accepted expression for the energy shift Δ [their equation (49)].

3-4 Resonances assisted by an oscillating field

In all of the above, we have assumed that the coupling $\hat{W}$ was imposed by the choice of the atomic species. The external magnetic field controlled the relative position of the closed channel with respect to the open channel, but the coupling itself depended only on the shape of the wave functions of the incident state and the bound state $|\phi_0\rangle$.

It is possible to enrich the possibilities offered by Fano–Feshbach resonances by using an electromagnetic field, optical or microwave, to couple the incident open channel to any closed channel, not necessarily close in

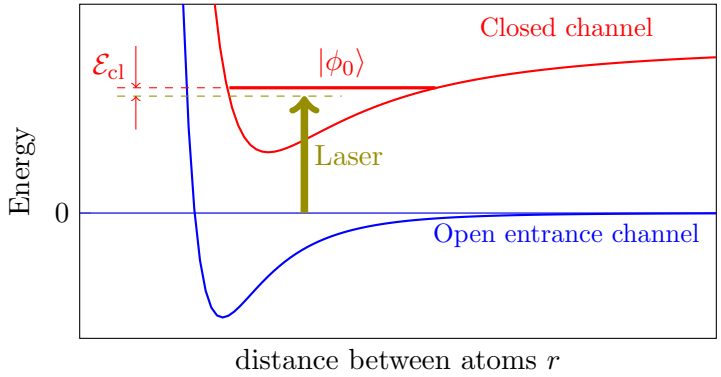

Figure 12. *Principle of a one-photon optical Fano–Feshbach resonance. A light beam couples in a quasi-resonant way the input channel, a scattering state of the electronic ground level to a bound state of an electronically excited level.*

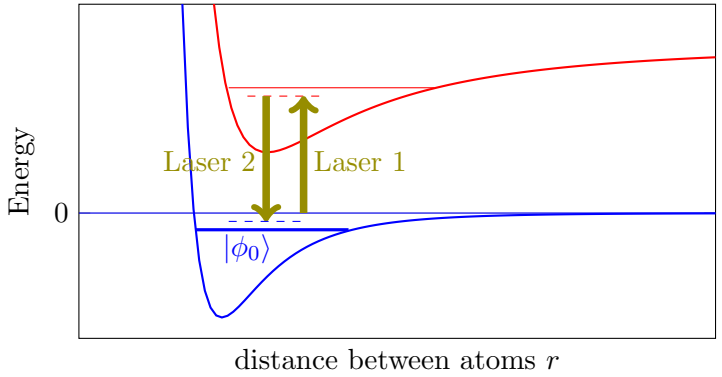

Figure 13. *Principle of a two-photon optical Fano–Feshbach resonance. A pair of light beams couples in a quasi-resonant way the input channel, a scattering state of the electronic ground level, to a bound state of the electronic ground level, via a virtual transition to an excited electronic state.*

energy. The tunability provided by the magnetic field B is replaced by the choice of the frequency of the oscillating field. The coupling W becomes proportional to the amplitude of this field and can be adjusted at will.

The first proposal in this sense was made by Fedichev, Kagan, et al. (1996) and implemented by Theis, Thalhammer, et al. (2004). These are optical Fano–Feshbach resonances where the input channel, which has two atoms in the electronic ground state, is coupled to a closed channel which has one atom in an excited electronic state and the other in the ground state (figure 12). A variant, explored by Thalhammer, Theis, et al. (2005), consists in using a two-photon (stimulated Raman) transition, to find a closed channel with two atoms in their ground state (figure 13).

The experiments of Theis, Thalhammer, et al. (2004) and Thalhammer, Theis, et al. (2005) confirmed the theoretical predictions concerning the modification of the scattering length. But they also highlighted an intrinsic limitation of this method, related to the heating due to the randomness of the spontaneous emission of photons. More precisely, in the energy denominator involved in the expression of the scattering amplitude, deduced for example from the expression of the matrix $\hat{T}(E)$ given in (60), it is necessary to add an imaginary term $\mathrm{i}\Gamma_e$, corresponding to the natural width of the electronic excited state. This imaginary term gives an imaginary part to the scattering length, i.e. a loss term (which can be considerable in practice) when injected in the Gross–Pitaevskii equation. One can consult Bohn & Julienne (1999) for a detailed treatment of this heating mechanism.

Another approach has been proposed by Papoular, Shlyapnikov, et al. (2010) and is shown in figure 14 [see also Kaufman, Anderson, et al. (2009) and Tscherbul, Calarco, et al. (2010)]. It consists in using a microwave coupling between the open and closed channels. Then, there is no passage through an excited state and thus no additional heating. The important point to note in this case is that the wavelength of the microwave field used is very large compared to the range of the interaction potentials between atoms. We can therefore consider that $W(r)$ is independent of r. However, we have shown in §3-1 that the desired modification of the scattering length involves the matrix elements

$$\langle\phi_0|\hat{W}|\psi_{\boldsymbol{k}}^{\rm op}\rangle \approx W\,\langle\phi_0|\psi_{\boldsymbol{k}}^{\rm op}\rangle. \tag{68}$$

It is therefore necessary that the two states $|\phi_0\rangle$ and $|\psi_{\boldsymbol{k}}^{\rm op}\rangle$ have a non-zero overlap, and in particular that they are not orthogonal. Since they are

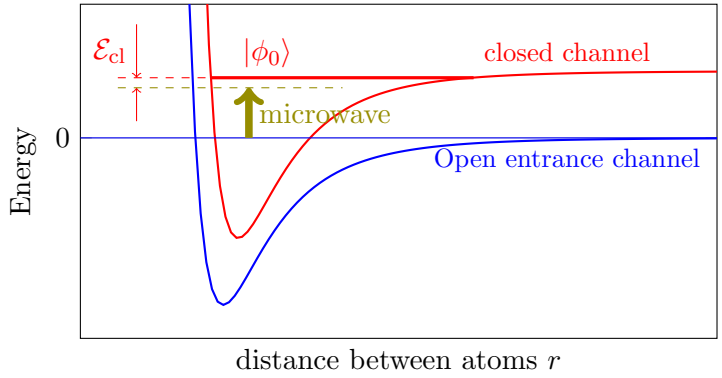

Figure 14. *Microwave assisted Fano–Feshbach resonance, obtained by a coupling between the two hyperfine sublevels of the electronic ground state.*

each eigenstates of a Hamiltonian $\hat{p}^2/2m_{\rm r} + V_\alpha(r)$, this means that the two Hamiltonians in question must be "significantly different" from each other. For alkali metal atoms, this condition can be fulfilled all the better if the triplet and singlet scattering lengths are far apart and if the two channels involved have significantly different weights on these singlet and triplet branchs.

4 Some recent experiments

Since their initial observation for atomic gases by Inouye, Andrews, et al. (1998), Fano–Feshbach resonances have played a considerable role in quantum fluid physics. It is not our intention here to review these very many experimental studies, or even to cite them. We refer interested readers to the review article of Chin, Grimm, et al. (2010) which gave, at least at the time of its publication, a complete state-of-the-art of experimental knowledge in this field. In the following paragraphs, we will limit ourselves to give (without concern for completeness) three recent remarkable examples. As these experiments use different protocols, this part will give us the opportunity to discuss three diagnostic techniques for the presence of

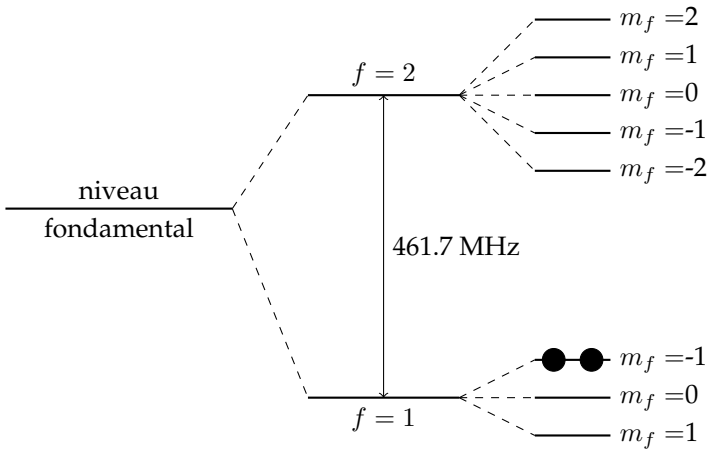

Figure 15. *Position of the hyperfine levels of the electronic ground state of a ^{39}K atom in the presence of a magnetic field. The experiment of Chapurin, Xie, et al. (2019) is conducted with atoms prepared in the $|f = 1, m_f = -1\rangle$ state.*

a resonance: bound state spectroscopy, thermalization kinetics of a trapped gas and atom losses.

4-1 Precision measurements on potassium 39

Chapurin, Xie, et al. (2019) recently conducted an experiment on potassium-39, the purpose of which was to test some aspects of three-body physics. A key part of their analysis involved two-body interactions in a ^{39}K gas (bosons) in the presence of a magnetic field of about 30 Gauss. In this experiment, atoms are prepared in the $|f = 1, m_f = -1\rangle$ state, i.e. the higher energy state of the $f = 1$ hyperfine sublevel.

Starting from about 10^5 atoms confined in an optical trap at a temperature of 300 nK, the magnetic field is swept through the value corresponding to the Fano–Feshbach resonance, which allows to adiabatically transfer an important fraction of the atoms to an assembly of dimers in the state $|\phi_0\rangle$ (Köhler, Góral, et al. 2006). The non-transferred atoms are eliminated

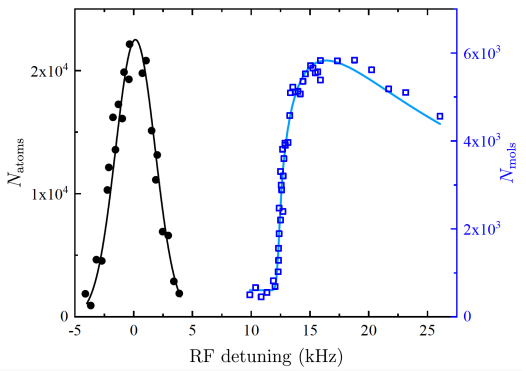

Figure 16. *Blue squares: radio-frequency spectrum of dissociation of ^{39}K dimers for a magnetic field of 33.9575 (3) G. The origin of the x-axis is shifted by 446.834413 MHz. The black points are obtained for a gas of atoms and allow to calibrate the experiment. Figure extracted from* Supplemental Material *of Chapurin, Xie, et al. (2019).*

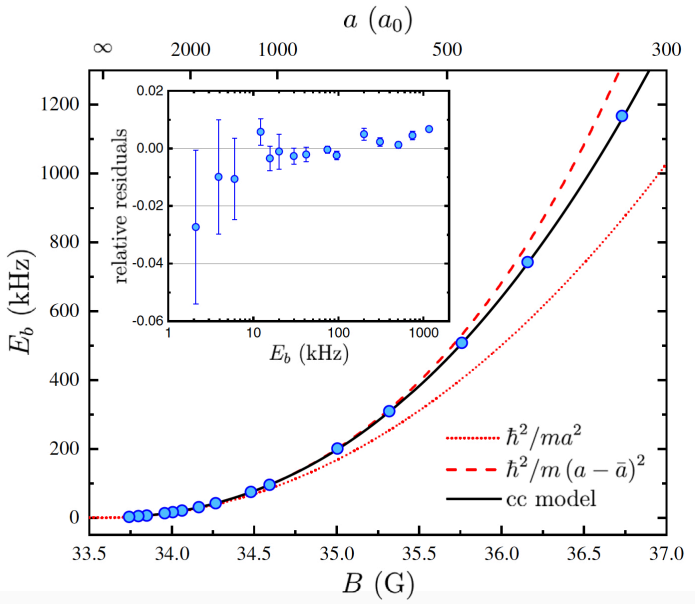

Figure 17. *Measurement of the binding energy of the ^{39}K dimer in the vicinity of the Fano–Feshbach resonance. The universal prediction is plotted with a red dotted line. The black curve is the prediction from a numerical calculation including 5 coupled spin channels. The red dashed curve is a refined version of the universal prediction. Figure extracted from Chapurin, Xie, et al. (2019).*

thanks to a light pulse which pushes them out of the trap.

The main tool is radio-frequency (rf) spectroscopy which consists in making one of the atoms of the dimer switch to the $|f = 2, m_f = 0\rangle$ state, then counting the atoms thus transferred according to the frequency of the rf. A typical example is shown in figure 16. We can see the spectrum recorded for the dimer gas (in blue) and the equivalent signal for an atomic gas. A precise modeling of the shift between the two curves allows to deduce the binding energy for this value of the field, $E_{\text{bound}}/h = 12.274\,\text{kHz}$.

This experiment is repeated for different values of the magnetic field around the Fano–Feshbach resonance, producing the data in figure 17. The magnetic field interval corresponds to a variation of the scattering length a between 16 nm and $+\infty$ ($R_{\text{vdW}} = 3.3\,\text{nm}$ for ^{39}K).

For this curve, the (weak) correction of the dimer energy related to the confinement potential has been taken into account. The fit with a theoretical model taking into account the five coupled channels for this s-wave resonance (see §3) is excellent and leads to the determination of the position of the resonance with an unprecedented accuracy: $B_0 = 33.5820\,(14)\,\text{G}$.

This precision allowed Chapurin, Xie, et al. (2019) to improve very significantly the modeling of singlet and triplet potentials for a pair of ^{39}K atoms.

We can see in this figure that only the central part of the resonance is well described by the universal model although $a \geq 5\,R_{\text{vdW}}$ on the explored range. This proves that this resonance does not fall into the category of broad resonances. More precisely, Chapurin, Xie, et al. (2019) related their data to the s_{res} parameter of Chin, Grimm, et al. 2010 (identical to our Δ/E_{vdW} parameter introduced above) to find $s_{\text{res}} \approx 2.6$. It is thus an "intermediate" resonance, located at the border between broad and narrow resonances.

Note that in order to describe the resonance with this degree of accu-

racy, modeling by the usual formula (52) is not sufficient and a second pole must be included, i.e. a 5-parameter modeling.

4-2 Orbital resonances for ytterbium 173

For alkali metal species, each atom carries an electron spin $1/2$. The interaction between two atoms in their electronic ground state depends on the exchange symmetry of the electronic wave function. An orbital wave function which is symmetric [resp. antisymmetric] by exchange of the two electrons is associated with an antisymmetric [resp. symmetric] spin state, i.e. the singlet state $S = 0$ [resp. triplet $S = 1$]. The different scattering channels contain varying parts of the singlet and triplet potentials, and the coupling between these channels gives rise to the resonances discussed so far.

A class of atoms that plays an important role in cold gas physics concerns atoms with two peripheral electrons, such as strontium or ytterbium. For an atom prepared in its ground state g, the orbital angular momentum L of the two electrons is zero as well as their spin angular momentum S, so that the total angular momentum J is also zero. The $S = 0$ value prevents the possibility of setting up a Fano–Feshbach resonance of the same type as for the alkali metal atoms, at least when the atoms are all prepared in their electronic ground state. Even though these atoms may have a nuclear spin I, the interaction potential between atoms will not depend on the spin state of the nuclei[4] and the collision can be considered as "single-channel".

A way around this impossibility was proposed by Zhang, Cheng, et al. (2015), and then realized experimentally a few months later by Höfer, Riegger, et al. (2015) and Pagano, Mancini, et al. (2015). Zhang, Cheng, et al. (2015) suggested to take advantage of very long-lived excited electronic states, in particular the $^3\mathrm{P}_0$ state; it is a state

- of orbital angular momentum $L = 1$ (hence the notation "P");
- of electronic spin $S = 1$ (triplet state, hence the notation "3"), thus different from the spin $S = 0$ of the ground state (this difference contributes to the very long lifetime);
- of total angular momentum (orbital+spin) $J = 0$, which reinforces the stability of this state because it cannot de-excite to the ground state by a one-photon transition, a transition $J = 0 \to J = 0$ being forbidden by the selection rules of light-matter interaction.

For ^{173}Yb, the lifetime of the $^3\mathrm{P}_0$ state is of the order of 20 s, which is extremely long on the atomic scale.

The idea put forward by Zhang, Cheng, et al. (2015) is to consider a pair of atoms, one in the ground state $^1\mathrm{S}_0$, the other in the $^3\mathrm{P}_0$. They consider the fermionic isotope ^{173}Yb which has a nuclear spin $I = 5/2$; in the presence of an external magnetic field, this results in each of the two electronic levels considered, $^1\mathrm{S}_0$ and $^3\mathrm{P}_0$, being split into six states corresponding to $m_I = -\frac{5}{2}, -\frac{3}{2}, \ldots, +\frac{5}{2}$. Since we are dealing with nuclear magnetism, the splittings are very small (factor $\sim 10^{-3}$ compared to electronic magnetism), but this is sufficient to create the necessary control parameter.

Among the multiple possible pairs for the nuclear spins of the two atoms, one selects a pair denoted $(m_I^\downarrow, m_I^\uparrow) \equiv (\downarrow, \uparrow)$ (one chooses $m_I^\downarrow \neq m_I^\uparrow$). The important point is that the Landé factors g_g and g_e of the two states $^1\mathrm{S}_0$ and $^3\mathrm{P}_0$ are not equal. Therefore, the two states

$$|g\uparrow; e\downarrow\rangle \quad \text{and} \quad |g\downarrow; e\uparrow\rangle \tag{69}$$

do not have the same energy: the energy difference reads[5] $\mu_\mathrm{n} B\,(g_e - g_g)(m_I^\downarrow - m_I^\uparrow)$, where μ_n is the nuclear magneton. This energy difference can be varied by changing the applied magnetic field. We will suppose in what follows that the first of these two states is the one of lower energy.

We now take into account the fact that the atoms are fermions and we focus on an s-wave collision, i.e. a spatial wave function symmetric in the exchange of the positions of the two atoms. This is possible because the atoms are not in the same internal state: the global antisymmetric character of the state of the two atoms can be ensured by these internal variables.

[4] This invariance with respect to nuclear spin leads to a $SU(N)$ symmetry for the interaction potential, $N = 2I + 1$ being the number of nuclear spin states.

[5] The energy difference for ^{173}Yb is $h \times 113$ Hz for $B = 1$ Gauss and $m_I^\downarrow - m_I^\uparrow = 1$. The origin of the difference between g_g and g_e lies in a slight hyperfine coupling between the $^3\mathrm{P}_0$ and $^3\mathrm{P}_1$ states.

More precisely, we pose

$$|\psi\rangle = \frac{1}{\sqrt{2}}\left(|g\uparrow; e\downarrow\rangle - |e\downarrow; g\uparrow\rangle\right) \tag{70}$$

which corresponds to the nuclear + electronic state of the open channel (low energy), and

$$|\phi\rangle = \frac{1}{\sqrt{2}}\left(|g\downarrow; e\uparrow\rangle - |e\uparrow; g\downarrow\rangle\right) \tag{71}$$

which corresponds to the closed channel (high energy).

Like the singlet and triplet potentials for one-electron atoms, the interaction potential between the two atoms depends on the symmetric or antisymmetric nature of the orbital electronic state. The electronic and nuclear parts of the two eigenstates of interest here are

$$|\pm\rangle = \frac{1}{2}\left(|ge\rangle \pm |eg\rangle\right) \otimes \left(|\uparrow\downarrow\rangle \mp |\downarrow\uparrow\rangle\right), \tag{72}$$

each characterized by a scattering length, $a_\pm$, for s-wave collisions.

Let us consider a collision between low-energy atoms initially prepared in the $|\psi\rangle$ state written in (70). This state $|\psi\rangle$ is a linear combination of the two $|\pm\rangle$ states:

$$|\psi\rangle = \frac{1}{\sqrt{2}}\left(|+\rangle + |-\rangle\right) \tag{73}$$

and is therefore not an eigenstate of the interaction Hamiltonian. During the collision, it is coupled to the closed channel state $|\phi\rangle$. After the collision, the atoms emerge in $|\psi\rangle$ but the accumulated phase shift depends on the coupling with $|\phi\rangle$.

For a resonance to occur due to this coupling, there must be in the closed channel a bound state of energy close to the dissociation limit of the open channel. This is indeed the case for the $|+\rangle$ channel which is associated with a large and positive scattering length (Scazza, Hofrichter, et al. 2014; Cappellini, Mancini, et al. 2014; Cappellini, Mancini, et al. 2015). The bound state has a binding energy of $h \times 32\,\mathrm{kHz}$.

We present in figure 18 data extracted from Höfer, Riegger, et al. (2015); they show the variation with the magnetic field B of the thermalization time of an equilibrated mixture of 60,000 atoms in the pair of states

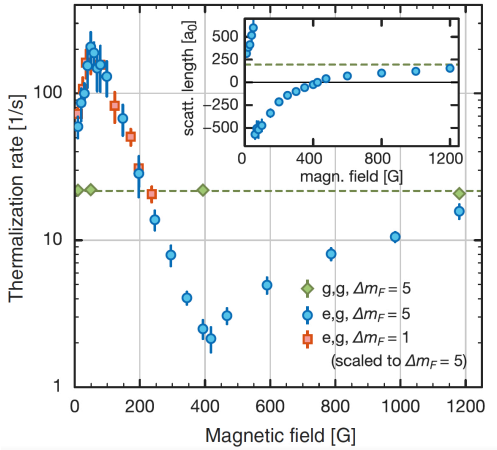

Figure 18. *Orbital resonance for ^{173}Yb. Thermalization rates in a $|g\uparrow, |e\downarrow\rangle$ mixture (blue and red dots) and $|g\uparrow, |g\downarrow\rangle$ (green dots). The red [resp. blue] points correspond to $m_I^\uparrow = -m_I^\downarrow = \frac{1}{2}$ [resp. $\frac{5}{2}$]. The B field has been resized by a factor of 5 for the red points to show the universality of the result. Figure taken from Höfer, Riegger, et al. (2015).*

$|g\uparrow\rangle, |e\downarrow\rangle$, and for comparison a mixture $|g\uparrow\rangle, |g\downarrow\rangle$. This mixture is confined in an anisotropic dipole trap and one measures the time needed for an excess of energy along one axis of the trap to be distributed along the 3 axes, as expected for the equipartition of the energy. This time is inversely proportional to the effective section of elastic collision, thus to the square of the scattering length. We can see that this time varies by two orders of magnitude around the resonance for the mixture $|g\uparrow\rangle, |e\downarrow\rangle$ while it is independent of B for the mixture $|g\uparrow\rangle, |g\downarrow\rangle$. Such resonances can open new perspectives in the realization of topological superfluids (Cornish 2015).

4-3 The case of lanthanides Er and Dy

Lanthanide atoms such as erbium or dysprosium have very different characteristics from other atoms commonly used in quantum gas experiments such as the alkali metals or alkaline earths. The orbital angular momen-

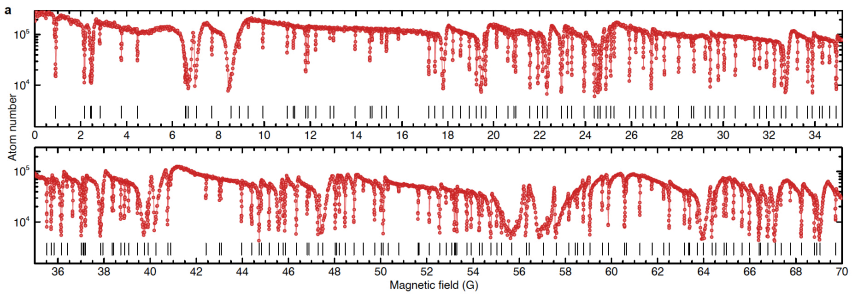

Figure 19. *Number of ^{168}Er atoms having "survived" in a light trap after a duration of 400 ms in the presence of a B magnetic field. Each narrow peak indicates an increased loss due to a Fano–Feshbach resonance. Figure taken from Frisch, Mark, et al. (2014).*

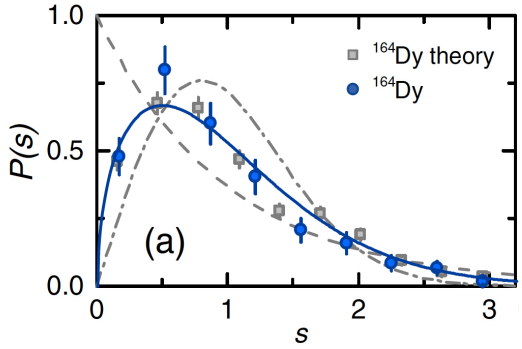

Figure 20. *Normalized distribution of the gap between two successive ^{164}Dy resonances. The blue points correspond to measurements and the grey points to the result of a coupled-channel calculation. The dashed curve gives the expected result for a regular Hamiltonian, the dotted one the result for a chaotic Hamiltonian (Wigner-Dyson law). We see that the resonances "repel" each other, but not as much as expected by the Wigner-Dyson law. Figure extracted from Maier, Kadau, et al. (2015).*

tum of the electrons in the electronic ground state is not zero. Added to the spin angular momentum, this leads to very large magnetic moments: $10\mu_B$ for dysprosium, thus magnetic dipole-dipole interactions 100 times larger than for alkali metal atoms. The interactions between lanthanide atoms show a marked anisotropy, on the one hand because of these magnetic dipoles and on the other hand because of the van der Waals interactions, which acquire a significant anisotropic part (of the order of 10% of the isotropic part) coming from the orbital angular momentum of the electrons

For lanthanide atoms of angular momentum J in their electronic ground state, there are $(J+1)^2$ non-degenerate potential curves leading to $(J+1)^2$ independent scattering lengths, to be compared with the two singlet and triplet channels of the alkali metal atoms. This leads to a very large number of possibilities for Feshbach resonances in a given magnetic field range; this number is further increased by the fact that the Zeeman shift of the different states for a given field is much larger than for the alkali metal atoms, due to the large magnetic moment.

To locate these Feshbach resonances, a frequently used technique is to measure the rate of atomic losses in a trapped cloud as a function of the applied magnetic field. In the vicinity of a resonance, the probability of finding a pair of atoms close to each other is strongly increased and two- or three-body loss processes are therefore favored. A two-body loss corresponds to the flip of an electron spin during the collision, the released Zeeman energy being converted into kinetic energy. A three-body process leads to the formation of a strongly bound dimer, the third body carrying away the energy released by this formation.

We show in figure 19 an example of result obtained by Frisch, Mark, et al. (2014) for a gas of ^{168}Er atoms at a temperature of 330 nK. There are 190 resonances in a magnetic field interval of 70 Gauss. This number is considerable: one would find on average less than one resonance on an interval of this width for alkali metal atoms.

Frisch, Mark, et al. (2014) and Maier, Kadau, et al. (2015) have taken advantage of this large number of resonances, obtained for both erbium and dysprosium, to perform a statistical analysis. They studied in particular the distribution of the gaps between two consecutive resonances, an example of which is shown in figure 20. It can be seen that the successive resonances "repel" each other, i.e. the probability of finding two resonances

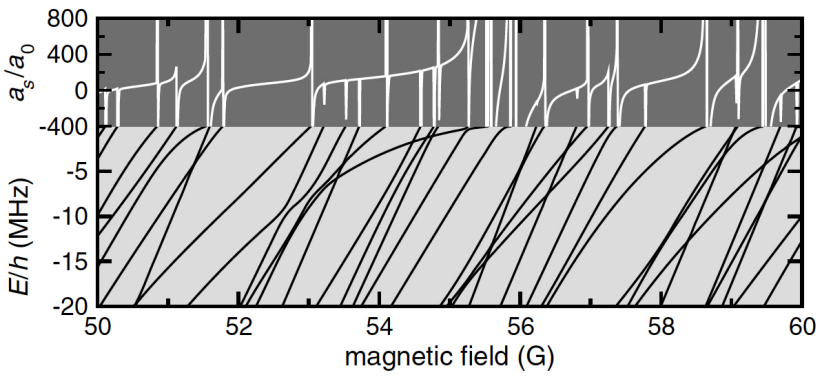

Figure 21. *Top: scattering length estimated by a coupled-channel calculation for ^{168}Er. Bottom: spectrum of weakly bound states. A Fano–Feshbach resonance occurs each time a bound state crosses the zero energy and disappears in the continuum. Figure extracted from Maier, Kadau, et al. (2015).*

with a small separation is smaller than if these resonances were randomly distributed.

The distribution of the positions of the resonances of ^{168}Er as the magnetic field is varied is directly related to the spectrum of the bound states of the Hamiltonian of the problem, for a given magnetic field. This point is illustrated in figure 21, where the energies of the bound states, shown here for ^{168}Er, have been obtained by a coupled-channel calculation. Now the spectrum of the Hamiltonian, more precisely the distribution $P(s)$ of the interval s between successive eigenvalues, gives information about the nature of the underlying motion. If this motion is regular, a collection of decoupled harmonic oscillators for example, the distribution $P(s)$ will be a Poisson distribution. If this motion is chaotic and the Hamiltonian is described by a real symmetric random matrix, we expect a Wigner-Dyson distribution $\propto s\, \mathrm{e}^{-\pi s^2/4}$.

We can see in figure 20 that the repulsion of the positions of the Fano–Feshbach resonances, if it is indeed present, is not as strong as the one expected for the Wigner-Dyson law. This result, confirmed by the numerical calculation, indicates that the Hamiltonian is neither completely regular nor completely chaotic in this range of magnetic field[6].

[6]The Brody parameter allows one to characterize the deviation of the measured distribution with respect to Poisson and Wigner–Dyson distributions. For a magnetic field $\sim$ 30 Gauss, the value of this parameter deduced from the coupled-channel calculation is ~ 0.5 for ^{164}Dy or ^{168}Er.

Appendix: bound state for our resonance model

As for the study of scattering states in the previous chapter, our starting point for the search of possible bound states will be the first of the two eigenvalue equations (2-3) :

$$(E - \hat{H}_0)|\psi\rangle = \hat{W}|\phi\rangle. \tag{74}$$

Its solution is written thanks to the resolvent operator $\hat{G}_0$ (without free term since we consider $E < 0$):

$$|\psi\rangle = \hat{G}_0(E)\,\hat{W}|\phi\rangle. \tag{75}$$

It is now a question of finding the energy (or energies?) E for which this equation is compatible with the second eigenvalue equation (3):

$$(E - E_{\rm cl})|\phi\rangle = \hat{W}|\psi\rangle. \tag{76}$$

To do this, recall that $|\phi\rangle = \alpha|\phi_0\rangle$ and project (76) onto $|\phi_0\rangle$:

$$(E - E_{\rm cl})\alpha = \langle\phi_0|\hat{W}|\psi\rangle = \alpha\langle\phi_0|\hat{W}\,\hat{G}_0(E)\,\hat{W}|\phi_0\rangle \tag{77}$$

hence the equation to determine E:

$$E - \langle\phi_0|\hat{W}\,\hat{G}_0(E)\,\hat{W}|\phi_0\rangle = E_{\rm cl}. \tag{78}$$

To make this equation more explicit, let us take the result obtained in the previous chapter for the matrix element involved in the left-hand side of this equation:

$$\langle\phi_0|\hat{W}\,\hat{G}_0(E)\,\hat{W}|\phi_0\rangle = \frac{1}{(2\pi)^3}\int \frac{|\langle\phi_0|\hat{W}|\boldsymbol{q}\rangle|^2}{E - \varepsilon(\boldsymbol{q}) + {\rm i}0_+}\,{\rm d}^3q, \tag{79}$$

After angular integral and replacement of E by $-\hbar^2\kappa^2/2m_{\rm r}$, we obtain

$$\begin{aligned}\langle\phi_0|\hat{W}\,\hat{G}_0(E)\,\hat{W}|\phi_0\rangle &= -\frac{2}{\pi}\int \frac{q^2\,g^2(q)}{q^2+\kappa^2}\,{\rm d}q \\ &= -\Delta + \frac{2\kappa^2}{\pi}\int \frac{g^2(q)}{q^2+\kappa^2}\,{\rm d}q\end{aligned} \tag{80}$$

which, using $\tilde{E_{\rm cl}} \equiv E_{\rm cl} - \Delta$ finally leads to

$$\frac{\hbar^2}{2m_{\rm r}}\left[\kappa^2 + \frac{4m_{\rm r}}{\pi\hbar^2}\int_0^{+\infty}\frac{\kappa^2\,g^2(q)}{q^2+\kappa^2}\,{\rm d}q\right] = -\tilde{E_{\rm cl}}. \tag{81}$$

The left-hand side of this equation is obviously positive and is moreover an increasing function of κ, with values ranging from 0 to $+\infty$. To have a (unique) solution to this equation, it is necessary and sufficient that the right-hand side is also positive, i.e. $\tilde{E_{\rm cl}} < 0$. According to (8), this corresponds to the regime $a > 0$.

We see on (81) that the choice $\tilde{E_{\rm cl}} = 0$ leads to the solution $\kappa = 0$. Let us now check that for $\tilde{E_{\rm cl}}$ sufficiently small, so a sufficiently large, we find the universal law (13). For that, let us notice first that when $\kappa \to 0$, the integral appearing in the left member of (81) diverges in $q = 0$. For κ small but not zero, this integral is therefore dominated by small values of q. We can replace $g(q)$ by $g_0 \equiv g(0)$ to find:

$$\kappa \to 0 : \qquad \int_0^{+\infty}\frac{g^2(q)}{q^2+\kappa^2}\,{\rm d}q \approx g_0^2\int_0^{+\infty}\frac{1}{q^2+\kappa^2}\,{\rm d}q = \frac{\pi g_0^2}{2\kappa}. \tag{82}$$

When $\kappa \to 0$, this term becomes dominant in the $[\ldots]$ of (81), which simplifies to

$$\kappa g_0^2 \approx -\tilde{E_{\rm cl}} \tag{83}$$

or by using (8) :

$$\kappa \approx \frac{1}{a} \qquad \Rightarrow \quad E_{\rm bound} \approx -\frac{\hbar^2}{2m_{\rm r}a^2}. \tag{84}$$

This is the expected result: for $a > 0$ and in the small $|\tilde{E_{\rm cl}}|$ regime, the energy of the bound state is related to the scattering length by the universal relation (13).

References

Abeelen, F. A. van & B. J. Verhaar (Jan. 1999), "Determination of collisional properties of cold Na atoms from analysis of bound-state photoassociation and Feshbach resonance field data"en, in *Physical Review A* **59**, pp. 578–584.

Abraham, E. R. I., W. I. McAlexander, C. A. Sackett & Randall G. Hulet (Feb. 1995), "Spectroscopic Determination of the s -Wave Scattering Length of Lithium", in *Physical Review Letters* **74**, pp. 1315–1318.

Araujo, Luis EE. de, Jonathan D. Weinstein, Stephen D. Gensemer, Fredrik K. Fatemi, Kevin M. Jones, Paul D. Lett & Eite Tiesinga (2003), "Two-color photoassociation spectroscopy of the lowest triplet potential of Na2", in *The Journal of Chemical Physics* **119**, pp. 2062–2074.

Arndt, M., M. Ben Dahan, D. Guéry-Odelin, M. W. Reynolds & J. Dalibard (1997), "Observation of a zero-energy resonance in Cs-Cs collisions", in *Phys. Rev. Lett.* **79**, p. 625.

Bahns, JT, PL Gould & WC Stwalley (2000), "Formation of Cold (Tâ©$\frac{1}{2}$ 1 K) Molecules", in *Advances In Atomic, Molecular, and Optical Physics* **42**, pp. 171–224.

Barrow, David A & Ronald A Aziz (1988), "The neon–argon potential revisited", in *The Journal of chemical physics* **89**, pp. 6189–6194.

Bergeman, T., M. G. Moore & M. Olshanii (2003), "Atom-Atom Scattering under Cylindrical Harmonic Confinement: Numerical and Analytic Studies of the Confinement Induced Resonance", in *Phys. Rev. Lett* **91**, p. 163201.

Berkhout, J. J., O. J. Luiten, I. D. Setija, T. W. Hijmans, T. Mizusaki & J. T. M. Walraven (1989), "Quantum reflection: Focusing of hydrogen atoms with a concave mirror", in *Phys. Rev. Lett.* **63** (16), pp. 1689–1692.

Berry, Michael V & KE Mount (1972), "Semiclassical approximations in wave mechanics", in *Reports on Progress in Physics* **35**, p. 315.

Beth, Erich & George E Uhlenbeck (1937), "The quantum theory of the non-ideal gas. II. Behaviour at low temperatures", in *Physica* **4**, pp. 915–924.

Bethe, Hans & Rudolf Peierls (1935), "Quantum theory of the diplon", in *Proceedings of the Royal Society of London. Series A-Mathematical and Physical Sciences* **148**, pp. 146–156.

Bohn, John L. & P. S. Julienne (1999), "Semianalytic theory of laser-assisted resonant cold collisions", in *Phys. Rev. A* **60** (1), pp. 414–425.

Boisseau, C, E Audouard & J Vigué (1998), "Quantization of the highest levels in a molecular potential", in *EPL (Europhysics Letters)* **41**, p. 349.

Boisseau, C, E Audouard, J Vigué & VV Flambaum (2000), "Analytical correction to the WKB quantization condition for the highest levels in a molecular potential", in *The European Physical Journal D-Atomic, Molecular, Optical and Plasma Physics* **12**, pp. 199–209.

Borkowski, M., R. Ciuryło, P. S. Julienne, S. Tojo, K. Enomoto & Y. Takahashi (2009), "Line shapes of optical Feshbach resonances near the intercombination transition of bosonic ytterbium", in *Phys. Rev. A* **80** (1), p. 012715.

Borkowski, Mateusz, Alexei A. Buchachenko, Roman Ciuryło, Paul S. Julienne, Hirotaka Yamada, Yuu Kikuchi, Kakeru Takahashi, Yosuke Takasu & Yoshiro Takahashi (2017), "Beyond-Born-Oppenheimer effects in sub-kHz-precision photoassociation spectroscopy of ytterbium atoms", in *Phys. Rev. A* **96** (6), p. 063405.

Braaten, Eric, Masaoki Kusunoki & Dongqing Zhang (2008), "Scattering Models for Ultracold Atoms", in *Annals of Physics* **323**, pp. 1770–1815.

Breit, G (1947), "The scattering of slow neutrons by bound protons. I. Methods of calculation", in *Physical Review* **71**, p. 215.

Busch, Thomas, Berthold-Georg Englert, Kazimierz Rzażewski & Martin Wilkens (1998), "Two cold atoms in a harmonic trap", in *Foundations of Physics* **28**, pp. 549–559.

Cappellini, G., M. Mancini, G. Pagano, P. Lombardi, L. Livi, et al. (2014), "Direct Observation of Coherent Interorbital Spin-Exchange Dynamics", in *Phys. Rev. Lett.* **113** (12), p. 120402.
– (2015), "Erratum: Direct Observation of Coherent Interorbital Spin-Exchange Dynamics [Phys. Rev. Lett. 113, 120402 (2014)]", in *Phys. Rev. Lett.* **114** (23), p. 239903.
Casimir, H. B. G. & D. Polder (1948), "The Influence of Retardation on the London-van der Waals Forces", in *Phys. Rev.* **73** (4), pp. 360–372.
Castin, Y & F Werner (2012), "The Unitary Gas and its Symmetry Properties", in *The BCS–BEC Crossover and the Unitary Fermi Gas*, ed. by W. Zwerger, Springer.
Castin, Yvan (2007), "Basic theory tools for degenerate Fermi gases", in *Ultra-cold Fermi Gases*, ed. by M. Inguscio, W. Ketterle & C. Salomon, Proceedings of the Enrico Fermi Varenna School (2006).
Chapurin, Roman, Xin Xie, Michael J. Van de Graaff, Jared S. Popowski, Jose P. D'Incao, Paul S. Julienne, Jun Ye & Eric A. Cornell (Dec. 2019), "Precision Test of the Limits to Universality in Few-Body Physics", in *Physical Review Letters* **123**, p. 233402.
Chen, Yue, Da-Wu Xiao, Ren Zhang & Peng Zhang (2020), *Analytical solution for the spectrum of two ultracold atoms in a completely anisotropic confinement*, arXiv: 2002.02168.
Chin, Cheng, Rudolf Grimm, Paul Julienne & Eite Tiesinga (2010), "Feshbach resonances in ultracold gases", in *Rev. Mod. Phys.* **82** (2), pp. 1225–1286.
Ciuryło, R., E. Tiesinga, S. Kotochigova & P. S. Julienne (2004), "Photoassociation spectroscopy of cold alkaline-earth-metal atoms near the intercombination line", in *Phys. Rev. A* **70** (6), p. 062710.
Cohen-Tannoudji, Claude & David Guéry-Odelin (2011), *Advances in Atomic Physics*, World Scientific.
Comparat, Daniel (1999), "Molecules froides: formation de molecules froides par photoassociation d'atomes froids de cesium. mise en evidence de forces a longue portee entre atomes froids excites de cesium", PhD thesisParis 11.
– (2004), "Improved LeRoy–Bernstein near-dissociation expansion formula, and prospect for photoassociation spectroscopy", in *The Journal of chemical physics* **120**, pp. 1318–1329.
Cornish, Simon (2015), "Controlling Collisions in a Two-Electron Atomic Gas", in *Physics* **8**, p. 125.
Côté, R., E. J. Heller & A. Dalgarno (1996), "Quantum suppression of cold atom collisions", in *Phys. Rev. A* **53** (1), pp. 234–241.
Courteille, Ph., R. S. Freeland, D. J. Heinzen, F. A. van Abeelen & B. J. Verhaar (July 1998), "Observation of a Feshbach Resonance in Cold Atom Scattering", in *Physical Review Letters* **81**, pp. 69–72.
Coxon, John A & Photos G Hajigeorgiou (2010), "The ground X Σ 1 g+ electronic state of the cesium dimer: Application of a direct potential fitting procedure", in *The Journal of chemical physics* **132**, p. 094105.
Crubellier, A, O Dulieu, F Masnou-Seeuws, M Elbs, H Knöckel & E Tiemann (1999), "Simple determination of Na 2 scattering lengths using observed bound levels at the ground state asymptote", in *The European Physical Journal D-Atomic, Molecular, Optical and Plasma Physics* **6**, pp. 211–220.
Deiß, Markus, Björn Drews, Johannes Hecker Denschlag, Nadia Bouloufa-Maafa, Romain Vexiau & Olivier Dulieu (2015), "Polarizability of ultracold molecules in the rovibrational ground state of", in *New Journal of Physics* **17**, p. 065019.
DeMarco, B., J. L. Bohn, J. P. Burke, M. Holland & D. S. Jin (1999), "Measurement of p-Wave Threshold Law Using Evaporatively Cooled Fermionic Atoms", in *Phys. Rev. Lett.* **82** (21), pp. 4208–4211.
Demtröder, Wolfgang (2010), *Atoms, molecules and photons*, Springer.
Derevianko, A., J. F. Babb & A. Dalgarno (2001), "High-precision calculations of van der Waals coefficients for heteronuclear alkali-metal dimers", in *Phys. Rev. A* **63** (5), p. 052704.
Druzhinina, V. & M. DeKieviet (2003), "Experimental Observation of Quantum Reflection far from Threshold", in *Phys. Rev. Lett.* **91** (19), p. 193202.
Duine, Rembert A & Henk TC Stoof (2004), "Atom–molecule coherence in Bose gases", in *Physics Reports* **396**, pp. 115–195.
Dulieu, Olivier, Maurice Raoult & Eberhard Tiemann (2006), "Cold Molecules: a chemistry kitchen for physicists?", in *Journal of Physics B: Atomic, Molecular and Optical Physics* **39**.
Efimov, V (1971), "Weakly-bound states of three resonantly-interacting particles", in *Sov. J. Nucl. Phys* **12**, p. 101.
Escobar, Y. N. Martinez de, P. G. Mickelson, P. Pellegrini, S. B. Nagel, A. Traverso, M. Yan, R. Côté & T. C. Killian (2008), "Two-photon photoassociative spectroscopy of ultracold ^{88}Sr", in *Phys. Rev. A* **78** (6), p. 062708.

Fano, U. (1961), "Effects of Configuration Interaction on Intensities and Phase Shifts", in *Phys. Rev.* **124** (6), pp. 1866–1878.
Fedichev, P. O., M. W. Kagan, G. V. Shlyapnikov & J. T. M. Walraven (1996), "Influence of Nearly Resonant Light on the Scattering Length in Low-Temperature Atomic Gases", in *Phys. Rev. Lett.* **77**, p. 2913.
Feshbach, Herman (1958), "Unified Theory of Nuclear Reactions", in *Annals of Physics* **5**, pp. 357–390.
– (1962), "A unified theory of nuclear reactions. II", in *Annals of Physics* **19**, pp. 287–313.
Feynman, R. P. (1939), "Forces in Molecules", in *Phys. Rev.* **56** (4), pp. 340–343.
Flambaum, V. V., G. F. Gribakin & C. Harabati (Mar. 1999), "Analytical calculation of cold-atom scattering", in *Physical Review A* **59**, pp. 1998–2005.
Frisch, Albert, Michael Mark, Kiyotaka Aikawa, Francesca Ferlaino, John L Bohn, Constantinos Makrides, Alexander Petrov & Svetlana Kotochigova (2014), "Quantum chaos in ultracold collisions of gas-phase erbium atoms", in *Nature* **507**, pp. 475–479.
Gao, Bo (1998a), "Quantum-defect theory of atomic collisions and molecular vibration spectra", in *Phys. Rev. A* **58** (5), pp. 4222–4225.
– (1998b), "Solutions of the Schrödinger equation for an attractive $1/r^6$ potential", in *Physical Review A* **58**, pp. 1728–1734.
– (1999), "Breakdown of Bohr's Correspondence Principle", in *Phys. Rev. Lett.* **83** (21), pp. 4225–4228.
– (2000), "Zero-energy bound or quasibound states and their implications for diatomic systems with an asymptotic van der Waals interaction", in *Phys. Rev. A* **62** (5), p. 050702.
– (2001), "Angular-momentum-insensitive quantum-defect theory for diatomic systems", in *Phys. Rev. A* **64** (1), p. 010701.
– (2004), "Binding energy and scattering length for diatomic systems", in *Journal of Physics B: Atomic, Molecular and Optical Physics* **37**, p. 4273.
Gerber, Ian (2006), "Description des forces de van der Waals dans le cadre de la théorie de la fonctionnelle de la densité par un traitement explicite des interactions de longue portée", PhD thesisNancy-I: Université Henri Poincaré.
Gogolin, Alexander O., Christophe Mora & Reinhold Egger (2008), "Analytical Solution of the Bosonic Three-Body Problem", in *Phys. Rev. Lett.* **100** (14), p. 140404.
Goldberger, Marvin L & Kenneth M Watson (2004), *Collision theory*, Dover Publications.
Goral, Krzysztof, Thorsten Koehler, Simon A Gardiner, Eite Tiesinga & Paul S Julienne (2004), "Adiabatic association of ultracold molecules via magnetic-field tunable interactions", in *Journal of Physics B: Atomic, Molecular and Optical Physics* **37**, p. 3457.
Gribakin, G. F. & V. V. Flambaum (July 1993), "Calculation of the scattering length in atomic collisions using the semiclassical approximation", in *Physical Review A* **48**, pp. 546–553.
Grisenti, R. E., W. Schöllkopf, J. P. Toennies, G. C. Hegerfeldt, T. Köhler & M. Stoll (2000), "Determination of the Bond Length and Binding Energy of the Helium Dimer by Diffraction from a Transmission Grating", in *Phys. Rev. Lett.* **85** (11), pp. 2284–2287.
Guan, Qingze, V Klinkhamer, R Klemt, JH Becher, A Bergschneider, PM Preiss, S Jochim & D Blume (2019), "Density Oscillations Induced by Individual Ultracold Two-Body Collisions", in *Physical review letters* **122**, p. 083401.
Guéry-Odelin, David, Francesca Zambelli, Jean Dalibard & Sandro Stringari (1999), "Collective oscillations of a classical gas confined in harmonic traps", in *Phys. Rev. A* **60** (6), pp. 4851–4856.
Haller, Elmar, Mattias Gustavsson, Manfred J Mark, Johann G Danzl, Russell Hart, Guido Pupillo & Hanns-Christoph Nägerl (2009), "Realization of an excited, strongly correlated quantum gas phase", in *Science* **325**, pp. 1224–1227.
Heaven, Michael C, Jeremy M Merritt & Vladimir E Bondybey (2011), "Bonding in beryllium clusters", in *Annual review of physical chemistry* **62**, pp. 375–393.
Heitler, Walther & Fritz London (1927), "Wechselwirkung neutraler Atome und homöopolare Bindung nach der Quantenmechanik", in *Z. Physik* **44**, p. 455.
Höfer, M., L. Riegger, F. Scazza, C. Hofrichter, D. R. Fernandes, M. M. Parish, J. Levinsen, I. Bloch & S. Fölling (2015), "Observation of an Orbital Interaction Induced Feshbach Resonance in Yb 173", in *Physical Review Letters* **115**, p. 265302.
Huang, K. (1987), *Statistical Mechanics*, New York: Wiley.
Huang, Kerson & Chen Ning Yang (1957), "Quantum-mechanical many-body problem with hard-sphere interaction", in *Physical review* **105**, p. 767.

Inouye, S., M. Andrews, J. Stenger, H. J. Miesner, D. M. Stamper-Kurn & W. Ketterle (1998), "Observation of Feshbach resonances in a Bose–Einstein condensate", in *Nature* **392**, p. 151.

Jaskula, J.-C., M. Bonneau, G. B. Partridge, V. Krachmalnicoff, P. Deuar, K. V. Kheruntsyan, A. Aspect, D. Boiron & C. I. Westbrook (2010), "Sub-Poissonian Number Differences in Four-Wave Mixing of Matter Waves", in *Phys. Rev. Lett.* **105** (19), p. 190402.

Jelassi, Haikel, Bruno Viaris de Lesegno & Laurence Pruvost (2008), "Reexamination of the LeRoy-Bernstein formula for weakly bound molecules", in *Phys. Rev. A* **77** (6), p. 062515.

Joachain, Charles Jean (1975), *Quantum collision theory*.

Kaufman, A. M., R. P. Anderson, Thomas M. Hanna, E. Tiesinga, P. S. Julienne & D. S. Hall (2009), "Radio-frequency dressing of multiple Feshbach resonances", in *Phys. Rev. A* **80** (5), p. 050701.

Kerman, Andrew J, Cheng Chin, Vladan Vuletić, Steven Chu, Paul J Leo, Carl J Williams & Paul S Julienne (2001), "Determination of Cs–Cs interaction parameters using Feshbach spectroscopy", in *Comptes Rendus de l'Académie des Sciences-Series IV-Physics* **2**, pp. 633–639.

Khaykovich, L., F. Schreck, G. Ferrari, T. Bourdel, J. Cubizolles, L. D. Carr, Y. Castin & C. Salomon (2002), "Formation of a matter-wave bright soliton", in *Science* **296**, p. 1290.

Kitagawa, Masaaki, Katsunari Enomoto, Kentaro Kasa, Yoshiro Takahashi, Roman Ciuryło, Pascal Naidon & Paul S. Julienne (2008), "Two-color photoassociation spectroscopy of ytterbium atoms and the precise determinations of s-wave scattering lengths", in *Phys. Rev. A* **77** (1), p. 012719.

Köhler, Thorsten, Krzysztof Góral & Paul S. Julienne (2006), "Production of cold molecules via magnetically tunable Feshbach resonances", in *Rev. Mod. Phys.* **78** (4), pp. 1311–1361.

Kokkelmans, S. J. J. M. F., J. N. Milstein, M. L. Chiofalo, R. Walser & M. J. Holland (May 2002), "Resonance superfluidity: Renormalization of resonance scattering theory", in *Physical Review A* **65**, p. 053617.

Kolos, W. & C. C. J. Roothaan (1960), "Accurate Electronic Wave Functions for the H_2 Molecule", in *Rev. Mod. Phys.* **32** (2), pp. 219–232.

Kołos, W & L Wolniewicz (1975), "Improved potential energy curve and vibrational energies for the electronic ground state of the hydrogen molecule", in *Journal of Molecular Spectroscopy* **54**, pp. 303–311.

Kolos, Wlodzimierz, Krzysztof Szalewicz & Hendrik J Monkhorst (1986), "New Born–Oppenheimer potential energy curve and vibrational energies for the electronic ground state of the hydrogen molecule", in *The Journal of chemical physics* **84**, pp. 3278–3283.

Kostrun, Marijan, Matt Mackie, Robin Côté & Juha Javanainen (2000), "Theory of coherent photoassociation of a Bose-Einstein condensate", in *Phys. Rev. A* **62** (6), p. 063616.

Kunitski, Maksim, Stefan Zeller, Jörg Voigtsberger, Anton Kalinin, Lothar Ph H Schmidt, Markus Schöffler, Achim Czasch, Wieland Schöllkopf, Robert E Grisenti, Till Jahnke, et al. (2015), "Observation of the Efimov state of the helium trimer", in *Science* **348**, pp. 551–555.

Lamporesi, G., J. Catani, G. Barontini, Y. Nishida, M. Inguscio & F. Minardi (2010), "Scattering in Mixed Dimensions with Ultracold Gases", in *Phys. Rev. Lett.* **104** (15), p. 153202.

Landau, L. D. & E. M. Lifshitz (1975), *Mécanique quantique*, Editions Mir.

Lepers, Maxence, J-F Wyart & Olivier Dulieu (2014), "Anisotropic optical trapping of ultracold erbium atoms", in *Physical Review A* **89**, p. 022505.

LeRoy, Robert J. & Richard B. Bernstein (1970), "Dissociation Energy and Long Range Potential of Diatomic Molecules from Vibrational Spacings of Higher Levels", in *The Journal of Chemical Physics* **52**, pp. 3869–3879.

LeRoy, Robert J, Nikesh S Dattani, John A Coxon, Amanda J Ross, Patrick Crozet & Colan Linton (2009), "Accurate analytic potentials for Li $_2$ (X $^1\Sigma_g^+$) and Li_2 (A $^1\Sigma_u^+$) from 2 to 90 Å, and the radiative lifetime of Li (2 p)", in *The Journal of chemical physics* **131**, p. 204309.

Li, H., J.-F. Wyart, O. Dulieu, S. Nascimbene & M. Lepers (2017), "Optical trapping of ultracold dysprosium atoms: transition probabilities, dynamic dipole polarizabilities and van der Waals C_6 coefficients", in *Journal of Physics B: Atomic, Molecular and Optical Physics* **50**, p. 014005.

Li, P, W Xie & KT Tang (2010), "The van der Waals potential of the magnesium dimer", in *The Journal of chemical physics* **133**, p. 084308.

Lim, T. K., Sister Kathleen Duffy & William C. Damer (1977), "Efimov State in the ^{4}He Trimer", in *Phys. Rev. Lett.* **38** (7), pp. 341–343.

Lippmann, B. A. & Julian Schwinger (1950), "Variational Principles for Scattering Processes. I", in *Phys. Rev.* **79** (3), pp. 469–480.

London, Fritz (1930), "Zur theorie und systematik der molekularkräfte", in *Zeitschrift für Physik* **63**, pp. 245–279.

Lutz, Jesse J & Jeremy M Hutson (2016), "Deviations from Born-Oppenheimer mass scaling in spectroscopy and ultracold molecular physics", in *Journal of Molecular Spectroscopy* **330**, pp. 43–56.

Maier, T, H Kadau, M Schmitt, M Wenzel, I Ferrier-Barbut, T Pfau, Albert Frisch, Simon Baier, Kiyotaka Aikawa, Lauriane Chomaz, et al. (2015), "Emergence of chaotic scattering in ultracold Er and Dy", in *Physical Review X* **5**, p. 041029.

Massignan, Pietro & Yvan Castin (2006), "Three-dimensional strong localization of matter waves by scattering from atoms in a lattice with a confinement-induced resonance", in *Phys. Rev. A* **74** (1), p. 013616.

Matsunaga, Nikita & Andreas A Zavitsas (2004), "Comparison of spectroscopic potentials and an a priori analytical function. The potential energy curve of the ground state of the sodium dimer, X $^1\Sigma_g^+$ Na_2", in *The Journal of chemical physics* **120**, pp. 5624–5630.

Messiah, Albert (1962), *Quantum mechanics: volume II*, North-Holland Publishing Company Amsterdam.

Mies, Frederick H. & Maurice Raoult (2000), "Analysis of threshold effects in ultracold atomic collisions", in *Phys. Rev. A* **62** (1), p. 012708.

Mitroy, J. & M. W. J. Bromley (2003), "Semiempirical calculation of van der Waals coefficients for alkali-metal and alkaline-earth-metal atoms", in *Phys. Rev. A* **68** (5), p. 052714.

Moal, S., M. Portier, J. Kim, J. Dugué, U. D. Rapol, M. Leduc & C. Cohen-Tannoudji (2006), "Accurate Determination of the Scattering Length of Metastable Helium Atoms Using Dark Resonances between Atoms and Exotic Molecules", in *Phys. Rev. Lett.* **96** (2), p. 023203.

Moerdijk, A. J., B. J. Verhaar & A. Axelsson (1995), "Resonances in ultracold collisions of Li 6 , Li 7 , and Na 23", in *Physical Review A* **51**, pp. 4852–4861.

Mott, Nevill Francis & Harrie Stewart Wilson Massey (1949), *The theory of atomic collisions*, Clarendon Press.

Naidon, Pascal & Shimpei Endo (May 2017), "Efimov physics: a review", in *Reports on Progress in Physics* **80**, p. 056001.

Naidon, Pascal & Ludovic Pricoupenko (2019), "Width and shift of Fano-Feshbach resonances for van der Waals interactions", in *Phys. Rev. A* **100** (4), p. 042710.

Nayak, V. U., D. O. Edwards & N. Masuhara (1983), "Scattering of ^{4}He Atoms Grazing the Liquid-^{4}He Surface", in *Phys. Rev. Lett.* **50** (13), pp. 990–992.

Nishida, Yusuke & Shina Tan (2008), "Universal Fermi Gases in Mixed Dimensions", in *Phys. Rev. Lett.* **101** (17), p. 170401.

Ogilvie, JF & Frank YH Wang (1992), "Potential-energy functions of diatomic molecules of the noble gases I. Like nuclear species", in *Journal of molecular structure* **273**, pp. 277–290.

Olshanii, Maxim (1998), "Atomic scattering in the presence of an external confinement and a gas of impenetrable bosons", in *Physical review letters* **81**, p. 938.

Olshanii, Maxim & Ludovic Pricoupenko (2001), "Rigorous Approach to the Problem of Ultraviolet Divergencies in Dilute Bose Gases", in *Phys. Rev. Lett.* **88** (1), p. 010402.

Pachomow, Evgenij, Veit Peter Dahlke, Eberhard Tiemann, Fritz Riehle & Uwe Sterr (2017), "Ground-state properties of Ca_2 from narrow-line two-color photoassociation", in *Physical Review A* **95**, p. 043422.

Pagano, G., M. Mancini, G. Cappellini, L. Livi, C. Sias, J. Catani, M. Inguscio & L. Fallani (Dec. 2015), "Strongly Interacting Gas of Two-Electron Fermions at an Orbital Feshbach Resonance", in *Physical Review Letters* **115**, p. 265301.

Papoular, D. J., G. V. Shlyapnikov & J. Dalibard (2010), "Microwave-induced Fano-Feshbach resonances", in *Phys. Rev. A* **81**, p. 041603.

Pasquini, T. A., Y. Shin, C. Sanner, M. Saba, A. Schirotzek, D. E. Pritchard & W. Ketterle (2004), "Quantum Reflection from a Solid Surface at Normal Incidence", in *Phys. Rev. Lett.* **93** (22), p. 223201.

Perrin, A., H. Chang, V. Krachmalnicoff, M. Schellekens, D. Boiron, A. Aspect & C. I. Westbrook (2007), "Observation of Atom Pairs in Spontaneous Four-Wave Mixing of Two Colliding Bose-Einstein Condensates", in *Phys. Rev. Lett.* **99** (15), p. 150405.

Pethick, Christopher & Henrik Smith (2008a), *Bose-Einstein condensation in dilute gase*sen, 2nd ed, Cambridge ; New York: Cambridge University Press.

Pethick, C.J. & H. Smith (2008b), *Bose–Einstein Condensation in Dilute Gases, Second Edition*, Cambridge University Press.

Petrov, D. S. (Jan. 2003), "Three-body problem in Fermi gases with short-range interparticle interaction"en, in *Physical Review A* **67**, p. 010703.

Petrov, D. S., M. Holzmann & G. V. Shlyapnikov (2000), "Bose–Einstein Condensation in Quasi-2D Trapped Gases", in *Phys. Rev. Lett.* **84**, p. 2551.

Pillet, P, N Vanhaecke, C Lisdat, D Comparat, Olivier Dulieu, Anne Crubellier & Françoise Masnou-Seeuws (2003), "Ultra-cold molecules: Formation, trapping and prospects", in *Physica Scripta* **2003**, p. 7.

Pitaevskii, L. & S. Stringari (2016), *Bose–Einstein Condensation and Superfluidity*, 2nd edition, Oxford: Oxford University Press.

Plattner, G-R & Ingo Sick (1981), "Coherence, interference and the Pauli principle: Coulomb scattering of carbon from carbon", in *European Journal of Physics* **2**, p. 109.

Porsev, S. G., M. S. Safronova, A. Derevianko & Charles W. Clark (2014), "Long-range interaction coefficients for ytterbium dimers", in *Phys. Rev. A* **89** (1), p. 012711.

Porsev, SG & A Derevianko (2006), "High-accuracy calculations of dipole, quadrupole, and octupole electric dynamic polarizabilities and van der Waals coefficients C_6, C_8, and C_{10} for alkaline-earth dimers", in *Journal of Experimental and Theoretical Physics* **102**, pp. 195–205.

Roberts, J. L., N. R. Claussen, James P. Burke, Chris H. Greene, E. A. Cornell & C. E. Wieman (1998), "Resonant Magnetic Field Control of Elastic Scattering in Cold ^{85}Rb", in *Phys. Rev. Lett.* **81** (23), pp. 5109–5112.

Saffman, M., T. G. Walker & K. Mølmer (2010), "Quantum information with Rydberg atoms", in *Rev. Mod. Phys.* **82** (3), pp. 2313–2363.

Safronova, MS, SG Porsev & Charles W Clark (2012), "Ytterbium in quantum gases and atomic clocks: van der Waals interactions and blackbody shifts", in *Physical review letters* **109**, p. 230802.

Scazza, Francesco, Christian Hofrichter, Moritz Höfer, PC De Groot, Immanuel Bloch & Simon Fölling (2014), "Observation of two-orbital spin-exchange interactions with ultracold SU (N)-symmetric fermions", in *Nature Physics* **10**, pp. 779–784.

Schiff, Leonard I (1968), *Quantum Mechanics*, McGrawHill.

Schöllkopf, Wieland & J Peter Toennies (1994), "Nondestructive mass selection of small van der Waals clusters", in *Science* **266**, pp. 1345–1348.

Shimizu, Fujio (2001), "Specular Reflection of Very Slow Metastable Neon Atoms from a Solid Surface", in *Phys. Rev. Lett.* **86** (6), pp. 987–990.

Slater, John C. (1968), *Quantum Theory Of Matter*, McGraw-Hill.

Söding, J., D. Guery-Odelin, P. Desbiolles, G. Ferrari & J. Dalibard (1998), "Giant spin relaxation of an ultracold cesium gas", in *Phys. Rev. Lett.* **80**, p. 1869.

Stwalley, William C & He Wang (1999), "Photoassociation of ultracold atoms: a new spectroscopic technique", in *Journal of molecular spectroscopy* **195**, pp. 194–228.

Tang, K. T., J. P. Toennies & C. L. Yiu (1995), "Accurate Analytical He-He van der Waals Potential Based on Perturbation Theory", in *Phys. Rev. Lett.* **74** (9), pp. 1546–1549.

Tang, KT & J Peter Toennies (1984), "An improved simple model for the van der Waals potential based on universal damping functions for the dispersion coefficients", in *The Journal of chemical physics* **80**, pp. 3726–3741.

Tang, KT & JP Toennies (2003), "The van der Waals potentials between all the rare gas atoms from He to Rn", in *The Journal of chemical physics* **118**, pp. 4976–4983.

Thalhammer, Gregor, Matthias Theis, Klaus Winkler, Rudolf Grimm & Johannes Hecker Denschlag (2005), "Inducing an optical Feshbach resonance via stimulated Raman coupling", in *Phys. Rev. A* **71** (3), p. 033403.

Theis, M., G. Thalhammer, K. Winkler, M. Hellwig, G. Ruff, R. Grimm & J. Hecker Denschlag (2004), "Tuning the Scattering Length with an Optically Induced Feshbach Resonance", in *Phys. Rev. Lett.* **93**, p. 123001.

Thorsheim, H. R., J. Weiner & P. S. Julienne (1987), "Laser-induced photoassociation of ultracold sodium atoms", in *Phys. Rev. Lett.* **58** (23), pp. 2420–2423.

Tiesinga, E., B. J. Verhaar & H. T. C. Stoof (1993), "Threshold and resonance phenomena in ultracold ground-state collisions", in *Phys. Rev. A* **47** (5), pp. 4114–4122.

Tomza, Michał, Krzysztof Jachymski, Rene Gerritsma, Antonio Negretti, Tommaso Calarco, Zbigniew Idziaszek & Paul S. Julienne (July 2019), "Cold hybrid ion-atom systems", in *Reviews of Modern Physics* **91**, p. 035001.

Tsai, C. C., R. S. Freeland, J. M. Vogels, H. M. J. M. Boesten, B. J. Verhaar & D. J. Heinzen (Aug. 1997), "Two-Color Photoassociation Spectroscopy of Ground State Rb_2", in *Physical Review Letters* **79**, pp. 1245–1248.

Tscherbul, T. V., T. Calarco, I. Lesanovsky, R. V. Krems, A. Dalgarno & J. Schmiedmayer (2010), "rf-field-induced Feshbach resonances", in *Phys. Rev. A* **81** (5), p. 050701.

Verhaar, B. J., E. G. M. van Kempen & S. J. J. M. F. Kokkelmans (2009), "Predicting scattering properties of ultracold atoms: Adiabatic accumulated phase method and mass scaling", in *Phys. Rev. A* **79** (3), p. 032711.

Volz, Thomas, Stephan Dürr, Niels Syassen, Gerhard Rempe, Eric van Kempen & Servaas Kokkelmans (2005), "Feshbach spectroscopy of a shape resonance", in *Phys. Rev. A* **72** (1), p. 010704.

Vuletic, Vladan, Andrew J. Kerman, Cheng Chin & Steven Chu (1999), "Observation of Low-Field Feshbach Resonances in Collisions of Cesium Atoms", in *Phys. Rev. Lett.* **82** (7), pp. 1406–1409.

Walker, Thad G. & M. Saffman (2008), "Consequences of Zeeman degeneracy for the van der Waals blockade between Rydberg atoms", in *Phys. Rev. A* **77** (3), p. 032723.

Walraven, JTM (1990), "Atomic hydrogen and liquid helium surfaces", in *Fundamental systems in quantum optics*, ed. by J. Dalibard, JM Raimond & J. Zinn-Justin, Elsevier Science Publishers, Amsterdam.

Weber, Tino, Jens Herbig, Michael Mark, Hanns-Christoph Nägerl & Rudolf Grimm (2003), "Bose-Einstein condensation of cesium", in *Science* **299**, pp. 232–235.

Weiner, John, Vanderlei S. Bagnato, Sergio Zilio & Paul S. Julienne (1999), "Experiments and theory in cold and ultracold collisions", in *Rev. Mod. Phys.* **71** (1), pp. 1–85.

Werner, Félix & Yvan Castin (Nov. 2012), "General relations for quantum gases in two and three dimensions. II. Bosons and mixtures", in *Physical Review A* **86**, p. 053633.

Wigner, E (1933), "Über die streuung von Neutronen an Protonen", in *Zeitschrift für Physik* **83**, pp. 253–258.

Wynar, Roahn, RS Freeland, DJ Han, C Ryu & DJ Heinzen (2000), "Molecules in a Bose-Einstein condensate", in *Science* **287**, pp. 1016–1019.

Xiao, Dawu, Ren Zhang & Peng Zhang (2019), "Confinement Induced Resonance with Weak Bare Interaction in a Quasi 3+0 Dimensional Ultracold Gas", in *Few-Body Systems* **60**, p. 63.

Yamaguchi, Yoshio (1954), "Two-Nucleon Problem When the Potential Is Nonlocal but Separable. I", in *Phys. Rev.* **95** (6), pp. 1628–1634.

Yao, Xing-Can, Ran Qi, Xiang-Pei Liu, Xiao-Qiong Wang, Yu-Xuan Wang, et al. (June 2019), "Degenerate Bose gases near a d-wave shape resonance", in *Nature Physics* **15**, pp. 570–576.

Yin, GP, P Li & KT Tang (2010), "The ground state van der Waals potentials of the strontium dimer and strontium rare-gas complexes", in *The Journal of chemical physics* **132**, p. 074303.

Yoshida, Shuhei M. & Masahito Ueda (2015), "Universal High-Momentum Asymptote and Thermodynamic Relations in a Spinless Fermi Gas with a Resonant p-Wave Interaction", in *Phys. Rev. Lett.* **115** (13), p. 135303.

Yu, Zhenhua, Joseph H. Thywissen & Shizhong Zhang (2015), "Universal Relations for a Fermi Gas Close to a p-Wave Interaction Resonance", in *Phys. Rev. Lett.* **115** (13), p. 135304.

Zavitsas, Andreas A (2006), "The potential energy curve of the ground state of the potassium dimer, X $^1\Sigma_g^+$ K_2", in *The Journal of chemical physics* **124**, p. 144318.

Zhang, Ren, Yanting Cheng, Hui Zhai & Peng Zhang (2015), "Orbital Feshbach Resonance in Alkali-Earth Atoms", in *Physical Review Letters* **115**, p. 135301.

Zhao, Yan & Donald G Truhlar (2006), "Comparative DFT study of van der Waals complexes: rare-gas dimers, alkaline-earth dimers, zinc dimer, and zinc-rare-gas dimers", in *The Journal of Physical Chemistry A* **110**, pp. 5121–5129.